UNIVERSITÉ DE MONTRÉAL

VISCOUSLY DAMPED CONTROLLED ROCKING RESPONSE FOR COST EFFECTIVE SEISMIC DESIGN OF STEEL STRUCTURES

LOUIS-PHILIPPE POIRIER
DÉPARTEMENT DES GÉNIES CIVIL, GÉOLOGIQUE ET DES MINES
ÉCOLE POLYTECHNIQUE DE MONTRÉAL

MÉMOIRE PRÉSENTÉ EN VUE DE L'OBTENTION
DU DIPLÔME DE MAÎTRISE ÈS SCIENCES APPLIQUÉES
(GÉNIE CIVIL)
AOÛT 2008

Your file Votre référence
ISBN: 978-0-494-46072-6
Our file Notre référence
ISBN: 978-0-494-46072-6

UNIVERSITÉ DE MONTRÉAL

ÉCOLE POLYTECHNIQUE DE MONTRÉAL

Ce mémoire intitulé:

VISCOUSLY DAMPED CONTROLLED ROCKING RESPONSE FOR COST EFFECTIVE SEISMIC DESIGN OF STEEL STRUCTURES

présenté par: POIRIER Louis-Philippe
en vue de l'obtention du diplôme de: Maîtrise ès sciences appliquées
a été dûment accepté par le jury d'examen constitué de:

Mme KOBOEVIC Sanda, Ph.D., présidente
M. TREMBLAY Robert, Ph.D., membre et directeur de recherche
M. BOUAANANI Najib, Ph.D., membre et codirecteur de recherche
M. MASSICOTTE Bruno, Ph.D., membre

AKNOWLEGDGEMENTS

First and foremost I would like to thank my research director and co-director Mr. Robert Tremblay and Mr. Najib Bouaanani for their help, efforts and advice that they have provided me during the realisation of this research program. I greatly enjoyed working with them and the technical knowledge they have offered me will greatly benefit my career.

Financial support for this study was provided by Bureau d'Études Spécialisées inc. (B.É.S. inc.) and the Natural Sciences and Engineering Research Council of Canada (NSERC - Collaborative Research and Development program). Special thanks to Mr. Stéphane Rivest and Mr. Luciano Fronteddu, associates at B.É.S. inc. for their continuous interest, support, and most valuable technical input in the course of the project.

I want to express my appreciation to the technical staff of the Structural Engineering Laboratory of Ecole Polytechnique of Montreal. In particular, Mr. Vivien René, Undergraduate Research Assistant and Mr. Martin Leclerc, Research Engineer. Their contribution to the shake table test program is greatly appreciated.

Thanks to my employer Stavibel inc., in particular to Mr. Mario Lévesque for his continuous mentoring and for providing me important career opportunities as well as allowing me some leeway with my work schedule in order to complete my thesis. I would also like to acknowledge the help of Mr. Dominic Ouellet with the preparation of some figures contained in this paper.

Finally, I can not thank enough my friends and family for their support and encouragements throughout this process. Special thanks to my soon-to-be wife Jessica for her patience and understanding. You are a constant reminder of how complete my life is.

RÉSUMÉ

Certains inconvénients économiques existent avec la méthode de conception par capacité actuellement prescrite par les codes nord-américains pour la conception sismique de bâtiments en acier utilisant des systèmes de contreventement concentriques. Premièrement, avec cette méthode, des efforts plus élevés doivent être considérés pour la conception des diaphragmes du toit et des étages, ainsi que la conception des fondations, pour assurer que la dissipation d'énergie prévue par la plastification des diagonales soit atteinte. Ceci peut causer une augmentation du coût de construction par rapport aux anciennes pratiques de conception. Deuxièmement, d'importantes déformations inélastiques permanentes sont à prévoir suite à un sévère tremblement de terre, pour les bâtiments conçus avec cette méthode. Ceci va occasionner des réparations coûteuses et, possiblement, un remplacement total, ce qui peut engendrer une perturbation aux opérations du bâtiment sur une longue période de temps.

Ce mémoire présente un système de contreventement innovateur conçu et détaillé spécifiquement pour basculer (soulèvement permis) sous les effets d'un tremblement de terre, pour réduire les efforts sismiques transmis à la structure du bâtiment. Ce système inclus des amortisseurs visqueux fixés verticalement entre les fondations et la base des colonnes pour dissiper de l'énergie et contrôler les déplacements latéraux de la structure, tout en limitant les forces d'impact subies par les colonnes.

Les motivations pour un tel système sont discutées et que les caractéristiques principales du système sont évaluées à travers une étude paramétrique effectuée sur le système de soulèvement sismique contrôlé avec amortissement visqueux (SSCAV) pour des structures typiques de 2-, 4- et 6-étages situées à Montréal, Vancouver et Los Angeles à l'aide d'analyses temporelles non-linéaires. L'étude démontre que le système performe très bien dans des zones sismiques à base et moyenne intensité, tel que Montréal et Vancouver. Le système réduit considérablement les efforts sur les

fondations comparativement à un système de contreventement conventionnel fixé aux fondations, ce qui peut diminuer de façon significative les coûts de constructions. L'étude démontre également que les structures peuvent être conçues de façon à éviter toute déformation résiduelle et dommage structural suite à un tremblement de terre, ce qui peut réduire considérablement les coûts de réparation et les périodes d'arrêt d'opération. Les résultats pour le site de Los Angeles indiquent que le système SSCAV peut occasionner des déplacements inter-étages excessif dans des régions sismiques à haute intensité avec des tremblements de terre de type impulsif, même avec l'utilisation d'amortisseurs à haute capacité. Une méthode de recentrage additionnelle doit être couplée au système SSCAV pour augmenter la performance du système dans de telles régions sismiques.

Des tests physiques sur des amortisseurs visqueux et des tests sur table vibrante d'un spécimen à grande échelle de deux-étages ont été effectués pour évaluer la performance générale du système et pour valider la précision des modèles numériques à reproduire correctement le comportement du système proposé. Les résultats des programmes d'essais expérimentaux ont démontrés que le système SSCAV s'est comporté tel que prévu lors de la conception, donc sans dommage structural. Les comparaisons avec les modèles d'éléments finis soulignent que les modèles analytiques présentement disponibles peuvent être utilisés avec confiance pour prédire les déformations subies par des contreventements équipés d'amortisseurs visqueux non-linéaire. Par contre, une certaine caution doit être exercée lors de l'interprétation des résultats des forces axiales fournis par les modèles numériques.

ABSTRACT

Several cost related drawbacks exist with the current capacity design approach provided by the North American standards for the seismic design of steel buildings with concentrically braced frames. Firstly, this procedure results in amplified design forces for the sizing of roof and floor diaphragms, as well as the foundations in order to ensure that the intended energy dissipation mechanism in the braces can be achieved, which can lead to major increases in construction costs compared to past practices. Secondly, so-designed buildings are expected to sustain significant inelastic deformations after a strong ground motion earthquake. This will necessitate lengthy and costly repairs and, even, total replacement, while creating disruption of the building functions for long periods of time

This paper presents an innovative braced frame system specifically designed and detailed to rock at its base under earthquake solicitations, to reduce the earthquake forces subjected onto a building structure. The system includes viscous dampers that are vertically mounted between the foundation and the column bases to dissipate energy and control the structure lateral displacements, while limiting the impact forces induced in the columns.

The motivation for such a system is discussed and the main features of the system are highlighted through a parametric study performed on the viscously damped controlled seismic rocking (VDCSR) system for typical 2-, 4- and 6-storey structures located in Montreal, Vancouver and Los Angeles using non-linear time history analyses. The study demonstrates that the VDCSR system performed very well in low and moderate seismic regions, such as the Montreal and Vancouver. The system leads to considerably lowered foundations loads compared to conventional fixed base seismic force resisting systems, which can result in significant cost savings during construction. The study also showed that the structures can be designed to avoid any residual

deformation and structural damage after strong ground motion, thus reducing considerably the repair costs and disruption periods after a severe earthquake event. The results for the Los Angles site indicate that the VDCSR system in high seismic regions where impulsive type ground motions are expected may result in excessive inter-storey drift demand, even if high capacity viscous dampers are used. It is believed that additional self-centering capability should be added to the system to enhance the response of the system in these seismic zones.

Physical testing of viscous damper units and shake table testing of a large scale 2-storey viscously damped rocking braced steel frame from the parametric study is performed to evaluate the overall performance of the system and to validate the adequacy of the numerical models to accurately reproduce the response of the proposed system. The results of the test programs showed that the VDCSR system behaved as intended in design, thus without structural damage. Comparisons with finite element models suggest that currently available simple finite element models can be used with confidence to predict the deformation demand on rocking braced frames equipped with nonlinear viscous dampers. However, caution must be exercised in the interpretation of the axial force outputs provided by the numerical models.

CONDENSÉ EN FRANÇAIS

1. Introduction

Certains inconvénients économiques existent avec la méthode de conception par capacité actuellement prescrite par les codes nord-américains pour la conception sismique de bâtiments en acier utilisant des systèmes de contreventement concentriques. Premièrement, avec cette méthode, des efforts plus élevés doivent être considérés pour la conception des diaphragmes du toit et des étages, ainsi que la conception des fondations, pour assurer que la dissipation d'énergie prévue par la plastification des diagonales soit atteinte. Ceci peut causer une augmentation du coût de construction par rapport aux anciennes pratiques de conception. Deuxièmement, d'importantes déformations inélastiques permanentes sont à prévoir suite à un sévère tremblement de terre, pour les bâtiments conçus avec cette méthode. Ceci va occasionner des réparations coûteuses et, possiblement, un remplacement total, ce qui peut engendrer une perturbation aux opérations du bâtiment sur une longue période de temps.

Ce mémoire présente un système de contreventement innovateur conçu et détaillé spécifiquement pour basculer (soulèvement permis) sous les effets d'un tremblement de terre, pour réduire les efforts sismiques transmis à la structure du bâtiment. De plus, ce système permet aux composantes du contreventement de travailler à l'intérieur de leurs limites élastiques, donc le bâtiment subit aucun dommage résiduel suite à un tremblement de terre. Le système a été baptisé le 'système de **S**oulèvement **S**ismique **C**ontrôlé avec **A**mortissement **V**isqueux' (SSCAV). Le système SSCAV a été développé par le Bureau d'Études Spécialisées inc., en collaboration avec l'École Polytechnique de Montréal. Celui-ci inclus des amortisseurs visqueux fixés verticalement entre les fondations et la base des contreventements pour dissiper de l'énergie et contrôler les déplacements latéraux de la structure, tout en limitant les forces d'impact subies par les colonnes. Ce système pourrait être utilisé autant dans la conception d'un nouveau bâtiment que dans la réhabilitation sismique d'un bâtiment existant.

Les objectives du projet de recherche sont les suivants: (1) Trouver une méthode de conception simplifiée, pour la phase 'avant projet', afin de déterminer si l'utilisation du système SSCAV est souhaitable et pour déterminer les propriétés optimales requises. (2) Évaluer la performance sismique du système proposé pour une variété de bâtiments et de conditions sismiques. (3) Vérifier expérimentalement le comportement du système et l'assemblage fondation/amortisseur/colonne sous l'effet de charges cycliques et valider la capacité des modèles numériques à reproduire adéquatement le comportement du système proposé.

Pour accomplir ces objectifs, the projet a été divisé en quatre tâches. La première tâche est une revue littéraire de la littérature dédiée aux investigations et aux développements touchant le soulèvement sismique des bâtiments, pour identifier les paramètres qui influencent ce type de comportement. La deuxième tâche est l'évaluation de trois méthodes simplifiées, développées pour prédire les déplacements sismiques de structures qui basculent sur leurs fondations, pour développer une procédure de conception préliminaire. La troisième tâche est une étude paramétrique sur une variété de bâtiments hypothétiques, pour déterminer les conditions auxquelles le système SSCAV est bénéfique et pour déterminer les caractéristiques de l'amortisseur requises pour ces conditions. La dernière tâche est un programme expérimental effectué sur un spécimen d'essai demi-échelle du système SSCAV. Ce programme d'essai est effectué pour évaluer le comportement réel du système soumis à des tremblements de terre et à divers autres signaux, pour valider l'exactitude des modèles d'éléments finis utilisés dans l'étude paramétrique.

2. Revue littéraire

La revue littéraire était axée sur l'identification des paramètres principaux qui peuvent influencer le comportement de bâtiments permis de basculer sur leurs fondations. Le concept de basculement est considéré comme une méthode d'isolation sismique qui permet de dissocier les mouvements du sol et de la base d'un bâtiment. Les

premières études sur ce concept datent des années 1960 et 1970 (Housner 1963; Meek 1975). Des programs d'essais expérimentaux et des études analytiques ont été effectués aux États-Unis sur des structures d'acier de 3- et 9-étages, avec et sans ancrages pour retenir le soulèvement des contreventements (Kelly et Tsztoo 1977; Clough and Huckelbridge 1977; Huckelbridge 1977). Les cas sans ancrages ont démontrés que l'effet de basculement réduit considérablement les charges latérales soumissent à la superstructure en comparaison avec les cas avec ancrages, représentant une économie potentiel pour le coût de la structure. De plus, il fut démontré que l'ajout de dissipateur d'énergie, tel que des plaques qui plastifient en torsion à la base des colonnes, permet de réduire les déformations latérales de la structure. Les résultats expérimentaux ont été reproduits efficacement par des analyses non-linéaires temporelles. D'autres essais sur table vibrante ont été effectués aux États-Unis sur des cadres d'acier et de béton avec soulèvement des colonnes permis et des systèmes d'isolation à la base (Griffith et al. 1988a, 1988b). Une bonne performance des systèmes a été observée, par contre les tests ont démontré que l'impact de la colonne sur la fondation crée des vibrations qui peuvent exciter les modes à haute fréquence de la structure pouvant causer des dommages au bâtiment. Des tests récents ont été complétés au Japon par Midorikawa et al. (2003) sur des structures multi-étagés avec des plaques de base conçues pour dissiper de l'énergie par plastification en flexion. Ces tests ont confirmé que ce type de système se comporte très bien.

La bonne performance d'un bâtiment en béton réel de 4-étages, pendant le tremblement de terre de San Fernando en 1971, a été attribuée à la réponse en basculement des fondations et l'interaction non-linéaire entre le sol et la structure pendant les vibrations intense du tremblement de terre (Rutemberg et al., 1982). Des études analytiques sur des murs de refend en béton dans le ouest Canadien, par Filiatrault et al. (1992) et Anderson (2003), ont démontrées que la motion de basculement permet de réduire les forces induites à la structure sans crée des déformations trop importantes. Basé sur cette étude, le basculement des fondations est

maintenant permis explicitement pour des bâtiments par le Code National du Bâtiment du Canada 2005.

Le basculement des fondations a également été proposé pour des piles de pont (Priestley et al., 1996). Ce concept a été utilisé pour la réhabilitation sismique de ponts existants (Rodriguez et Ingham, 1996; Dowdell et Hamersley, 2000). L'approche permet de réduire les forces d'inerties latérales et de concentrer les dommages structuraux, si présents, à la base des piles, où les réparations sont plus facilement effectuées (Dowdell et Hamersley, 2000). Pour réduire les impacts dynamiques à base des colonnes, des dissipateurs d'énergie ont été proposés. Pollino et Bruneau (2004a, 2004b) ont complété récemment des essais utilisant se concept pour des piles en treillis d'acier. Les résultats de l'investigation démontrent l'efficacité du système à contrôler la motion de basculement et de fournir une capacité de recentrage qui protège le pont de toute déformations résiduelles suite à un tremblement de terre.

3. Méthodes simplifiées

Dans le but de développer une méthode de conception simplifiée pour la phase préliminaire de design, trois méthodes analytiques ont été évaluées dans le cadre du projet : Substitute Substructure technique (Priesley et al., 1996), Energy Balance method (Anderson, 1993) et Equal Energy method (Anderson, 1993). Ces méthodes ont été proposées pour prédire le déplacement horizontal, dû au basculement, que subissent des structures lorsque soumises à des charges latérales de tremblement de terre. Une telle valeur pourrait être utilisée pour prévoir le comportement d'une structure munie du système SSCAV.

L'évaluation a été effectuée à l'aide de quatre structures de type bloc rigide et quatre structures à un degré de liberté. Une structure de type bloc rigide est une structure qui ne subit aucunes déformations internes lors de la motion de basculement, tandis qu'une

structure à un degré de liberté subit des déformations internes en plus du basculement. Les méthodes simplifiées ont été utilisées pour évaluer le déplacement des structures pour quatre tremblements de terre. Les résultats ont été comparés aux prédictions de modèles numériques non-linéaires par d'éléments finis, effectués avec le programme d'analyse SAP2000 (Computer & Structures inc., 2007). Les résultats démontrent que l'efficacité des méthodes varie d'une structure à l'autre et d'un tremblement de terre à un autre. Toutes les méthodes ont prédit très précisément les déplacements dans certains cas et n'étaient pas très précises dans d'autres cas. Les conclusions de l'étude démontrent que les méthodes simplifiées proposées ne fournissent pas un niveau de confiance assez élevé pour remplacer des analyses plus complètes effectuées à l'aide de modèle par éléments finis. Une étude plus approfondie est requise pour développer une méthode de conception préliminaire analytique pour le système SSCAV.

Une deuxième évaluation a été complétée pour déterminer l'efficacité du programme d'éléments finis SAP2000 à reproduire correctement le mouvement de basculement causé par des tremblements de terre. Ceci a été accompli en comparant les résultats de modèles d'éléments finis à ceux obtenus en utilisant la méthode analytique établie par Yim et Chopra (1983). Les résultats de l'évaluation démontrent que SAP2000 reproduit correctement la motion de basculement, donc est une bonne référence pour l'évaluation des méthodes simplifiées. En plus, cette évaluation a démontré que SAP2000 est un programme approprié pour l'étude paramétrique, effectuée en deuxième tâche.

4. Étude paramétrique

Une étude paramétrique à été effectuée à l'aide d'analyses numériques par éléments finis avec SAP2000 pour évaluer le comportement du système SSCAV incorporé dans des bâtiments de 2-, 4- et 6-étages situés à Montréal, Vancouver et Los Angeles. L'élancement des contreventements (2.81 m, 5.625 m et 9.0 m) et le ratio entre le poids sismique et le poids vertical des contreventements (positionné à l'intérieur et sur le périmètre du bâtiment) ont été variés pour déterminer l'influence de ces paramètres sur

le comportement du système. Pour cette étude, des amortisseurs aux paramètres non-linéaires donnés par la formule $F_d = C \cdot v^{\gamma}$ ont été utilisés où F_d est la force, C est une constante, v est la vitesse de l'amortisseur et γ est le paramètre de non-linéarité influençant la vitesse. Un facteur γ égale à 0.25 a été sélectionné pour que la force dans les amortisseurs atteigne rapidement une valeur maximale prédéfinie à des hautes vitesses, permettant une conception élastique de la structure pour résister à cette valeur maximale. Dans l'étude, une valeur optimale pour la constante C a été déterminée pour chacun des bâtiments de façon à limiter les déplacements inter-étages aux limites du code Canadien (NRCC, 2005) ou celles du code Californien (ICCCBSC, 2001).

Les résultats de l'étude démontrent que le système SSCAV anéanti presque entièrement les efforts de soulèvement à la base des contreventements. Les forces verticales vers le bas sont également réduites considérablement comparativement à un contreventement conventionnel à base fixe. Les réductions d'efforts verticaux produites par l'utilisation du système SSCAV représentent un gain important dans le coûts de construction des ancrages et des fondations. Durant le processus de basculement, une colonne du contreventement doit supporter le poids gravitaire total des deux colonnes. Malgré cette punition, les forces axiales dans les colonnes demeurent plus petites (Vancouver et Los Angeles) ou similaire (Montréal) que les forces considérées pour la conception d'un contreventement conventionnel à base fixe. Pour les bâtiments de 2-étages à Montréal et Los Angeles, les efforts de cisaillement à la base sont généralement réduits avec l'utilisation du système SSCAV, par rapport au cisaillement calculé avec le concept de 'capacité design', requis pour des conceptions conventionnelles. Lorsque la hauteur de la structure augmente, le comportement de basculement a tendance à devenir déphasé par rapport aux efforts de cisaillement à la base, réduisant les effets positifs du système SSCAV. Le cisaillement à la base devient donc plus élevé qu'un contreventement traditionnel. À Vancouver, le cisaillement à la base est plus élevé pour tous les bâtiments considérés dans l'étude. Pour tous les bâtiments (Montréal, Vancouver et Los Angeles) les efforts axiaux dans les diagonales sont plus élevés en

comparaison aux efforts prévus pour des contreventements à base fixe. Par contre, l'augmentation est moins importantes lorsque l'élancement du système SSCAV ou le ratio entre la masse verticale et la masse sismique sont réduits.

L'étude démontre que les structures peuvent être conçues de façon à éviter toute déformation résiduelle et dommage structural suite à un tremblement de terre, ce qui peut réduire considérablement les coûts de réparation et les périodes d'arrêt d'opération. Les résultats pour le site de Los Angeles indiquent par contre, que le système SSCAV peut occasionner des déplacements inter-étages excessif dans des régions sismiques à haute intensité avec des tremblements de terre de type impulsif, même avec l'utilisation d'amortisseurs à haute capacité. Une méthode de recentrage additionnelle doit être couplée au système SSCAV pour augmenter la performance du système dans de telles régions sismiques.

5. Programme expérimental

Un programme expérimental sur la table sismique du laboratoire de structures d'Hydro-Québec à l'École Polytechnique de Montréal a été développé pour un bâtiment de 2-étages tiré de l'étude paramétrique. Un cadre de contreventement demi-échelle fixé sur des amortisseurs visqueux a été utilisé pour le programme expérimental. Le cadre spécimen a été conçu suivant des strictes relations de similitude, utilisant la méthode de similitude avec accélération modifié (Merzouq, 2006), pour obtenir un modèle à demi-échelle qui se comporte exactement comme un modèle pleine grandeur.

Un programme d'essai préliminaire aux tests sur la table sismique a été complété pour calibrer les amortisseurs visqueux aux valeurs requises pour la table vibrante. Les amortisseurs ont été fourni pas LCL-Bridge Technology Products Inc. Les amortisseurs ont été soumis à une variété de protocoles de chargement incluant des signaux à vitesses constantes, des signaux sinusoïdaux harmoniques et des signaux de déplacement provenant des analyses non-linéaires de l'étude paramétrique. Les résultats des tests

Un des objectifs principaux du programme expérimental était de valider que les modèles numériques pouvaient prédire correctement le comportement de bâtiments équipés du système SSCAV, afin de confirmer que les résultats de l'étude paramétrique sont valides et que le modèle numérique peut être utilisé pour des conceptions futures. Des simulations numériques ont été effectuées avec le programme d'éléments finis SAP2000 pour reproduire le comportement du cadre expérimental mesuré dans les tests sur la table sismique. Une comparaison des résultats démontre que le modèle numérique peut prédire très précisément les déplacements horizontaux et de soulèvement du cadre expérimental pour tous les cas de chargement considérés. Par contre, les résultats démontrent que les efforts axiaux des colonnes et des diagonales sont surestimés par le modèle numérique. Ceci est causé par une réponse numérique à haute fréquence qui n'est pas observée dans les tests expérimentaux. Cependant, cette surestimation n'est pas présente pour les signaux harmoniques à fréquence constante. Une investigation plus approfondie est requise pour expliquer ce phénomène. Néanmoins, les résultats de l'étude démontrent que les modèles d'analyses peuvent prédire efficacement les déformations d'un système basculant équipé d'amortisseurs visqueux non-linéaires. L'interprétation des efforts axiaux donnés par les modèles numériques doit être faite avec précaution. Ceci est autant vrai pour les résultats de l'étude paramétrique.

6. Conclusion

Ce projet a adressé quelques aspects d'un nouveau système innovateur de contreventement pour la résistance sismique de structures en acier. Ce système démontre des caractéristiques intéressantes. Les résultats du programme d'étude sont prometteurs et suggèrent que le système SSCAV proposé, a le potentiel de devenir une solution économique pour une performance sismique améliorée dans des conditions sismiques à base et moyenne intensité. Des études plus approfondies sont requises pour répondre à quelques questions soulevées lors de l'étude, ainsi que pour évaluer quelques points non traitées dans le cadre du projet : les effets de la composante verticale des tremblements

Un des objectifs principaux du programme expérimental était de valider que les modèles numériques pouvaient prédire correctement le comportement de bâtiments équipés du système SSCAV, afin de confirmer que les résultats de l'étude paramétrique sont valides et que le modèle numérique peut être utilisé pour des conceptions futures. Des simulations numériques ont été effectuées avec le programme d'éléments finis SAP2000 pour reproduire le comportement du cadre expérimental mesuré dans les tests sur la table sismique. Une comparaison des résultats démontre que le modèle numérique peut prédire très précisément les déplacements horizontaux et de soulèvement du cadre expérimental pour tous les cas de chargement considérés. Par contre, les résultats démontrent que les efforts axiaux des colonnes et des diagonales sont surestimés par le modèle numérique. Ceci est causé par une réponse numérique à haute fréquence qui n'est pas observée dans les tests expérimentaux. Cependant, cette surestimation n'est pas présente pour les signaux harmoniques à fréquence constante. Une investigation plus approfondie est requise pour expliquer ce phénomène. Néanmoins, les résultats de l'étude démontrent que les modèles d'analyses peuvent prédire efficacement les déformations d'un système basculant équipé d'amortisseurs visqueux non-linéaires. L'interprétation des efforts axiaux donnés par les modèles numériques doit être faite avec précaution. Ceci est autant vrai pour les résultats de l'étude paramétrique.

6. Conclusion

Ce projet a adressé quelques aspects d'un nouveau système innovateur de contreventement pour la résistance sismique de structures en acier. Ce système démontre des caractéristiques intéressantes. Les résultats du programme d'étude sont prometteurs et suggèrent que le système SSCAV proposé, a le potentiel de devenir une solution économique pour une performance sismique améliorée dans des conditions sismiques à base et moyenne intensité. Des études plus approfondies sont requises pour répondre à quelques questions soulevées lors de l'étude, ainsi que pour évaluer quelques points non traitées dans le cadre du projet : les effets de la composante verticale des tremblements

de terre, les forces d'impact générées par le contact des colonnes avec les fondations et l'effet que le type de sol a sur le comportement du système.

TABLE OF CONTENTS

LIST OF TABLES

Tables of Chapter 3

Tables of Chapter 4

Tables of Chapter 5

Tables of Chapter 6

Tables of Chapter 7

LIST OF FIGURES

Figures of Chapter 1

Figures of Chapter 2

Figures of Chapter 3

Figures of Chapter 4

Figures of Chapter 5

Figures of Chapter 6

Figures of Chapter 7

LIST OF SIGNS AND ABBREVIATIONS

a	acceleration
$a_{rocking}$	acceleration needed to initiate rocking
b	½ width of the foundation mat (Chopra and Yim)
c	lateral damping coefficient (Chopra and Yim)
c_f	damping value of foundation (Chopra and Yim)
C	damping coefficient
CM	center of mass
E	modulus of elasticity
E_c	elastic energy (EE method)
E_i	inelastic energy (EE method)
F	force
g	gravitational acceleration
H, h	height
I_o	inertia of foundation mat (Chopra and Yim)
k	stiffness
k_f	stiffness of foundation mat (Chopra and Yim)
K	gage factor
KE	kinetic energy
L	length
m	mass
m_o	mass of foundation mat (Chopra and Yim)
P	gravity load
PE	potential energy
M_r	resisting moment capacity
r	coefficient of restitution (SS technique)

R	hypotenuse between the point of rotation and the center of mass (SS technique)
R_g	gage resistance
S_a	spectral acceleration
S_d	spectral displacement
S_v	spectral velocity
t	time
T	period
u	lateral displacement (Chopra and Yim)
$\ddot{u}$	acceleration of gravity (Chopra and Yim)
V	elastic force (EE method)
V_E	equivalent lateral force (SS technique)
V_l	vertical displacement left base (Chopra and Yim)
V_o	overturning force (EE method)
V_r	vertical displacement right base (Chopra and Yim)
w	weight
γ	nonlinear parameter of the velocity
$\in$	strain
ξ	damping ratio
ξ_e	equivalent damping ratio
ξ_v	vertical damping ratio
σ	stress
θ	angle of base rotation
Ø	angle between hypotenuse R and a vertical line (SS technique)
ω	natural vibration frequency
ω_v	vertical vibration frequency
Δ	displacement
Δ_c	structural displacement

Δ_c	elastic displacement (EE method)
Δ_i	inelastic displacement (EE method)
Δ_r	rocking displacement

LIST OF APPENDICES

CHAPTER 1

INTRODUCTION

1.1. Introduction

The conventional earthquake design method used for buildings is to provide seismic force resisting systems (SFRS) that passively resist earthquakes through a combination of strength, deformability and energy absorption. During strong ground shaking, the SFRSs deform well beyond the elastic limit and dissipate the energy of the earthquake through inelastic plastic deformations and increased flexibility. This is the approach that has been adopted in Canada. The 2005 National Building Code of Canada (NBCC) provides special provisions to achieve satisfactory inelastic seismic performance for various SFRSs used in building construction using the capacity design principal (National Research Council of Canada, 2005). This principle allows for the dissipation of the seismic input energy through the localized damage of a chosen constituent of the SFRS, called the plastic hinge, through cyclic inelastic response, while the remainder of the system is provided with enough capacity to resists elastically to the maximum anticipated forces.

The design of steel buildings in Canada is governed by the provisions given by the CAN/CSA–S16-01 standard (CSA, 2001; CSA, 2005). The four major types of SFRS used in steel buildings are concentrically braced frames, eccentrically braced frames, moment resisting frames and frame plate shear walls. All of these SFRS are designed using the principles of capacity design. Several ductility levels (R_d factors) are available for each of these systems, varying from 1.5 to 5.0. The R_d factor is the ductility-related force modification factor reflecting the capability of a structure to dissipate energy through inelastic behaviour of the weak link in the SFRS (plastic hinge). It is left up to the designer's discretion to select the ductility level wanted, but the design criteria become more severe as the R_d factor is increased. This has a

significant impact on the surrounding components of the building such as the connections, the floor and roof diaphragms, the columns and the foundations, since these components must be designed with a significant reserve in strength to remain elastic during the earthquake solicitation. Complying with these design requirements has impacted significantly the cost of building structures.

Previous studies and post earthquake observations have demonstrated numerous advantages associated with allowing the SFRS of a building to rock at its base under strong ground motions. This foundation rocking creates a fuse between the ground and the structure which diminishes the force demand on the structure, which could represent a viable and cost effective seismic strategy. This type of strategy is now permitted for buildings by the NBCC 2005.

This thesis presents an innovative braced frame system specifically designed and detailed to rock at its base under earthquake solicitations, to reduce the earthquake forces subjected onto a building structure, while working within the elastic limits of the SFRS components. Therefore, no damage occurs to the structure following an earthquake. This system has been named the 'Viscously Damped Controlled Seismic Rocking system' (VDCSR).

1.2. The proposed VDCSR system

The proposed VDCSR system was developed by Bureau d'Études Spécialisées Inc. (B.E.S inc.), in collaboration with researchers from Ecole Polytecnique of Montreal. This system is composed of viscous dampers vertically mounted between the foundation and the bases of SFRS. Figure 1.1 illustrates one possible setup for the VDCSR system. In this case, the viscous dampers are introduced at the base of a concentrically braced steel frame. Steel casings are securely embedded with anchors rods in the concrete foundation at the base of each of the columns of the braced frame. The columns are designed with shop welded tubular steel shear lugs under the

base plates such that horizontal reactions are transferred by direct bearing. The upper parts of the viscous dampers are bolt-connected underneath the column base plates. The dampers allow for vertical uplift of the columns and, thereby, rocking response of the braced frame. Downward movement of the columns is prevented by direct bearing of the column base plates against the top end of the steel casing and the top surface of the surrounding concrete foundation. Alternative arrangements are possible such as securing the dampers to the foundation next to the columns, with the moveable part of the dampers being connected to a bracket welded on the side of the columns, or the use of horizontal struts connecting the column bases to the foundations for the transfer of the horizontal reactions. This system can also be introduced in retrofit projects to reduce the lateral force demand on the existing SFRSs.

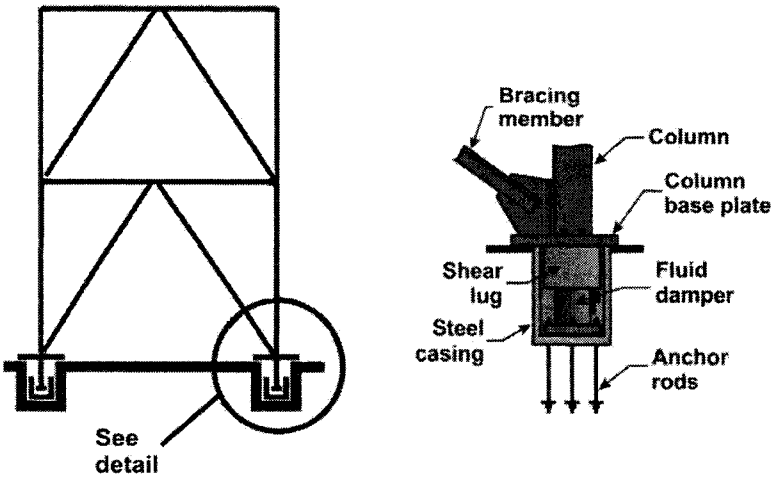

Figure 1.1: Example of a possible setup for the VDCSR.

1.3. Objectives

The objective of this project is threefold:

- To find a simplified design approach, for the preliminary design stage, to determine the optimum properties needed for the VDCSR system needed to optimise the benefits of using this system.
- To assess the enhancement of the seismic performance generated by the proposed system for various structures and seismic conditions.
- To verify experimentally the response of the proposed damper system and the foundation/fluid damper/column assembly under cyclic loading and validate the adequacy of the numerical models to reproduce the response of the proposed system.

1.4. Methodology

To accomplish these objectives, the project is divided into four tasks:

The first task is a literature review devoted to theoretical investigations and developments on the rocking response of structures, to identify the key parameters influencing this response. A summary of this review is presented in Chapter 2.

The second task is an evaluation of three simplified design approaches used to predict the rocking response of structures. The predictions obtained from these simplified methods are compared to finite element models to determine which would be best suited for preliminary design purposes. A description of the simplified methods and the results of the evaluation are presented in Chapter 3.

The third task is a parametric study performed on a variety of hypothetical buildings to determine the range of applicability of the VDCSR system and collect information on the damper characteristic that are needed to cover this range. The findings of this study are presented in Chapter 4.

The final task is an experimental test program on a test specimen of the VDCSR system. This test program is used to evaluate the real life performance of the system subjected to earthquakes and various other signals to validate the accuracy of the computer models used in the parametric study. To accomplish this task a half-scaled model is designed. Chapter 5 presents the procedure used to develop the experimental test program for the shake table. Also, tests are performed on two individual dampers to calibrate them to the properties required for the shake table test program. Chapter 6 describes this test program as well as the results of the experimental tests. Finally, Chapter 7 presents the shake table test program and the results of the comparison performed with finite element models.

CHAPTER 2

LITERATURE REVIEW

2.1. Introduction

This chapter presents a summary of the most relevant literature devoted to theoretical investigations and developments on the rocking response of structures. The focus of the review was on the identification of key parameters that can influence the rocking response.

2.2. The concept of seismic isolation applied to buildings

Naeim (2001) wrote a handbook that covers many of the aspects of seismic design. Chapter 14 covers exclusively the design of structures with seismic isolation. Seismic isolation systems are systems that modify the seismic response of a building in such a way that it prevents most of the horizontal movements of the ground from being transmitted to the building. Therefore, the seismic loads imposed onto the building are greatly reduced. According to this book, the concept of isolating structures from the damaging effects of earthquakes is not new. The first patent for a seismic isolation scheme was issued in 1909 and since that time several proposals with similar objectives have been made. The most common seismic isolation systems are illustrated in Figure 2.1. These systems include the use of elastomeric bearings, rollers, friction slip plates, cable suspension, sleeved piles, and, as is proposed in this program, rocking foundations.

This reference also enumerates the basic elements to any practical seismic isolation system, which are:

i. A system that increases the flexibility of the structure so that the period of vibration of the system is lengthened sufficiently to reduce the force response of the earthquake;
ii. A damper or energy dissipater to control the relative displacements between the building and the ground to a practical design level; and

iii. A means of providing rigidity under low service loads such as wind and minor earthquakes.

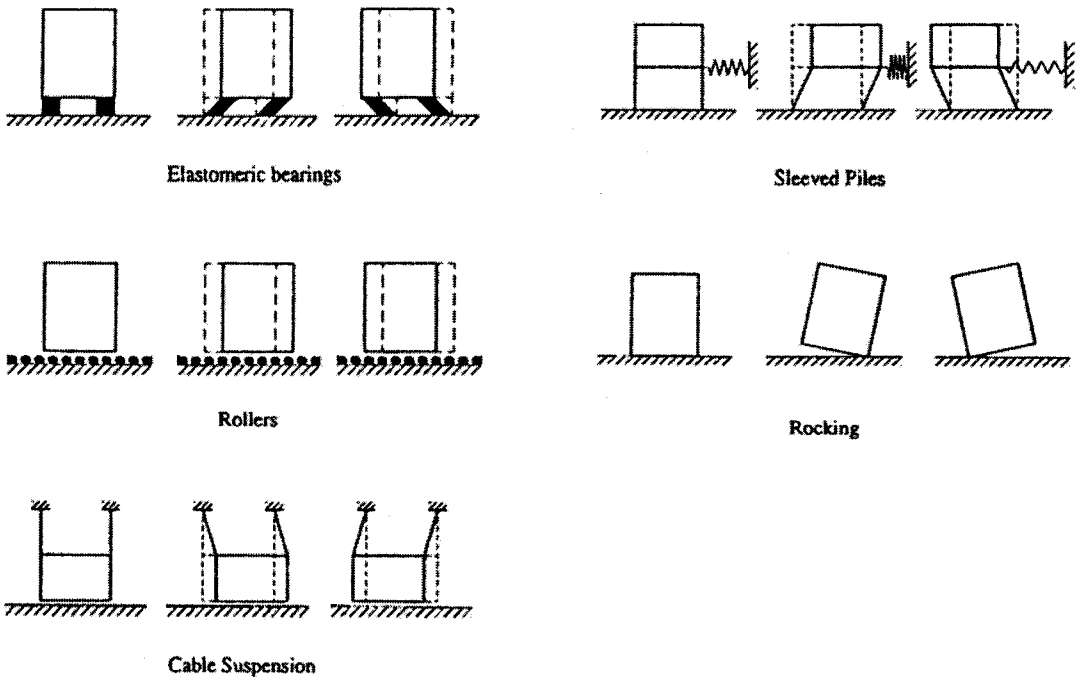

Figure 2.1: Seismic isolation systems (adapted from Naeim, 2001).

Lengthening the period of vibration of a structure is beneficial for the response to the earthquake excitations since the force input onto the structure is significantly reduced. Figures 2.2 (a) and (b) illustrate idealized response curves for the base shear forces and the lateral displacements of a structure. It is observed on the force response spectrum that an increased period reduces the force input; however, as illustrated on the displacement response spectrum, the displacement of the system is increased, which is not beneficial. The displacement of a building during an earthquake must be limited to avoid damages to building contents, architectural facades, partitions, piping and ductwork, ceilings, building equipments and elevators, which may cause increasingly high repair costs. Therefore, the displacements must be controlled by supplementary damping provided by mechanical dampers or energy dissipation devices. Adding

additional damping to a building is beneficial for both the displacement demand and the force demand imposed onto the structure. Figures 2.3 (a) and (b) illustrate idealized force and displacement spectrum. As illustrated, both the force and the displacement demand are reduced when increasing the damping values.

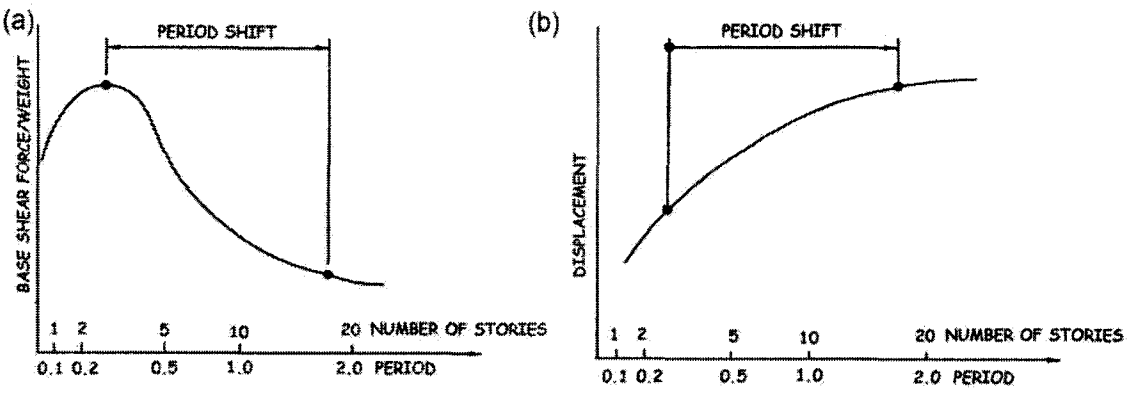

Figure F2.2: (a) Effects of a shift in period on the base shear spectrum (Naeim, 2001).
(b) Effects of a shift in period on the displacement spectrum (Naeim, 2001).

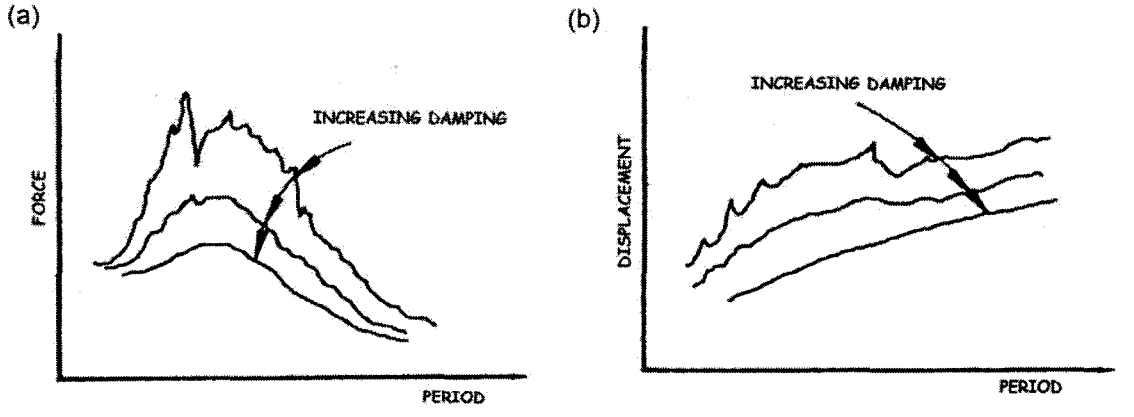

Figure 2.3: (a) Effects of an increase in damping on the force spectrum (Naeim, 2001).
(b) Effects of an increase in damping on the displacement spectrum (Naeim, 2001).

2.3. Rocking as a seismic isolation technique

Rocking is one of the seismic isolation techniques that can be applied to buildings. Intentionally designing column uplifting capability at the base of a structure or allowing foundation rocking creates a fuse between the ground and the structure that elongates the

period of the building and, thereby, reduces the force demand on the structure under strong earthquake ground motions.

This concept was first examined back in the 1960's by Housner (1963) who was the first to recognize the correlation between foundation uplift and the good performance of seemingly unstable structures during earthquakes. He questioned himself following the Chilean earthquake of 1960 about the behaviour of golf-ball-on-tee type of elevated water tanks that survived the ground shaking, while more stable appearing structures were severely damaged. He investigated the dynamics of a rigid block rocking on a rigid horizontal base. Representing the ground accelerations as rectangular pulses and half sinusoidal wave pulse, equations were derived to determine the minimum acceleration required to overturn a block. Using an energy approach, Housner presented an approximate analysis of the dynamics of a block subjected to earthquake excitations. The results of the study demonstrated that the stability of a tall slender block, subjected to a seismic ground motion is much greater than would be inferred from its stability against a static horizontal force, which is often employed to represent the effects of an earthquake. He also developed a formula to estimate the dissipation of energy resulting from rocking. Energy is dissipated in the impact that occurs every time the pole of rotation changes from one corner of the base to the other.

In the 1970's, Meek (1975) was the first to analytically investigate the effects of foundation uplift on the earthquake response of flexible structures. He presented methods which allow the influence of tipping to be considered in the dynamic analysis of single-mass models of structures subjected to simple transient ground motions. The investigation concluded that rocking leads to a favourable reduction in the maximum transverse deformation and shear forces imposed on a structure in comparison to fixed-base behaviour. By contrast, however, it was concluded that rocking can endanger the stability of the structure's compression members or lead to foundation failure caused by the short duration high intensity normal forces that are generated when the foundation

slams into renewed contact with the ground. A further investigation was needed to evaluate the impact forces.

Priestley et al. (1978) performed an evaluation of the equations for a rocking block proposed by Housner and concluded that some of his assumptions were unconservative. An extension of Housner's theory led Priestley and al. to develop a simple method for predicting maximum displacement of rocking by use of displacement response spectra and an equivalent elastic representation of the rocking system. This approach was developed to provide an estimate on the rocking response of buildings, bridge piers, chimneys and other structures. Shake table tests were also performed on a simple structural model to validate the effectiveness of this estimating approach. According to the authors, the agreement between the results of the tests and the predictions was reasonably good.

In the late 1970's, Yim et al. (1980) developed a numerical procedure and a computer program to solve the nonlinear equations of motion governing the rocking motion of rigid blocks on rigid bases subjected to vertical and horizontal ground motions. They performed a parametric study using these numerical methods to determine the parameters affecting the overturning response of blocks subjected to earthquake ground motions. The results of the study demonstrated that the response of a rigid block is very sensitive to small changes in size, slenderness ratio and the characteristics of the ground motion, but that no systematic trends were observed. However, using probabilistics, it was determined that the probability that a block overturns is increased with an increase in ground motion intensity, increase in slenderness ratio of the block, and a decrease in its size.

In the early 1980's, Yim and Chopra (1983) pursued their investigation on the rocking motion, but now dealing with flexible structures. They performed an analytical study to understand better the effects of transient foundation uplift on the response of

flexible structures, so that the related reduction in earthquake forces may be considered in the design of structures. They used mathematical models incorporating the effects of soil flexibility and the mechanics of uplifting and impact. The model used for the evaluations is illustrated in the following chapter (Figure 3.8). It is a flexible single-degree-of-freedom (SDOF) system supported by a foundation mat resting on a simple two spring-damper soil/foundation model. The evaluations demonstrated that the earthquake response of uplifting structures is controlled by the following parameters:

i. the natural vibration frequency of the structure;
ii. the slenderness ratio;
iii. the ratio between the mass of the superstructure and the mass of the foundation;
iv. the vertical vibration frequency of the soil;
v. the damping ratio of the structure; and
vi. the damping ratio of the soil.

It was also demonstrated that the base shear forces are reduced for short period structures allowed to uplift and that slender structures have a higher tendency to rock, thus resulting in greater reductions in shear forces. Although the vertical components of the ground motion were neglected in their study, the authors believed that this parameter may have a significant influence on the dynamic response of flexible structures.

At approximately the same time, Psycharis and Jennings (Psycharis et al., 1983; Psycharis, 1982) performed an analytical investigation on the effects of lift-off on the dynamic behaviour of both rigid block structures and flexible structures in order to put forth approximate methods of analysis to evaluate the rocking response of these structures. In their evaluation, two types of soil/foundation models that permit uplift were evaluated: the Winkler foundation model and the two-spring foundation model. Also, vertical dampers were included into these models to determine the effects of this

component on the rocking motion of the structures. Figure 2.4 illustrates the two damped soil/foundations models used for the rigid block structures. The same models where also used for the flexible structures.

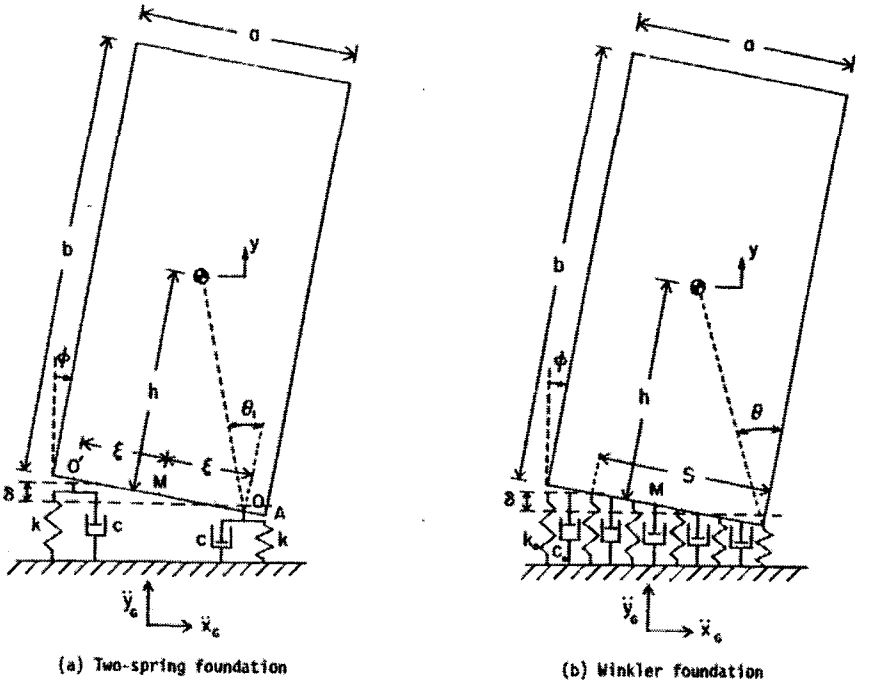

Figure 2.4: Soil/foundation models (Psycharis, 1982).

This investigation demonstrated interesting comparison results for the two foundation models, in which it was observed that an equivalence exists between the two. Therefore, one can always work with the much simpler two-spring foundation model. As for the rocking motion of the structures, it was observed that the rocking periods of the rigid blocks were dependant on the amplitude of the impulse and were increased with the amount of lift-off obtained. For flexible structures, the fundamental period of the structures, compared to the period before lift-off, was increased in the same way as for the rigid blocks. The increase was dependant on the amplitude of the impulse and the amount of lift-off obtained. The second mode and higher modes of frequency were not significantly affected by uplift or the soil/foundation interaction. When vertical dampers were added to the foundation model, the investigation demonstrated that the apparent

ratio of critical damping had a tendency to decrease with the amount of lift-off obtained. They determined that the dashpots (viscous dampers) were the most effective way to account approximately for the energy dissipation during impact, when the uplifted column comes back down. In conclusion, the report states that there is no general consensus on whether or not the rocking motion is beneficial for flexible structures. The deflection of the structure and the resulting stresses are dependant on the parameters of the building and the characteristics of the earthquake excitation.

In the late 1970's, experimental test trials were performed on rocking structures. Clough and Huckelbridge (1977) performed an extensive shake table test program and an analytical study on a 3-storey concentrically braced steel frame. Figure 2.5 (a) illustrates the test setup used. Tests were performed with uplift allowed and without uplift (fixed base condition). The results of these tests were compared to those of numerical analyses performed with a nonlinear dynamic program. The objective of the study was to investigate the seismically induced overturning effect in a simple structural system, both with and without anchorages provided, to evaluate the nonlinear analytical techniques available at that time. It was demonstrated that the analytical results were in good agreement with the experimental results. Also, the test results demonstrated clearly that the structural response quantities were reduced by the uplift phenomenon, in comparison to the fixed based case. According to the authors, the action of the uplift response mechanism as a structural 'fuse' was clearly evident. However, considerably large relative storey displacements were observed when uplift was allowed. Nevertheless, it was concluded that allowing column uplift in building frames can lead to more rational and economical designs.

Huckelbridge (1977) pursued his shake table test program and analytical study and tested a 9-storey two-dimensional steel frame subjected to various earthquake ground motions. Figures 2.5 (b) illustrates the test setup used. The objective of this study was to observe the uplifting behaviour of a more complex system, to compare the uplifting

behaviour to a fixed-base system and evaluate the potential of including rocking into the design of structural systems. The results demonstrated that the rocking response was beneficial even to a more complex structural system. The author believed that allowing column uplift could lead to more economical designs, particularly when foundation costs are considered; however, a rational design including provisions for column uplift is required.

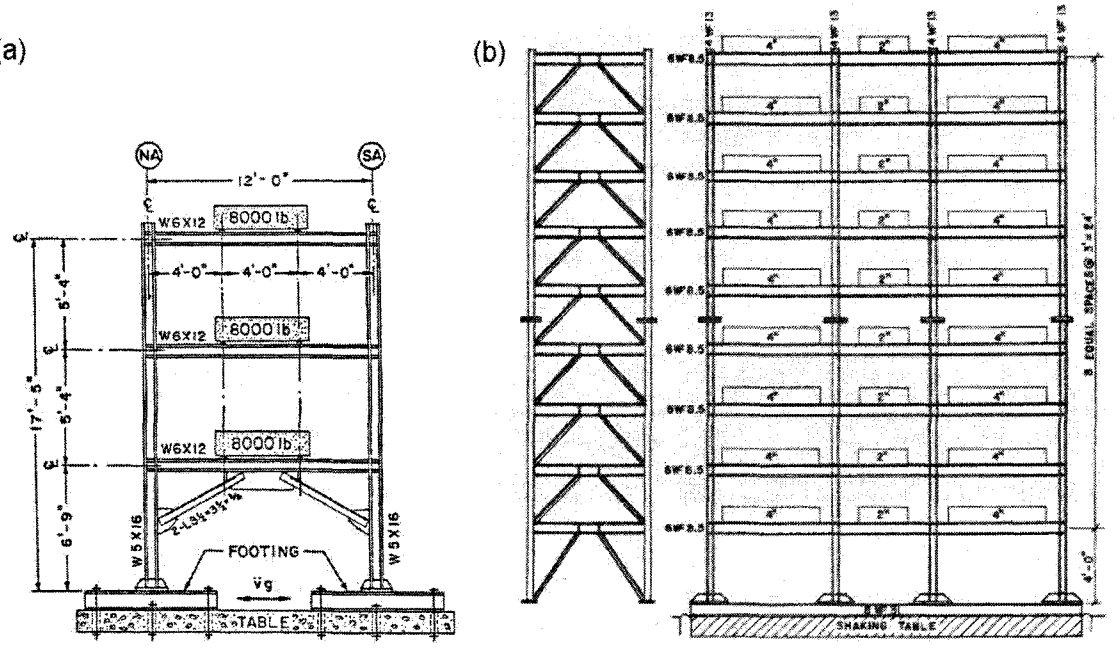

Figure 2.5: (a) Test setup for the 3-storey frame (Clough et al., 1977).
(b) Test setup for the 9-storey frame (Huckelbridge, 1977).

The principal of rocking foundations has been observed and used in real life applications. In the early 1980's, dynamic analyses were performed by Rutemberg and al. (1982) to understand the seismic response of the 4-storey reinforced concrete structure of the Veterans Hospital Building 41, located in San Francisco, during the February 9th 1971 San Fernando earthquake. The objective of the investigation was to understand how a building that was designed to withstand a lateral force coefficient of only 10 percent survived a maximum base shear of 60 to 130 percent of the weight of

the building. Two-dimensional dynamic models incorporating partial uplift and soil yielding were used to explain this phenomenon. According to the authors, the results of the study showed fairly convincingly that one of the keys to the successful response of the structure was the nonlinear soil-structure interaction involving rocking of the foundation.

In the late 1990's, design offices started employing the rocking concept for the seismic retrofit of existing bridge piers. Rodriguez and Ingham, (1996) used numerical nonlinear analyses to design the seismic retrofit of the Golden Gate Bridge in San Francisco, California, which included the rocking motion of the pier towers. Dowdell and Hamersley (2001) also used nonlinear dynamic analyses to determine the seismic retrofit strategy for the Lions' Gate Bridge North Approach in Vancouver, Canada. The strategy was to permit the 24 steel bents to rock on their concrete pedestals when subjected to earthquake ground motions. Numerical computations were undertaken to study the effectiveness of the seismic retrofit. One of the areas of concern that was addressed by the nonlinear analysis was the dynamic impact of the columns on the foundations. The analyses demonstrated that the impact created two different effects that increased the bent loads. The first is caused by a pressure wave that is propagated through the columns which induce stresses that are proportional to the velocity at the time of impact. The second is caused by a horizontal/vertical coupling effect which originates at the time of impact and affects the vertical vibration modes of the bent. Additional reinforcements were added to the columns to account for the impact forces; however altogether, the retrofit was deemed a robust, cost effective solution.

In the new National Building Code of Canada (NBCC 2005) (National Research Council of Canada, 2005), foundation rocking is now explicitly allowed for buildings. This is following analytical studies that have been performed by Filiatrault et al. (1992) and Anderson (2003) on shear wall structures in western Canada. These studies demonstrated that foundation rocking permitted to reach both ultimate objectives, which

are to reduce the force demand imposed onto a structure, without increasing excessively the lateral displacement of that structure. However, this could only be achieved if the foundations have minimum resistance to rocking. This new concept in the NBCC 2005 is covered in clause 4.1.8.15.(6) for the design of the SFRSs and clause 4.1.8.16.(1) for the design of the foundations. Clause 4.1.8.15.(6) states that the design of the SFRS need not exceed the maximum values associated with foundation rocking, provided that the R_d and R_o factors are conform to the type of SFRS used and that the foundations are designed in accordance to clause 4.1.8.16.(1). Clause 4.1.8.16.(1) states that when foundations are allowed to rock, the design forces need not exceed those determine in the dynamic analysis or the equivalent static force analysis using an R_dR_o value equal to 2.0.

2.4. Rocking with energy dissipation devices

Following the interesting developments found for the use of rocking as a seismic isolation technique, several energy dissipation devices have been proposed in combination to the rocking motion, to improve on this concept. Although many have demonstrated the benefits of creating a fuse between the ground and the structure that elongates the period of the building through allowed uplift of the columns, it has also been shown that this technique has a tendency of creating larger displacements to the structure. The theory behind adding the energy dissipation devices to the system is that these devices will allow for a control of the displacements of the structure, without taking away from the benefits of the rocking.

Following the successful shake table test trials performed by Clough and Huckelbridge (1977) on a 3-storey concentrically braced frame in the late 1970's to evaluate the effects of rocking, Kelly et al. (1977) performed shake table tests on the same three-storey test specimen but with additional energy dissipating steel twisting plates attached to the base of the columns. Figure 2.6 illustrates the test setup used. The objective of this investigation was to evaluate the effectiveness of this base isolation

system in reducing the effects of an earthquake ground motion on the frame. The results of the shake table tests were compared to the results obtained by Clough and Huckelbridge for the fixed base specimen and the specimen allowed to uplift. The results demonstrated that the response of the system with the energy dissipation devices was dependant on the type of earthquake excitation applied to the frame. Although it performed less favourably to impulsive loadings, such as the Pacoima Dam record, it presented great advantages over the fixed base response and certain advantages over the free rocking response when subjected to a less impulsive ground motion, such as the El Centro record.

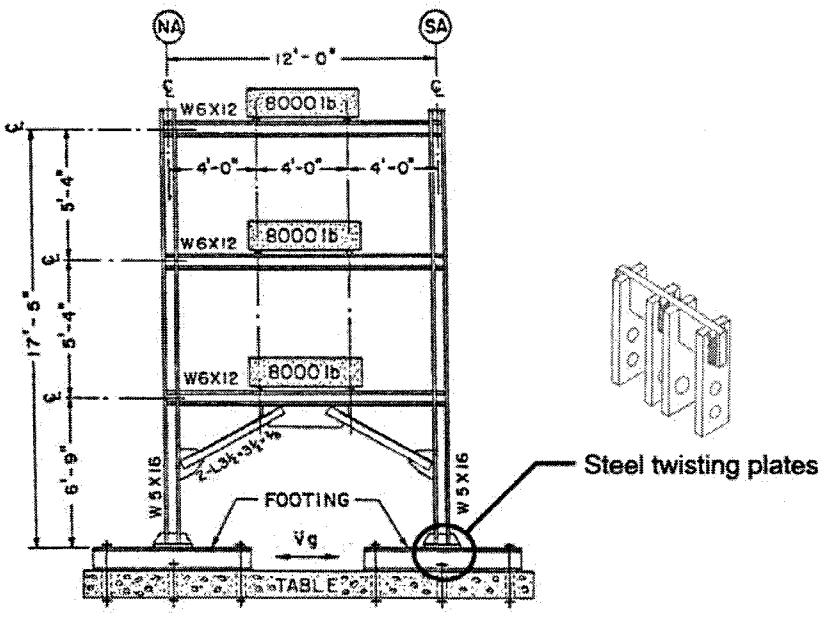

Figure 2.6: Test setup used for the rocking frame with steel twisting plates (adapted from Kelly et al., 1977).

Another type of energy dissipation device, used in combination with the rocking motion, was examined by Griffith et al. (1988a; 1988b) in the late 1980's. They performed earthquake simulator tests on a 1/5 scale seven-storey reinforced concrete building and a 1/4 scale nine-storey braced steel frame to evaluate the feasibility of using base isolation bearings pads to structures subject to column uplift during strong

ground motions. Two types of elastomeric bearing pads were tested, one made of neoprene and the other made of natural rubber with lead plugs. Figure 2.7 illustrates the test setup used for the shake table test program on the 9-storey braced steel frame. The results of the studies demonstrated that the base isolation of medium-rise structures provides significant reductions in base shear and story accelerations as compared to the cases with fixed bases. The tests were not conclusive on which elastomeric bearing was the most efficient. Both bearings proved to be effective isolators, but each demonstrated certain advantages over the other.

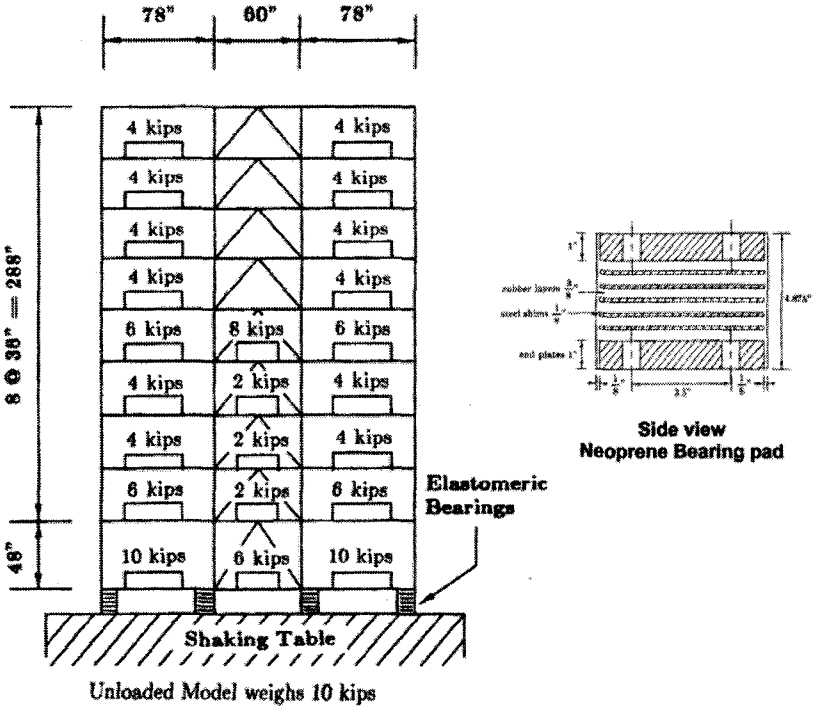

Figure 2.7: Test setup for the steel frame with elastomeric bearings (adapted from Griffith et al., 1988).

In the early 2000's, Midorikawa et al. (2003) completed shake table tests on a 3-storey one by two bay concentrically braced steel frame with a base plate yielding system. The principle of the base plate yielding system is presented in Figure 2.8. The authors categorized their system as one of the simplest forms of a smart structural

system, which is define as structural systems with a certain level of autonomy relying on the embedded functions of sensors, actuators and processors that can automatically adjust structural characteristics in response to the change in external disturbances and environments, towards structural safety and serviceability as well as the elongation of structural life. The objective of the study was to compare the seismic response of the yielding plate system to the response of a fixed based structure. The results of the study demonstrated that the yielding plate system was successful in allowing rocking to occur and reduced effectively the seismic force responses and the response displacement of the building structure, compared to the fixed based specimen. However, the forces in the columns were affected by the impact landing of the base plates on the way down following uplift.

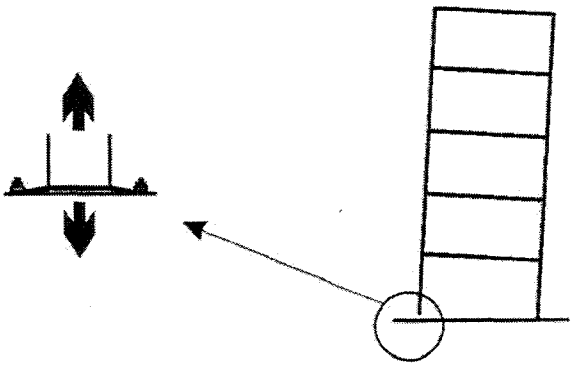

Figure 2.8: Principle of the base plate yielding system (Midorikawa et al., 2003).

2.5. Rocking self-centering structural systems

Rocking self-centering structural systems are systems that are based on the concept of rocking systems with energy dissipating devices, however including the interesting characteristic of returning the structure to its original position following an earthquake excitation, with no residual deformations to the structure. Filiatrault et al. (2004) describe the three key parameters to an optimal earthquake resisting system which are encompassed by a self-centering system:

i. A system that incorporates the nonlinear characteristics of yielding structures in order to limit the induced seismic forces and provide additional damping.
ii. A system that includes self-centering properties allowing the structural system to return to its original position after an earthquake.
iii. A system that reduces or eliminate cumulative damages to the main structural elements.

Self-centering systems have been tested on bridge piers, post-tensioned rocking wall systems (Figure 2.9 (a)), concrete beam/column joints, steel frame connections (Figure 2.9 (b)), cantilever wall systems (Figure 2.9 (c)) and confined masonry wall systems.

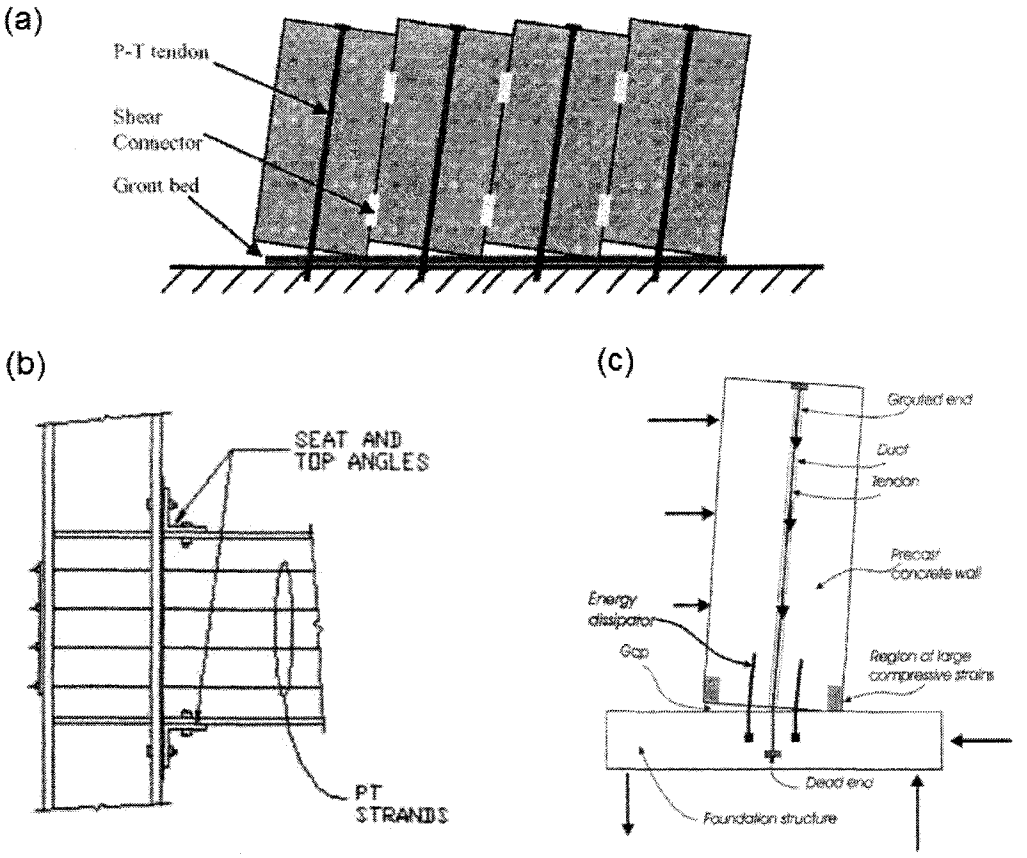

Figure 2.9: (a) Post-tensioned rocking wall system (Filiatrault et al., 2004).
(b) Post-tension steel frame connections (Filiatrault et al., 2004).
(c) Hybrid reinforced concrete cantilever wall system (Filiatrault et al., 2004).

Palermo et al. (2004) performed push-pull and nonlinear time-history analyses on single and multi-degree of freedom bridge systems to compare a proposed hybrid (or controlled rocking) system to a traditional monolithic system. The proposed hybrid system combines the used of post-tensioned (PT) unbounded tendons, which act as the self centering system, and the use of energy dissipaters such as mild steel reinforcement bars. Figure 2.10 (a) illustrates the hysteric flag-shape hysteresis behaviour obtained by the system which is typical to self-centering systems. Figure 2.10 (b) illustrates the comparison analysis performed for the hybrid system. The results of the study

demonstrated the efficiency of the system. The authors qualify it as a promising alternative to traditional earthquake resisting systems. The analyses demonstrated that the rocking motion leads to a significant damage reduction in the pier element. The only repairs needed following an earthquake are to the sacrificial energy dissipating devices. An adequate calibration of the ratio between the self-centering and the energy dissipation characteristics is fundamental to control the maximum displacements at the top of the structure.

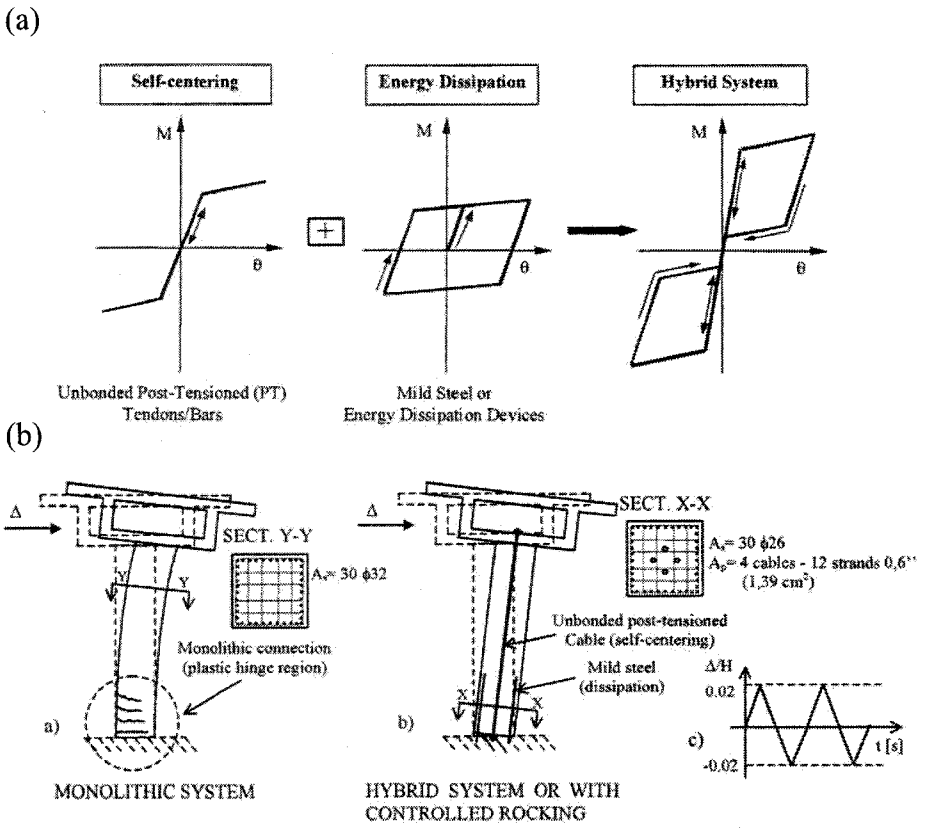

Figure 2.10: (a) Flag-shape hysteresis behaviour of the hybrid system (Palermo et al,, 2004).

(b) Comparison analysis performed for the hybrid system (Palermo et al., 2004)

Toranzo et al. (2004) completed a shake table test program to evaluate the use of a rocking confined masonry wall system with hysteretic energy dissipation provided by mild steel devices designed to yield in flexure during the rocking of the wall. Figure 2.11 illustrates the test setup used and the details of the energy dissipating devices. The masonry wall is confined within the concrete columns and beams of the building. The energy dissipaters are externally attached to the foundation beam. An interesting feature of the dissipation devices is that as well as yielding in flexure during uplift, they provide a lateral support in shear to the base of the wall. This system is proposed for seismically prone countries with limited technology. The results of the test trials demonstrated that the performance of the system was excellent and highly predictable.

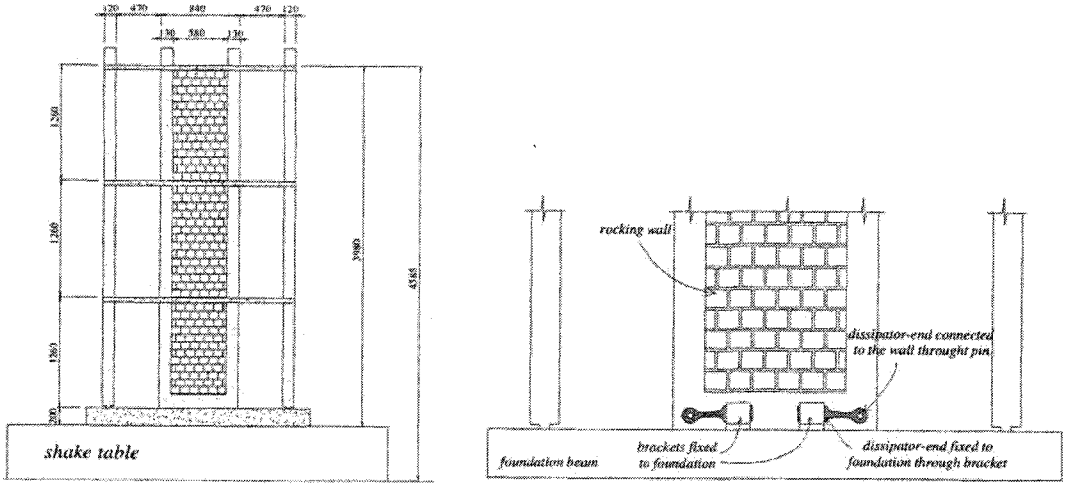

Figure 2.11: Test setup for the rocking confined masonry wall system (Toranzo et al., 2004).

Pollino and Bruno (2007) recently completed shake table tests and numerical analyses to investigate the use of a seismic retrofit technique to allow for controlled rocking of bridge steel truss piers. Displacement based passive energy dissipation devices are implemented at the base of the columns to better control the rocking

response. Figure 2.12 illustrates a retrofitted bridge steel truss pier using the proposed controlled rocking approach. The objective of the study was to evaluate the behaviour of the system through a parametric study of various parameters and establish a capacity based design procedure for the energy dissipaters (buckling-restrained braces, or BRBs). The results of the investigation demonstrated the efficiency of the system in controlling the rocking motion and providing a re-centering capacity while leaving the bridge with no residual displacements following the earthquake. A set of design constraints are also proposed to assist design engineers in achieving target design objectives such as maximum column impact forces, peak bridge lateral deformations, ductility demands on the BRBs and self-centering.

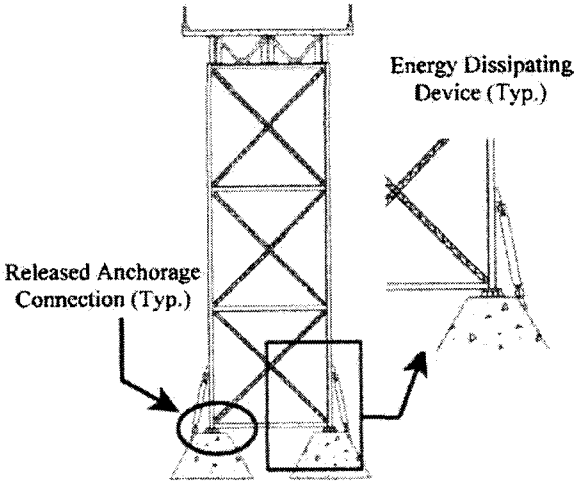

Figure 2.12: Controlled rocking approach used on a retrofitted bridge pier (Pollino et al., 2007).

2.6. Viscously Damped Controlled Seismic Rocking system

The VDCSR system proposed in this thesis fulfills all the requirements of a rocking self-centering structural system. It encompass the benefits of rocking while providing energy dissipation, supplementary damping and lateral displacement control through the use of viscous dampers vertically mounted at the base of the columns. The self-centering of the building is achieved by the dead loads in the columns which applies downward forces onto the dampers and bring the SFRS back to its original position. Considering

that the rocking SFRS is properly designed, no structural damage is expected following a severe ground motion excitation. The system remains completely elastic. It is believed that the seismic dampers will significantly reduce the high intensity impact forces generated when the columns comes into renewed contact with the ground following the rocking motion. More tests are still required to demonstrate this, but a reduction in the impact forces is expected, compared to a case where no dampers are provided. This added benefit would help avoid affecting the stability of the compression members or avoid foundation failure which was a concern to many of the previously stated researchers.

The type of damper proposed for the VDCSR system is a viscous damper. Taylor (1999), from Taylor Devices Inc., one of the world leaders in shock control devices, provides an overview of this type of product. A damper is defined as an element which can be added to a system to provide forces which are resistive to motion, thus a means of energy dissipation. For a viscous damper the output response is described by equation E2.1, where **F** is the resistance force, **C** is the damping constant, **v** is the end to end velocity across the damper and γ is the exponent of non-linearity on the velocity.

$$\mathbf{F} = C \cdot v^{\gamma} \qquad [E2.1]$$

The use of dampers in structural applications is not a new concept. Many buildings have been designed with added-on dampers to provided supplementary damping to the system. As illustrated in Figures 2.3 a) and b), additional damping has beneficial effects on the force and displacement response of the structure. The energy input from a seismic ground motion is not absorbed by the structure itself, but by the supplemental damping elements provided. Many damping devices exist, such as hysteretic dampers, visco-elastic dampers, yielding elements, friction devices, plastic hinges and rubber bearings. However, as described by Taylor, viscous dampers are well suited for building applications, compared to other types of dampers, since the force response of a viscous

damper is dependant only on the velocity. This results in an out of phase response between the deflection and the velocity of the structure, meaning that when the displacement is maximum (i.e. stress is maximum and velocity is zero) the damping forces are zero and when the displacement is zero (i.e. stress is zero and velocity is maximum) the damping forces are maximum. Therefore, viscous dampers are expected not to increase the stresses in the system, unlike other types of dampers. Figure 2.13 illustrates a typical response curve for a viscous damper and a typical schematic drawing of a viscous damper.

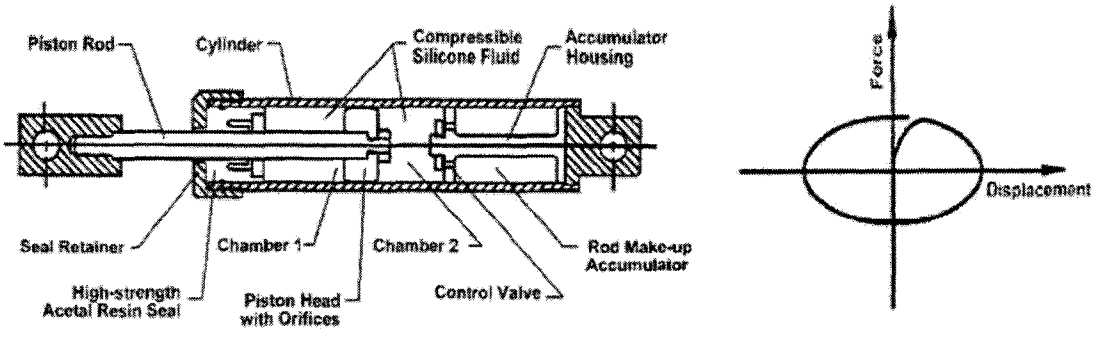

Figure 2.13: Response curve and schematic drawing of a viscous damper (Taylor, 1999).

CHAPTER 3

SIMPLIFIED METHODS FOR PREDICTING ROCKING

3.1. Introduction

Many researchers have demonstrated through experimental and theoretical studies that allowing a structure to rock on it's foundation, when subjected to lateral loads, reduces the forces absorbed by the structure. This is potentially a very useful technique for the seismic design of buildings. However, the rocking motion of a structure is a complex phenomenon. Nonlinear dynamic analyses are highly recommended to represent this motion (Priesley and al., 1996), which may be time consuming. Simplified methods have been proposed to calculate the maximum displacement that a rocking structure would incur when subjected to an earthquake motion. These methods might turn out to be valuable in a preliminary design stage to determine the rocking potential of a structure. The following chapter presents three methods:

i. The substitute substructure technique (Priesley et al., 1996);
ii. The energy balance method (Anderson, 1993);
iii. The equal energy method (Anderson, 1993).

These methods are fully described in this chapter and presented in a step-by-step format. The simplified methods are then used to calculate analytically the displacement of rigid blocks and single-degree-of-freedom (SDOF) structures allowed to rock on their foundations. The results of the simplified methods are compared to finite element analyses using the program SAP2000 (Computers & Structures inc, 2007). Finally, this chapter presents a numerical analysis performed to evaluate the finite element program SAP2000 and its capacity to correctly compute the nonlinear rocking phenomenon. This analysis was require to verify the pertinence of using SAP2000 as a valid reference for

the simplified methods, as well as the pertinence of using this finite element program for the parametric study presented in the following chapter.

3.2. Description of the simplified methods

3.2.1. Substitute substructure technique

The Substitute Substructure (SS) technique, as described by Priestley et al. (1996) is a simple iterative method used to predict the maximum displacement of a rocking system subjected to the lateral forces of an earthquake. This method was developed to provide an estimate on the rocking response of buildings, bridge piers, chimneys and other structures and is an extension of the equations for the rocking motion of rigid blocks proposed by Housner (1963). The SS technique calculates an equivalent damping ratio due to rocking, which is used to compute the displacement, velocity and acceleration response spectrums for the earthquake motion. From these response spectrums, a trial and error procedure is used to determine the response period and the equivalent displacement of the structure. This method approximates the rocking motion of single-degree-of-freedom (SDOF) systems with constant damping, whose period depends on the amplitude of rocking.

Figure 3.1 illustrates the simplified SDOF structure used to demonstrate the step by step procedure of the SS technique, assuming a rigid foundation, thus the point of rotation at the edge of the structure and no tensile force restraining the uplift motion.

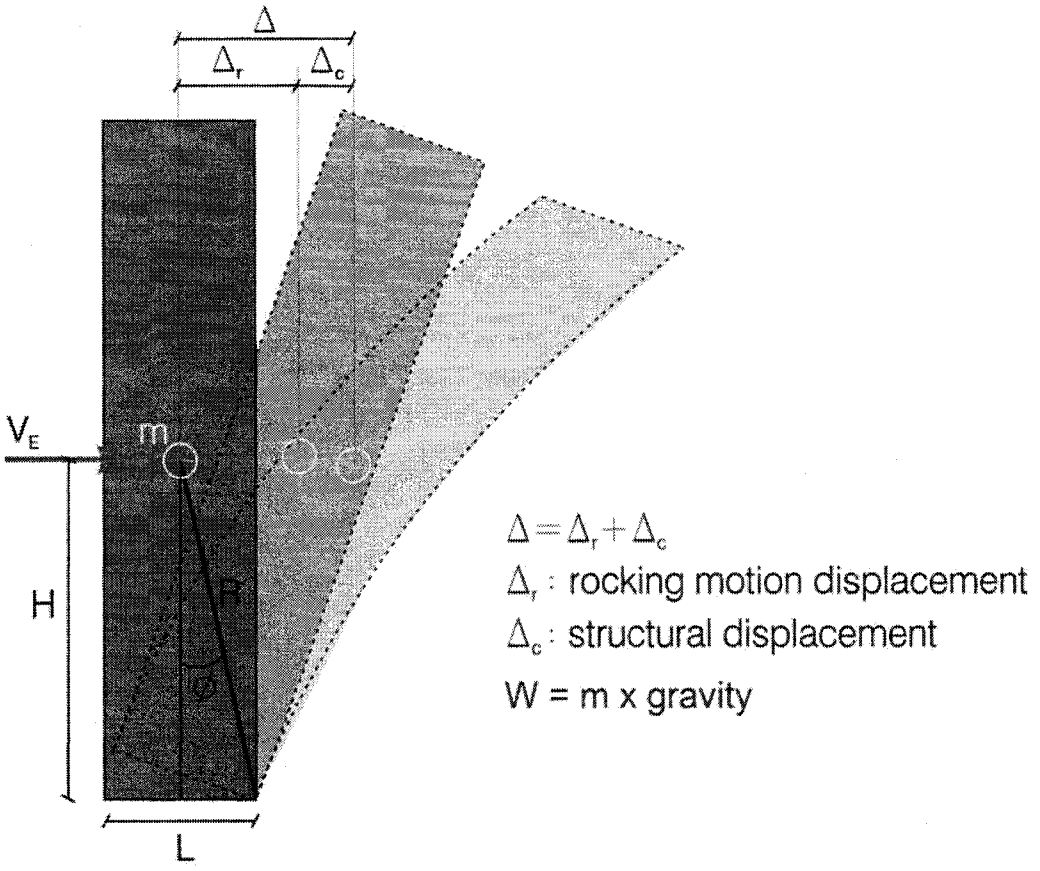

Figure 3.1: Geometric properties of the structure.

The step-by-step procedure to apply this method is as follows:

Step 1 is to verify that the structure will rock under the demand of a given earthquake; this simplified method is useless if the earthquake does not have the energy required to create uplift. To determine this, it is necessary to obtain the acceleration spectrum of the earthquake and determine the maximum acceleration for the period and damping ratio of the structure, assuming it has a fixed base. Equations 3.1 and 3.2 are used to calculate the resisting moment capacity of the structure (M_R) and the acceleration required to obtain this value ($a_{rocking}$)

$$M_R = W \cdot \frac{L}{2} \qquad [3.1]$$

$$a_{rocking} = \frac{M_R}{H \cdot W} = \frac{gL}{2 \cdot H} \qquad [3.2]$$

where W is the weight of the rigid block, L the length of its base, and H the height of the center of mass as illustrated in Figure 3.1. If the maximum acceleration of the earthquake surpasses the value of $a_{rocking}$ then the SS technique may be used to approximate the maximum rocking displacement of the structure.

Step 2 is to calculate an equivalent viscous damping ratio which simulates the effects of energy dissipation due to the rocking motion. The equivalent damping ratio (ξ_e) can be expressed by

$$\xi_e = 48 \cdot (1 - r) \qquad [3.3]$$

where r is the coefficient of restitution, representing the ratio between the kinetic energy before and after impact during rocking motion. It can be calculated using the equation

$$r = \left[1 - \frac{m \cdot R^2 \cdot (1 - \cos 2\phi)}{I_0}\right]^2 \qquad [3.4]$$

where m is the total mass of the structure, R the hypotenuse between the center of mass and the turning point, $\emptyset$ the angle between a vertical line and the line connecting the centroid and the center of rotation, and I_0 the mass moment of inertia of the block about the point of rotation.

Δ is the total displacement of the centre of mass, which is an addition of the displacement due to rocking (Δ_r) and the displacement of the structure (Δ_c). Δ_c is a function of the rigidity of the structure and is calculated using the fixed base period of

the structure and the displacement response spectrum of the ground motion. V_E is the equivalent shear force required to obtain the displacement Δ.

Step 3 is the beginning of the iterative process. An initial value for the maximum displacement (Δ_0) is randomly selected, which leads to the computation of the corresponding lateral force V_{E1} and the corresponding period T_1 using equations 3.5 to 3.7. Δr is calculated by subtracting Δ_c to Δ.

$$V_E = \frac{W \cdot L/2 - W \cdot \Delta}{H + (\Delta_r \cdot L)/(2 \cdot H)} \quad [3.5]$$

$$k = \frac{V_E}{\Delta} \quad [3.6]$$

$$T = 2\pi\sqrt{\frac{W}{g \cdot k}} \quad [3.7]$$

Using the calculated period (T_1) and the equivalent damping ratio (ξ_c) calculated in step 2, the displacement of the structure (Δ_1) is found from the displacement response spectrum. The displacement Δ_1 is then used in equations 3.5 to 3.7 to determine V_{E2} and the corresponding period T_2 to obtain the displacement Δ_2. The iteration process continues until convergence is found between Δ_n and Δ_{n-1} obtained at iterations *n* and *n*-1, respectively.

3.2.2. Energy Balance Method

The energy balance method, as described by Anderson (1993), is a simplified method which uses the kinetic energy of an earthquake to approximate the maximum displacement of a SDOF structure. The kinetic energy of an earthquake transferred to a single-degree-of-freedom structure is equated to the potential energy increase of the mass moving upwards as the structure rotates. Using this principle, the lateral displacement is calculated using the following step-by-step procedure.

Step 1 is to calculate the kinetic energy *KE* by using either the spectral velocity (S_v) of the earthquake according to Equation 3.8, or the spectral acceleration (S_a) according to Equation 3.9

$$KE = \frac{1}{2}\frac{W}{g}(S_v)^2 \qquad [3.8]$$

$$KE = \frac{1}{2}\frac{W}{g}\frac{T^2}{(2\pi)^2}(S_a)^2 \qquad [3.9]$$

where W is the lateral weight of the structure, g the acceleration of gravity and T the fundamental period of the structure. Figure 3.2 illustrates the geometric properties of the structure used for the energy balance method.

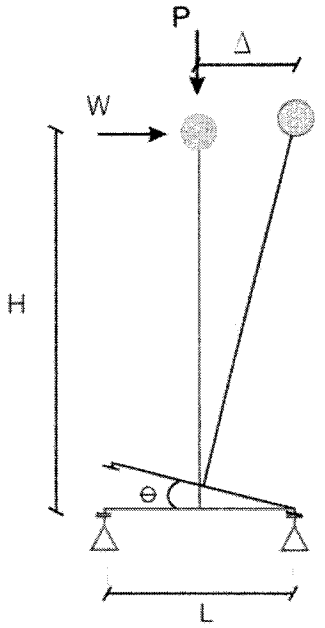

Figure 3.2: Geometric properties of the structure used to apply the energy balance method.

Step 2 is to set the kinetic energy calculated in step 1 equal to the potential energy increase of the structure as it rotates about its end support and to solve for the angle θ defining the rotation of the structure. The potential energy is expressed by Equation 3.10

$$PE = P \cdot \frac{L}{2} \cdot \theta \qquad [3.10]$$

where P is the vertical weight of the structure and L the distance between the supports. The rotation angle θ can be obtained using either Equation 3.11 which uses the spectral velocity of the earthquake or Equation 3.12 which uses the spectral acceleration of the earthquake.

$$\theta = \frac{W}{g \cdot P} \cdot \frac{S_v^{\,2}}{L} \qquad [3.11]$$

$$\theta = \frac{W}{g \cdot P} \cdot \frac{T^2 S_a^{\,2}}{(2\pi)^2 \cdot L} \qquad [3.12]$$

Step 3 is to calculate the lateral displacement Δ of the structure using the angle of rotation θ calculated in step 2. This lateral displacement can be approximated using equation 3.13

$$\Delta \approx H \cdot \tan\theta \qquad [3.13]$$

3.2.3. Equal Energy Method

The equal energy method is based on the concept that the elastic lateral energy and the inelastic lateral energy of a building are equal for buildings with short periods. This equivalence originates from the principal that the area under the lateral load deflection diagram of an elastic and an inelastic system are equal. The application of this concept to rocking systems is proposed by Anderson (1993). The maximum inelastic rocking displacement caused by an earthquake motion is obtained from the elastic displacement and the lateral load deflection curve of a building as described in the following procedure.

Step 1 is to determine the fundamental period (T) and the stiffness (k) of the system using the geometrical and physical properties of the structure.

Step 2 is to determine the maximum elastic displacement (Δ_e) of the structure using the spectral displacement of the earthquake motion assuming fixed base conditions.

Step 3 is to determine the elastic lateral force (V_e) using the stiffness and the elastic displacement of the structure. The resulting elastic lateral energy (E_e) is equal to the area below the load displacement curve as illustrated in Figure 3.3.

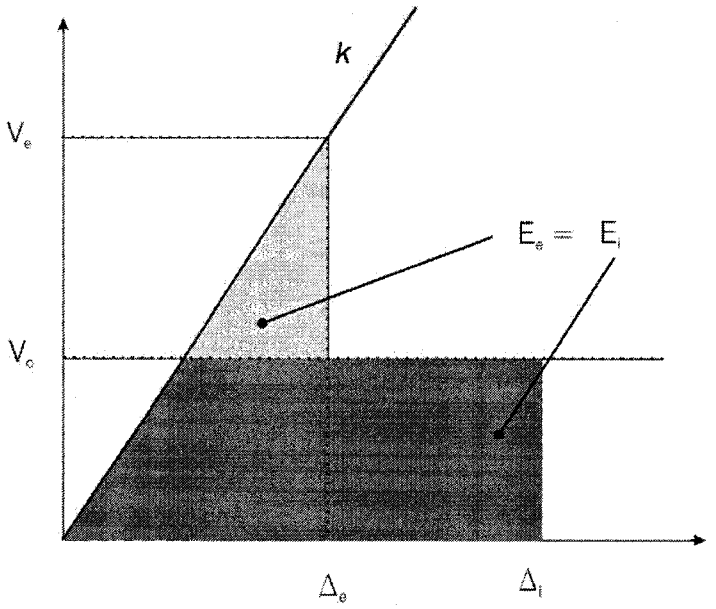

Figure 3.3: Lateral load deflection curve used for the Equal Energy method

Step 4 is to calculate the lateral load required to cause the structure to overturn (V_o). This value is calculated using Equation 3.14

$$V_o = \frac{P \cdot L/2}{H} \qquad [3.14]$$

where P is the vertical weight of the structure, H is the height of the center of mass and L is the distance between the supports.

Step 5 is to solve for the inelastic rocking displacement (Δ_i) by equating the inelastic energy (E_i) to the elastic energy (E_e) and using the area under the curve where the upper bound lateral load value is set to the overturning load (V_o).

3.3. Evaluation of the simplified methods

Two evaluations of the simplified methods are completed to determine their effectiveness to predict the maximum rocking displacement of a structure submitted to various lateral load inputs. The first is performed using rigid blocks and the second using a single degree of freedom structures (SDOF). The results of the simplified methods are compared to those from finite element analyses, which are assumed to represent more accurately the actual rocking response of the structures.

3.3.1. Rigid block structures

A rigid block structure is a system that rotates uniformly without any deformation of the core (column). It has a rigid body motion with zero internal strain. The angle of rotation at the bottom of the structure is identical to the rotation at the top of the structure. The uplift displacement of the system is linearly related to the lateral displacement. The rigid block structures used for the evaluation of the simplified methods are presented in Figure 3.4.

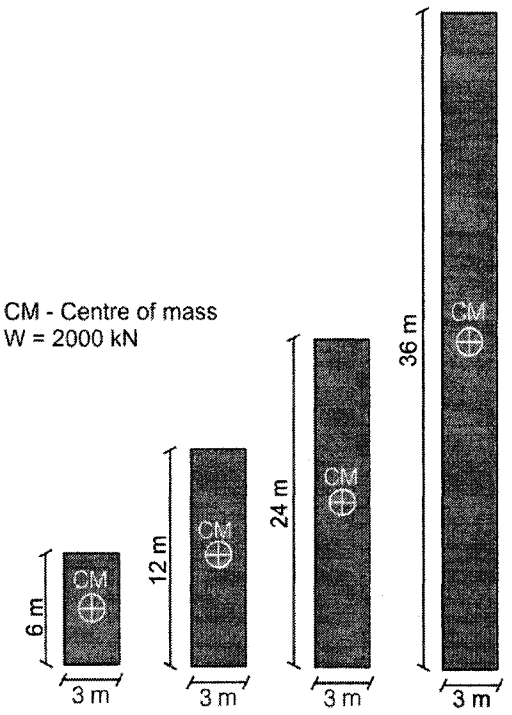

Figure 3.4: Rigid blocks used for the evaluation of the simplified methods.

The selected structures had varying slenderness ratios, while the remaining parameters, width and weight were left unchanged. The support width L was constant at 3 m, while the height H of the structures was set to 6 m, 12 m, 24 m and 36 m. The structures were subjected to four different ground motions. Two ground motions were real earthquakes: Imperial Valley Earthquake (El Centro, 1940) and Kern Country Earthquake (Taft, 1952). One ground motion was a simulated earthquake for eastern Canada (M701001, Magnitude 7 at a distance of 100 km from the origin) and the final ground motion was a simple sine wave (T = 0.6 sec, 20 cycles). The four time histories were calibrated to have a maximum acceleration of 0.2 m/s^2 to insure that overturning did not occur. The time histories and resulting spectrums are presented in Appendix A.

As a basis of comparison, the simplified methods were compared to a simple 2D model in the finite element program SAP2000 (Computer & Structures inc., 2007). The blocks are modeled by a mass connected to a rigid column and a rigid foundation mat,

connected to supports that allow uplift. The column and foundation mat are massless elements. The entire mass of the block is lumped at the center of mass which is located at half the height of the block. Figure 3.5 illustrates the properties of the finite element models.

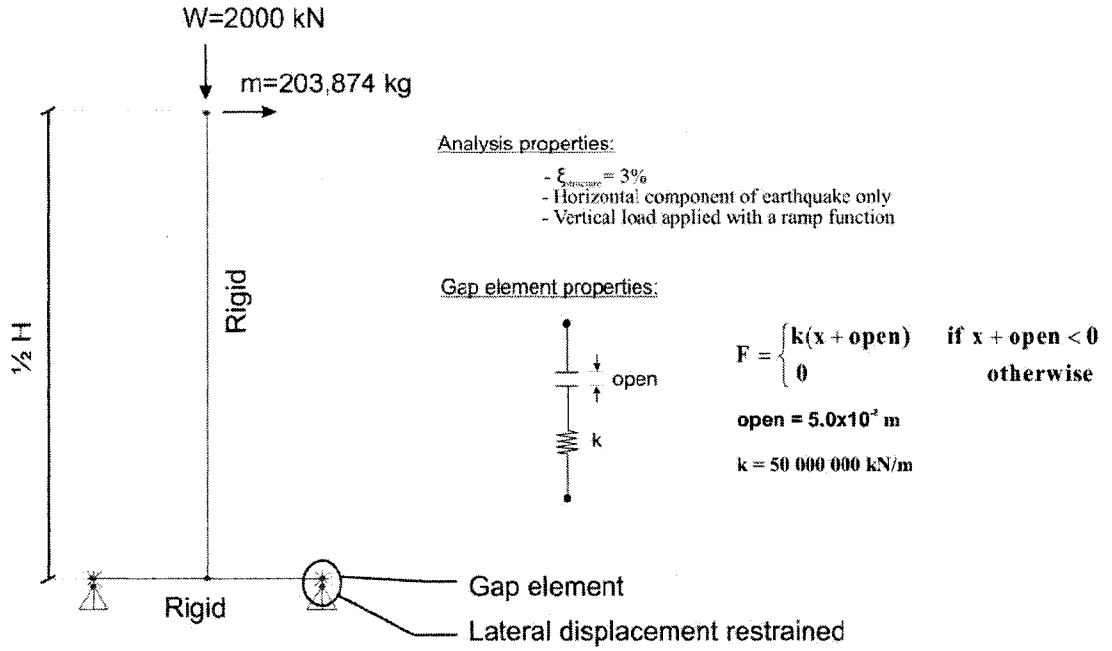

Figure 3.5: Properties of the finite element models used to analyse the rigid blocks (Computer & Structures inc., 2007).

As illustrated in Figure 3.5, the support conditions of the blocks are obtained using gap elements. These nonlinear elements are composed of contact plates in series with a spring (Computer & Structures inc., 2007). The contact plates allow a transfer of downward forces in compression, but have no resistance in tension, and are thus open when subjected to upward forces. The spring is used to specify the stiffness of the gap element. The stiffness of the spring had to be set to a value which did not alter to significantly the fundamental period of the structure, without being completely rigid to avoid numerical problems. Therefore the stiffness of the vertical support springs was

chosen so that the first mode period of the block was not changed by more that 10% from the period of the same block having fixed supports, as recommended by Anderson (1996). The 'open' value used for the gap elements was close to zero. Zero was not used to avoid computational errors in the finite element model.

The calculations performed for each of the simplified method are included in Appendix B. The following assumptions were made. The damping ratio of the structures was assumed to be 3%, which is a typical value for buildings and the SS was applied technique considering $I_0 = mR^2$ and $\Delta_c = 0$ for the rigid block.

Table 1.1 presents a comparison between the results from the three simplified methods and the finite element analysis (in grey). It is observed that very little to no rocking occurred for the 6 m and 12 m blocks. The intensity of the lateral input was not great enough to create overturning. The substitute substructure (SS) technique and the equal energy method were both efficient in predicting this response. Rocking did occur for the 24 m and 36 m blocks. All three methods were able to predict that rocking would occur. Compared to the finite element model, the energy balance method was the most precise for the El Centro and Taft lateral inputs, while the SS technique was the most accurate for the M701001 and sin inputs. Highlighted in yellow is the method that was the most similar to the finite element analysis.

Table 3.1: Results of the simplified methods for the rigid blocks.

	H = 6m				H = 12m				H = 24m				H = 36m			
	Δ_{max} (mm)				Δ_{max} (mm)				Δ_{max} (mm)				Δ_{max} (mm)			
Earthquake	SS Technique	Energy Balance Method	Equal Energy Method	Finite Element Analysis	SS Technique	Energy Balance Method	Equal Energy Method	Finite Element Analysis	SS Technique	Energy Balance Method	Equal Energy Method	Finite Element Analysis	SS Technique	Energy Balance Method	Equal Energy Method	Finite Element Analysis
El Centro	0	12	0	0	3	24	1	1	53	47	17	42	161	71	80	53
Taft	0	11	0	0	1	21	0	1	84	42	20	37	81	64	215	38
M701001	0	3	0	0	1	5	3	2	23	10	16	20	35	15	55	23
Sin Wave	0	20	0	0	0	39	0	0	67	78	9	54	79	118	85	47

3.3.2. SDOF structures

A single degree of freedom system is the simplest way to reproduce the behaviour of many structural engineering problems. It can be used to idealise the response of mechanical systems and structures subjected to dynamic loads. The equivalent SDOF model of a building structure is represented by a single mass with a vertical frame element having a rigidity equivalent to the rigidity of the building. For the purpose of this analysis, the SDOF structures also have a rigid foundation mat to add the dimension of width in order to obtain the points of rotation. Figure 3.6 illustrates the SDOF structures used for the evaluation of the simplified methods.

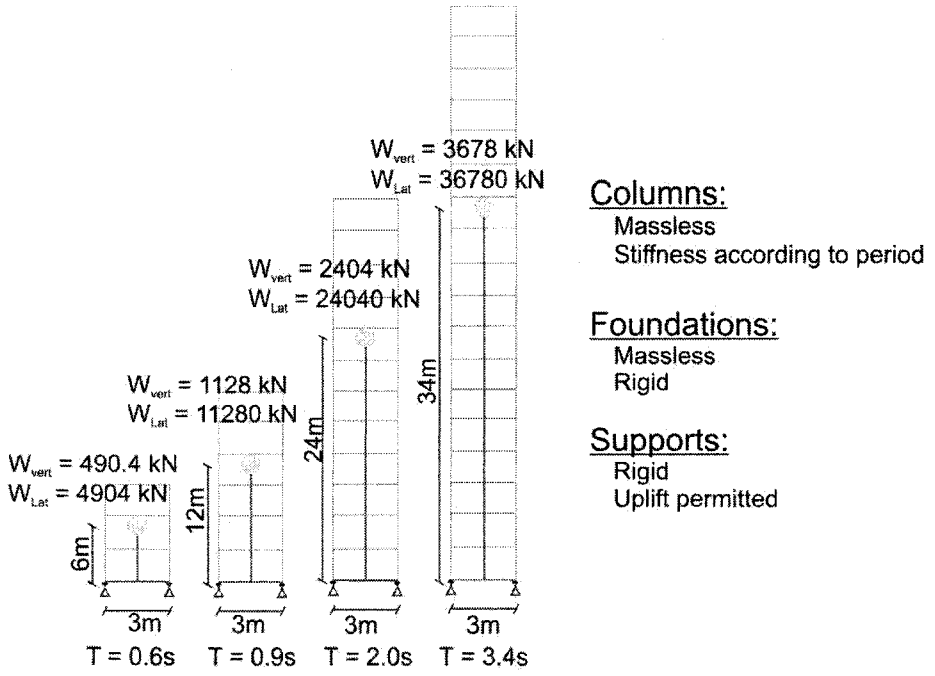

Figure 3.6: Structures used for the single degree of freedom analyses.

The simple SDOF structures were selected to represent a braced frame from a 3-, 6-, 12- and 18-storey building as shown in Figure 3.6. For the purpose of this analysis, the center of mass was lumped at 2/3 the height of each frame. The lateral seismic weight was assumed to be 10 times the vertical weight. The weight and period of each frame

were selected to be representative of actual buildings. The structures were subjected to the same ground motions as the trials on the rigid blocks.

For basis of comparison, the simplified methods were compared to a simple 2D finite element model in SAP2000. They were modeled by a mass connected to a column and a rigid foundation mat on supports that allow uplift. Gap elements were used for the supports. As for the rigid blocks, the stiffness of the vertical support springs was chosen so that the first mode period was not altered by more than 10% from the period of the structure assuming fixed supports (Anderson, 2003). The dimensions of the columns were adjusted to obtain the required periods. The column and foundation mat are massless elements. Figure 3.7 illustrates the properties of the finite element models used.

		Height H (m)	Period T (s)	Vertical Weight W (kN)	Lateral Mass M (kg)	Column Width X (m)	Column Rigidity K (kN/m)
Frame	3 Storeys	6	0.6	490.4	500000	0.61	540831.1
	6 Storeys	12	0.9	1126.0	1150000	1.25	56049.6
	12 Storeys	28	2.0	2403.6	2045000	1.88	24181.0
	18 Storeys	36	3.4	3678.0	3750000	2.29	12806.6

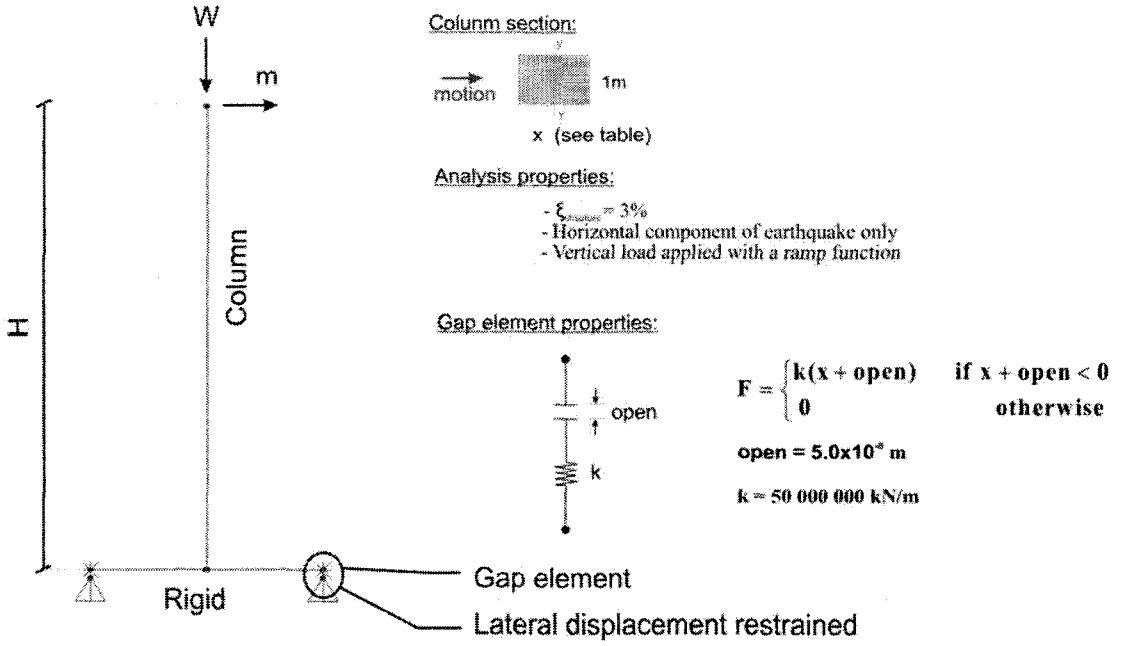

Figure 3.7: Properties of the finite element models used for the SDOF trials.

The calculations performed for each of the simplified methods are included in Appendix B. The structural damping ratio was assumed to be 3%, which is a typical value for steel buildings. The following assumptions were made for the SS technique: $I_0 = mR^2$ and $\Delta_c = 0$ assuming that $\Delta_c << \Delta_r$.

Table 2.2 compares results obtained using the three simplified methods and the finite element analyses (in grey). It is observed that rocking occurred for all four structures. All three of the simplified methods predicted this response. The precision of the methods compared to the finite element analysis varies from one structure to the other and from

one lateral input to the other. The SS technique was the most often similar to the finite element model. The similarity between the two is excellent in some cases, especially for the 3- and 6-storey storey frames. Among the two energy-based methods, the energy balance method was the most similar to the finite element analyses for the 3- and 6-storey frames, while the equal energy method was the most similar for the 12- and 18-storey frames. Highlighted in yellow is the method that was the most similar to the finite element analysis.

Table 3.2: Results of the simplified methods for the SDOF structures.

	2 storey frame (T=0.6s)				4 storey frame (T=0.9s)				8 storey frame (T=2.0s)				12 storey frame (T=3.4s)			
	Δ_{max} (mm)				Δ_{max} (mm)				Δ_{max} (mm)				Δ_{max} (mm)			
Earthquake	SS Technique	Energy Balance Method	Equal Energy Method	Finite Element Analysis	SS Technique	Energy Balance Method	Equal Energy Method	Finite Element Analysis	SS Technique	Energy Balance Method	Equal Energy Method	Finite Element Analysis	SS Technique	Energy Balance Method	Equal Energy Method	Finite Element Analysis
El Centro	56	118	43	51	103	237	46	104	138	474	115	111	160	711	92	111
Taft	48	106	24	85	81	212	55	77	120	424	99	98	135	636	68	268
M701001	11	25	13	27	32	49	15	41	57	99	24	77	59	148	32	56
Sin Wave	64	196	75	60	84	392	101	82	90	784	148	256	91	1176	134	372

Evaluations of the simplified methods were completed using rigid block structures and single-degree-of-freedom (SDOF) structures. The evaluations demonstrate that none of the simplified methods was predominantly correct. The results were dependant on the structure and the type of lateral ground motion. The results of the methods were compared to finite element analysis models, which is the most effective way to predict the actual behaviour of structures without physically testing them. However, the output of a finite element model is only as good as the input. The right assumptions and parameters must be used and a good understanding of the program is required of the user to obtain valuable results. It is a mistake to have blind faith in the results of a numerical program. Validations must always be performed. The following section presents an evaluation completed to validate the modeling parameters and assumptions used in SAP2000 to predict the rocking motion.

3.4. Evaluation of the finite element modeling of a rocking structure

A trial was performed to validate the effectiveness of using finite element models in SAP2000 to simulate the rocking motion of a structure on its foundation. This validation is based on nonlinear dimensionless analytical equations for the rocking motion of single-degree-of-freedom (SDOF) structures developed by Chopra and Yim (1983). The authors presented dimensionless curves illustrating various rocking responses. These curves were used to evaluate the accuracy of two finite element models of SDOF rocking structures created in SAP2000.

First, a description of the Chopra and Yim method is presented, followed by the results of the numerical analysis performed by Chopra and Yim. This section also presents the results of the finite element models and compares them to the results of the numerical analysis performed by Chopra and Yim (1983).

3.4.1. Chopra and Yim method

The Chopra and Yim method reproduces numerically the nonlinear motion of rocking by dividing this complicated problem into a series of distinct simple to solve problems. The method takes into account the support conditions of the SDOF system during the rocking motion, creating three linear equations. The three conditions are defined as:

i. Contact at both ends;
ii. Left edge uplift;
iii. Right edge uplift.

The structural system considered is an idealized representation of a single story structure with a mass m, a lateral stiffness k and a lateral damping coefficient c. The structure is supported by a massless column connected to a foundation mat of mass m_o resting on two spring-damper elements as illustrated in Figure 3.8.

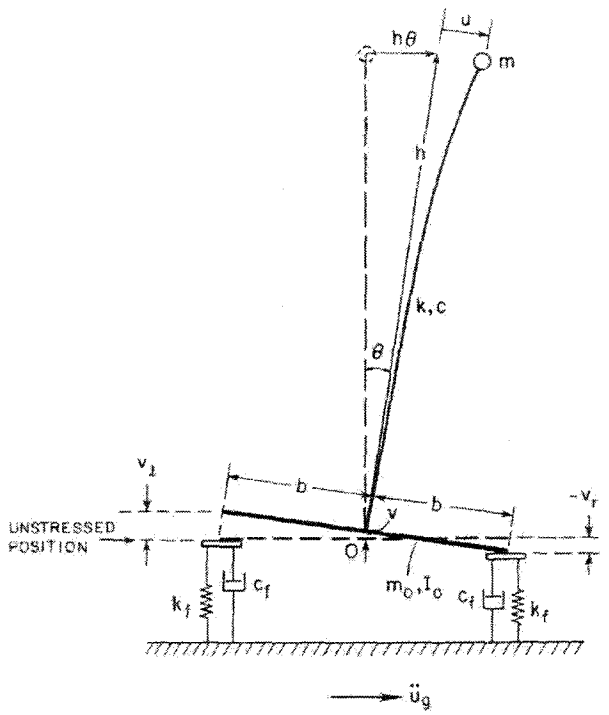

Figure 3.8: Model definition (Chopra and Yim, 1983).

The support element illustrated in Figure 3.8 is a spring and a damper combined in parallel to represent the soil conditions. This element provides a reaction force in the downward direction, but no reaction force in the upward direction. The structure is thus free to uplift. When lateral forces are applied to a structural system which is allowed to uplift, the maximum base shear that can be developed under static conditions is limited to the force that produces uplift. Therefore, maximum base shear V_c can be computed using Equation 3.15. The resulting structural displacement u_c caused by this base shear is calculated using Equation 3.16 and the incipient uplift rotation θ_c of the foundation mat by Equation 3.17.

$$V_c = (m + m_o) g \frac{b}{h} \qquad [3.15]$$

$$u_c = \frac{(m+m_o)g}{k}\frac{b}{h} \qquad [3.16]$$

$$\theta c = \frac{(m+m_o)g}{2k_f b} \qquad [3.17]$$

According to Chopra and Yim (1983), the rocking response of any SDOF system depends on the six following dimensionless parameters:

i) $\omega = \sqrt{k/m}$, the natural frequency of the structure assuming bounded supports;

ii) $\xi = c/2m\omega$, the damping ratio of the structure;

iii) $\beta = \omega_v / \omega$, where $\omega_v = \sqrt{2k_f/(m+m_o)}$ is the vertical vibration frequency of the system with its foundation bounded to the supports;

iv) $\xi_v = 2c_f / 2(m+m_o)\omega_v$, the damping ratio in vertical vibration of the system with its foundation bounded to the supports;

v) $\alpha = h/b$, the slenderness ratio parameter;

vi) $\gamma = m_o / m$, ratio between the mass of the foundation and the mass of the superstructure.

3.4.2. Analytical analysis performed by Chopra and Yim

Chopra and Yim (1983) used the equation of motion they developed to study, through numerical analyses, the response of SDOF structures subjected to free vibration and to seismic loads. Two support conditions were studied. The first was with a bounded contact, where the foundation mat was fixed to the supports preventing uplift, thus the springs were active in the upward direction. The second support condition was with an unbounded contact, where uplift was permitted, thus the springs had no stiffness in the upward direction.

For the free vibration analysis, an initial velocity was applied to the structure. A normalized value for the initial velocity was defined using Equation 3.18, where $\dot{x}_c(0)$

is the initial velocity that creates the maximum displacement. This velocity is calculated using Equation 3.19.

$$\bar{\dot{x}}(0) = \dot{x}(0) / \dot{x}_c(0) \qquad [3.18]$$

$$\dot{x}_c(0) = \frac{\sqrt{\alpha^2 + \beta^2}}{\alpha\beta} \frac{g}{\omega} \qquad [3.19]$$

Two cases where studied, one without damping and the other with damping; the results are presented in Figures 3.9 and 3.10. The parameters used for both case studies where $\alpha = 10$, $\beta = 8$, $\gamma = 0$ and $\bar{\dot{x}} = 2$. For the example with damping, equivalent damping ratios used where $\xi = 0.05$ and $\xi_v = 0.4$, whereas these values were set to zero for the example without damping.

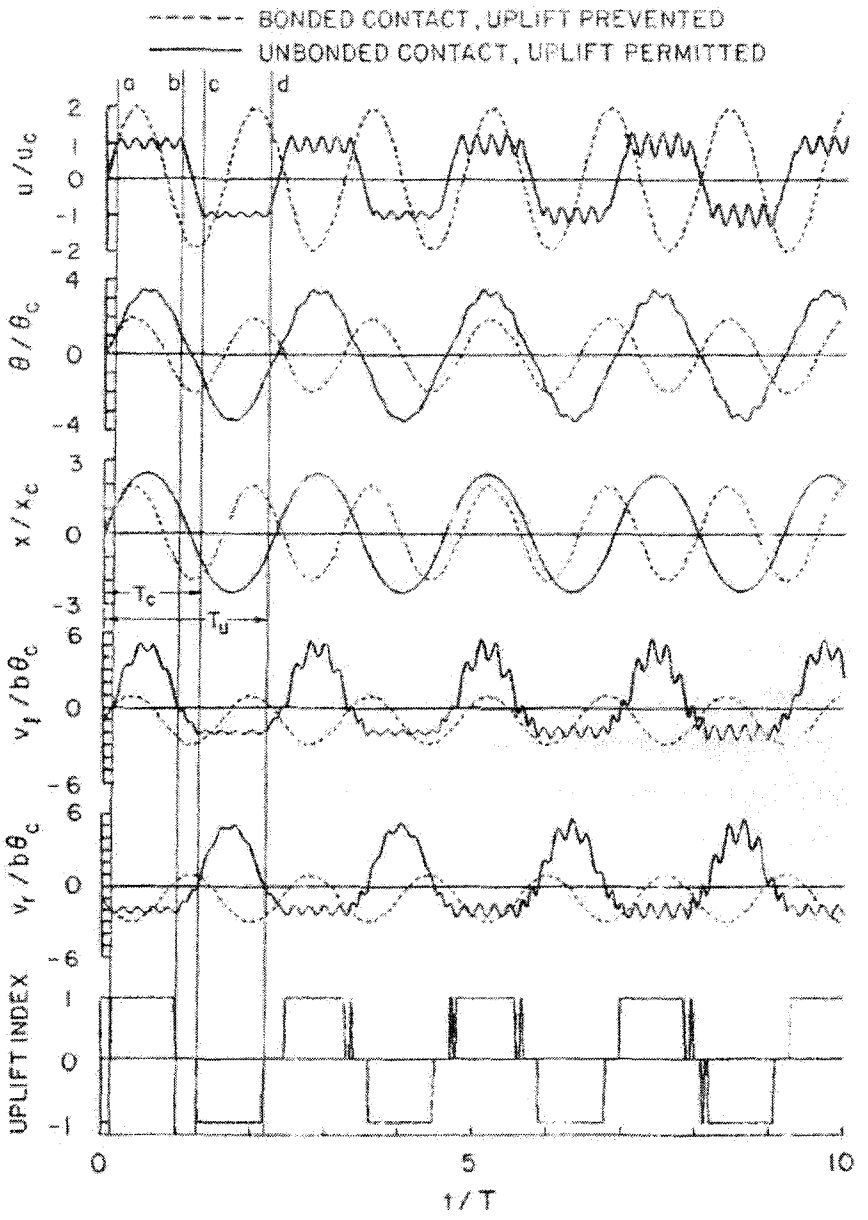

Figure 3.9: Analytical results – Free vibration response without damping (Chopra and Yim, 1983).

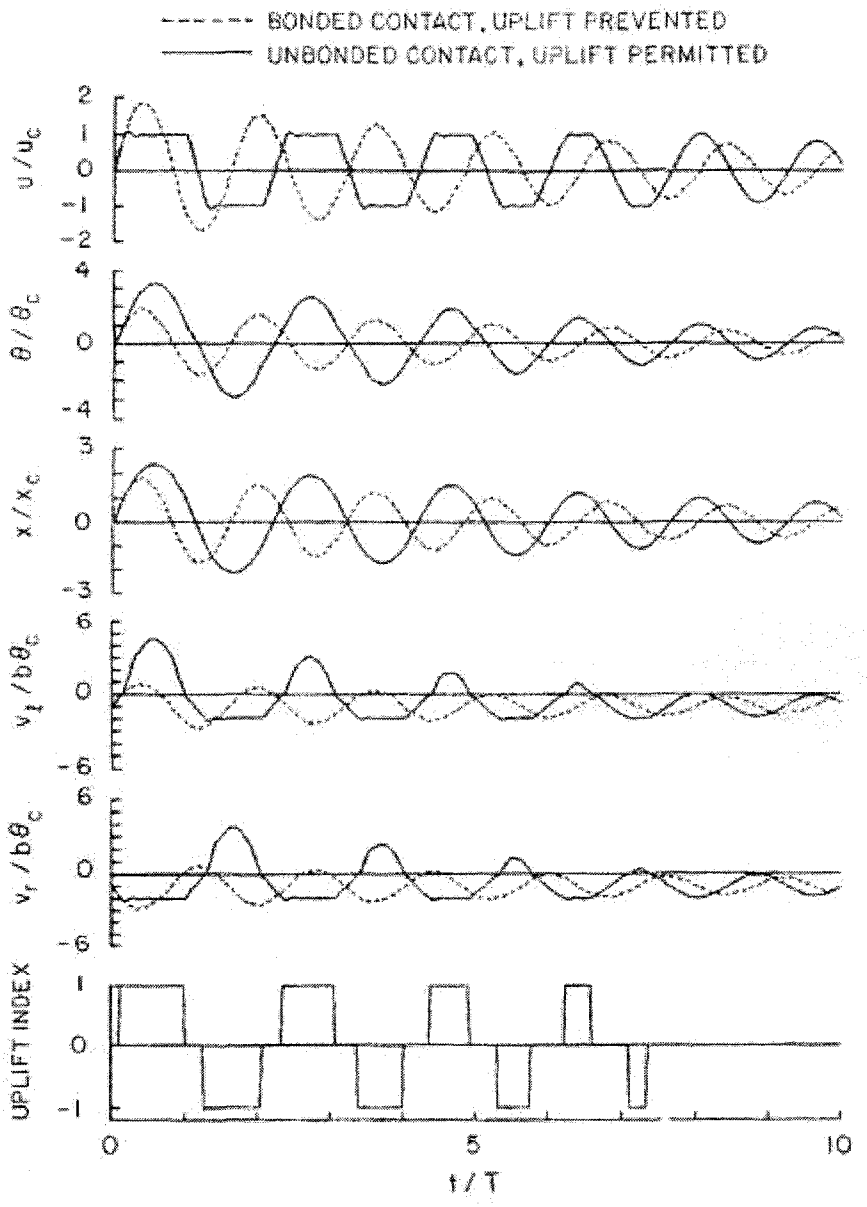

Figure 3.10: Analytical results – Free vibration response with damping (Chopra and Yim, 1983).

For the earthquake response analysis, one case was studied. The north-south component of the 1940 El Centro ground motion was used with a SDOF structure having the following properties: $\alpha = 10$, $\beta = 8$, $\gamma = 0$, $T = 1.0s$, $\xi = 0.05$ and $\xi_v = 0.4$. The results are presented in Figure 3.11.

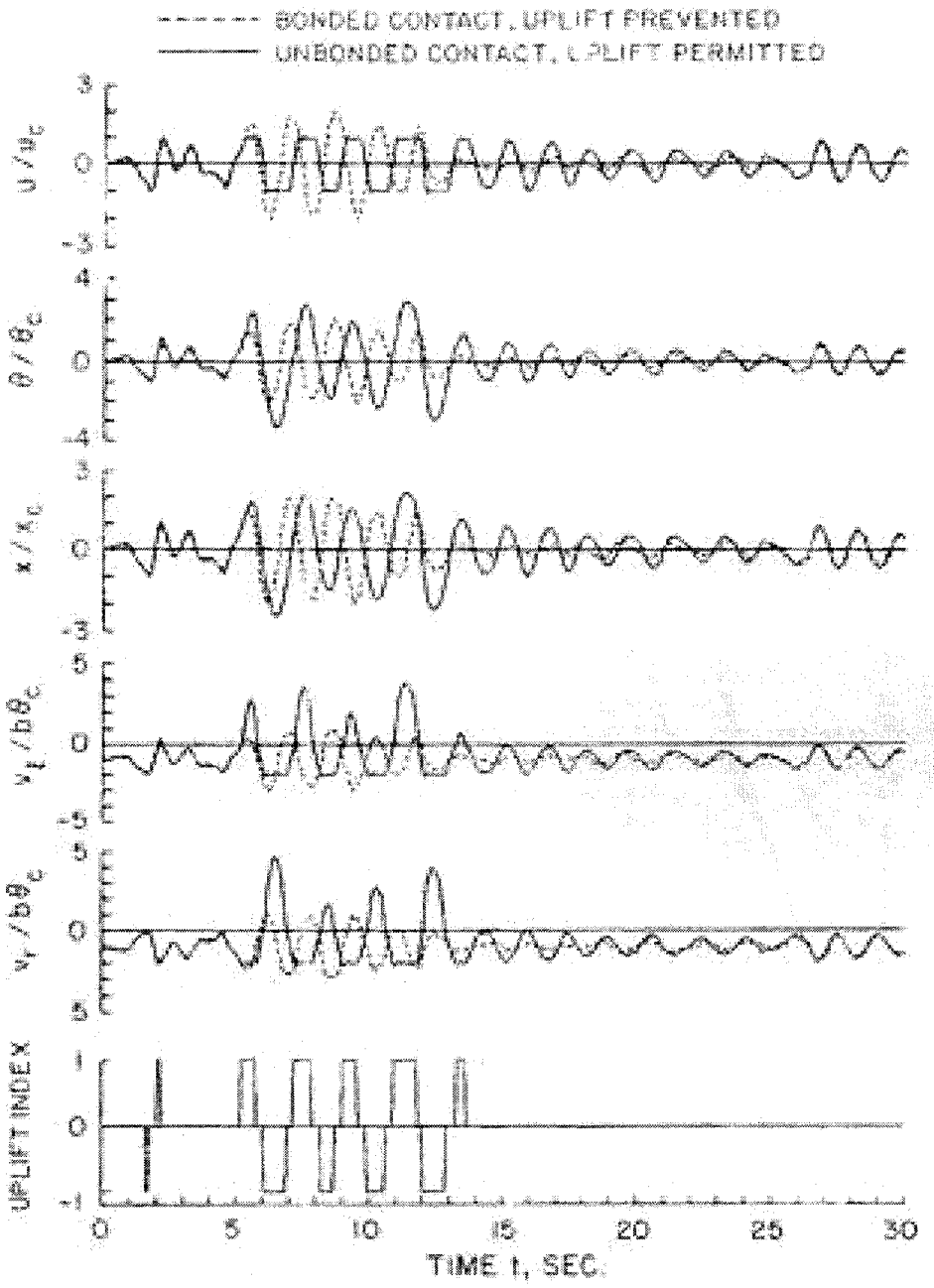

Figure 3.11: Analytical results – Earthquake response (Chopra and Yim, 1983).

Chopra and Yim were able to develop a numerical method using dimensionless parameters to describe the rocking motion of SDOF structures. Using this method, they demonstrated the key components involved in the rocking motion. They also demonstrated that the base shear forces are reduced for short period structures allowed to uplift and that slender structures have a higher tendency to rock thus resulting in greater reductions in shear forces.

3.4.3. Finite element analysis using SAP2000

To validate the use of SAP2000 models to reproduce the rocking motion, a finite element analysis was performed using the same conditions and parameters used in the analytical analysis performed by Chopra and Yim (1983), presented in the previous section. The response of a SDOF structure subjected to free vibration and to seismic loads was evaluated.

For the free vibration analysis, two cases were studied: one with damping and the other without damping. For the earthquake analysis, the 1940 El Centro ground motion was used. The dimensions and properties of the structure were selected to satisfy the same dimensionless parameters as the numerical analysis, thus $\alpha = 10$, $\beta = 8$, $\gamma = 0$ and $T = 1.0$ s. The damping ratios ξ and ξ_v were set to 0.05 and 0.4 respectively for the case with damping, and to zero for the case without damping. The properties used for the finite element model are illustrated in Figure 3.12.

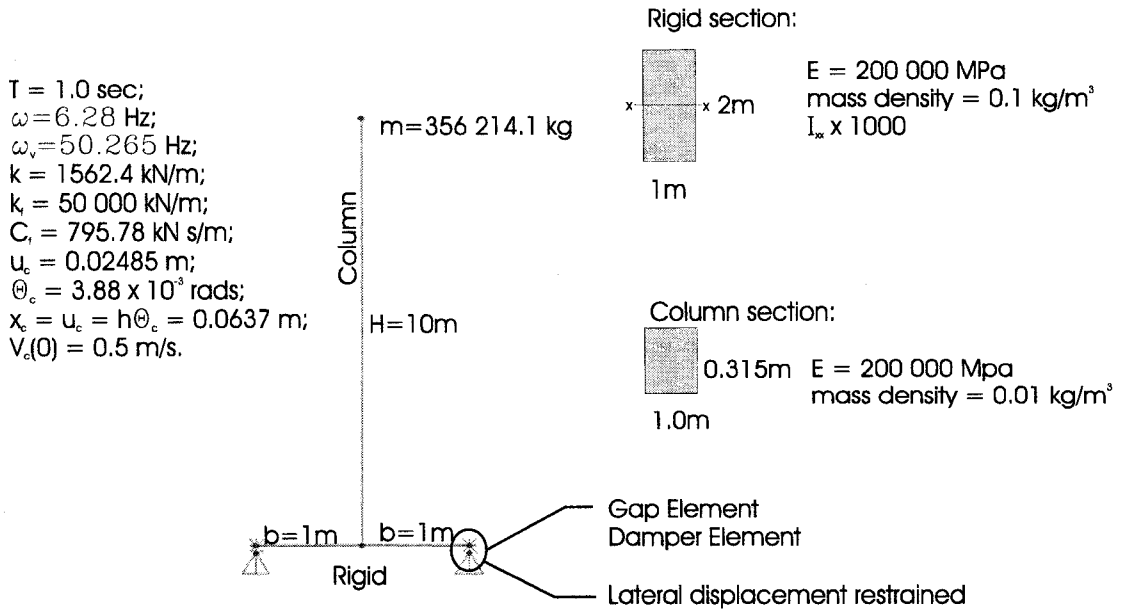

Figure 3.12: Finite element model of the structure with a period T = 1.0 s.

The results of the free vibration analyses are presented in Figures 3.13 and 3.14, and those of the earthquake analyses are presented in Figure 3.15.

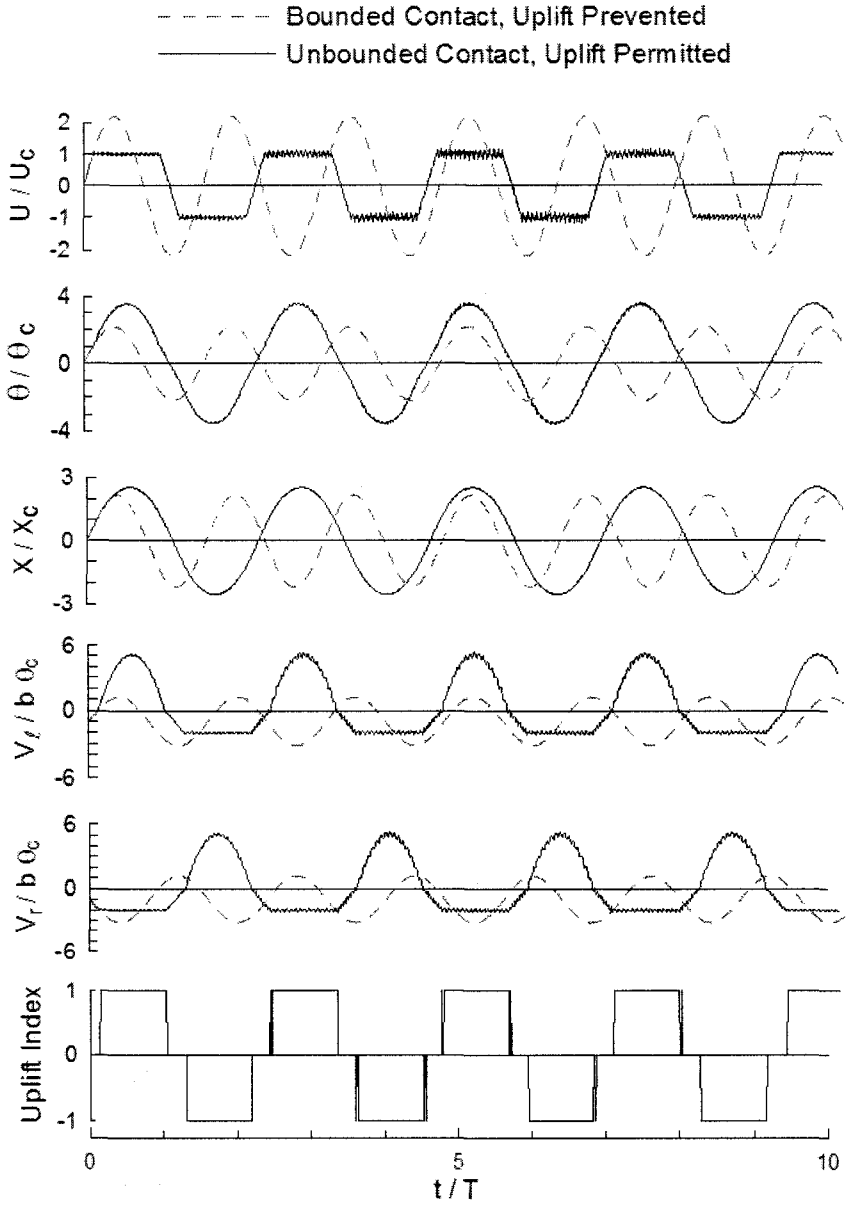

Figure 3.13: Finite element results – Free vibration response without damping.

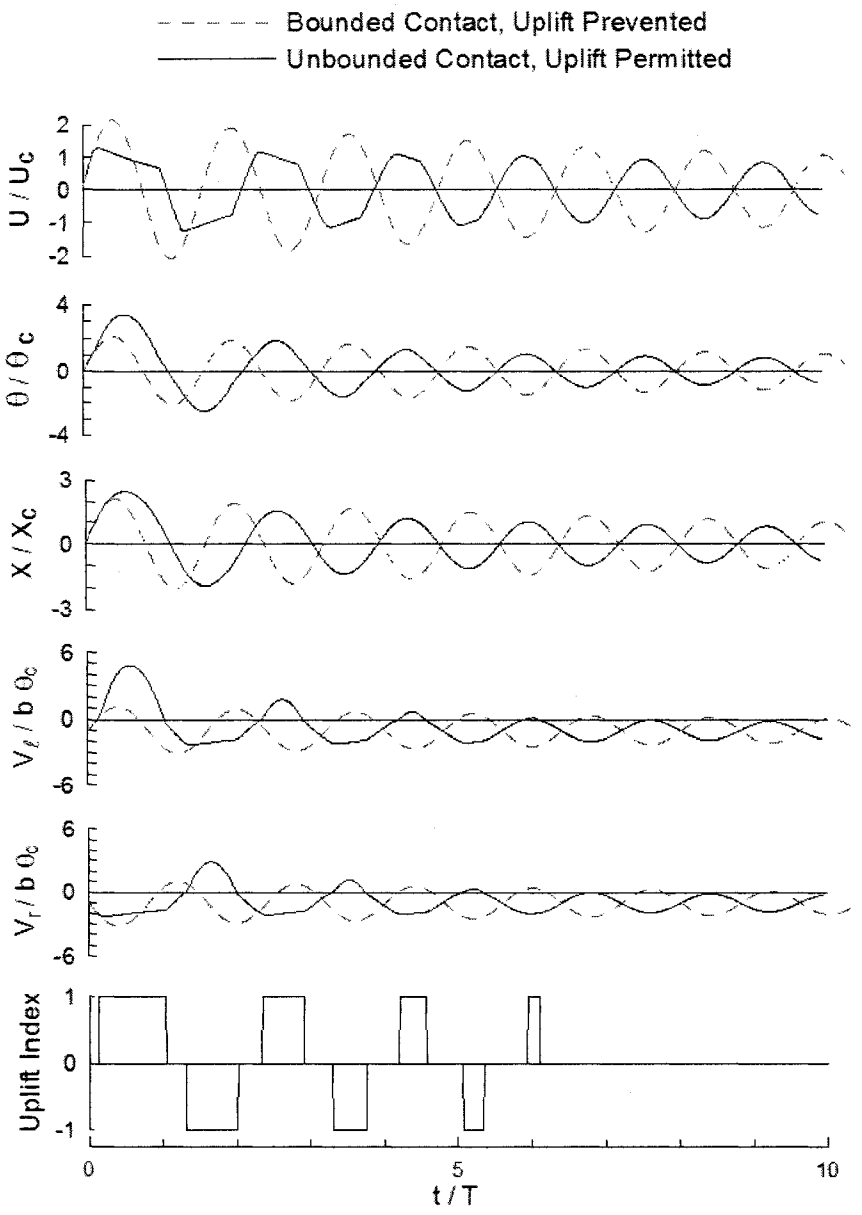

Figure 3.14: Finite element results – Free vibration response with damping.

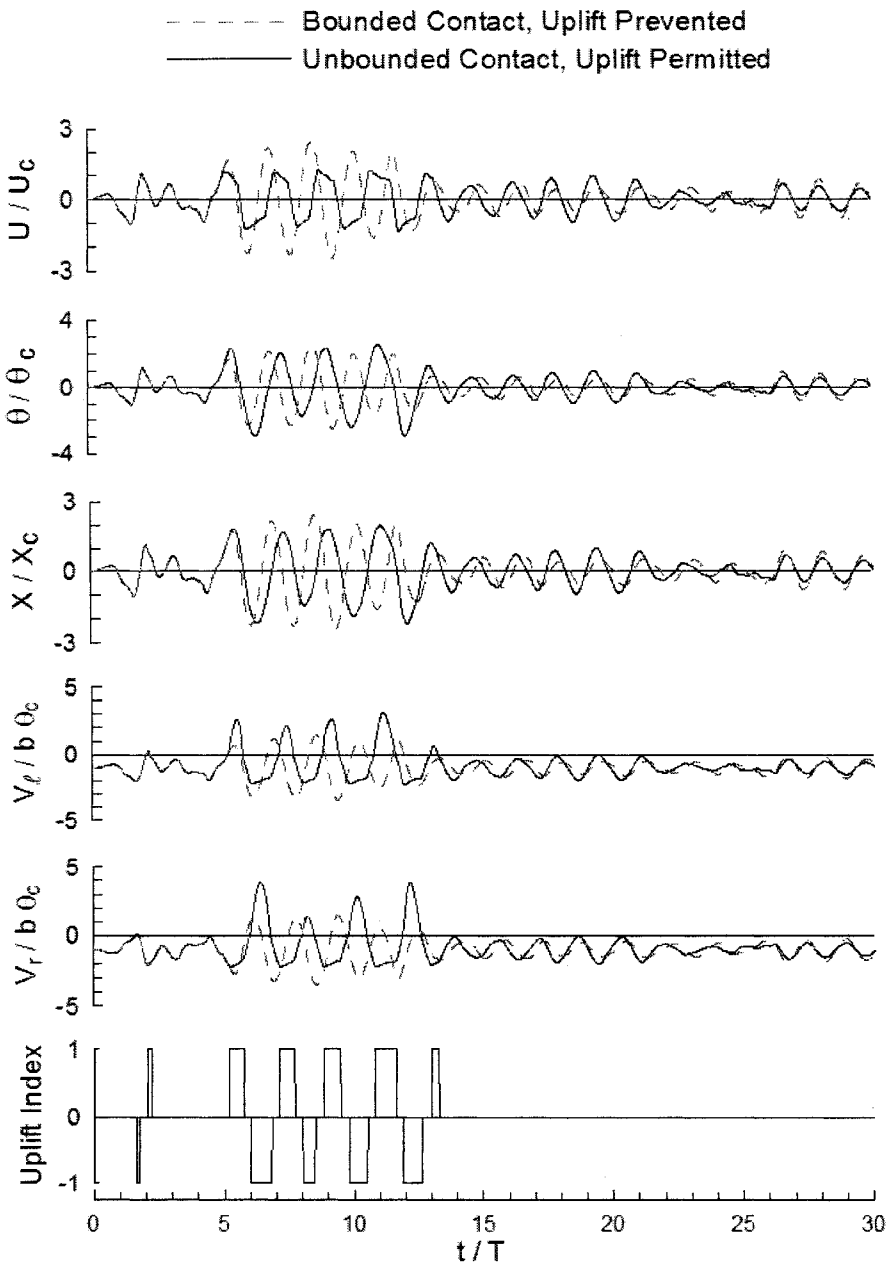

Figure 3.15: Finite element results – Earthquake response.

3.4.4. Comparison

For the case without damping, Figures 3.9 and 3.13, the results from the finite element analysis are exactly the same as the result of the analytical analysis. The only difference observed was with the second order displacements of the U/U_c graphs. The frequency is greater and the amplitude is smaller in the analysis performed with the finite element model.

For the case with damping, Figures 3.10 and 3.11, the results from the finite element analysis are very similar to the results of the analytical analysis. However, the plateaus observed in the U/U_c graph for the finite element analysis are not as flawless as the ones observed in the analytical analysis. Also, the response period of the finite element model is slightly smaller than the one observed in the analytical analysis.

For the earthquake analysis, Figures 3.11 and 3.15, the general response and most importantly the maximum responses of the two analyses are equivalent.

3.5. Conclusion

This chapter presented three simplified methods which have been proposed to predict the rocking motion of structures for preliminary design considerations. The three methods were the Substitute Substructure technique, the Energy Balance method and the Equal Energy method. Example problems using rigid blocks and SDOF structures were performed to evaluate the effectiveness of these simplified methods to correctly estimate the maximum rocking displacement caused by ground motion earthquakes and sinusoidal pulses. Nonlinear finite element models using SAP2000 were used as a basis of comparison for the simplified methods. The results demonstrated that the effectiveness of the methods was dependant on the structure and the ground motion. None of the techniques were predominantly more accurate than the other, although all of them predicted very accurately the displacement in certain cases. It is the author's

opinion that these methods are no replacement for more complete nonlinear dynamic analyses.

A second evaluation was performed to determine the ability of the finite element program SAP2000 to accurately simulate the rocking motion of systems subjected to various input signals. This was accomplished by comparing the results of finite element models to those obtained using the dimensionless analytical method proposed by Yim and Chopra. It can be concluded that the finite element modeling used to reproduce the rocking response of a structure is correct. Therefore, it was justified to use the finite element program SAP2000 as a reference for the evaluation of the simplified methods. Also, this evaluation demonstrated that SAP2000 is an appropriate program which can be used for the parametric study presented in the following chapter.

CHAPTER 4

PARAMETRIC STUDY

4.1. Introduction

The previous chapters reviewed the literature available on the subject and presented simplified methods to approximately assess the rocking potential of structures. In this chapter, a parametric study is carried out to determine the type of buildings that would benefit most from a rocking motion with the use of seismic viscous dampers. A building was selected for the parametric study. Different building parameters were varied to evaluate the impact these parameters have on the response of the building. This chapter presents the parameters of the study, followed by a description of the lateral load inputs, the finite element models used to evaluate the performance of the seismic dampers and, finally, the results of the study.

4.2. Parameters of the study

A parametric study was performed to evaluate the behaviour of the Viscously Damped Controlled Seismic Rocking (VDCSR) system on various buildings. This study was believed to be necessary to determine what type of building and which geographical regions would benefit most from this system.

A simple 45 m by 45 m building layout was selected for the study. The layout is presented in Figure 4.1. The selected building is a steel building with a floor and roof structure composed of a 63 mm thick concrete slab on a 38 mm deep steel deck, supported by W-shaped beams and columns. The building has five 9 m bays in the east/west direction and eight 5.625 m bays in the north/south direction. The seismic force resisting system used for the building was a set of two moderately ductile (Type MD) concentrically chevron braced frames (CBF), in each direction. The dead load weight of the roof, floors, exterior wall and interior partitions were 3.0 kPa, 3.5 kPa,

1.2 kPa and 1.0 kPa, respectively. These loads represent the weight of the structure and the weight of the architectural finishes. The floor live load considered was 3.8 kPa, whereas the roof live load was dependant on the location of the building. The building is classified as being of normal importance.

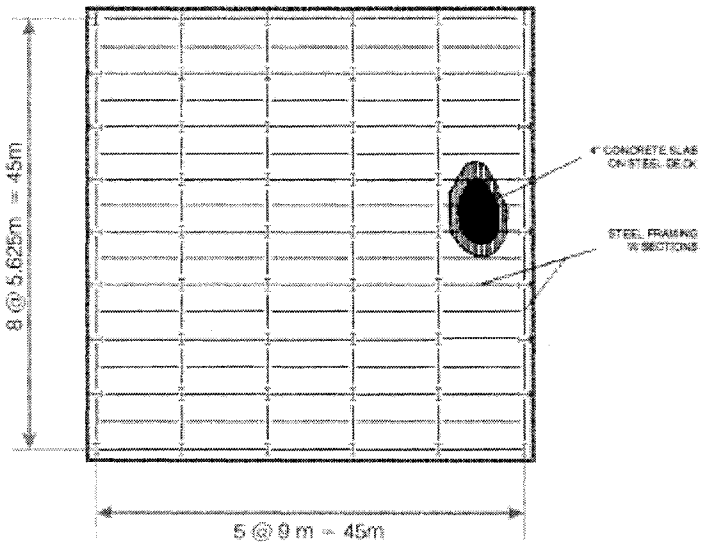

PLAN VUE

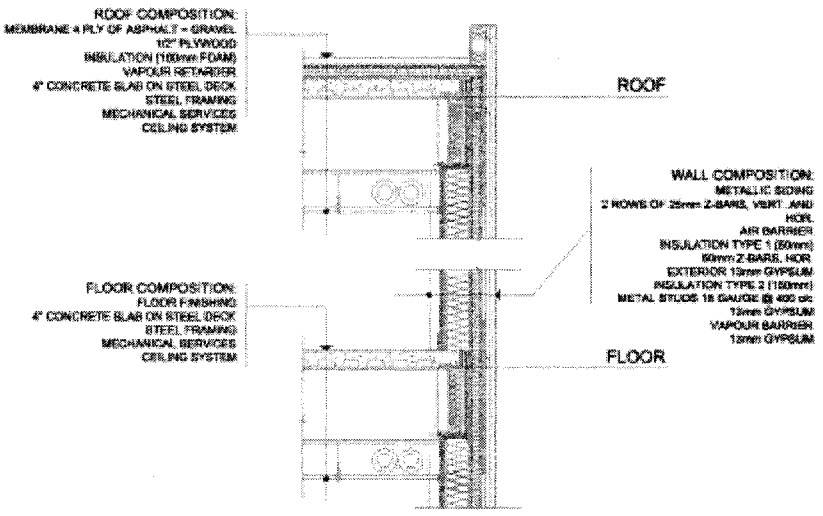

COMPOSITIONS

Figure 4.1: Plan view and cross-section.

The following parameters were used for the study:

i. *Number of storeys.* The number of storeys was changed. The seismic responses of 2-, 4- and 6-storey buildings were evaluated. The three buildings are illustrated in Figure 4.2.

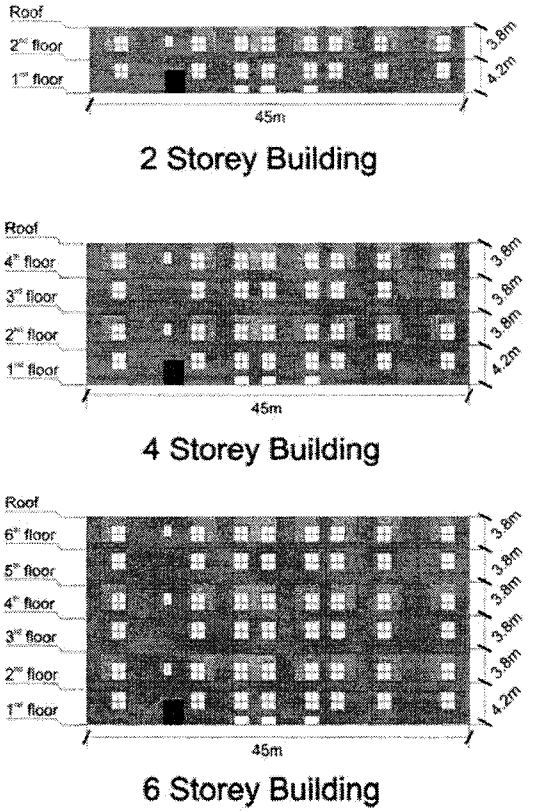

Figure 4.2: Elevations of the buildings considered in the parametric study.

ii. *Location.* Different locations were considered. The response of the buildings was evaluated for Montreal (QC), Vancouver (BC), and Los Angeles (CA). Lateral load inputs, on the form of ground motion time histories representative of each of the local seismic conditions, were used for the evaluation. The applicable building codes for each of these sites were used, thus the National Building Code of Canada (NBCC) (National Research Council of Canada, 2005) for Montreal and Vancouver, and the California Building Code (CBC) (International Code Council and the California Building Standards Commission, 2001) for Los

Angeles . In Montreal and Vancouver, Site Class C condition (very dense soil or soft rock) was assumed whereas Site Class D (stiff soil) was adopted for the buildings in Los Angeles. Figure 4.3 illustrates the location of these cities on a map of North America and indicates the roof live loads used for each city. For Montreal and Vancouver, the roof load is due to snow. In Los Angeles, it represents the minimum roof live load.

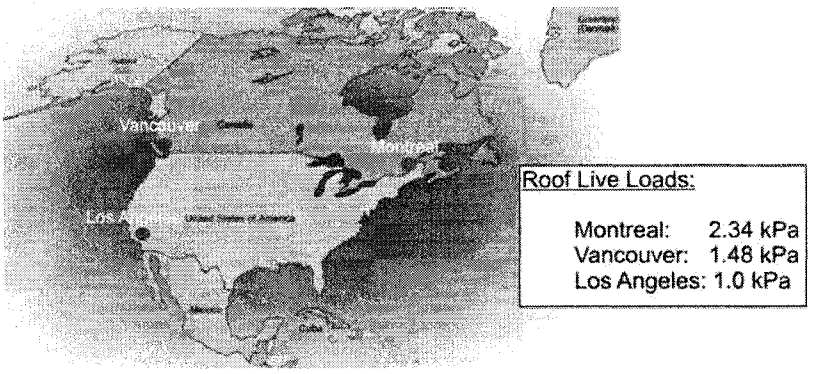

Figure 4.3: Locations of the buildings assumed for the parametric study.

iii. *Slenderness ratio.* The effect of the slenderness of the braced frames on the performance of the VDCSR system was evaluated. Slenderness is the ratio between the height and the width of the rocking braced frame. As illustrated in Figure 4.4 a) and b), the seismic analyses performed in the east/west direction were on braced frames with a 9 m wide footprint and the seismic analyses performed in the north/south direction were on braced frames with a 5.625 m wide footprint. For the 2-storey building in Montreal, the case of a 2.81 m wide footprint was also investigated. This frame is illustrated on Figure 4.4 c).

iv. *Vertical load to seismic load ratio.* The effect of the ratio of vertical load to seismic load supported by the braced frames on the performance of the VDCSR system was evaluated. Interior and exterior braced frames were considered in the study to examine the influence of the gravity load carried by the bracing bents.

As illustrated in Figure 4.4 a) and b), the interior frames support nearly twice as much vertical loads as the exterior frames.

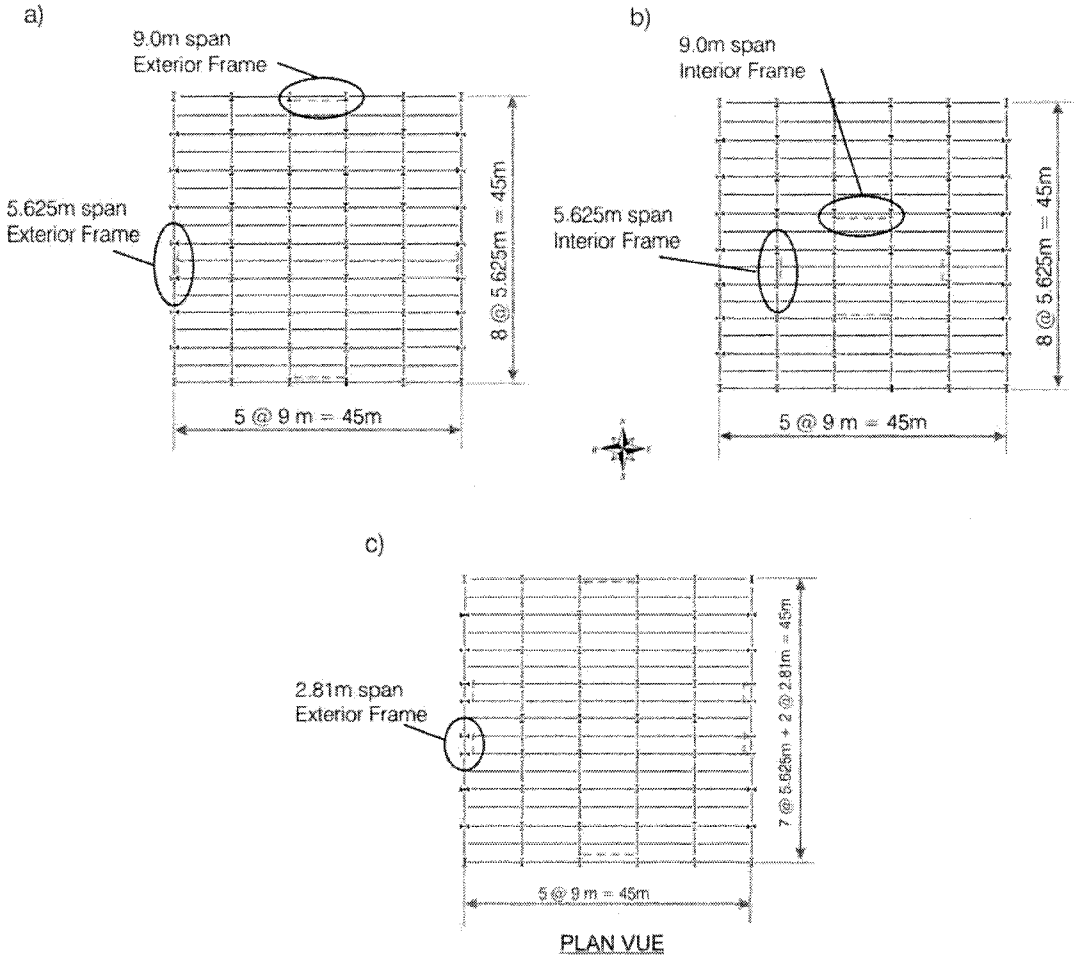

Figure 4.4: Braced frames considered in the parametric study.

v. *Base conditions.* The building frames were evaluated using four different base conditions. Three values for the damping constant were used for the VDCSR system: 100-kNs/m, 500 kN-s/m and 1000 kN-s/m. The fourth condition was a fixed base condition, which represents the response of a conventional building construction, anchored to its foundations.

4.3. Earthquake loads

The earthquake loads used for the parametric study were acceleration time history inputs from real and simulated earthquakes. Different signals were selected for each of the three locations. These signals were representative of the local seismic activity, thus the west coast earthquakes were of larger amplitude and of smaller dominant frequency than the eastern North-American earthquakes. The following section presents the seismic records used for each of the three sites.

4.3.1. Montreal

Twelve earthquake records were selected for Montreal. All twelve were artificial earthquakes with a probability of exceedance of 2% in 50 years, created to replicate the seismic characteristics of eastern Canada (Tremblay and Atkinson, 2001). All the inputs were scaled to match as closely as possible the design response spectrum of Montreal specified in the 2005 National Building Code of Canada. The magnitude, hypocentral distance (R), the peak horizontal acceleration (PHA), and the scaling factors of all records are presented in Table 4.1. The scaled acceleration time histories and the scaled acceleration spectra for the twelve time histories are presented in Appendix C.

Table 4.1: Description of the earthquake records used for Montreal.

Earthquakes used for Montreal					
Identification	Description	Magnitude (M)	R (km)	PHA (g)	Scale Factor
E01	Artificial Earthquake E60301	6.0	30	0.42	0.85
E02	Artificial Earthquake E60302	6.0	30	0.51	0.85
E03	Artificial Earthquake E60501	6.0	50	0.24	1.50
E04	Artificial Earthquake E60502	6.0	50	0.18	1.50
E05	Artificial Earthquake E70301	7.0	30	0.95	0.30
E06	Artificial Earthquake E70302	7.0	30	1.00	0.30
E07	Artificial Earthquake E70501	7.0	50	0.50	0.60
E08	Artificial Earthquake E70502	7.0	50	0.62	0.60
E09	Artificial Earthquake E70701	7.0	70	0.30	0.90
E10	Artificial Earthquake E70702	7.0	70	0.28	0.90
E11	Artificial Earthquake E701001	7.0	100	0.24	1.00
E12	Artificial Earthquake E701002	7.0	100	0.26	1.00

4.3.2. Vancouver

Twenty earthquake records were selected for Vancouver. Ten were from real occurrences and ten were from artificial earthquakes with a probability of recurrence of 2% in 50 years (Tremblay and Atkinson, 2001). All the inputs were scaled to match as closely as possible the response spectrum of Vancouver specified in the 2005 National Building Code of Canada. A description of the real seismic records is shown in Table 4.2, which includes the date and location of the occurrence, magnitude, hypocentral distance (R), the station and component where the record was measured, the peak horizontal acceleration (PHA) and the scaling factors. A description of the artificial seismic records is shown in Table 4.3, which includes the magnitude, hypocentral distance (R), the peak horizontal acceleration (PHA) and the scaling factors of these records. The scaled acceleration time histories and the scaled acceleration spectra for the ten real earthquakes and the ten simulated earthquakes are presented in Appendix D.

Table 4.2: Description of the real earthquake records used for Vancouver.

Real earthquakes used for Vancouver							
Ident.	Description	Magn.	R (km)	Station	Comp.	PHA (g)	SF
H01	Jan. 17, 1994 Northridge	MW 6.7	44	Castaic, Old Ridge Rd	90	0.57	0.65
H02	Jan. 17, 1994 Northridge	MW 6.7	30	Santa Monica City Hall	360	0.57	1.10
H03	Jan. 17, 1994 Northridge	MW 6.7	34	Los Angeles Baldwin Hills	360	0.17	1.76
H04	Feb. 9, 1971 San Fernando	MW 6.6	31	Castaic, Old Ridge Rd	291	0.27	1.50
H05	Apr. 24, 1984 Morgan Hill	MW 6.1	37	Gilroy Array Sta 6 - Ysidro	280	0.29	0.84
H06	Apr. 25, 1992 Cape Mendocino	MW 7.0	52	Eureka - Myrtle & West	90	0.18	1.20
H07	Oct. 18, 1989 Loma Prieta	MW 7.0	54	Stanford Univ.	360	0.29	1.03
H08	Oct. 18, 1989 Loma Prieta	MW 7.0	100	Presidio	90	0.20	1.30
H09	Apr. 13, 1949 West.Wash.	MW 7.1	76	Olympia, Test Lab	86	0.28	1.60
H10	June 28, 1992 Landers	MW 7.3	93	Barstow	90	0.14	2.03

Table 4.3: Description of the artificial earthquake records used for Vancouver.

Artificial earthquakes used for Vancouver					
Identification	Description	Magnitude (M)	R (km)	PHA (g)	Scale Factor
A01	Artificial Earthquake W60201	6.0	20	0.17	2.00
A02	Artificial Earthquake W60202	6.0	20	0.20	2.00
A03	Artificial Earthquake W65301	6.5	30	0.53	1.00
A04	Artificial Earthquake W65302	6.5	30	0.54	1.00
A05	Artificial Earthquake W65501	6.5	50	0.26	1.10
A06	Artificial Earthquake W65502	6.5	50	0.28	1.10
A07	Artificial Earthquake W72301	7.2	30	0.94	0.50
A08	Artificial Earthquake W72302	7.2	30	0.65	0.50
A09	Artificial Earthquake W72701	7.2	70	0.25	1.00
A10	Artificial Earthquake W72702	7.2	70	0.25	1.00

4.3.3. Los Angeles

Ten earthquake records were selected for Los Angeles. These records were selected from the set of 2% in 50 years (Maximum Credible Earthquake level) ground motion records at distance prepared for the SAC Steel Project for Site Class D in the Los Angeles area (Somerville et al., 1997). The SAC Steel Project is a joint venture of the Structural Engineers Association of California (SEA), the Applied Technology Council (ATC) and the California Universities for Research in Earthquake Engineering (CUREe). The objective of the project is to study the seismic design criteria for steel moment resisting frames. A description of the seismic records is given in Table 4.4. Note that the SAC designation is used herein and the scaling factors are those adopted in the SAC project. The scaled acceleration time histories and the scaled acceleration spectra for the ten earthquakes are presented in Appendix E.

Table 4.4: Description of the earthquake records used for Los Angeles.

Earthquakes used for Los Angeles					
Identification	Description	Magnitude (M)	R (km)	PHA (g)	Scale Factor
LA23	Loma Prieta Earthquake (1989)	7.0	3.5	0.42	0.82
LA24	Loma Prieta Earthquake (1989)	7.0	3.5	0.47	0.82
LA25	Northridge Earthquake (1994)	6.7	7.5	0.87	1.29
LA26	Northridge Earthquake (1994)	6.7	7.5	0.18	1.29
LA27	Northridge Earthquake (1994)	6.7	6.4	0.95	1.61
LA28	Northridge Earthquake (1994)	6.7	6.4	1.00	1.61
LA31	Elysian Park (simulated)	7.1	17.5	1.30	1.43
LA32	Elysian Park (simulated)	7.1	17.5	1.19	1.43
LA37	Palos Verdes (simulated)	7.1	1.5	0.71	0.90
LA38	Palos Verdes (simulated)	7.1	1.5	0.78	0.90

4.4. Finite element models

The parametric study was performed using nonlinear time history direct integration analyses in the finite element program SAP2000 (Computer & Structures, 2007). Simple two-dimensional models were used to perform the study. The P-delta effects were not considered in these analyses. The Hilber-Hughes-Taylor (alpha= -0.05) method was used as the time integration method with an output time step of 0.05 seconds. Figure 4.5 illustrates a numerical model used for a 6-storey building. In design and analysis, the effects of torsion were neglected. Therefore, only one frame and its base conditions were needed to evaluate the response of the structure as illustrated in Figure 4.5. The dimensions, the tributary vertical and lateral masses, the steel sections and the base conditions were all assumed to be representative of the characteristics of each of the buildings.

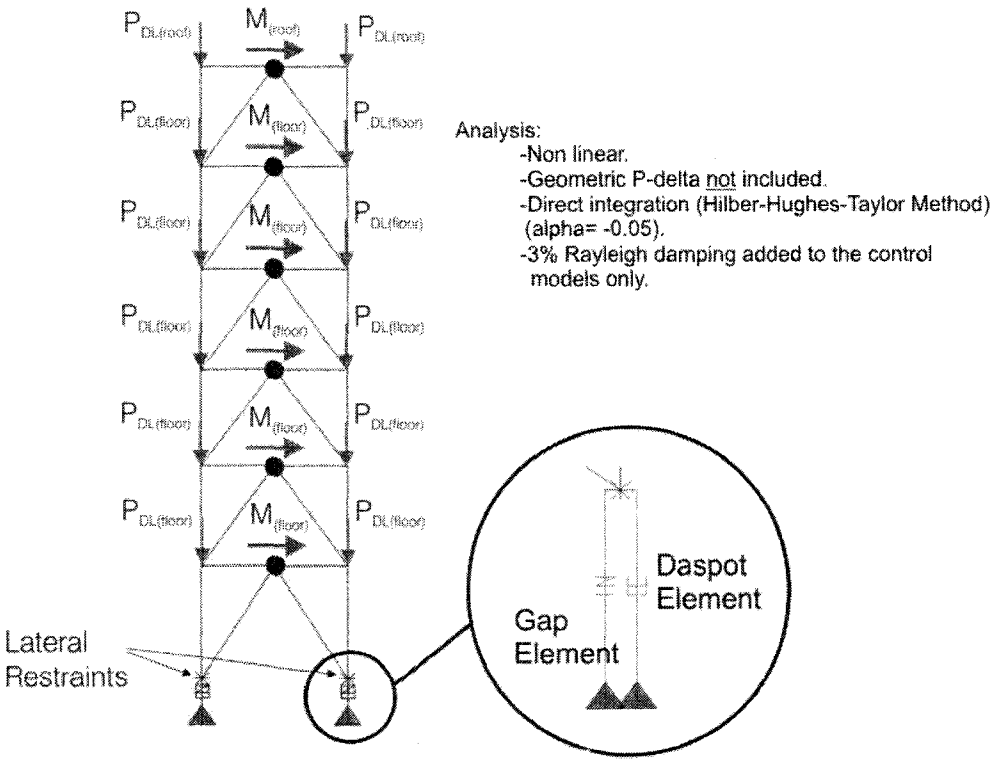

Figure 4.5: Example of a numerical model used for the parametric study.

The braced frames were designed using spectral analyses. The steel sections selected for the braced frames were chosen from the results of the spectral analyses and the evaluation of the inter-storey drift limits, according to the location of the building. The spectral analyses performed for Montreal and Vancouver were calibrated using the equivalent static force procedure of the NBCC 2005, with a ductility-based reduction factor R_d equal to 3, an over-strength reduction factor R_o equal to 1.3 and a C site class. The inter-storey drift ratio for these cities was limited to 2.5% of the storey height (NBCC 2005). The spectral analyses performed for Los Angeles were calibrated to the equivalent lateral force procedure of the CBC 2001, with an R factor equal to 6.0, an Ωo factor equal to 2.0, a C_d factor equal to 5.0 and a D Site Class. The inter-storey drift ratio for Los Angeles was limited to 2.0% the storey height (CBC 2001). The reductions permitted by the NBCC 2005 (80% V_d) and the CBC 2001 (85% V_d) for dynamic analyses were considered, where applicable.

Frame (Beam) elements in SAP2000 program were used to model the bracings. The properties of the steel sections selected from the spectral analysis were assigned to the frame elements. The end conditions of the beams and the diagonal braces were released in rotation to obtain pinned connections. At each level, horizontal masses were assigned to the central joints that corresponded to the floor (or roof) tributary seismic weight for the braced frame studied. Vertical loads were assigned to the beam-to-column joints to represent the tributary vertical weight of the floors supported by the columns. Only roof and floor dead loads were considered in the analysis as this represented a more critical condition for controlling rocking response. A ramp function was used to apply the vertical loads at a slow progressive rate onto the columns through a nonlinear static analysis in SAP2000 program. The static load effects were then used as the initial conditions for the nonlinear time history analyses. Rayleigh type damping equal to 5% of critical in the first two modes was specified for the fixed-based control models to account for the inherent damping of steel structures. No such damping was specified to the frames equipped with the VDCSR system. This was believed unnecessary and more conservative considering the high level of damping supplied by the seismic dampers. This assumption will be verified by the experimental shake table test results and the finite element models used to replicate these experimental results (Chapter 7).

A numerical model of the VDCSR system was created in SAP2000 by using a gap element and a damper element combined in parallel. As described in the previous chapter, the gap element is a nonlinear element in SAP2000, composed of contact plates in series with a spring. The contact plates allow a transfer of downward forces in compression, but have no resistance in tension, thus open when subjected to upward forces. The gap element acts as a contact surface for the column base. In a typical building, this element would represent a foundation wall or a footing. The damper element is a nonlinear element in SAP2000, composed of a dashpot in series with a spring element. Both elements are illustrated in Figure 4.6. The damper and gap

elements were introduced as the vertical base condition of the braced frames. The top joint of the system was fixed in the lateral direction.

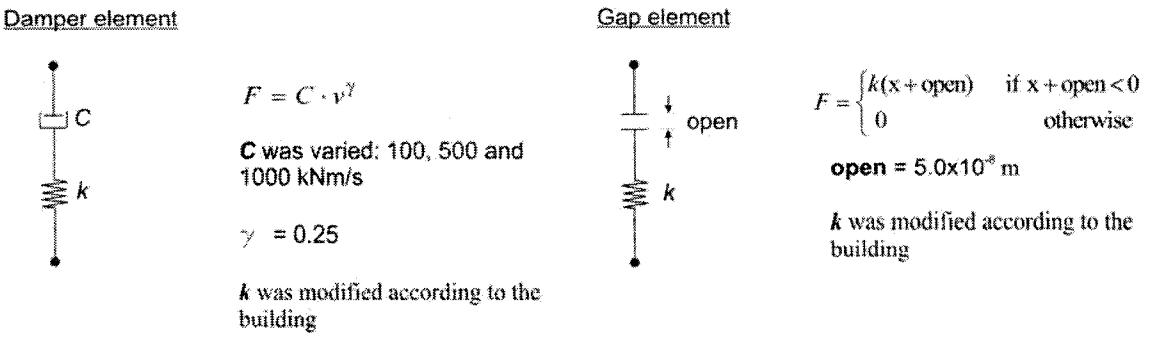

Figure 4.6: Description of the damper and gap elements in SAP2000 (Computer & Structures, 2007).

The stiffness k of the springs included in the damper and gap elements were modified according to the properties of the building. The same procedure as described in the preceding chapter was used, thus the stiffness of the springs had to be set to a value which did not alter too significantly the fundamental period of the structure, without being completely rigid. Therefore the stiffness of the vertical support springs was chosen so that the first mode period of the braced frame was not altered by more that 10% from the period of the same braced frame having fixed supports, as suggested by Anderson (1993). The combined axial rigidity of the gap and damper elements was in the range of 4 to 10 times the rigidity of the frame columns. The 'open' value used for the gap elements was close to zero. Zero was not used to avoid computational errors in the finite element model.

A total of 144 finite element models were created in SAP2000 to address every parameter described in the first section of this chapter. An identification system was established to simplify the characterization of the various models. The first part of the designation was to distinguish the width of the frame; '6' was used for the 5.625 m

frames and '9' was used for the 9 m frames. The second part of the identification name represents the position of the frame within the building; 'e' was used for the exterior frames and 'int' was used for the interior frames. The third part of the name corresponds to the number of storeys; '2' was used for the 2-storey frames, '4' was used for the 4-storey frames and '6' was used for the 6-storey frames. The fourth part of the name was to distinguish between the sites: 'mtl' was used for Montreal, 'van' was used for Vancouver and 'LA' was used for Los Angeles. The final part of the name is related to the base condition used for the frame; 'control' was for the fixed base condition, 'C100', 'C500' and 'C1000' were for the value of the damping coefficient used for the VDCSR system. For example, 9-e-6-van.C100 was the identification used for the 9 m wide exterior frame of the 6-storey building located in Vancouver, with the VDCSR system installed at the base of the frame with a damping coefficient of 100 kN-m/s.

Table 4.5 presents the characteristics of the braced frames used in the study, where W is the seismic weight of the building tributary to the braced frame, T_1 and T_2 are the periods of the first and second modes of vibration of the structure, and V is base shear to which the spectral analyses were adjusted, shown here as a percentage of the seismic weight (V/W). A complete list of all the frame sections and modeling parameters used for each of the finite element models is presented in Appendix F.

Table 4.5: Characteristics of the braced frames.

Brace frame				Characteristics			
Storeys	Span	Position	Location	W (kN)	T_1 (s)	T_2 (s)	V/W* (%)
2	2.81m	ext	Mtl	4156	0.94	0.4	9.4
	5.625m	int	Mtl	8312	0.66	0.29	9.4
			Van	8100	0.56	0.25	15.4
			LA	7725	0.48	0.22	23.3
		ext	Mtl	8312	0.66	0.29	9.4
			Van	8100	0.56	0.25	15.4
			LA	7725	0.48	0.22	23.3
	9m	int	Mtl	8312	0.53	0.23	9.4
			Van	8100	0.47	0.21	15.4
			LA	7725	0.41	0.19	23.3
		ext	Mtl	8312	0.53	0.23	9.4
			Van	8100	0.48	0.21	15.4
			LA	7725	0.41	0.19	23.3
4	5.625m	int	Mtl	17230	1.32	0.46	4.7
			Van	17020	1.12	0.41	9.6
			LA	16146	0.98	0.36	14.2
		ext	Mtl	17230	1.36	0.48	4.7
			Van	17020	1.14	0.42	9.6
			LA	16146	0.98	0.36	14.2
	9m	int	Mtl	17230	1.10	0.38	4.7
			Van	17020	0.92	0.24	9.6
			LA	16146	0.77	0.28	14.2
		ext	Mtl	17230	1.15	0.41	4.7
			Van	17020	0.95	0.25	9.6
			LA	16146	0.79	0.29	14.2
6	5.625m	int	Mtl	26154	2.31	0.75	2.8
			Van	25941	1.83	0.61	6.2
			LA	25567	1.60	0.53	10.5
		ext	Mtl	26154	2.52	0.78	2.8
			Van	25941	1.97	0.63	6.2
			LA	25567	1.60	0.53	10.5
	9m	int	Mtl	26154	1.80	0.61	2.8
			Van	25941	1.51	0.51	6.2
			LA	25567	1.24	0.45	10.5
		ext	Mtl	26154	1.95	0.66	2.8
			Van	25941	1.59	0.52	6.2
			LA	25567	1.29	0.46	10.5

* Base shear calculated using the appropriate building code. NBCC for Montreal and Vancouver (Rd = 3, R_0 = 1.3), reduction of 80% for dynamic analysis included where applicable. CBC for LA (R = 6, Ω_0 = 2), reduction of 85% for dynamic analysis where applicable.

4.5. Results of the parametric study

A total of 2016 time history analyses were performed. For each case, the following data was extracted from the finite element analysis results:

i. The lateral displacement of the central joints at each level;
ii. The axial force in each diagonal;
iii. The axial force in each column segment;
iv. The base shear;
v. The vertical base reactions (uplift and downward forces);
vi. The vertical displacement of the column base;
vii. The vertical velocity of the column base;
viii. The force in the seismic dampers.

Figures 4.7, 4.8 and 4.9 illustrate the location of the numerical data extracted from the finite element models and present the terminology used to identify the various frame components for the 2-storey, 4-storey and 6-storey frames respectively.

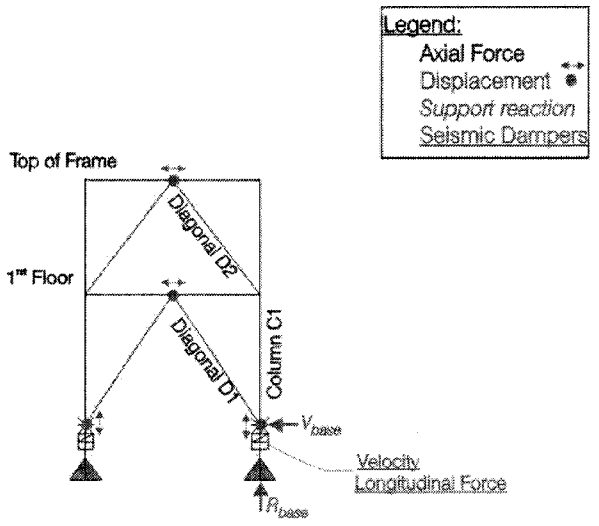

Figure 4.7: Numerical data extracted from the numerical models for the 2-storey frame.

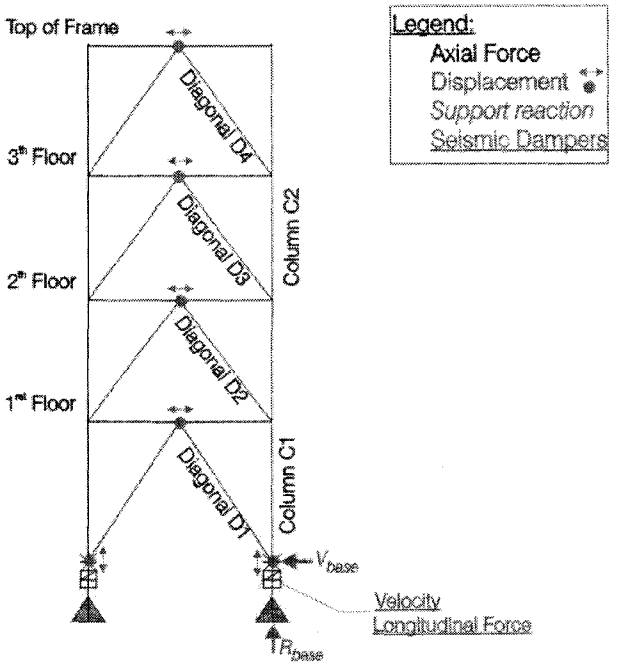

Figure 4.8: Numerical data extracted from the numerical models for the 4-storey frame.

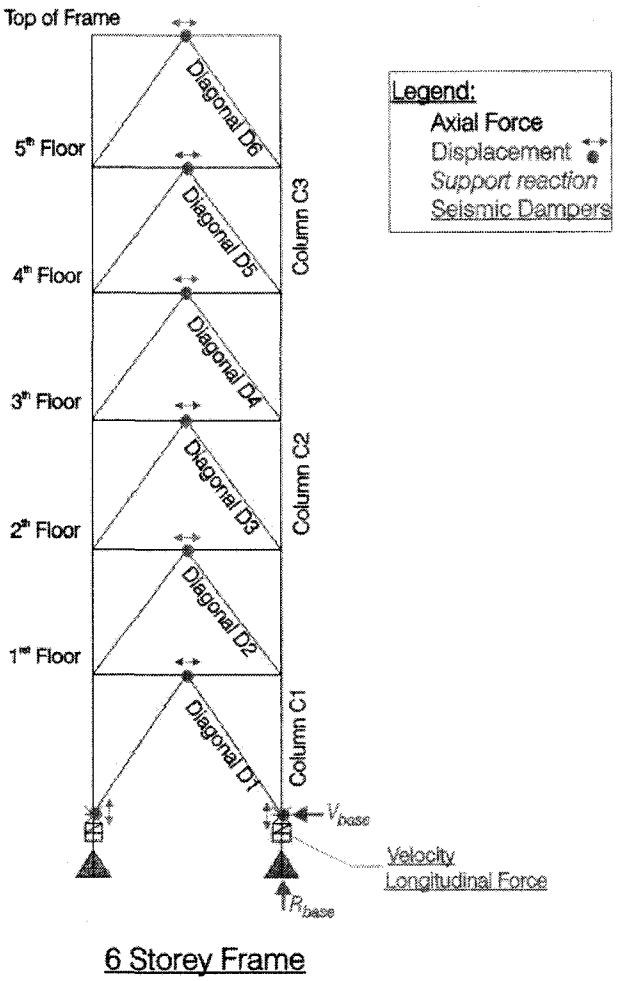

Figure 4.9: Numerical data extracted from the numerical models for the 6-storey frame.

The lateral displacement results were used to calculate the inter-storey drifts at each level of the braced frames. For all cases, the largest inter-storey drift was obtained at the uppermost level. It was observed that the displacement of the braced frames was controlled by the damping value used for the damper. The larger the damping coefficient, the smaller was the inter-storey drift. Inversely, however, the larger the damping coefficient, the smaller were the benefits of the system in terms of reducing the forces such as the vertical base reactions. Indeed, the system acted as a fixed base for larger values of the damping coefficient. Therefore, to maximise the benefits of the VDCSR system while respecting the inter-storey drift limit permitted by design codes,

the damping coefficient for the VDCSR system was selected by interpolation using the drift ratio versus the damping coefficient curves. Table 4.6 and Figure 4.10 illustrate this procedure for the analyses performed on the 6-e-4-van building. Table 4.6 presents the maximum drift ratio at the top of the frame for each of the twenty earthquake records used for Vancouver. The 50th percentile and the 84th percentile values were determined for each of the base conditions. Figure 4.10 illustrates the maximum drift versus the damping coefficient curves for this building. The optimal damping coefficient was determined to be 415 kN-s/m, which is the intersection between the drift limit of 0.025 and the 50th percentile drift ratio curve.

Table 4.6: Maximum inter-storey drift results for the 6-e-4-van building.

Top of Frame InterStory Drift									
Limit 0.025h_s = 0.095m									
		Base Condition							
		Fixed Base		C = 100 kN·s/m		C = 500 kN·s/m		C = 1000 kN·s/m	
		drift ratio	% limit	drift ratio	% limit	drift ratio	% limit	drift ratio	% limit
Time History	H01	0.014	56.1	0.027	107.7	0.022	88.5	0.020	79.3
	H02	0.013	52.4	0.027	108.8	0.014	56.6	0.012	46.1
	H03	0.012	47.2	0.023	93.6	0.019	75.8	0.014	56.2
	H04	0.011	45.9	0.020	78.9	0.014	56.9	0.014	55.7
	H05	0.018	70.7	0.010	40.2	0.008	34.0	0.009	34.7
	H06	0.012	46.7	0.025	98.2	0.021	83.5	0.019	76.1
	H07	0.013	50.5	0.017	67.3	0.019	75.8	0.020	79.0
	H08	0.014	55.6	0.024	95.8	0.021	83.2	0.017	66.3
	H09	0.009	37.4	0.022	87.1	0.018	73.6	0.014	56.5
	H10	0.013	52.2	0.087	346.3	0.046	184.2	0.024	96.0
	A01	0.011	43.2	0.020	78.8	0.015	58.8	0.014	54.2
	A02	0.015	61.5	0.032	129.5	0.025	101.2	0.023	92.4
	A03	0.009	35.3	0.036	145.8	0.036	143.6	0.034	137.5
	A04	0.023	91.4	0.070	281.3	0.044	174.2	0.028	110.2
	A05	0.011	43.1	0.015	59.8	0.013	51.3	0.011	43.3
	A06	0.013	50.2	0.030	120.0	0.026	105.2	0.022	88.6
	A07	0.012	48.5	0.053	210.6	0.034	135.9	0.025	101.0
	A08	0.010	39.7	0.031	123.2	0.026	103.5	0.016	62.9
	A09	0.010	39.4	0.040	159.1	0.026	104.5	0.019	77.1
	A10	0.007	29.9	0.033	131.2	0.020	82.0	0.018	72.9
	MAX	0.023	91.4	0.087	346.3	0.046	184.2	0.034	137.5
	50th	0.012	48.5	0.027	107.7	0.021	83.5	0.019	76.1
	84th	0.014	56.1	0.040	158.6	0.034	134.7	0.024	95.9

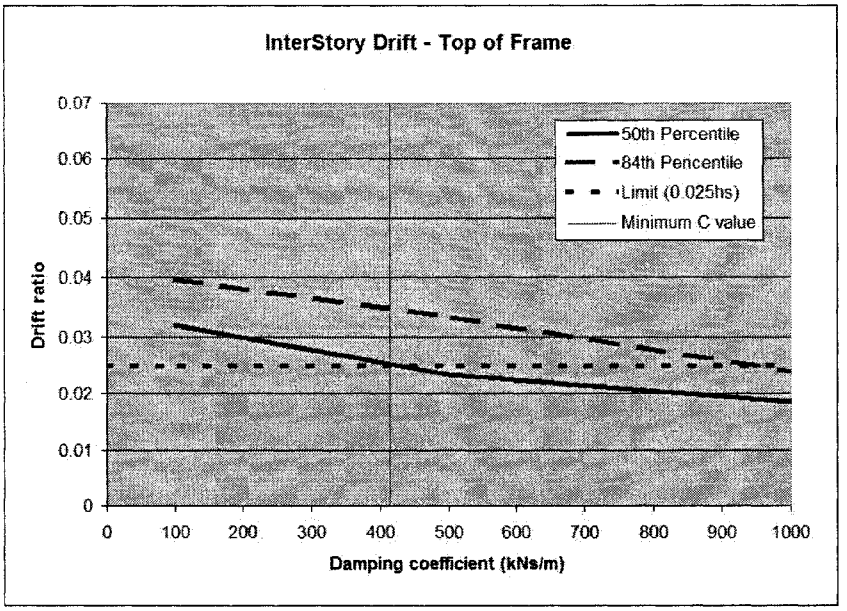

Figure 4.10: Drift ratio versus the damping coefficient curves for the 6-e-4-van building.

The described procedure was effective for all the analyses performed for the Vancouver site. An optimal damping value was selected for each of the buildings and an evaluation was performed on the behaviour of all the components of the frames using this selected parameter. Figure 4.11 presents the peak inter-storey drift ratios for all the building located in Vancouver. The values illustrated are for the 50^{th} and the 84^{th} percentile. This graph demonstrates the tendencies observed in the selection of the optimal damping coefficient for the viscous dampers. A higher damping value is required as the slenderness of the frame increases. However the height of the building and the position of the frame within the building (interior vs. exterior) do not have an important effect on the value required.

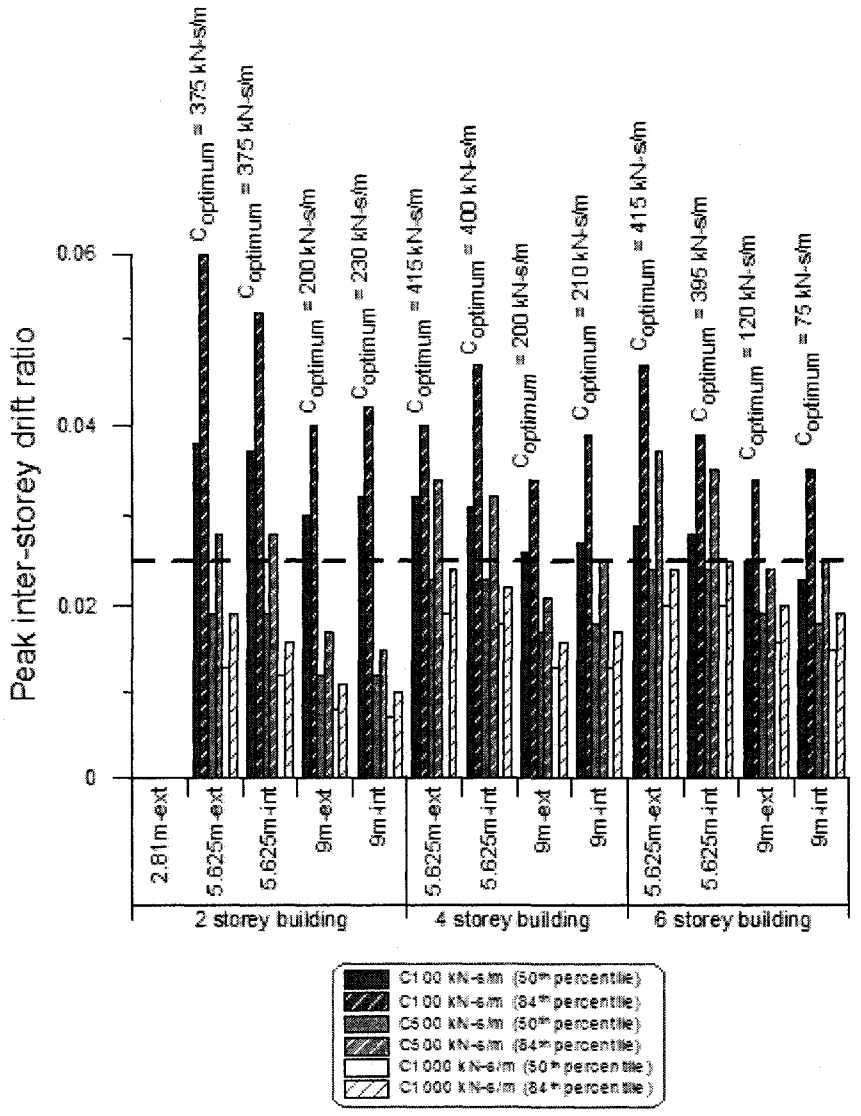

Figure 4.11: Peak inter-storey drift ratios for the buildings in Vancouver.

For the analyses performed in Montreal, the drift limit set by the building code was never reached for any of the buildings and damping values. The value of the damping coefficient was set to 100 kN-s/m, the lowest value used in the study. Although the damper was not required to control the rocking displacements of the frame, it was still beneficial in absorbing some of the impact between the columns and the foundation and in dissipating a portion of the energy from the earthquake motion. The behaviour of all the components of the frames was evaluated using this parameter. Figure 4.12 illustrates

the peak inter-storey drift ratios (50th and 84th percentile) for all the buildings located in Montreal.

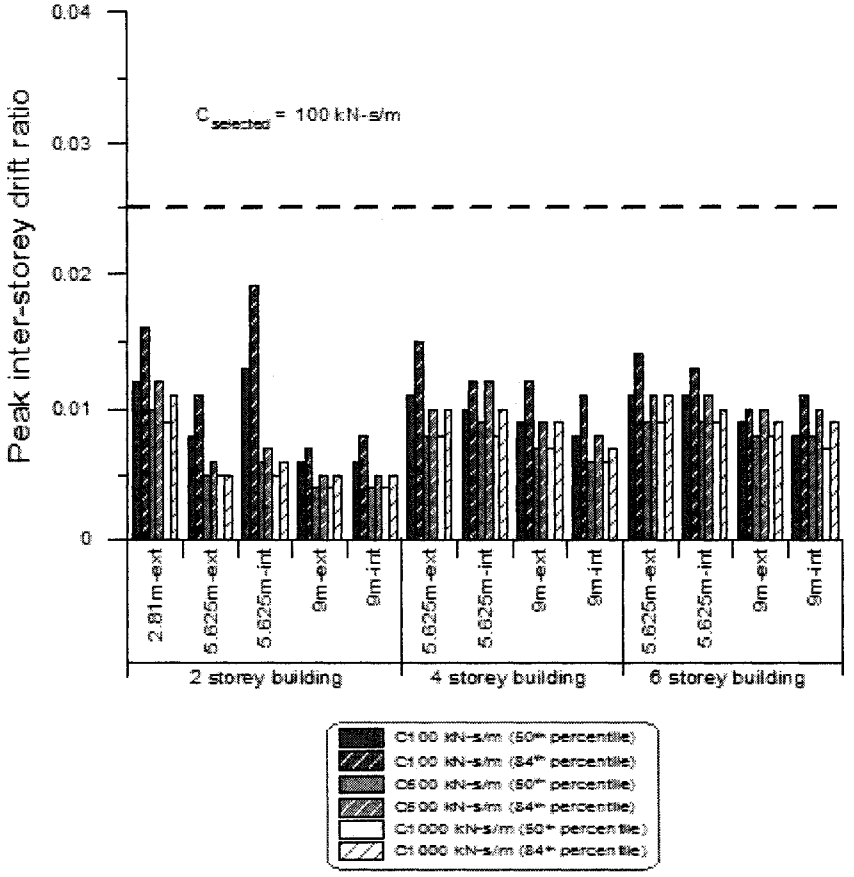

Figure 4.12: Peak inter-storey drift ratios for the buildings in Montreal.

Figure 4.13 shows the maximum peak inter-storey drifts for the Los Angeles site. Contrarily to what was observed for the Montreal site, the analyses resulted in inter-storey drifts all above the 0.02 limit permitted by the 2001 California Building Code. This suggests that the parameters used for the damping coefficients were not sufficient to control the rocking displacement of the buildings. Additional analyses were performed on four buildings using damping values of 1500, 2000 and 4000 kN-s/m. The results demonstrated that the drift limit was still exceeded even when specifying these higher damping levels for the VDCSR system. Figure 4.14 shows the uplift response at the base of the 6-e-4 frame for different values of C under one ground motion. The

rocking motion (uplift) reduces as the damping coefficient increases. However, the inter-storey drift ratios do not reduce significantly with an increase in the damping coefficient at these higher levels of damping. This is clearly observed on Figure 4.13 for the 4- and 6-storey frames. A very little reduction in drift is obtained between the damping coefficients of 500 and 1000 kN-s/m. Also, with an increased damping coefficient, the benefits of the VDCSR system disappear. The vertical forces on the foundation are increased to a level comparable to the fixed base condition. For certain ground motions, with the 2-storey buildings, increasing the damping coefficient had negative effects, such as increasing the inter-storey displacements and creating permanent foundation uplift. Figure 4.15 shows the response of the 2-storey 5.625 m span exterior braced frame subjected to the LA27 earthquake with a damping coefficient equal to 500, 1000 and 2000 kN-s/m. It is observed that an increase in damping has a negative effect on the rocking motion. For the damping coefficient of 2000 kN-s/m the momentum of the vertical dead load in the columns is not large enough to compress the dampers back to their original positions, following the earthquake solicitation. This is possibly du to computation errors in the finite element program.

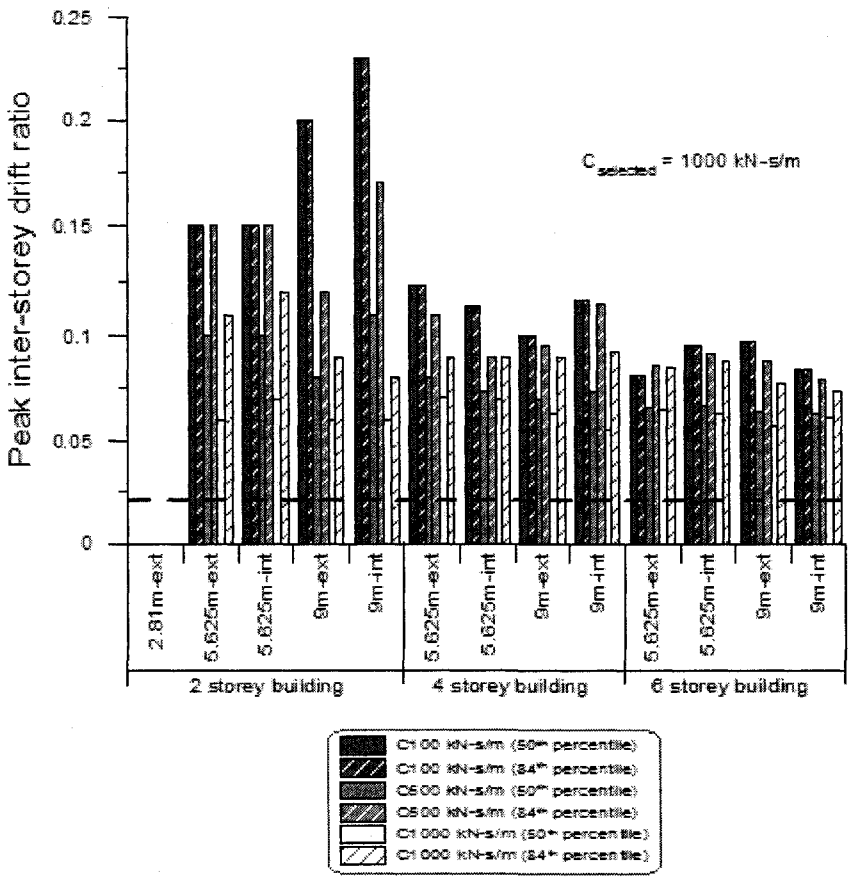

Figure 4.13: Peak inter-storey drift ratios for the buildings in Los Angeles.

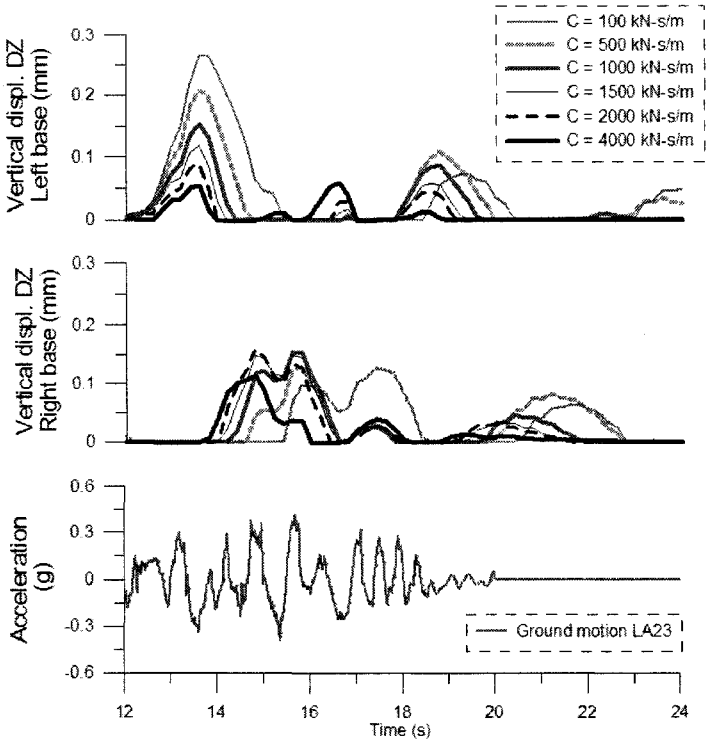

Figure 4.14: Effects of increasing the damping coefficient on the rocking motion.

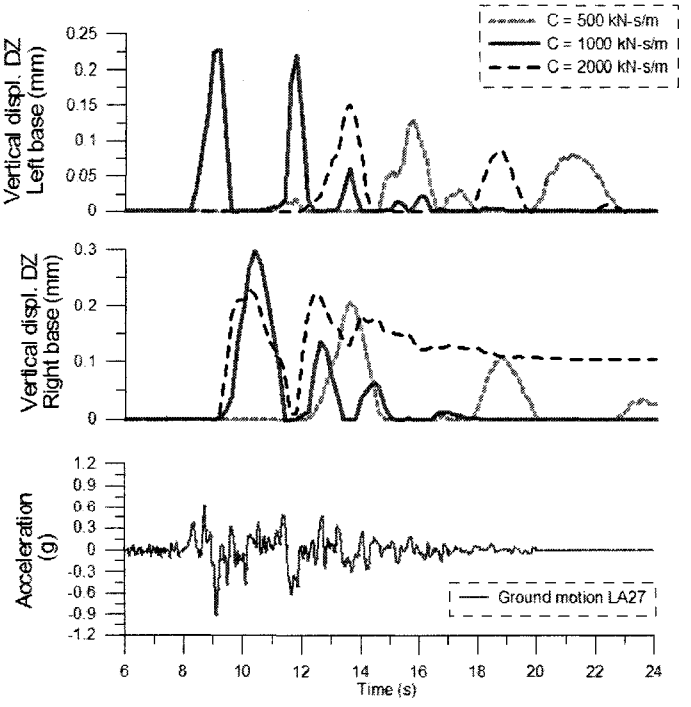

Figure 4.15: Rocking response of the 6-e-2-LA frame to the LA27 ground motion.

With the VDCSR system, the restoring force is provided only by the gravity loads supported by the rocking braced frame. The results for Los Angeles show that the drift demand on the system from MCE level ground motions that contain significant acceleration pulses is too high to keep the drifts within the prescribed code limit. In the U.S., conventional seismic force resisting systems are expected to only meet a life-safety performance objective under MCE ground motions and this is achieved by requiring that the probability of total structural collapse remains low under this earthquake level (ATC, 2008). No drift limit is prescribed for this hazard level. Several past studies have shown that structures designed according to U.S. codes experienced inter-storey drifts well in excess of the design inter-storey drift limit (e.g., Gupta and Krawinkler, 2000; Sabelli et al., 2003; Tremblay et al., 2008). In this context, the performance of the VDCSR system does not deviate significantly from current design practice and accepted performance levels for conventional seismic force resisting systems. However, it does not achieve the objectives of limited drifts with no structural damage nor residual deformations that can be achieved in sites of low or moderate seismic hazard level, such as Montreal and Vancouver. As discussed later, a superior performance could likely be achieved by providing the system with higher restoring force capacity.

For the purpose of comparison, the behaviour of the components of the frames was evaluated using the largest value of damping, thus a damping coefficient of 1000 kN-s/m. Although this may not represent an optimum design for a rocking system designed for enhanced seismic performance, this still provides a general overview of the expected response for buildings located in the Los Angeles area.

Detailed results for all the analyses performed for the Montreal, Vancouver, and Los Angeles sites are presented in the research Report No. SR08-06 (Poirier et al., 2008). This report includes the maximum inter-storey drift ratios at each level, maximum axial force for the diagonals and the columns, maximum base reactions and maximum lateral and uplift displacements for each of the earthquake records used. The results are

presented for each base condition and are plotted graphically according to the value of the damping coefficient used for the VDCSR system.

The time history analysis results obtained for the VDCSR system with the optimum damping level were compared to the results from the response spectrum analysis assuming a ductility factor R equal to 3.0 for Montreal and Vancouver, and 6.0 for Los Angeles. This evaluation was needed to determine the value of adding the VDCSR system in a building in comparison to a conventional seismic force resisting system. Figures 4.16, 4.17 and 4.18 illustrate the ratios between the median value of the peak axial forces in the diagonal bracing members in the VDCSR system, N, to the axial forces from spectral analysis, $N_{\text{spectral analysis}}$. Values lower than 1.0 in the figures indicates a gain in using the VDCSR system versus a conventional lateral force resisting system. These results are discussed later for each of the three sites.

Figures 4.19 and 4.20 illustrate the ratio between the median value of the peak axial forces in the columns, peak base shear forces, and peak uplift and downward reaction loads in the VDCSR system, N, to the corresponding forces from code capacity design procedure $N_{\text{capacity design}}$. The capacity design forces, as required by the applicable seismic design provisions (CSA-S16-2001 for Montreal and Vancouver and AISC 2005 for Los Angeles) are the values that would be used in the design of conventional braced frame systems. They represent the force demand associated to the development of the expected capacity of the bracing members selected from spectral analysis. In the figures, a value lower than 1.0 indicates a gain in using the VDCSR system versus a conventional lateral force resisting system.

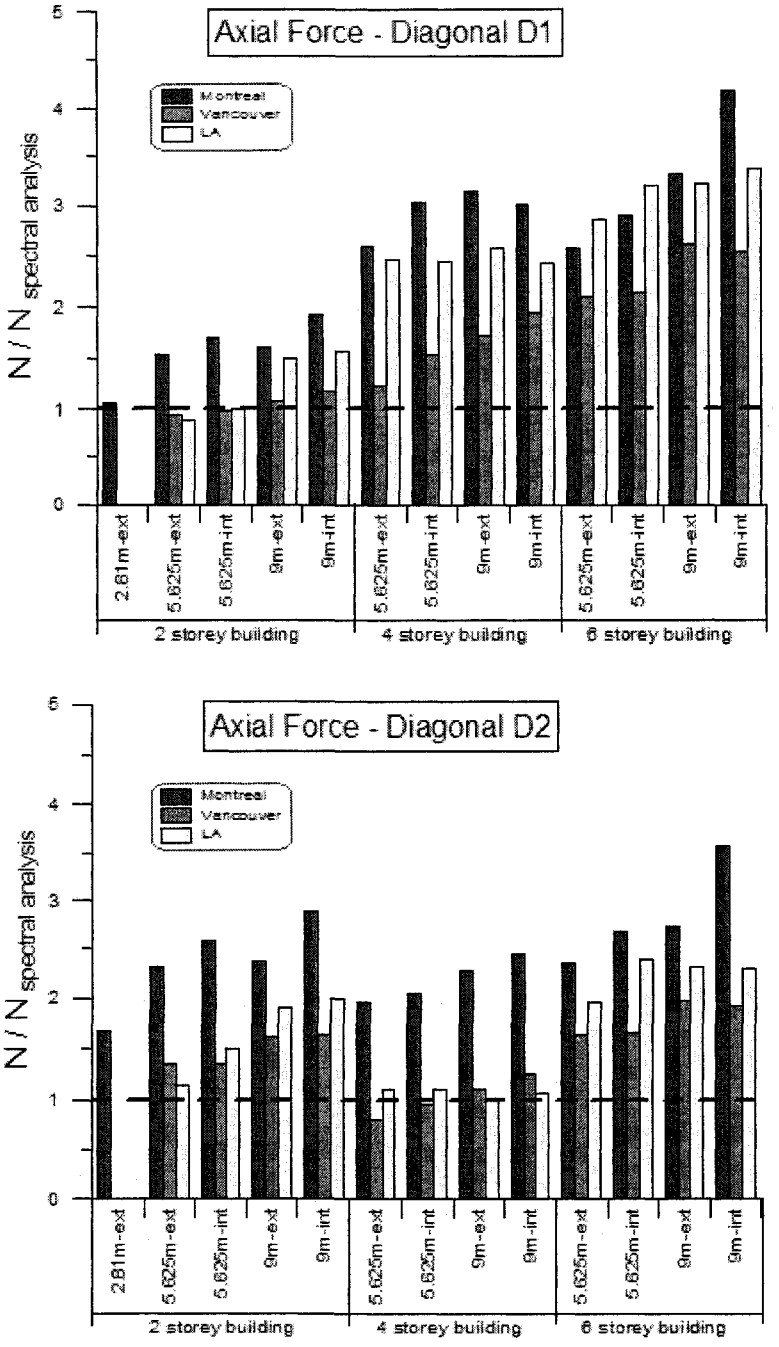

Figure 4.16: Axial force ratios for 1st and 2nd storey braces D1 and D2.

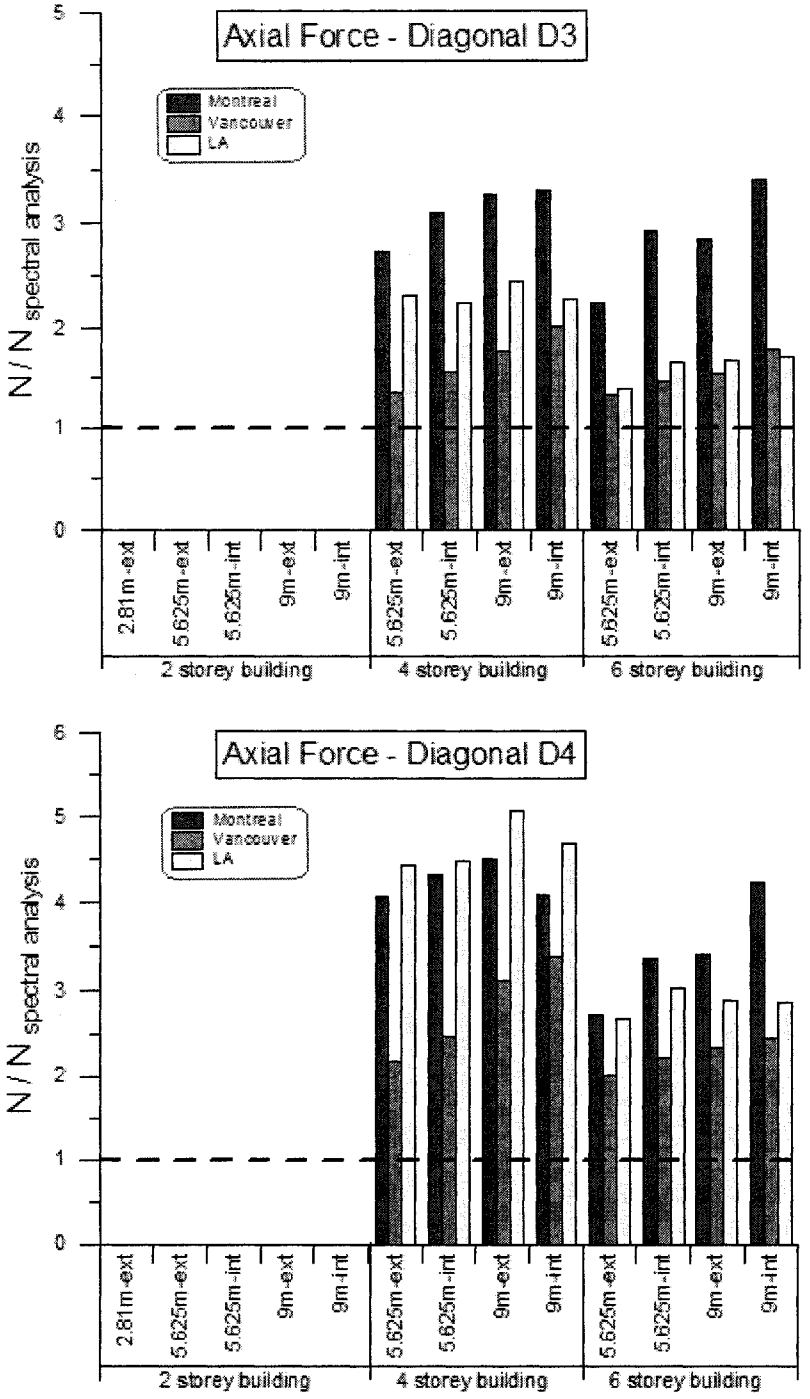

Figure 4.17: Axial force ratios for 3rd and 4th storey braces D3 and D4.

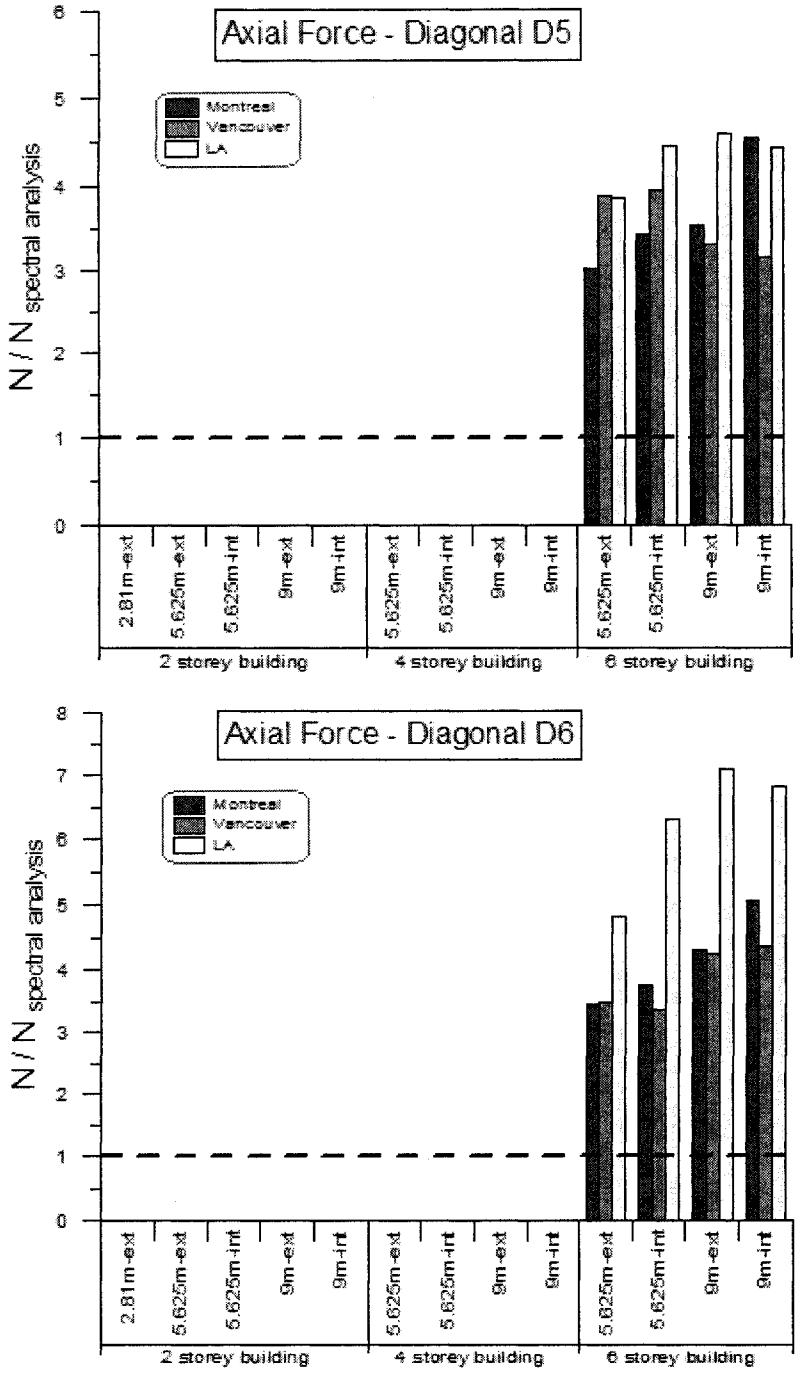

Figure 4.18: Axial force ratios for 5th and 6th storey braces D5 and D6.

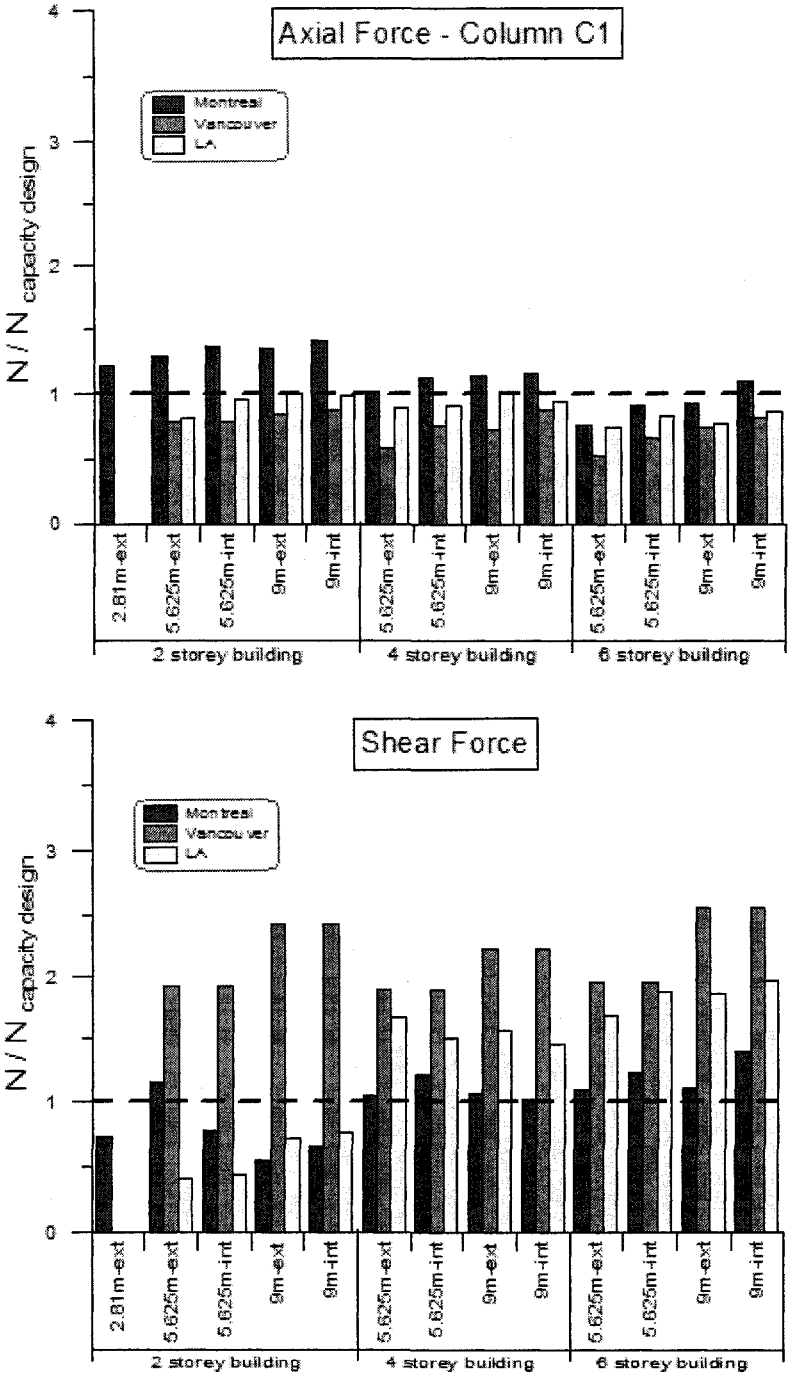

Figure 4.19: Axial force ratios for the 1st storey column (C1) and base shear ratios.

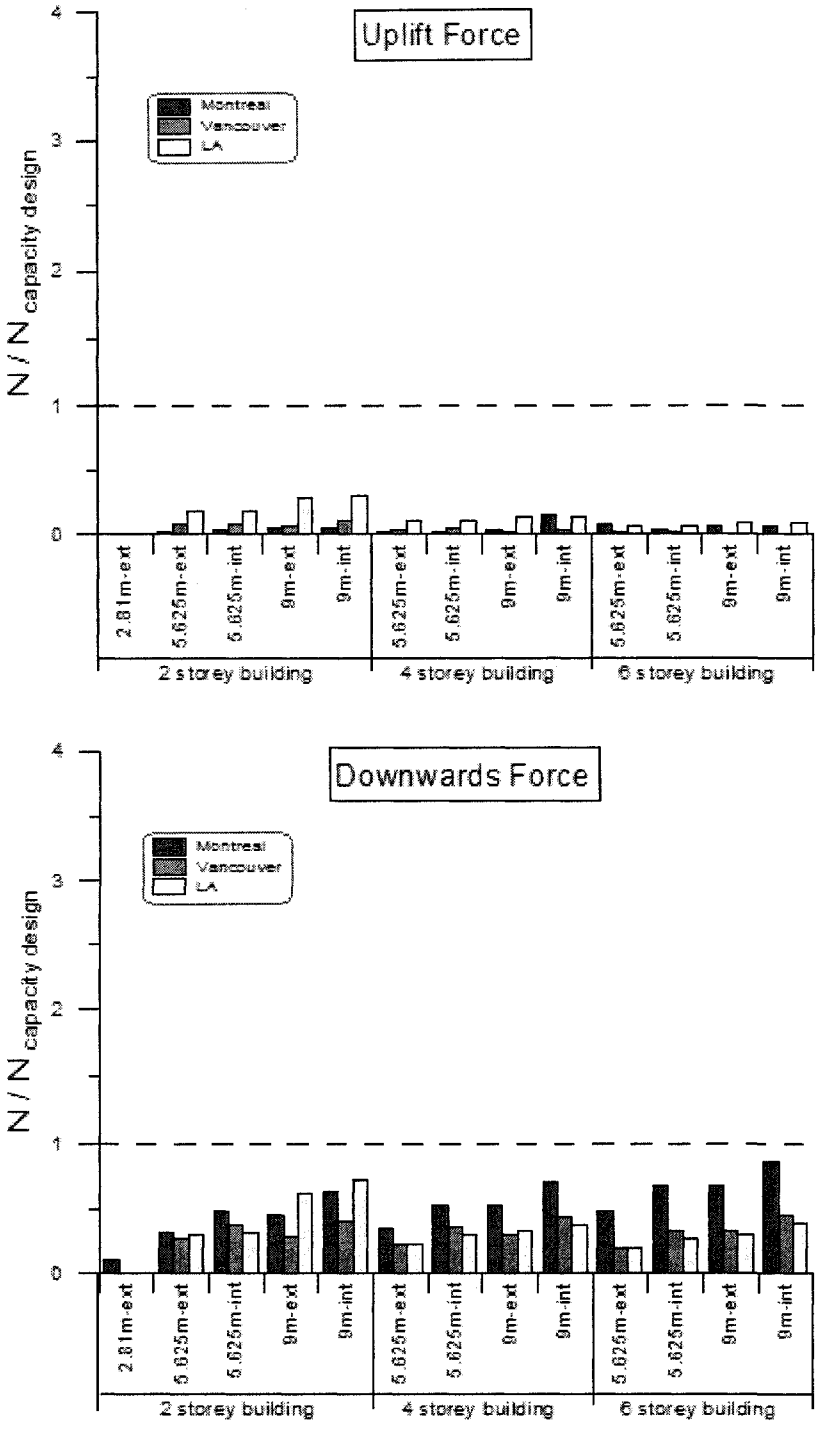

Figure 4.20: Uplift and downward base reaction ratios.

4.5.1. Results for Montreal

2-storey buildings. As observed in Figure 4.16, the axial forces in the bracing members are greater at both levels with the VDCSR system, compared to a conventional building designed using a spectral analysis. The increase in the axial forces varied from 1.1 to 1.9 for the first level and from 1.7 to 2.9 for the second level. The ratios generally decreased as the frame slenderness was increased, the reason being that more slender frames are more prone to rocking and, hence, attract lower seismic forces.

In Figures 4.19 and 4.20, the axial forces in column C1 were greater with the VDCSR system, compared to a conventional building. The forces were greater by a factor of 1.2 to 1.4. The base shear forces in the VDCSR however were smaller for all the buildings, varying between 0.5 and 0.8, except for for the 5.625 m wide exterior frame for which the ratio was equal to 1.2. An important reduction in the vertical base reactions was observed for all buildings. The ratios for the uplift forces varied from 0.01 to 0.05, and varied from 0.1 to 0.6 for the downward forces.

4-storey buildings. Figures 4.16 and 4.17 show that the brace axial forces were greater at all levels with the VDCSR system. The increase in the axial forces varied from 2.6 to 3.2 for the first level, from 1.9 to 2.5 for the second level, from 2.9 to 3.4 for the third level and from 4.0 to 4.4 for the fourth level. The increase is more pronounced for the 9 m frames. The higher values in the upper floors are attributed to the fact that brace forces in the upper levels are greatly influenced by higher mode response whereas first mode response is the one that is filtered most by rocking. The same reasoning explains the higher ratios observed for the 4-storey buildings compared to the 2-storey building; the response of the former being more influenced by higher modes. Figure 4.21 illustrates the relation between the base shear forces, the 1^{rst} brace (D1) axial forces and the overturning moment for a 2- and 6-storey frame in Montreal and a 6-storey frame in Vancouver. It is observed that the base shear force is a component of the axial force in the first lower diagonal. For the 2-storey frame in Montreal, the base shear is

synchronized with the overturning moment. Both are in sync with the vertical displacement of the column bases. However, the same cannot be said for the 6-storey frame. The overturning moment is not synchronized with the shear forces or the vertical displacement of the column bases. The second mode effects are more significant, therefore decreasing the benefits of rocking for the higher level diagonals. For buildings in Vancouver, the lower frequency content in the ground motions likely provides a lower contribution to the higher mode effects. This is demonstrated by the results for the 6-storey frame in Figure 4.21. The base shear forces are synchronized with the overturning moment and the vertical uplift displacement of the bases.

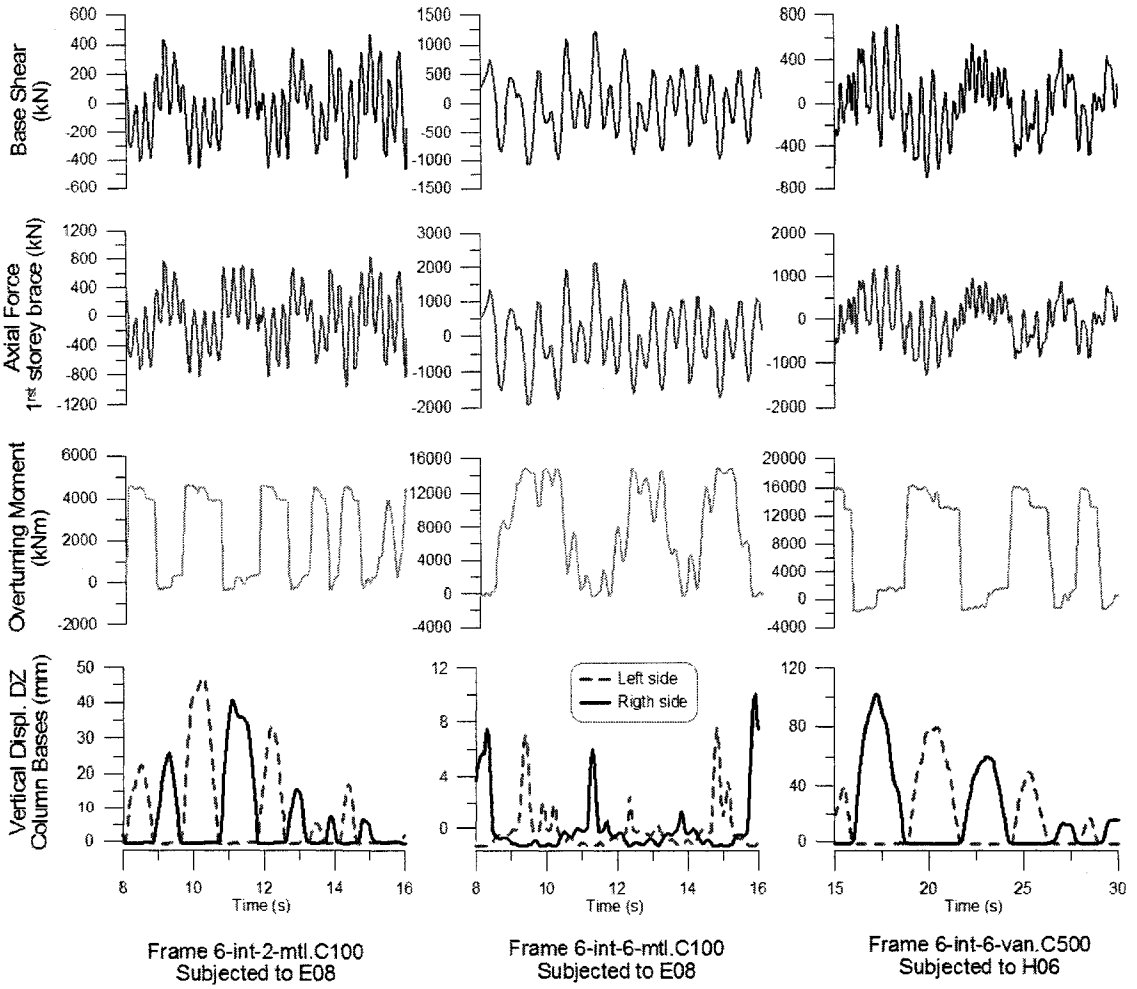

Figure 4.21: Relation between the base shear and the overturning moment.

As observed in Figures 4.19 and 4.20, the axial forces in column C1 and base shear forces are comparable to or slightly exceed those used in the design of a conventional braced frame. The ratios vary between 1.0 and 1.2. As was the case for the 2-storey frames, a significant reduction in vertical base reactions was observed for all buildings. The ratios vary from 0.02 to 0.2 for the uplift forces and from 0.4 to 0.7 for the downward forces.

6-storey buildings. In Figures 4.16, 4.17, and 4.18, the brace axial loads in the VDCSR system are larger than the response spectrum analysis results at all levels. The increase in the axial forces varied from 3.5 to 4.4 for the first level, from 2.4 to 3.6 for the second level, from 2.5 to 3.5 for the third level, from 2.8 to 4.3 for the fourth level, from 3 to 4.6 for the fifth level and from 3.5 to 5.0 for the sixth level. As for the shorter buildings, the highest ratios were obtained for the less slender frames. These values are higher than those obtained for the 4-storey frames, confirming that rocking is more effective when shear and overturning moment demand are in phase as is the case in lower buildings that have a first mode dominated response.

Except for the 9 m wide interior frame, the column axial loads in the VDCSR system are all smaller than those in the conventional CBF design (Figure 4.19). The force ratios vary between 0.75 and 1.1. The base shear forces in the VDCSR system exceeded those of the conventional system, with ratios varying from 1.1 to 1.4. Again, the VDCSR system resulted in reductions in the vertical base reactions for all buildings: The ratios are between 0.04 and 0.1 for the uplift forces and between 0.5 and 0.95 for the downward forces.

4.5.2. Results for Vancouver

2-storey buildings. In Figure 4.16, when compared to conventional CBF, the first-storey brace axial force demand in the VDCSR system is smaller for the buildings with the 5.625m wide braced frames and larger for the 9 m wide braced frames. The ratios varied

from 0.9 to 1.2. The axial forces in the diagonal members D2 increased by a factor of 1.4 to 1.6 with the VDCSR system. These ratios for Vancouver are much smaller than in Montreal, likely because the ground motions in western Canada are richer in lower frequency, resulting in reduced shear force demand for low-rise buildings.

Figures 4.19 and 4.20 show that the axial forces in column C1 were smaller in all VDCSR designs compared to the conventional frame system. The force ratios are included between 0.8 and 0.9. The force demand in the columns reduces when increasing the frame slenderness. The use of the VDCSR system resulted in higher base shear forces, from 1.9 to 2.5 times the values of the conventional CBF. The vertical base reactions reduced for all the buildings with uplift force ratios varying from 0.08 to 0.1 and downward forces ratios varying from 0.3 to 0.4.

4-storey buildings. As observed in Figures 4.16 and 4.17, the axial forces in the braces were greater at all levels with the VDCSR system, except at the second level of the 5.625 m wide braced frames. A ratio of 0.8 to 0.95 was observed at the 2nd level of these buildings. For the other buildings, the increase in the axial forces varied from 1.2 to 1.9 for the first level, from 1.1 to 1.3 for the second level, from 1.4 to 2.0 for the third level and from 2.2 to 3.3 for the fourth level. The 9 m frames experienced higher brace force demand. The ratios a larger increase than the 5.625m frames. Again, the ratios are lower in Vancouver compared to the frames with the same height in Montreal. The lower frequency content of the Vancouver ground motions likely results in a relatively lower contribution from higher modes as illustrated by Figure 4.21.

In Figure 4.19 and 4.20, the axial forces in column C1 in all VDCSR structures were smaller than in the conventional building. The force ratios were comprised between 0.6 and 0.9. Higher base shear forces were however observed for the VDCSR system, with ratios varying from 1.9 to 2.2. Lower vertical base reactions were observed in all

rocking frames, with uplift force ratios from 0.02 to 0.05 and downward force ratios from 0.2 to 0.4.

6- storey buildings. In Figures 4.16 to 4.18, the brace axial forces are greater at all levels of the VDCSR frames. The force ratios when compared to conventional CBF varied from 2.0 to 2.6 for the first level, from 1.6 to 2.0 for the second level, from 1.3 to 1.8 for the third level, from 2.0 to 2.5 for the fourth level, from 3.2 to 4.0 for the fifth level and from 3.4 to 4.4 for the sixth level.

Figures 4.19 and 4.20 show that the axial force demand in column C1 with the VDCSR system varies between 0.6 to 0.9 times the values in the conventional building. The shear forces were greater with the VDCSR system, the ratios varying from 1.9 to 2.2. An important reduction in the vertical base reactions was observed for all the buildings. The VDCSR system permitted to reduce the uplift and downward forces to a fraction of the CBF values: between 0.02 to 0.05 and between 0.2 to 0.4, respectively.

4.5.3. Results for Los Angeles

As mentioned previously, the use of the proposed VDCSR system at this site did not permit to reach the desired superior performance level that could be achieved at the other two sites. Therefore the results obtained for Los Angeles may not be representative of structures equipped with VDCSR systems that would be specially designed to fully take advantage of the rocking technology. For this reason, the results are not analysed in depth. Examination of Figures 4.16 to 4.18 reveals that the tendencies are similar to those observed for Montreal and Vancouver: an increase in brace axial loads and base shear forces and potential savings in column axial forces and vertical base reactions.

It is believed that the performance of the system at this site could have been improved if stiffer braced frames had been used. The behaviour could also be enhanced by increasing the restoring force capacity of the system. For example, the restoring

capacity could be increased by adding post tensioned self-centering cables that would help control the displacements. This approach has been adopted for the earthquake-resistant self-centering steel frame system currently being studied by Sause and al. (2007) in an on-going Network for Earthquake Engineering Simulation Research (NEES) project at Lehigh University. As illustrated in Figure 4.22, the CBF rocking response in this system is controlled by the post-tensioned vertical cables. A combination of this system with the VDCSR system could represent an interesting solution for buildings located in the Los Angeles area.

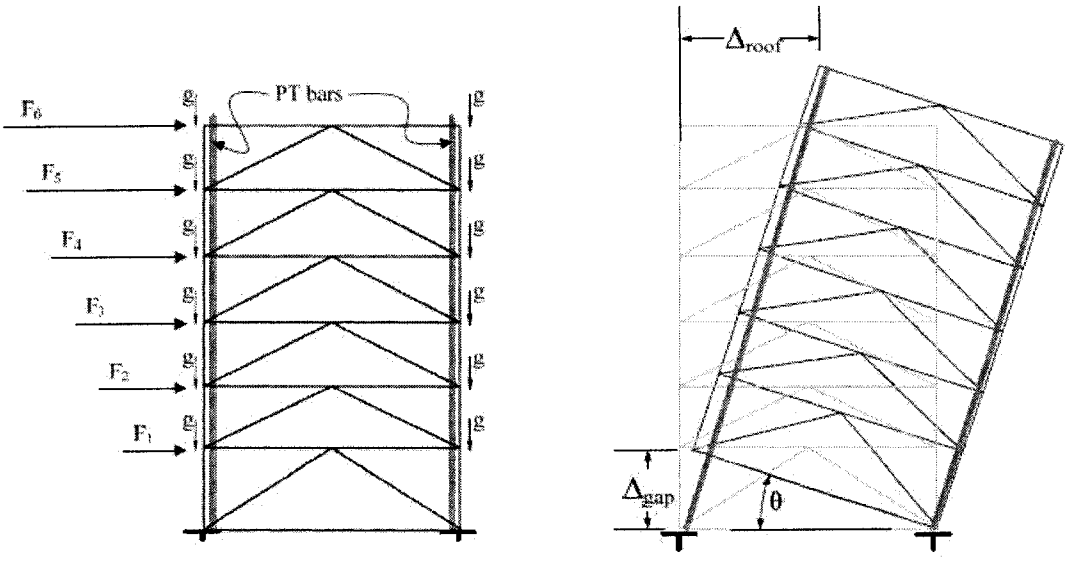

Figure 4.22: Self-centering post-tensioned lateral load resisting system (adapted from Sause and al. (2007).

4.5.4. Rocking period of the buildings

An evaluation was performed on all the buildings (Montreal, Vancouver and Los Angeles) to determine the rocking period of the structures for each of the earthquake ground motions used in the parametric study. The rocking periods of the braced frames were obtained by counting the number of occurrences uplift was observed on a given time period. For example, Figure 4.23 illustrates the uplift displacement of the right column base of the 2-storey, 5.625 m exterior span braced frame in Vancouver subjected to the H09 ground motion. As demonstrated, 9 uplift occurrences were observed in a time range of 14.8 seconds, yielding a rocking period equal to 1.64 seconds. Using the average rocking period values obtained for each of the buildings for the three seismic locations considered, the graph illustrated in Figure 4.24 was created to determine what trends could be observed for the rocking periods as a function of the fixed base fundamental period of vibration of the buildings. These trends are used to develop the test protocol for the calibration of the seismic dampers for the shake table test program, which is presented in Chapter 6.

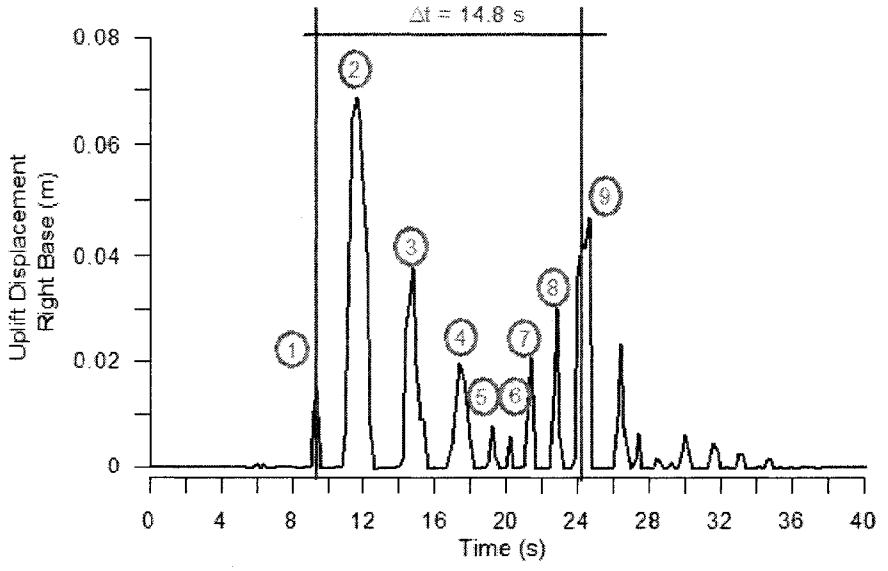

Figure 4.23: Rocking period calculated for the 6-e-2-van frame subjected to the H09 ground motion.

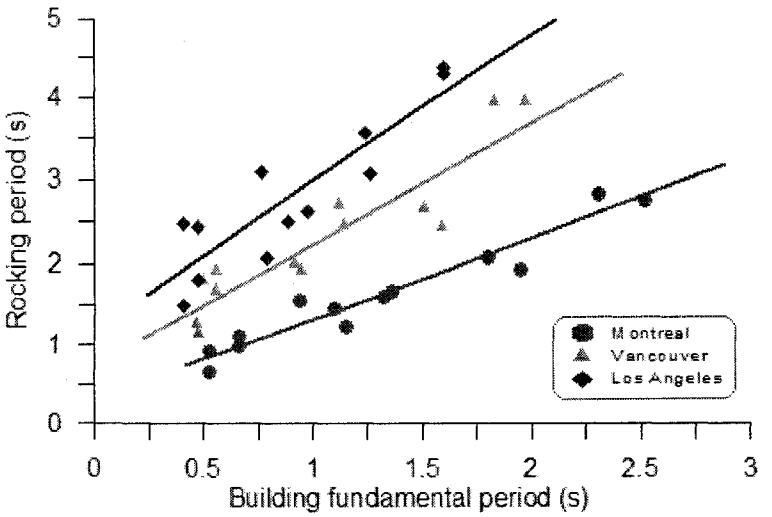

Figure 4.24: Relationship between the rocking period and the fundamental period of the buildings.

A relationship is observed between the two parameters illustrated in Figure 4.24. The rocking period is directly proportional to the fixed-base period of vibration. As the fixed base period increases, the rocking period also increases. It is observed that the rate of increase is greatest for Los Angeles, followed by Vancouver and then Montreal. For the range of buildings examined in the parametric study, the rocking period of the buildings varied between 0.6 seconds in Montreal to 4.5 seconds in Los Angeles. These two extremes are considered in the test protocol for the viscous dampers, presented in Chapter 6.

4.6. Comments on SAP2000

Before discussing the conclusions of the parametric study, certain comments must be made on the finite element program SAP2000 versions 9 to 11. This program has certain interesting features but also has aspects that are inconvenient that one should consider before using it as a tool for nonlinear time history analyses.

Firstly, the advantages: SAP2000 is an easy accessible (cost) program to professional engineering firms. It is user friendly and has a wide range of applications.

For example, the gap and damper elements were very well suited for the complex rocking motion. Also, SAP2000 allows for nonlinear time history analysis using direct integration methods with nonlinearity functions such as the P-delta effects and the P-delta large displacement effects.

Now the inconvenient aspects: The computation time is extremely long for nonlinear time history analyses. Many numerical models in the parametric study took over three days to solve. Inclusion of Rayleigh damping was impossible when the damper and/or gap elements were included as the base conditions. Proportional damping on the mass only was possible. The output files are very voluminous and require a lot of computer memory. Also, a more recent version of SAP2000 can open files saved in an older version, but all the analysis results are lost. Therefore analyses must be redone, which can be time consuming. In the two years required to complete this thesis, four upgrade of SAP2000 were required.

4.7. Conclusion

A parametric study was conducted using finite element numerical analyses to evaluate the response of the VDCSR system incorporated into 2-, 4- and 6-storey buildings located in three locations: Montreal, Vancouver and Los Angeles. The slenderness and the vertical weight to seismic mass ratios were varied to determine the influence of these parameters on the performance of the system. The following assumptions were used in the models to simplify the analyses:

i. A two dimensional analyses was performed, thus neglecting the effects of torsion.
ii. The ground motions were applied in the horizontal direction only. The vertical component was not considered.
iii. P-delta effects were not considered.

iv. The Hilber-Hughes-Taylor method was used as the time integration method, with an alpha factor equal to -0.05. This allowed for faster computation by the finite element program compared to the more common Newmark method.

The results of the study confirmed that the column uplift loads could be nearly entirely annihilated with the VDCSR system for all buildings. The downwards forces on the foundations could also be greatly reduced compared to conventional fixed base CBF designs. These gains offered by the VDCSR system can result in considerable cost savings for column anchorage and foundations. During the rocking process, one column of the braced frame must carry the total gravity loads supported by the bracing bay. In spite of this penalty, the peak axial loads in the columns remained lower (Vancouver and Los Angeles) or similar (Montreal) to the forces that must be considered in the design of a conventional fixed base steel braced frame. For the 2-storey buildings in Montreal and Los Angeles, the base shear forces in the VDCSR structures is generally lower than the capacity design values for a conventional chevron bracing. As the height of the building increases, the overturning moment response tends to lag behind the horizontal shear force demand and the benefits of rocking gradually diminish. The base shear forces then become larger than those found in conventional design. For Vancouver, the base shear forces are higher for all the buildings studied. For all buildings, the brace axial loads were also larger than what would be expected for fixed base chevron bracing. Smaller brace axial loads were obtained in the VDCSR system when reducing the frame slenderness ratio or the vertical weight to seismic mass ratio.

In view of the satisfactory results from this parametric study, the next step was to build an actual VDCSR system and perform shake table tests to validate the numerical finite element models that were used to predict the response of the system. The procedure that was adopted to develop the test specimen is presented in the following chapter.

CHAPTER 5

DESIGN OF A SCALED MODEL FOR USE IN THE EXPERIMENTAL TEST PROGRAM

5.1. Introduction

Experimental tests have always been of great importance to the scientific community. They allow researchers to examine accurate solutions of engineering problems in order to validate predictions made using mathematical methods. Test programs also help to point out some aspects that may have been neglected or underestimated in mathematical predictions. One of the main difficulties in structural engineering, in regards to laboratory testing, is the cost and size constraints to test programs. Constructing a full size dam, bridge or building for laboratory tests is more than often impossible. Another consideration is the capacity of the laboratory equipment and instrumentation. Limits must be set on the dimensions, weight and movement of experimental specimens in order to respect these constraints. This is why, more than often, experimental work is carried out on reduced scale models.

The following chapter presents a scaled test specimen and the corresponding testing setup. The test program is intended to validate the assumptions and accuracy of the finite element analysis models used in the parametric study presented in Chapter 4. The tests were performed on the earthquake simulator of the Hydro-Québec Structural Engineering Laboratory at École Polytechnique of Montreal.

5.2. Similitude Requirements

Experiment work performed on scaled models must follow the laws of dimensional analysis. Dimensional analysis is a method used to convert dimensional equations describing a problem into a set of functional relationships using independent dimensionless products of selected physical quantities. This method is based on the Buckingham π theorem (Buckingham, 1914) and is explained in depth by Moncarz

(1981). Moncarz stated that generally, the number of independent dimensionless products required for a given problem is equal to the number of physical quantities involved minus the number of fundamental quantities required to describe the dimensions of these physical quantities. The following ten physical quantities are believed to adequately describe the dynamic response of the specimens tested in this work:

$$F = (m, L, t, a, g, \Delta, E, \sigma, P, C) \qquad [5.1]$$

The fundamental quantities are the mass (m), length (L) and time (t). These three quantities can be used to define all the other physical quantities, which are the horizontal acceleration (a), the acceleration due to gravity (g), the displacement (Δ), the elastic Young's modulus (E), the stress (σ), the gravity load (P) and the damping coefficient of the damper (C). Applying the Buckingham π theorem, we can obtain the following dimensionless products:

$$G = \left\{ \frac{a}{g}, \frac{\Delta}{L}, \frac{\sigma}{E}, \frac{t^2 EL}{m}, \frac{ma}{EL^2}, \frac{mg}{P}, \frac{C\left(\frac{\Delta}{t}\right)^{\gamma}}{ma} \right\} \qquad [5.2]$$

We designate by *Prototype* the full scale actual braced frame, and by *Model* the reduced-scale test specimen. The scale factor for distance is $\alpha = L_{model}/L_{prototype}$. Steel is used for both the prototype and the model, which leads to $E_{model} = E_{prototype}$ and $\sigma_{model} = \sigma_{prototype}$. Finally, it is assumed that the nonlinearity in the damper response is the same in the prototype and model ($\gamma_{model} = \gamma_{prototype} = \gamma$). Under these assumptions, the ratios in equation 5.2 can be used to determine all the similitude requirements between the model and the prototype. Two commonly used scaling methods (Moncarz, 1981) are presented in table 5.1: the velocity similitude method and the acceleration with artificial mass similitude method. Also presented in table 5.1 is the modified acceleration similitude method (Merzouq, 2006). This method introduces a second scaling factor which is

applied to the acceleration, $\beta = a_{model}/a_{prototype}$. This third method was the one selected in the development of the test program because it requires less mass than the other methods, thus reducing the cost of fabrication of the experimental setup. However, one disadvantage of this method is that the vertical acceleration of the model (gravity) is not respected ($a/g \neq 1.0$ in the model). The acceleration due to gravity had to be increased by the β factor, which was not possible in the laboratory. The consequences of this shortcoming will be discussed later in this chapter.

Table 5.1: Modeling parameters for the similitude law methods.

			Similitude law method		
			Velocity Similitude	Acceleration Similitude	Modif. Acc. Similitude
Parameter	Units	Prototype	Model	Model	Model
Length	(m)	L	$L \cdot \alpha$	$L \cdot \alpha$	$L \cdot \alpha$
Acceration	(m/s^2)	a	a/α	a	$a \cdot \beta$
Gravity	(m/s^2)	g	g/α	g	$g \cdot \beta$
Time	(s)	t	$t \cdot \alpha$	$t \cdot \alpha^{0.5}$	$t \cdot (\alpha/\beta)^{0.5}$
Mass	(kg)	m	$m \cdot \alpha^3$	$m \cdot \alpha^2$	$m \cdot \alpha^2/\beta$
Force	(kN)	P	$P \cdot \alpha^2$	$P \cdot \alpha^2$	$P \cdot \alpha^2$
Frequency	(Hz)	f	f/α	$f/\alpha^{0.5}$	$f/(\alpha/\beta)^{0.5}$
Velocity	(m/s)	v	v	$v \cdot \alpha^{0.5}$	$v \cdot (\alpha \cdot \beta)^{0.5}$
Viscous Damp. Coeff.	(kNs/m)	C	$C \cdot \alpha^2$	$C \cdot \alpha^2/\alpha^{0.5}$	$C \cdot \alpha^2/(\alpha \cdot \beta)^{0.5}$
Mod. Elast.	(MPa)	E	E	E	E
Stress	(MPa)	σ	σ	σ	σ

5.3. Selection of the laboratory model

The selection of the laboratory model was a complex task. The first step was to determine the constraints of the laboratory program. Budget, size and laboratory equipment limitations were established and then considered in the selection of the model. Compromises had to be made to develop a realistic test specimen while considering these restrictions. It was decided to limit the total mass of the laboratory model to approximately 30 000 kg (295 kN) to meet the budget constraint and to ensure that the mass could be easily and safely handled in the laboratory. The dimensions and the capacity of the seismic shake table were also considered, these are illustrated in Figure 5.1. Using these limits, three test specimen options were developed for the laboratory test program.

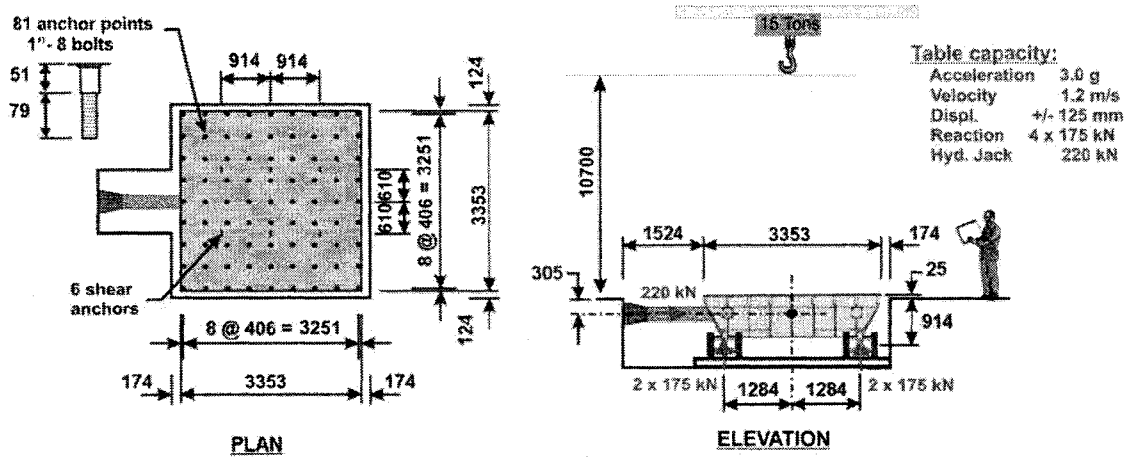

Figure 5.1: Shake table dimensions and capacity (adapted from Tremblay et al., 2005).

It was decided to use Vancouver as the design location for the snow loads and the seismic loads considering that the results from the parametric study were very promising for Vancouver, and that the force and displacement responses obtained in the study were in mid range between the results for Montreal and Los Angeles; not too low and not too high. Also, it was determined from the parametric study that a damping coefficient of 500 kN-s/m was the average optimum value for seismic isolation dampers to be included in low-rise buildings designed for Vancouver. This was considered a feasible value for the prototype.

For options 2 and 3, preliminary designs were required to select the steel sections for the prototype frame. It is our assumption, considering the results of the parametric study that the VDCSR system performs more efficiently than conventional fixed-base SFRSs. The preliminary design method used for the prototype frames involved selecting steel sections that can resist the elastic forces determined from spectral analyses in Vancouver, with the seismic forces reduced by the ductility factors considering a fixed-base SFRS. It was believed that the VDCSR system, at least for 2-storey or less buildings, could provide a higher force reducing effect than that provided by the

ductility of these conventional systems, thus selecting steel sections with an upper-bound force-resisting capacity. This design procedure needs to be validated for real design application. Not enough data is available at this time to determine a definite design methodology, but for the purposes of this research program, this method was deemed acceptable.

As described in section 5.6 of this chapter, the amplitude of the earthquake ground motions for Montreal were scaled up and the amplitude of the earthquake ground motions for Los Angeles were scaled down to meet the strength and deformation capacity of the laboratory test specimen designed for a seismic hazard typical of Vancouver, as well as the capacity limits of the earthquake simulator.

5.3.1. Option 1 – 2-storey building from the parametric study

The first option for the prototype is a 2-storey exterior braced frame from a building taken directly from the parametric study. Figure 5.2 illustrates the characteristics of the building used for this option.

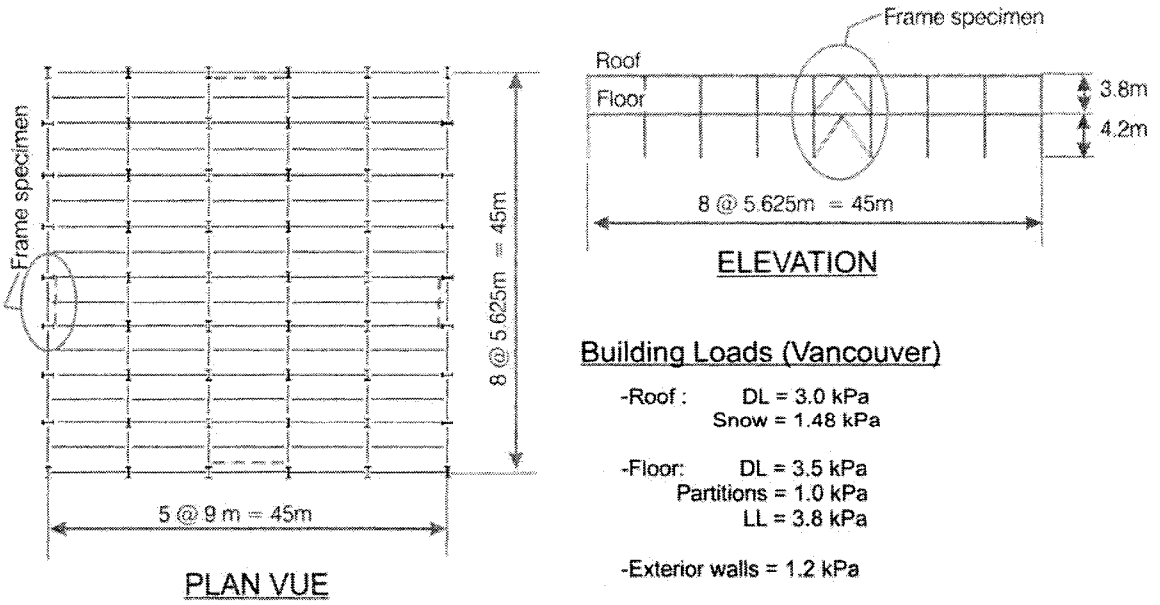

Figure 5.2: Option 1 – Building characteristics and design loads.

The prototype is a 5.625 m x 8 m 2-storey frame with a lateral tributary seismic mass equal to half the buildings' mass. The vertical loads in the columns are equal to the loads of the roof and floor tributary to the columns. Following are the calculations performed to obtain these values, where *TA* is the tributary area, *p* is the perimeter of the building tributary to the frame and *H* is the height of the exterior wall.

- Seismic mass (prototype):

$$TA = \frac{45m \times 45m}{2} = 1012.5m^2$$

$$p = \frac{2 \times (45m + 45m)}{2} = 90m$$

i. Roof mass

$$H_{wall} = \frac{1}{2} \times 3.8m = 1.9m$$

$$m_{\text{roof}} = \{(\text{DL}_{\text{roof}} + 25\%\text{Snow}) \times TA + \text{DL}_{\text{wall}} \times H_{\text{wall}} \times p\} \times \frac{1000}{g}$$

$$m_{\text{roof}} = \{(3.0kPa + (0.25) \times 1.48kPa) \times 1012.5m^2 + 1.2kPa \times 1.9m \times 90m\} \times \frac{1000}{9.81m/s^2}$$

$$m_{\text{roof}} = 368735kg$$

ii. Floor mass

$$H_{wall} = \frac{1}{2}(4.2m + 3.8m) = 4.0m$$

$$m_{\text{floor}} = \left\{\left(\text{DL}_{\text{floor}} + \frac{1}{2}\text{DL}_{\text{partitions}}\right) \times TA + \text{DL}_{\text{wall}} \times H_{\text{wall}} \times p\right\} \times \frac{1000}{g}$$

$$m_{\text{roof}} = \left\{\left(3.5kPa + \frac{1}{2} \times 1.0kPa\right) \times 1012.5\,m^2 + 1.2kPa \times 4.0m \times 90m\right\} \times \frac{1000}{9.81m/s^2}$$

$$m_{\text{floor}} = 456880kg$$

- Vertical loads (prototype):

$$TA = \frac{9m \times 5.625m}{2} = 25.31m^2$$

i. Roof load

$$P_{DL(roof)} = DL_{roof} \times TA$$

$$P_{DL(roof)} = 3.0kPa \times 25.31m^2$$

$$P_{DL(roof)} = 75.93kN \cong 76kN$$

ii. Floor load

$$P_{DL(floor)} = (DL_{roof} + DL_{partitions}) \times TA$$

$$P_{DL(floor)} = (3.5kPa + 1.0kPa) \times 25.31m^2$$

$$P_{DL(floor)} = 113.9kN \cong 114kN$$

This frame is taken directly from the parametric study. It had been designed for the seismic demand of Vancouver, using a spectral analysis with a ductility factor R_d equal to 3.0, an over-strength factor R_o equal to 1.3 and a C Site Class, as explained in Chapter 4. The prototype frame is illustrated in Figure 5.3, as well as the equivalent model frame using scale factors of α = 1/3 and β = 3.0. These scale factors were chosen to limit the total lateral mass of the laboratory model to 30 000 kg.

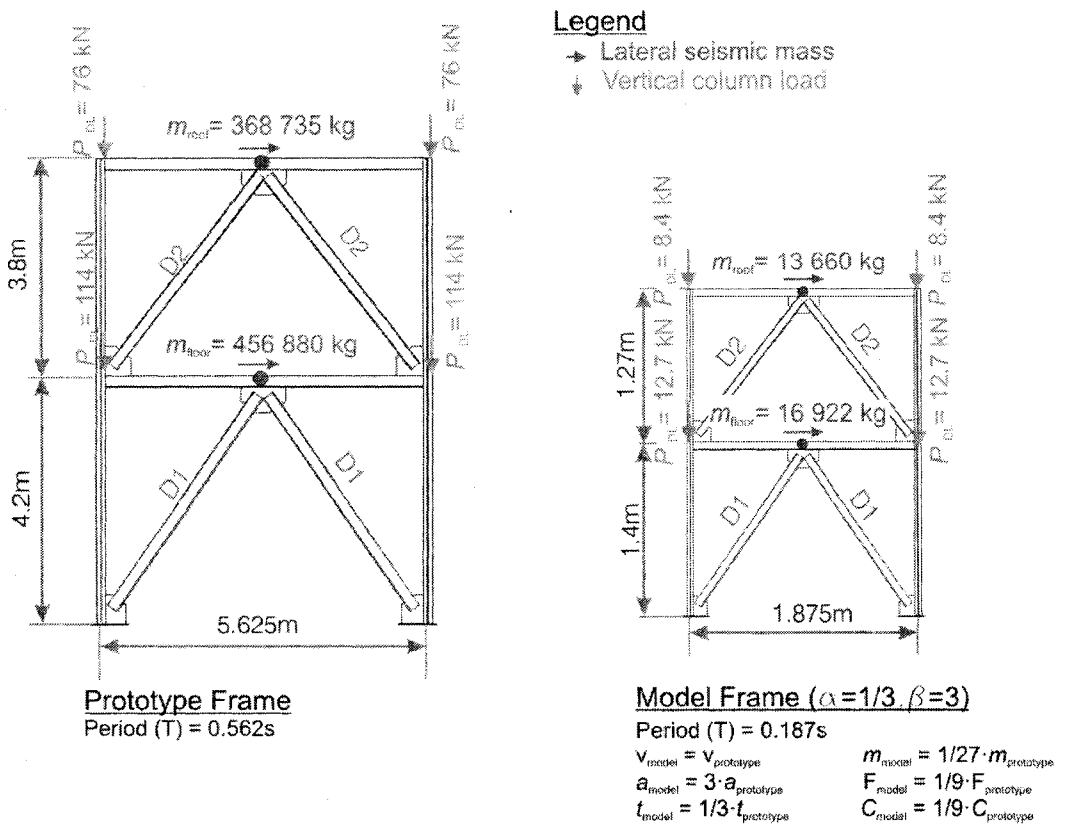

		Prototype Frame			Model Frame		
Frame Properties	Element	Section	As (mm^2)	I_x (mm^4)	Section	As (mm^2)	I_x (mm^4)
	Diagonals D1	HSS 178x178x9.5	5620	---	---	624	---
	Diagonals D2	HSS 152x152x9.6	4740	---	---	527	---
	Columns	W8x21	4000	$31.4x10^6$	---	444	0.39x106
	Beam roof	W12x19	3610	$54.3x10^6$	---	401	0.67x106
	Beam floor	W16x26	4990	$127x10^6$	---	554	1.56x106
Damper Properties	Element	Damping (C) (kN·s/m)	Stiffness (k) (kN/m)		Damping (C) (kN·s/m)	Stiffness (k) (kN/m)	
	Damper (γ=0.25)	500	$3.0x10^6$		55.6	$1.0x10^6$	

Figure 5.3: Option 1 – Properties of the prototype and model frame structures.

This option has several advantages over the other options described later. Firstly, the prototype building is taken directly from the parametric study. This is interesting due to the fact that the response of this building has already been analysed in depth (Chapter 4). Direct comparison between the test results and the results obtained from the numerical analysis models used in the parametric study would then have been possible. Secondly, the velocity of the model is equal to the velocity of the prototype. Considering

that velocity is the principal parameter involved in the behaviour of a viscous damper, this is thought to be an interesting advantage.

However, this option was not selected because it also has disadvantages that outweigh its advantages. The model frame has very small dimensions. With a scale factor $\alpha = 1/3$, the dimensions of the model are reduced by a factor of 3.0. The area of the sections is reduced by a factor of 9.0 and the moment of inertia of the cross-sections is reduced by a factor of 81. No existing steel shapes can satisfy these properties and a trade-off would have been necessary. In addition, the resulting damping coefficient C of the model dampers is reduced significantly to a value of 55.6 kN-s/m. The supplier of the dampers had indicated that this coefficient should be between 100 and 1000 kN-s/m for good performance. Therefore, this option's damping coefficient value is below the range of efficiency.

5.3.2. Option 2 – single-storey building with 1:1 scaling ratio for geometric dimensions

The second option for the prototype is a single-storey exterior braced frame taken from a building with a roof composition and a braced frame arrangement established to obtain a model with a scale factor α equal to 1.0, thus a 1:1 ratio for the model geometric dimensions, while limiting the total lateral mass to 30 000 kg using an acceleration ratio $\beta = 3.0$. This building represents a typical commercial building, such as a large retail store. Figure 5.4 illustrates the characteristics of the building used for this option.

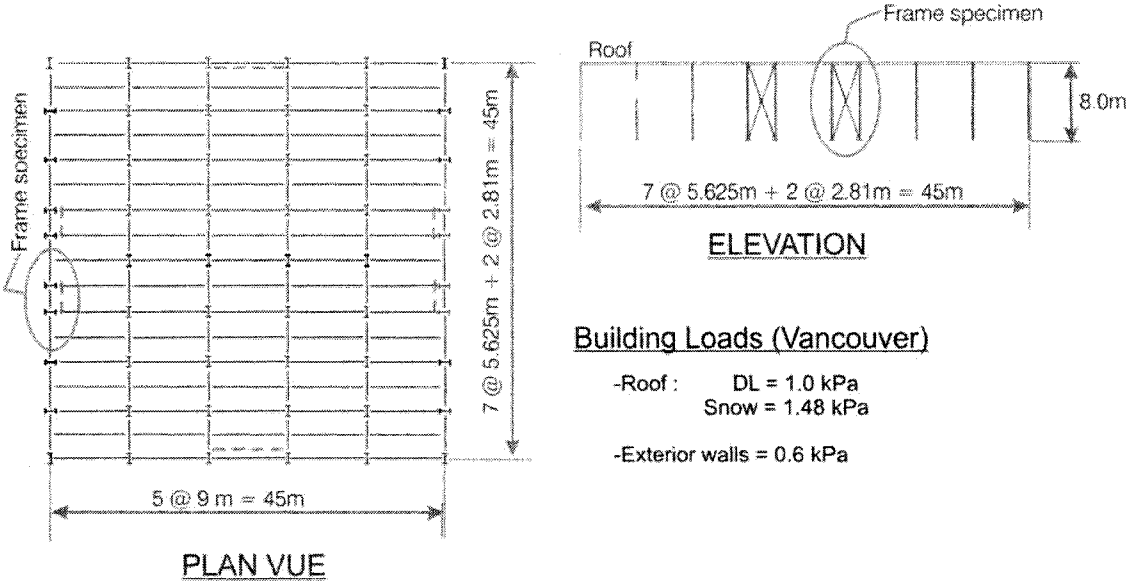

Figure 5.4: Option 2 – Building characteristics and design loads.

The prototype frame is a 2.81 m x 8 m single-storey frame with a lateral tributary seismic mass equal to one-quarter of the buildings mass. The vertical loads in the columns are equal to the loads of the roof tributary to the columns. Following are the calculations performed to obtain these values. The prototype frame is illustrated in Figure 5.5, as well as the equivalent model frame. The steel sections for the frame were selected following a preliminary design using a spectral analysis for the seismic demand of Vancouver, considering a system with a ductility factor R_d equal to 2 and an over-strength factor R_o equal to 1.3 corresponding to a concentrically braced tension only SFRS with limited ductility (NBCC, 2005).

- Seismic mass (prototype):

$$TA = \frac{45m \times 45m}{4} = 506.25m^2$$

$$p = \frac{2 \times (45m + 45m)}{4} = 45m$$

i. Roof mass

$$H_{wall} = \frac{1}{2} \times 8.0m = 4.0m$$

$$\mathrm{m_{roof}} = \{(\mathrm{DL_{roof}} + 25\%\mathrm{Snow}) \times TA + \mathrm{DL_{wall}} \times H_{\mathrm{wall}} \times p\} \times \frac{1000}{g}$$

$$m_{\mathrm{roof}} = \{(1.0kPa + (0.25) \times 1.48kPa) \times 506.25\,m^2 + 0.6kPa \times 4.0m \times 45m\} \times \frac{1000}{9.81m/s^2}$$

$$m_{\mathrm{roof}} = 81709kg$$

- Vertical loads (prototype):

$$TA = \frac{9m \times (2.81m + 5.625m)}{4} = 18.98m^2$$

i. Roof load

$$P_{\mathrm{DL(roof)}} = \mathrm{DL_{roof}} \times TA$$

$$P_{\mathrm{DL(roof)}} = 1.0kPa \times 18.98m^2$$

$$P_{\mathrm{DL(roof)}} = 18.98kN \cong 19kN$$

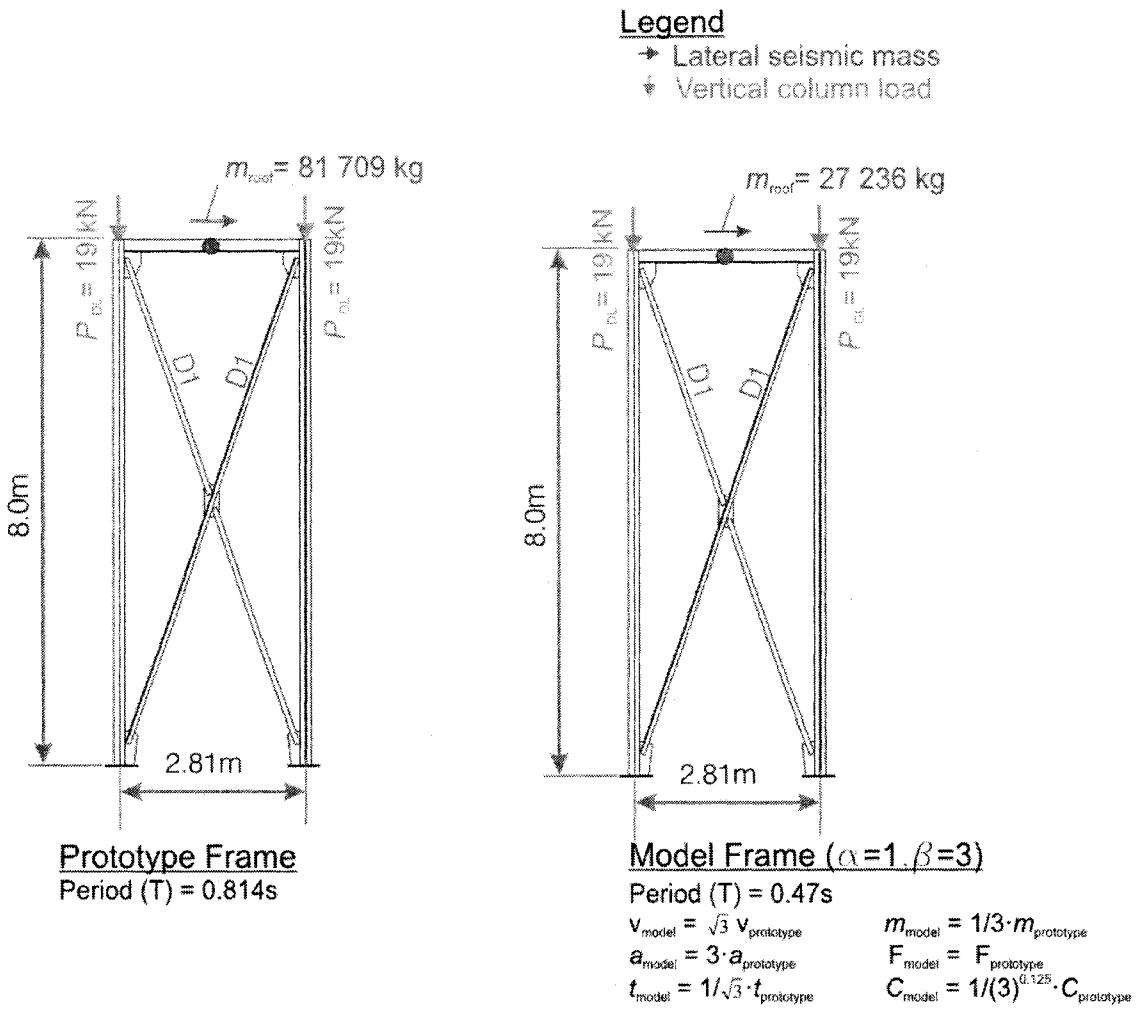

		Prototype Frame			Model Frame		
Frame Properties	Element	Section	As (mm^2)	I_x (mm^4)	Section	As (mm^2)	I_x (mm^4)
	Diagonals D1	2-L3x3x5/16	2170	---	2-L3x3x5/16	2170	---
	Columns	W8x10	1900	$12.7x10^6$	W8x10	1900	$12.7x10^6$
	Beam roof	W12x19	3610	$54.3x10^6$	W12x19	3610	$54.3x10^6$
Damper Properties	Element	Damping (C) (kN·s/m)	Stiffness (k) (kN/m)		Damping (C) (kN·s/m)	Stiffness (k) (kN/m)	
	Damper (γ=0.25)	500	$3.0x10^6$		436	$1.0x10^6$	

Figure 5.5: Option 2 – Properties of the prototype and model structures.

This option has certain advantages over the other ones. Firstly, with α = 1.0, the dimensions of the model are equal to the dimensions of the prototype. This is interesting due to the fact that all the steel sections required for the model are existing sections.

Secondly, the properties of the dampers in the model are practically unchanged, which is an important advantage. This option was not selected however because the characteristics of the braced frame, although advantageous, had no relevance to the parametric study presented previously. Single-storey buildings were indeed not considered.

5.3.3. Option 3 – Modified version of option 1

The third option for the prototype is a modified version of the first option. It is a 2-storey braced frame from a building taken from the parametric study, but with a modified roof composition (lighter), additional bracings and added columns to obtain a model specimen with scale factors α and β equal to 1/2 and 3.0, respectively, while limiting the total lateral mass to 30 000 kg as well as the vertical mass on the seismic table. Figure 5.6 illustrates the characteristics of the building used for this option.

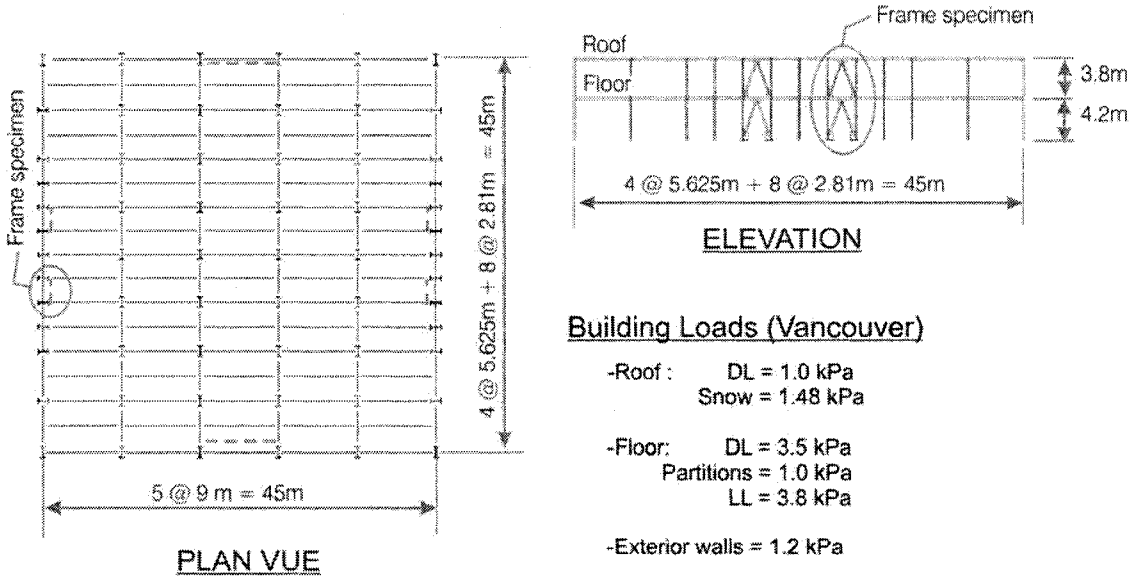

Figure 5.6: Option 3 – Building characteristics and design loads.

The prototype is a 2.81 m x 8 m 2-storey frame with a lateral tributary seismic mass equal to one-quarter of the buildings mass. The vertical loads in the columns are equal to the loads of the roof and the floor tributary to the columns. Following are the calculations performed to obtain these values. The prototype frame is illustrated in Figure 5.7, as well as the equivalent model frame using scale factors of α = 1/2 and β = 3.0. The steel sections for the frame were selected following a preliminary design using a spectral analysis for the seismic demand of Vancouver, considering a system with a ductility factor R_d equal to 3.0 and an over-strength factor R_o equal to 1.3 (concentrically braced chevron SFRS with moderate ductility).

- Seismic mass (prototype):

$$TA = \frac{45m \times 45m}{4} = 506.25m^2$$

$$p = \frac{2 \times (45m + 45m)}{4} = 45m$$

i. Roof mass

$$H_{wall} = \frac{1}{2} \times 3.8m = 1.9m$$

$$m_{roof} = \{(\mathrm{DL}_{roof} + 25\%\mathrm{Snow}) \times TA + \mathrm{DL}_{wall} \times H_{wall} \times p\} \times \frac{1000}{g}$$

$$m_{roof} = \{(1.0kPa + (0.25) \times 1.48kPa) \times 506.25m^2 + 1.2kPa \times 1.9m \times 45m\} \times \frac{1000}{9.81m/s^2}$$

$$m_{roof} = 81152kg$$

ii. Floor mass

$$H_{wall} = \frac{1}{2}(4.2m + 3.8m) = 4.0m$$

$$m_{floor} = \left\{\left(\mathrm{DL}_{floor} + \frac{1}{2}\mathrm{DL}_{partitions}\right) \times TA + \mathrm{DL}_{wall} \times H_{wall} \times p\right\} \times \frac{1000}{g}$$

$$m_{roof} = \left\{\left(3.5kPa + \frac{1}{2} \times 1.0kPa\right) \times 506.25m^2 + 1.2kPa \times 4.0m \times 45m\right\} \times \frac{1000}{9.81m/s^2}$$

$$m_{floor} = 228440kg$$

- Vertical loads (prototype):

$$TA = \frac{9m \times 2.81m}{2} = 12.7m^2$$

i. Roof load

$$P_{DL(roof)} = DL_{roof} \times TA$$

$$P_{DL(roof)} = 1.0kPa \times 12.7m^2$$

$$P_{DL(roof)} = 12.7kN \cong 13kN$$

ii. Floor load

$$P_{DL(floor)} = (DL_{roof} + DL_{partitions}) \times TA$$

$$P_{DL(floor)} = (3.5kPa + 1.0kPa) \times 12.7m^2$$

$$P_{DL(floor)} = 57.2kN \cong 57kN$$

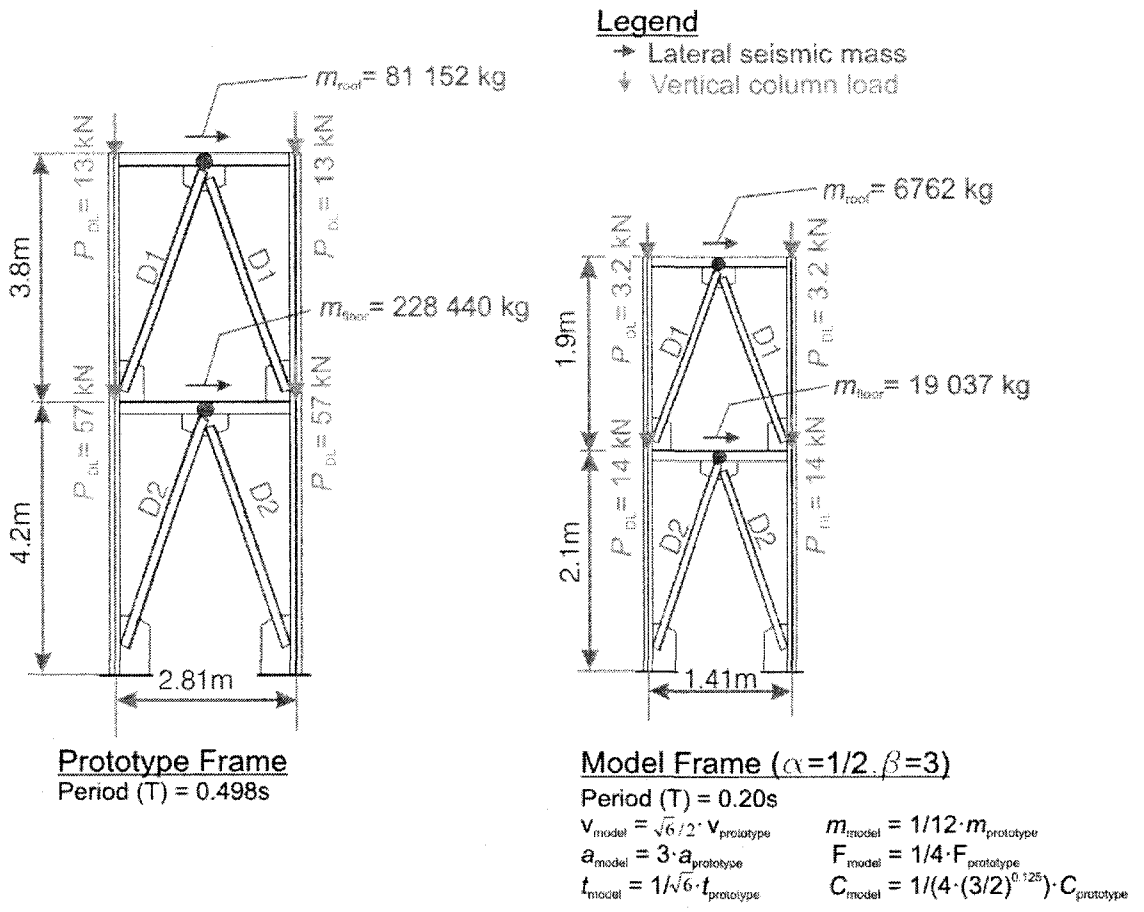

		Prototype Frame			Model Frame		
Frame Properties	Element	Section	As (mm^2)	I_x (mm^4)	Section	As (mm^2)	I_x (mm^4)
	Diagonals D1	HSS 152x152x13	6110	—	—	1528	—
	Diagonals D2	HSS 102x102x13	3790	—	—	948	—
	Columns	W8x28	5310	40.9×10^6	—	1328	2.6×10^6
	Beam roof	W8x10	1900	12.7×10^6	—	475	0.79×10^6
	Beam floor	W8x10	1900	12.7×10^6	—	475	0.79×10^6
Damper Properties	Element	Damping (C) (kN·s/m)	Stiffness (k) (kN/m)		Damping (C) (kN·s/m)	Stiffness (k) (kN/m)	
	Damper (γ=0.25)	500	3.0×10^6		119	1.5×10^6	

Figure 5.7: Option 3 – Properties of the prototype and model structures.

This option was the one selected for the laboratory test program for the following reasons. Firstly, the prototype building is very similar to those used in the parametric study; a 2-storey 45 m x 45 m building with a height of 8 m. Secondly, with $\alpha = 1/2$, the dimensions of the test model are of reasonable size to adequately reproduce the actual

building response. Thirdly, the resulting characteristics of the dampers in the model are within the range of efficient performance according to the manufacturer. The only disadvantage of this option is that with a reduction factor of 4 on the area and of 12 on the inertia of the sections, compromises are necessary with regards to the laws of similitude for the selection of the steel sections for the laboratory model. The effects of these compromises are discussed later in this chapter.

5.4. Validation of the similitude law requirements

The prototype and the model structures were analysed numerically using the SAP2000 structural finite element computer program (CSI, 2007). A nonlinear direct integration analysis considering the P-delta effects was performed for both the prototype and the model structures using a simple 2D finite element frame model. Material nonlinearity was however not included in the analysis and proportional damping was not added to the numerical models because it was believed that it would not be conservative to consider additional damping on top of the damping already provided by the seismic dampers. The Newmark time integration method was used with an output time step of 0.05 seconds for the prototype structure and 0.0204 seconds for the model structure according to similitude requirements. Three acceleration time-history records were used for comparison purposes, one from each city used in the parametric study: Montreal (E08), Vancouver (H09) and Los Angeles (LA31). A description of each seismic record is presented in Chapter 4. The amplitude and time scale of the seismic inputs were scaled using the adopted similitude laws for the model structure.

A numerical model of the seismic dampers was included at the base of the frame. It was created with a dashpot and a gap element acting in parallel. This numerical model was explained in depth in Chapter 4. Vertical masses equal to $P_{DL}/9.81 m/s^2$ were assigned to the beam/column joints to represent the gravity loads. The seismic masses, the vertical weights and the properties for the dampers used for the prototype and the model structures, are illustrated in Figure 5.7. The properties indicated for the dampers

characterize the dashpot and the gap elements combined. For the prototype structure, the dashpot element had a damping coefficient C equal to 500 kN-s/m and the dashpot and gap elements had each a rigidity k equal to $1.5\text{x}10^6$ kN/m, yielding a total rigidity equal to $3.0\text{x}10^6$ kN/m. For the model structure, the dashpot element had a damping coefficient C equal to 119 kN-s/m and both the dashpot and gap elements had a rigidity $\boldsymbol{k}$ equal to $0.75\text{x}10^6$ kN/m each, for a total rigidity equal to $1.5\text{x}10^6$ kN/m. Figure 5.8 illustrates the simple 2-dimensional finite element frame analysed using SAP2000.

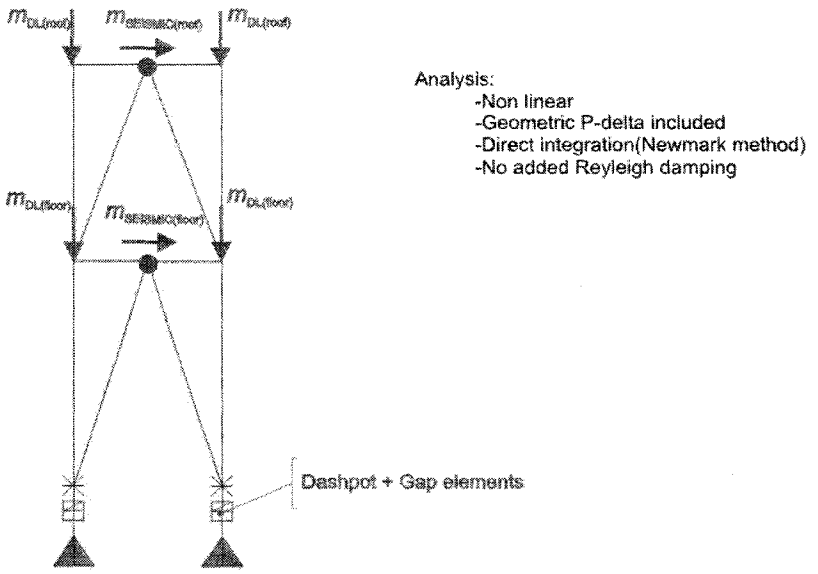

Figure 5.8: Finite element model of the theoretical model structure.

Figures 5.9 to 5.11 illustrate the results of the comparison between the prototype and the model structures for the seismic inputs E08, H09 and LA31 respectively. The results are very conclusive; the superimposed curves demonstrate that the selected similitude method is very efficient. The displacement responses and the vertical reactions (axial load in the dampers) of the two structures are perfectly matched. However, the axial loads in the columns and the diagonal braces, the base shear and the acceleration responses have the exact peaks and valleys, but the amplitude values for the model structure are slightly greater than those for the prototype structure.

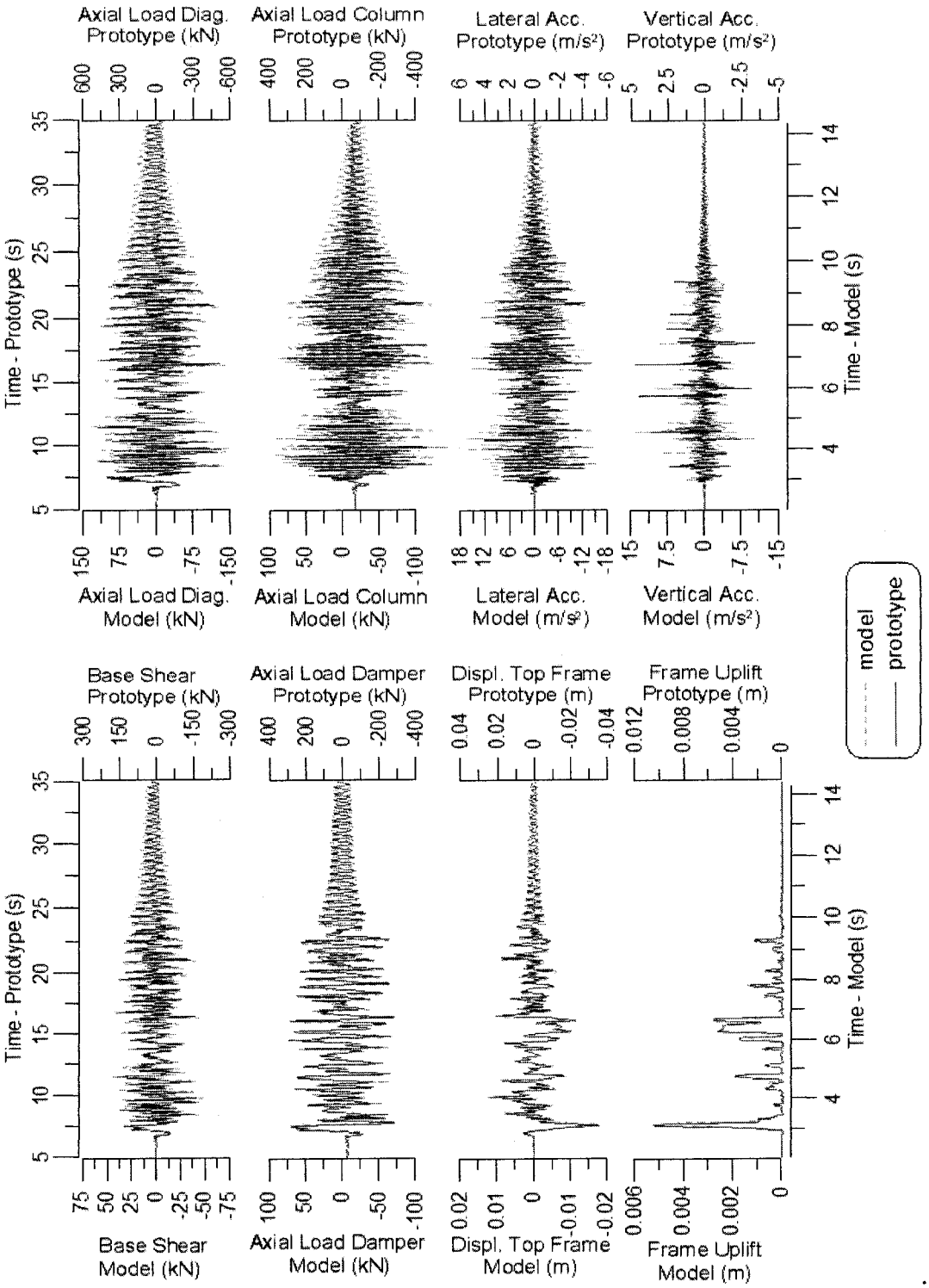

Figure 5.9: Comparison between the responses of the prototype and the model submitted to ground motion E08.

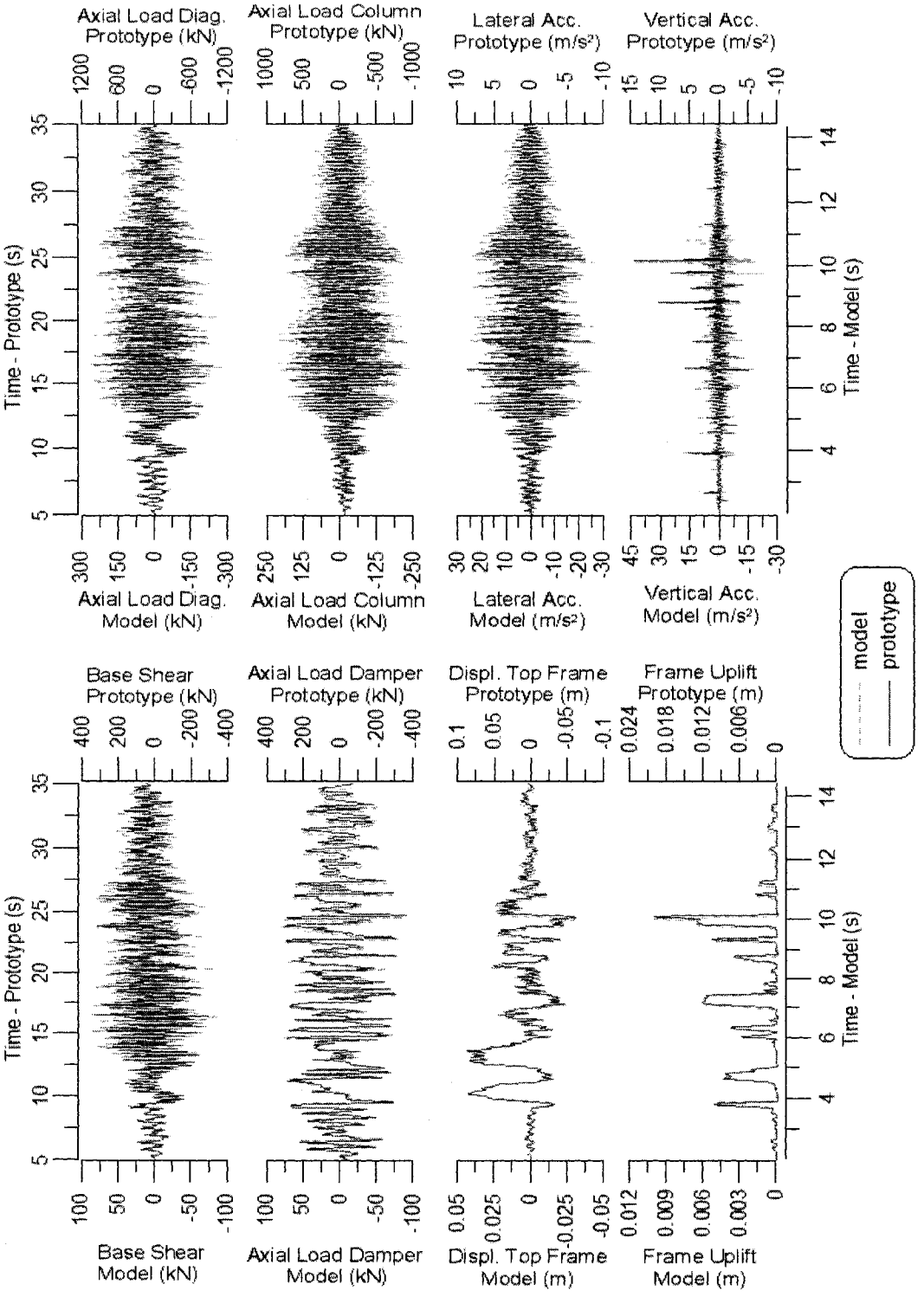

Figure 5.10: Comparison between the responses of the prototype and the model submitted to ground motion H09.

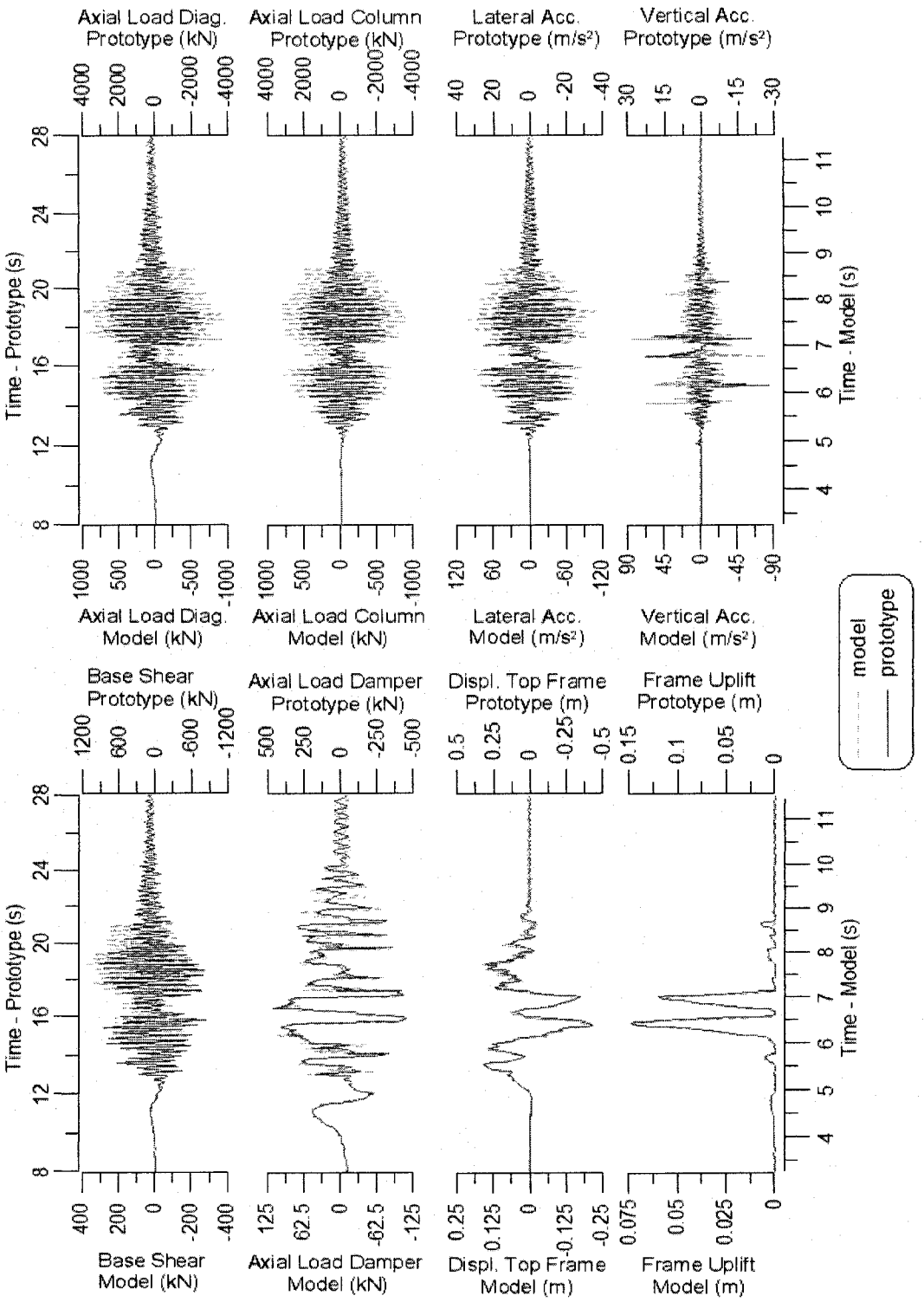

Figure 5.11: Comparison between the responses of the prototype and the model submitted to ground motion LA31.

As mentioned previously, by using the modified acceleration similitude procedure with an acceleration factor β equal to 3, which scales the accelerations of the model, we are unable to respect the laws of similitude for the vertical gravitation acceleration (g). The right vertical loads are nevertheless obtained by assigning masses (m_{DL}) equal to $P_{DL}/9.81$ m/s^2 and a vertical acceleration equal to 9.81 m/s^2 (1g). However, we questioned ourselves on whether this would have an influence on the response of the model, since the vertical mass inertia and the third mode of vibration (vertical axial mode) of the frame were not exact. Considering the imperfections observed between the model and the prototype structures, an analysis was performed using a second numerical model of the model structure with the laws of similitude perfectly respected. A vertical acceleration βg = 3 x 9.81 m/s^2= 29.43 m/s^2 is considered and the vertical loads are obtained using masses (m_{DL}) equal to $P_{DL}/29.43$ m/s^2. Figure 5.12 illustrates the comparison between the numerical results for the prototype structure and the two model structures subjected to ground motion H09. The Figure presents the base shear, the column axial load and the vertical and lateral acceleration responses between the 25th and 26th seconds of the analysis (prototype time). The response of the new model and the prototype are perfectly matched. The analysis demonstrates that by not following the laws of similitude for the vertical acceleration, imperfections exist between the response of the prototype and the model structures. The same was observed for the E08 and LA31 ground motions.

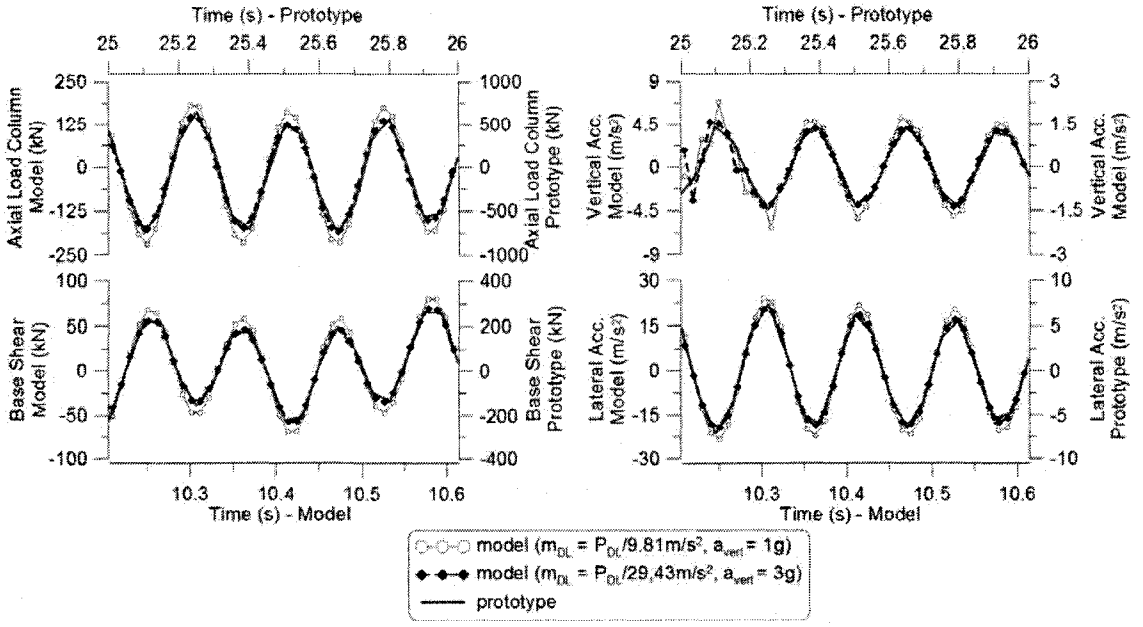

Figure 5.12: Comparison to evaluate the effects of the vertical acceleration (H09).

The values $P_{DL}/29.43$ m/s^2 could have been used in the test but member forces and stresses due to gravity loads would have been incorrect as the acceleration due to gravity in the laboratory could not be increased by 3.0. The decision was made to use masses equal to $P_{DL}/9.81$ m/s^2. It is noted that the only consequence of this shortcoming is that the model does not exactly represent the prototype. As discussed in the next section, other factors were to lead to small deviations from strict compliance to similitude requirements and it was anticipated that the model would not be exact. The main objective of the test program was to validate the numerical models used in the parametric study. Although a model as close as possible to the prototype structure is desirable, this validation is still possible with an imperfect model provided that the conditions that prevail in the laboratory are properly reproduced in the numerical model.

5.5. Laboratory test specimen

The laboratory test specimen was designed to replicate to the highest degree of accuracy the properties of the selected model structure previously described in Figure 5.7. However, the laboratory test specimen was built using existing steel sections. Therefore, the properties of the diagonals, the columns and the beams do not respect entirely the laws of similitude. The width, height, vertical column weight and the lateral seismic masses did however respect nearly perfectly the laws of similitude. Figure 5.13 illustrates schematically the characteristics of the test specimen fixed on the earthquake simulator.

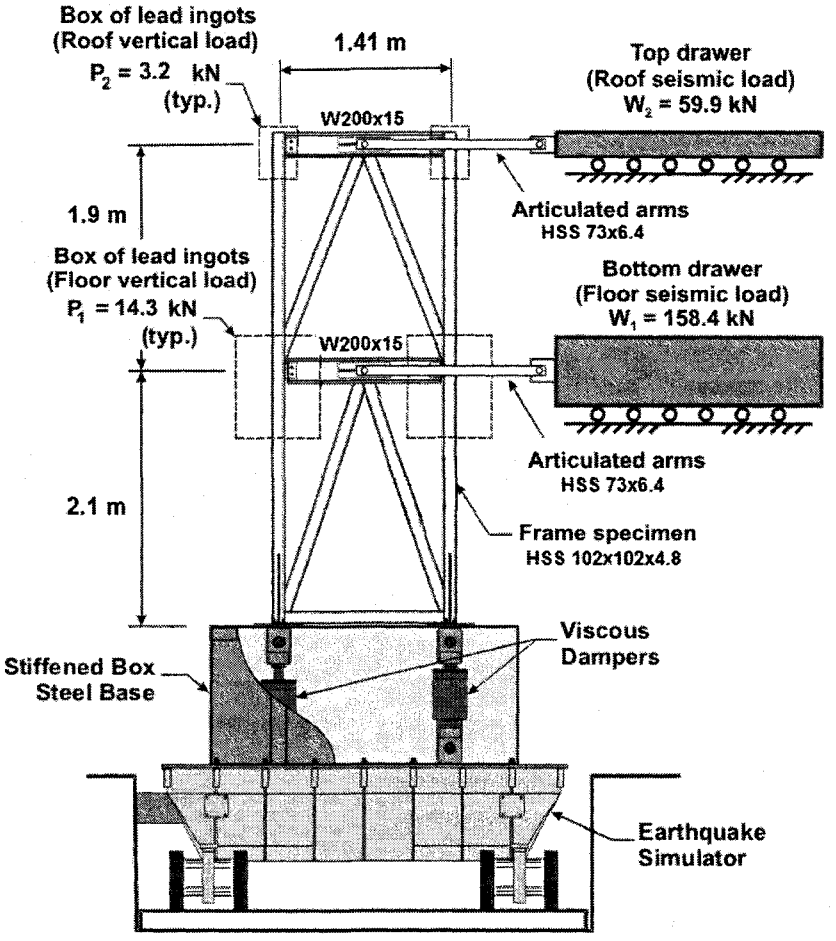

Figure 5.13: Illustration of the test specimen (adapted from Tremblay and al., 2008).

As illustrated in Figure 5.13, the test frame was installed on top of a stiffened steel casing, which was designed to enclose the viscous dampers supplied by LCL-Bridge Technology Products Inc, while providing enough rigidity to insure a synchronised movement between the table and the base of the frame. The vertical masses at the beam/column joints were obtained using lead ingots placed in steel casings rigidly connected to the frame. The lateral seismic masses were obtained by using a combination of concrete blocs and 25 mm thick steel plates mounted on guided roller bearings running on smooth stainless steel plates. These masses were connected to the test specimen by the means of pin-ended HSS73x6.4 steel tubes. An independent 2-storey steel structure was built next to the earthquake simulator to support the lateral masses. A more detailed description of the test specimen and the components of the test program setup are presented in chapter 7. A 3-dimensional render of the laboratory test setup is presented in Figure 5.14. A complete set of the structural construction blueprints are presented in Appendix G.

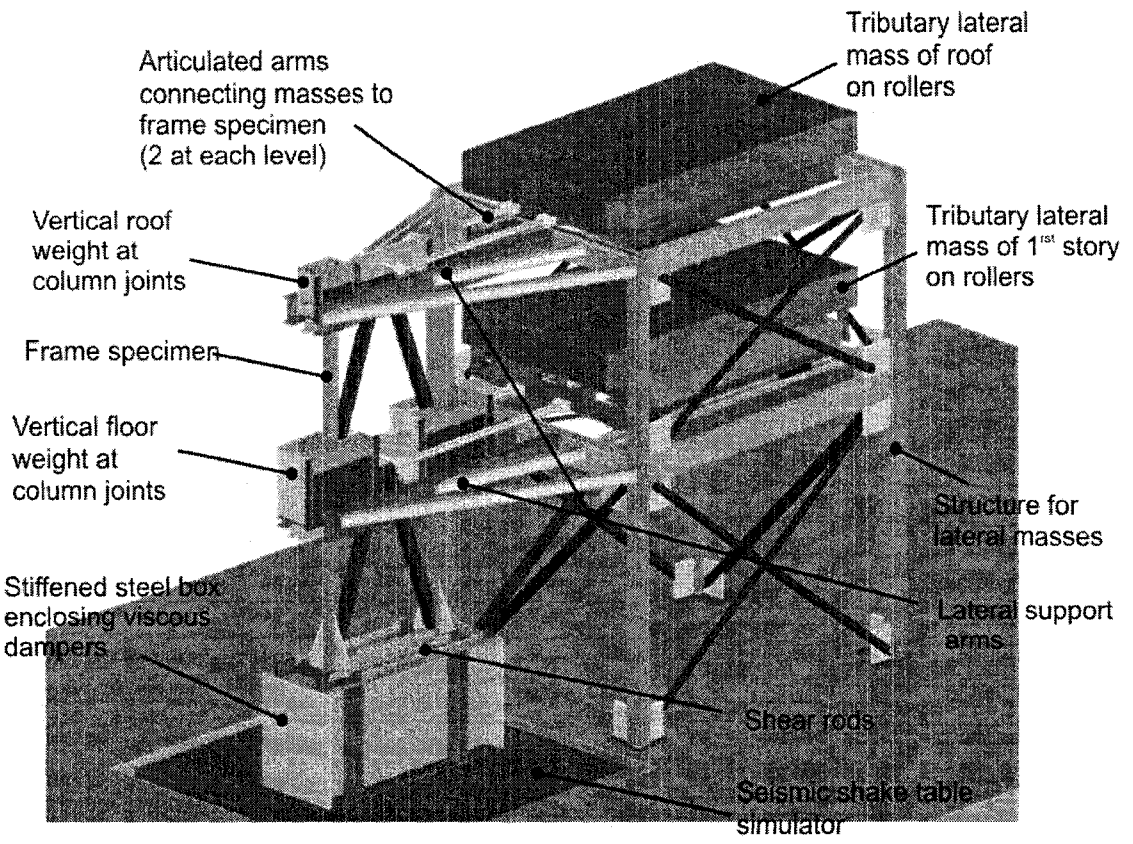

Figure 5.14: Laboratory test setup.

Numerical analyses using SAP2000 were performed to reproduce the response of the laboratory test specimen. The results of these analyses were compared to the results of the theoretical model structure (Figure 5.8) to evaluate the effects of the differences between the two structures. Also, these numerical analyses were used to calibrate the seismic ground inputs selected for the shake table test program. The construction blueprints were used to build the numerical model. This numerical model was a 2D replica of the laboratory test setup, thus the real steel sections were used. The rigid steel box and the seismic shake table simulator were included in the model as well as their masses. The exact weight of the lateral mass drawers and the vertical load boxes were calculated and included in the numerical analysis. The masses of the drawers were assigned to joints on rollers connected to the frame by the means of steel tubes. The

masses of the vertical load boxes including the mass of the lead ingots were assigned to the beam/column joints of the frame. Nonlinear analyses were performed using the Newmark method of direct integration with a time step of 0.0204 sec. The P-delta effects were considered. Material nonlinearity was however not included in the analysis and proportional damping was not added to the numerical model. Figure 5.15 illustrates the finite element model of the laboratory test specimen. The values and locations of the masses assigned to the frame are also shown. A diagram indicating the labels of the frame elements and a table listing all the properties of the frame elements used in the numerical model are included in Appendix H. It is noted that even if the masses at the beam-to-column joints were scaled using the acceleration due to gravity, the total mass at each level does comply with the similitude requirements. For instance, at the roof level, the total mass is equal to 6106 kg + 2 x 326.2 kg = 6758 kg, which very closely matches to the required value of 6762 kg (see Figu

re 5.7).

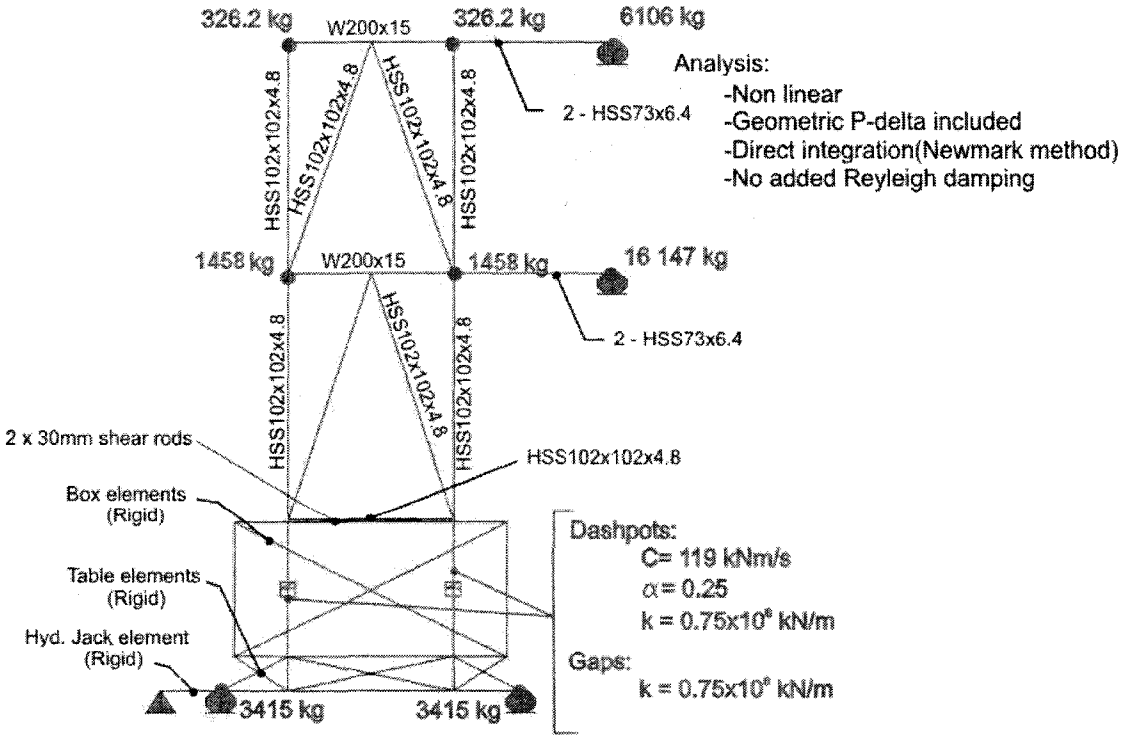

Figure 5.15: Finite element analysis model of the laboratory test specimen.

Figures 5.16 to 5.18 illustrate the results of the comparison between the numerical models of the theoretical model structure and the laboratory test specimen for the seismic inputs E08, H09 and LA31, respectively. It is noticed that the vertical and lateral displacements of the two structures are very similar, as well as the forces in the viscous dampers. However, the magnitudes of the base shear, axial loads in the columns and the diagonal braces and the vertical and lateral acceleration responses for the laboratory model were very different from those of the theoretical model. Additional analyses were performed to explain these differences. It was determined that the W200x15 floor and roof beams were responsible for these differences. The beams used for the laboratory model are 16 times more rigid than what should have been used according to the similitude laws. The stiffness of the beams has an impact on the axial loads in the diagonal members and the columns; therefore altering the base shear and the acceleration responses of the frame. Nevertheless, the general behaviour of the laboratory model is very similar to the behaviour of the theoretical model. Although not perfect considering similitude laws, the performance of the numerical model is satisfactory. Its primary objective is indeed to replicate the behaviour of the actual response of the shake table tests, and not to obtain a perfectly reduced scale test specimen.

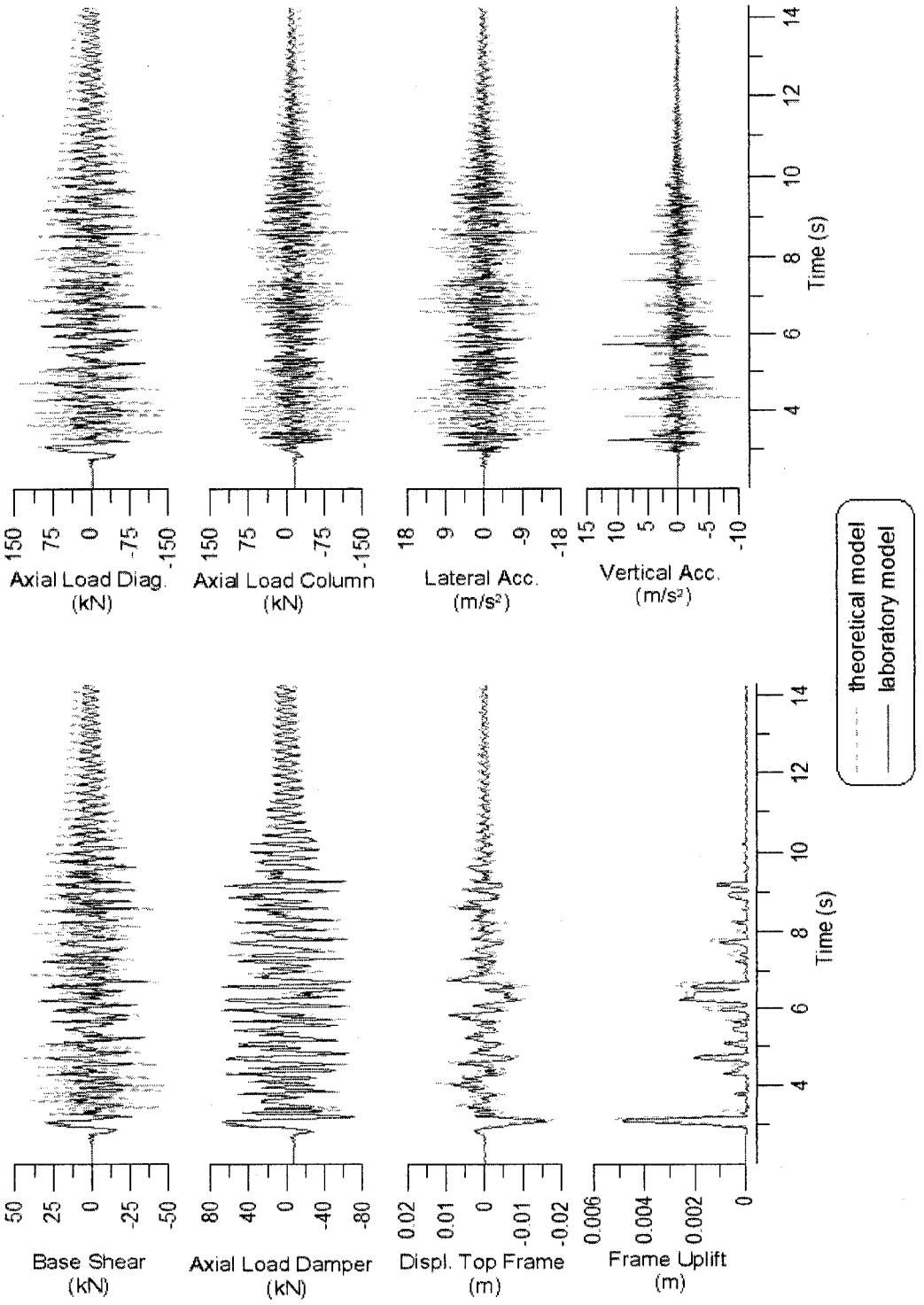

Figure 5.16: Comparison between the responses of the theoretical model and the laboratory model submitted to ground motion E08.

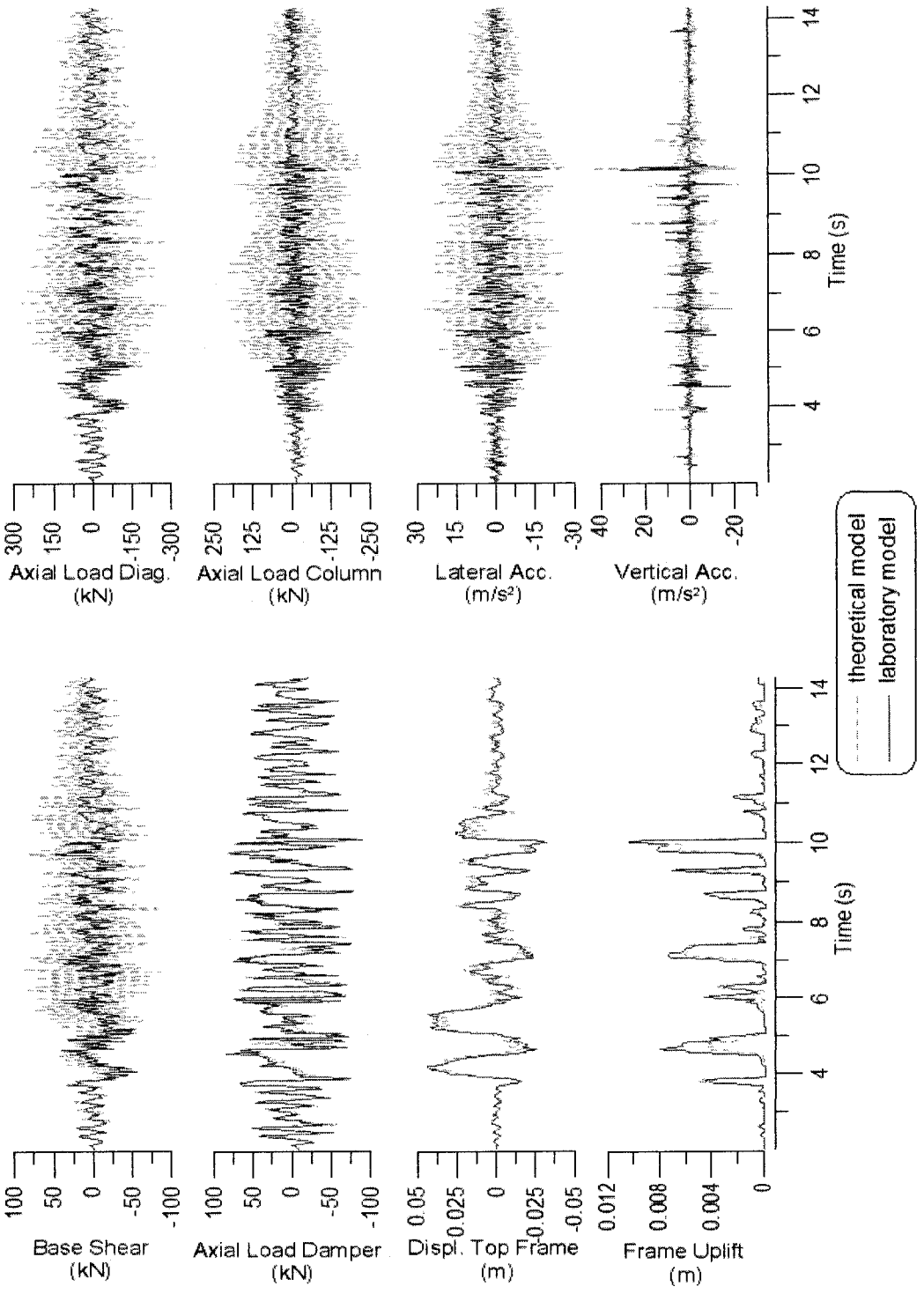

Figure 5.17: Comparison between the responses of the theoretical model and the laboratory model submitted to ground motion H09.

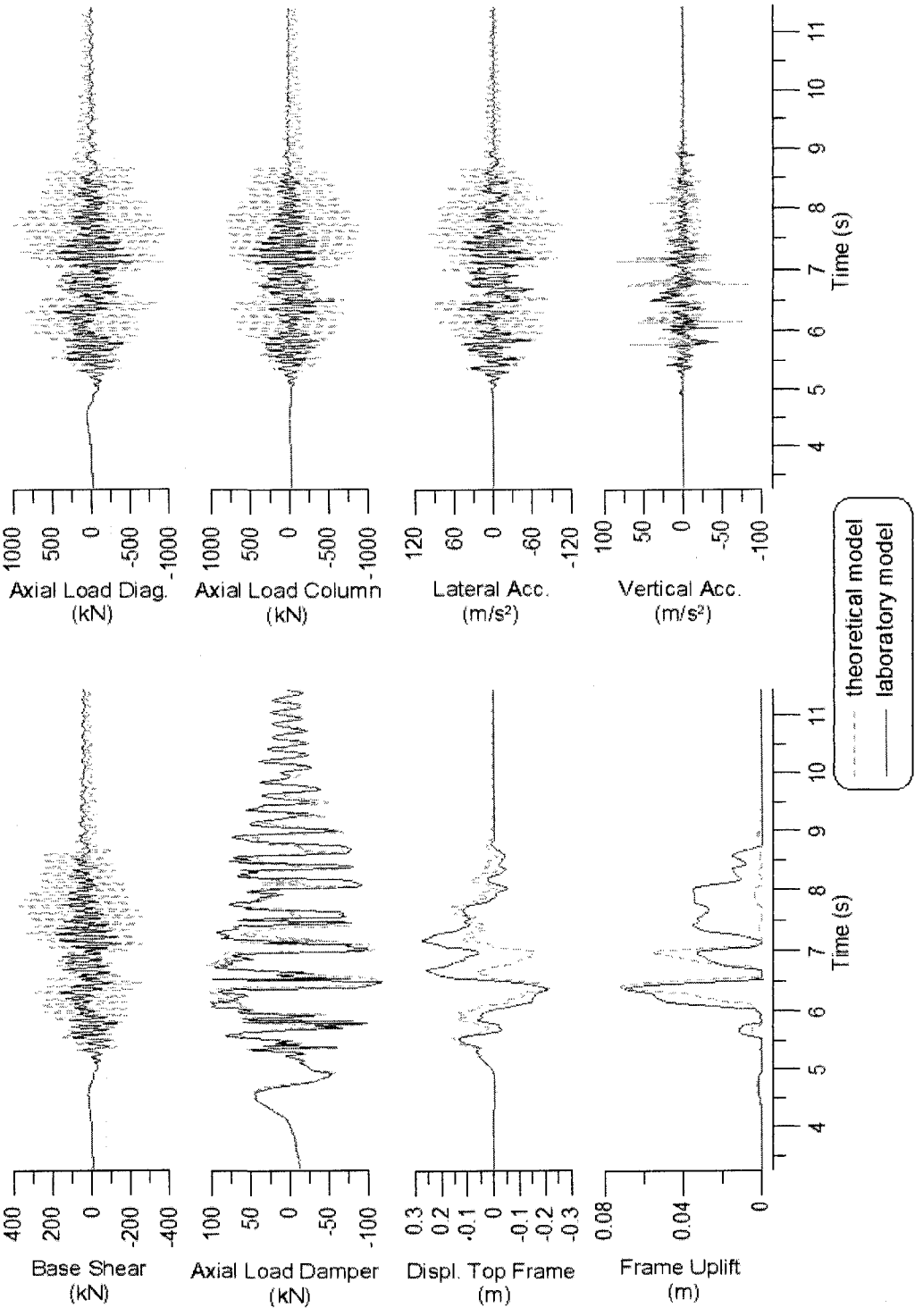

Figure 5.18: Comparison between the responses of the theoretical model and the laboratory model submitted to ground motion LA31.

5.6. Seismic inputs used for the laboratory test program

The acceleration time history records used in the scope of this study were presented previously in Chapter 4. From these 42 time history records, three earthquake records were chosen for each of the three sites: E08, E10 and E12 for Montreal, A04, H06 and H09 for Vancouver and LA28, LA31 and LA37 for Los Angeles.

The numerical model of the laboratory test specimen, presented in Figure 5.15, was used to scale the 9 seismic acceleration records according to the capacity of the earthquake simulator and the capacity of the test frame specimen. As illustrated on Figure 5.1, the shake table is limited to a peak horizontal acceleration, velocity and displacement equal to 3.0 g, 1.2 m/s, and ±125 mm, respectively. The vertical capacity of each of the four linear hydro-static bearings of the simulator is 175 kN and the dynamic capacity of the horizontal hydraulic actuator of the shake table is 220 kN. The maximum permitted uplift of the frame was limited to 75 mm, du to the configuration of the horizontal struts connecting the column bases to the foundations used for the transfer of the horizontal reactions in the laboratory test setup. The maximum axial load in the diagonal and column members was limited to 420 kN and 435 kN, respectively. The axial load in the viscous dampers was limited to 350 kN, which was the limit provided by the manufacturer. Figure 5.19 illustrates the maximum responses obtained for each ground motion. The red lines indicate maximum allowable limits.

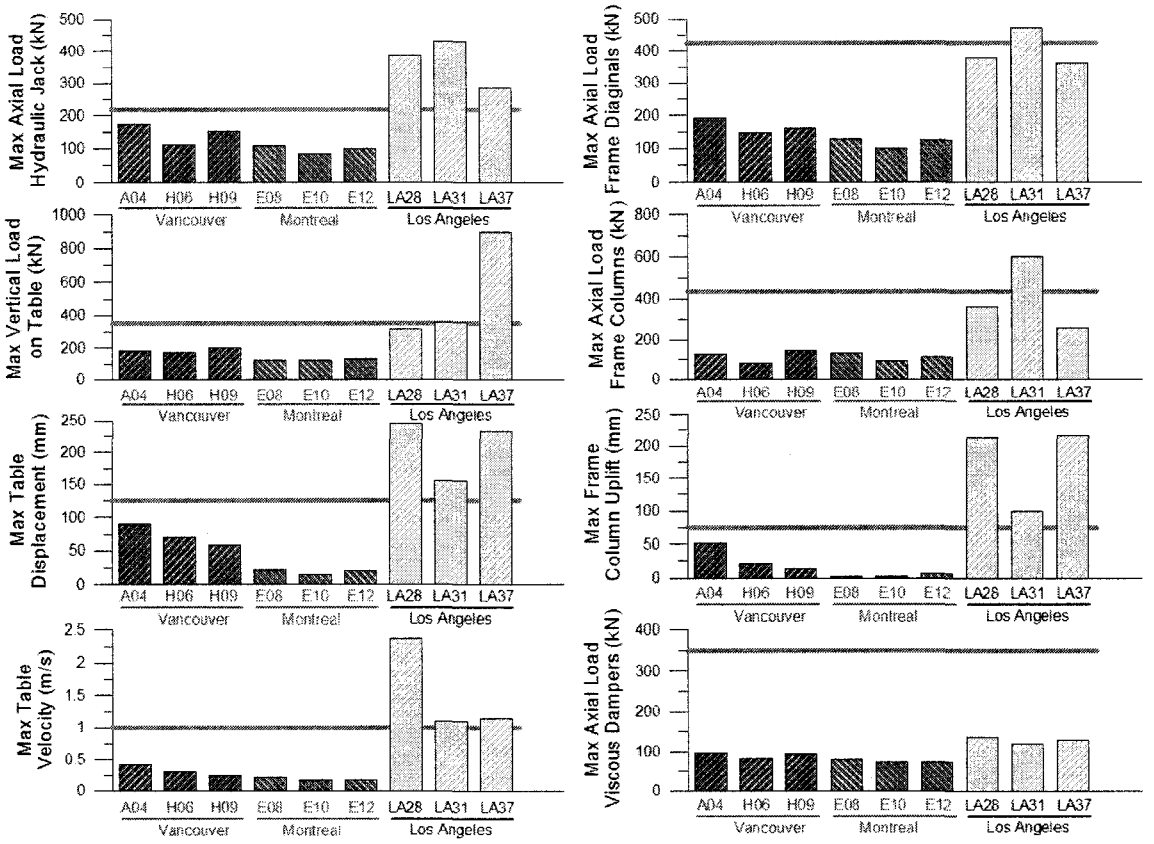

Figure 5.19: Analysis performed to scale the seismic records.

Using these results, the seismic records were scaled according to the capacity of earthquake simulator and the test frame. The magnitudes of the Vancouver records A04, H06 and H09 were left unchanged. The magnitudes of the Montreal records E08, E10 and E12 were scaled by a factor of 2.0. The magnitudes of the Los Angeles records LA28 and LA37 were scaled by a factor of 0.33, while the record LA31 was scaled by a factor of 0.5. The laboratory test setup was designed for the Vancouver ground motion inputs; therefore a scale factor of 1.0 was selected. The scale factors chosen for Montreal were selected to obtain interesting shake table test responses, to maximize the rocking motion of the test specimen, to push the laboratory test setup to its limits without exceeding them. The scale factors chosen for Los Angeles were selected to reduce the ground motion inputs to acceptable limits, considering the constraints of the test setup. Again, the optimum objective of the shake table test program was to validate the

adequacy of the numerical models to accurately reproduce the response of the proposed system and this can be achieved using scaled records. In addition, for all sites, the chosen scaling factors still permit to verify experimentally the response of the VDCSR system under relatively strong ground shaking producing a significant rocking response. It must be realised, however, that no conclusions can be drawn directly from these tests on the seismic performance of the system for the Montreal and Los Angeles sites as the model, including the dampers, was not designed specifically for the scaled ground motions used in the tests.

5.7. Conclusion

The objective of the work described in this chapter was to design a scaled model for the laboratory experimental test program. The modified acceleration similitude law method was selected to scale three prototype building options. One of the options was chosen, resulting in a half-scale model frame specimen for the laboratory.

Numerical analyses were performed to compare the response of the prototype, the theoretical model and the laboratory model. The analyses demonstrated that by following the laws of similitude, the response of the theoretical model was exactly the same as the prototype. However, for the laboratory specimen, certain compromises were required in the selection of the steel frame members. The response of the laboratory model was similar to the prototype, but was not perfectly synchronized, especially the axial forces in the frame members. It was concluded that the performance of the laboratory model was satisfactory, even though it did not respect perfectly the laws of similitude. The primary objective was to obtain a laboratory specimen for the shake table test program and attempt to reproduce it numerically with finite element analyses, not to obtain a perfectly scaled model specimen.

The following chapters present the experimental work performed on the test specimen.

CHAPTER 6

EXPERIMENTAL TEST PROGRAM – PART 1: SEISMIC DAMPERS

6.1. Introduction

The experimental tests were divided into two programs. The first, which is described in this chapter, was used to calibrate and evaluate the behaviour of the viscous dampers. The second program concerns the shake table tests discussed in the next chapter.

The viscous dampers used for the shake table test program were fabricated and supplied by LCL-Bridge Technology Products inc., a company specialized in bridge products such as expansion joints, bearing systems and seismic devices. These dampers are made of a steel cylinder-piston assembly filled with a silicone based fluid material. The viscous dampers were tested independently to validate there performance, verify that their behaviour could be reproduced using the nonlinear relationship adopted in the parametric study, and to calibrate them to the required specifications needed for the shake table test program. The following chapter presents the calibration procedure developed for the viscous dampers, the test program as well as the results of the experimental tests.

6.2. Calibration Procedure

The objective of the calibration procedure was to obtain viscous dampers calibrated to the mechanical properties of the scaled model (shake table specimen), as described in the previous chapter. The dampers supplied to us had been used in a previous experimental program at École Polytechnique de Montreal but their actual characteristics were unknown. Therefore, a test program was developed to evaluate the properties of the dampers in order to supply LCL-Bridge Technology Products inc. with

the data needed to adjust the parameters controlling the flow of the viscous fluid within the damper to obtain the target specifications.

The test program was conducted at the Hydro-Quebec Structural Engineering Laboratory at École Polytechnique of Montreal. The test setup is illustrated in Figure 6.1. The dampers were mounted in a load frame and were subjected to various displacement time histories using a high performance dynamic structural actuator with a force capacity of 1500 kN in tension and compression. The hydraulic actuator had a total stroke capacity of 300 mm and was equipped with a built-in displacement transducer as well as a load cell having a rated capacity of 1700 kN. It was powered by a 1360 lpm hydraulic power supply with 150 l accumulators on both the pressure and return lines. An MTS Flextest GT digital controller with a 2096 Hz internal clock was used to control the actuator.

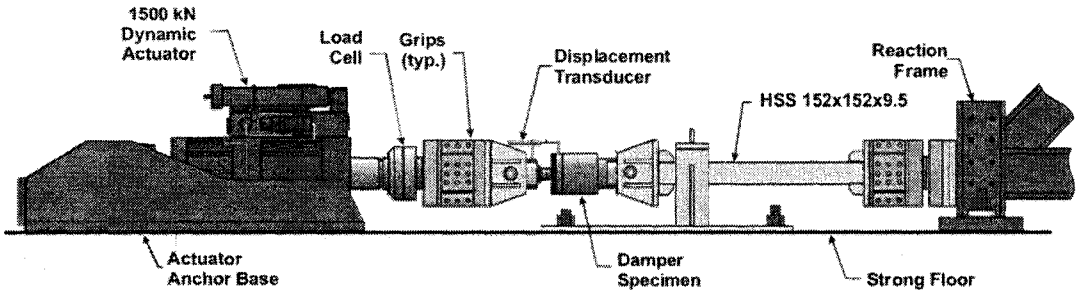

Figure 6.1: Test setup for the damper units (adapted from Tremblay et al. 2008).

Figures 6.2 and 6.3 are pictures of the test setup used for the experimental evaluations. The outputs measured with this setup were the force and the displacement of the damper. The acquisition rate during the tests was 205 Hz (0.0049 sec). The forces in the system were measured by the built-in load cell in the dynamic actuator. An external Linear Variable Differential Transformer (LVDT) was mounted directly to the damper specimen to measure the exact axial displacement of the piston. The displacements applied to the damper were controlled by this external LVDT to avoid unwanted errors du to any imprecision in the test setup. The velocity of the damper was

calculated by integration using the displacement output. Force vs. Displacement and Force vs. Velocity curves were plotted for each of the tests.

Figure 6.2: Picture of the seismic damper.

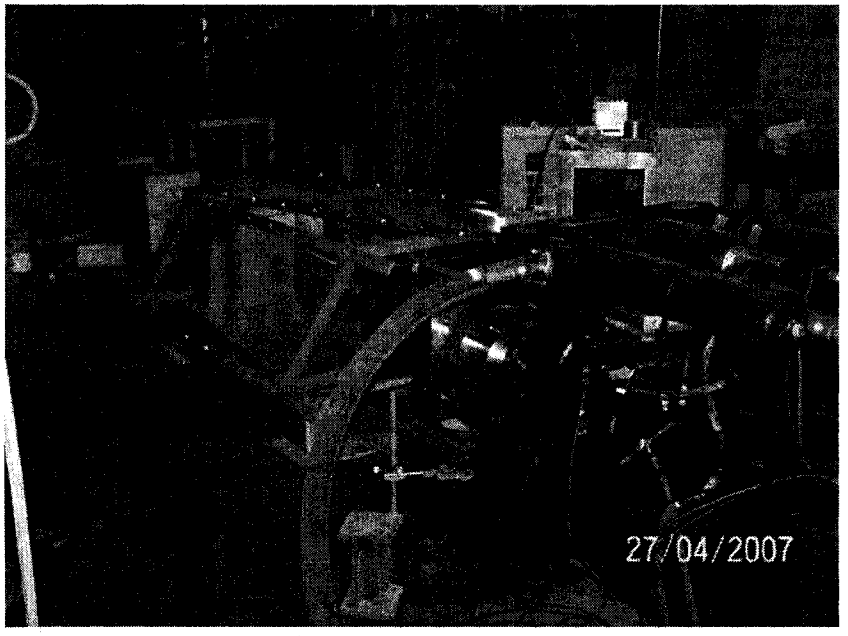

Figure 6.3: Picture of the experimental test setup.

Throughout the test program, the properties of the dampers were progressively modified to cover a wide range of applications. The properties varied from values that would be needed in typical building applications to the properties required for the shake table program. Equation 6.1 determines the force-velocity relationship governing the response of the nonlinear viscous dampers. The two constants characterizing the mechanical properties of the damper are the damping coefficient C and the damping exponent γ. The force F is a function of the velocity v of the damper.

$$F = C \cdot v^{\gamma} \qquad [6.1]$$

6.3. Test program

Four test series were developed for the test program. The first series were tests performed with a constant velocity. The second series were tests performed using sinusoidal inputs having a duration of one (1) complete cycle. The third series were tests performed using sinusoidal inputs of ten (10) cycles. The final series were tests performed using seismic displacement time history inputs from the parametric study. These test series were developed using the results from the parametric study presented in Chapter 4, while considering the capacity limits of the dampers supplied for the test program. The following section presents the capacity limits of the seismic dampers, followed by results of the parametric study and finally, a description of the four test series.

6.3.1. Capacity limits of the viscous dampers

Two viscous dampers were supplied by LCL-Bridge Products Technology inc. Table 6.1 lists the capacity limits of the viscous dampers supplied.

Table 6.1: Capacity limits of the viscous dampers provided by the manufacturer.

	Parameter		
	Force (kN)	Displacement (mm)	Velocity (mm/s)
Limit	350	±50	**

** Velocity limit varies according to the damping coefficient (C) of the viscous damper.

6.3.2. Results from the parametric study

The parametric study covered a wide range of building types and locations. The objective of the study was to evaluate the rocking response of buildings subjected to site specific earthquakes. The results of the study were used to develop the test series by taking into account the trends observed in the parametric study as well as the extreme cases.

As explained in Chapter 4, the rocking period of all the buildings examined in the parametric study was calculated and from this evaluation, it was observed that a relationship exists between the fixed base fundamental period of a building and its rocking period. This relation is site specific, as illustrated on Figure 4.24, therefore time history results for column displacement uplift from all three sites were used for the test protocol. The time histories were selected to cover the range of rocking period observed, which varied between 0.6 seconds in Montreal to 4.5 seconds in Los Angeles.

6.3.3. Test series

6.3.3.1. Test series 1: Constant velocity

A total of nine tests were included in test series 1. These tests were displacement pulse inputs with a maximum displacement limited to 80 mm at a constant velocity. Table 6.2 lists the parameters used for each of the 9 inputs. The selected velocity values were chosen in order to plot a representative curve for the force vs. velocity relationship for the viscous dampers. Figure 6.4 (a) illustrates the pulse displacement input used for the test series and Figure 6.4 (b) illustrates the velocity signal obtained for the displacement inputs.

Table 6.2: Description of the parameters used in test series 1.

Test name	Velocity (mm/s)	Max Displacement (mm)
S1.1	0.008	5
S1.2	0.5	5
S1.3	1	5
S1.4	10	80
S1.5	50	80
S1.6	100	80
S1.7	200	80
S1.8	400	80
S1.9	600	80

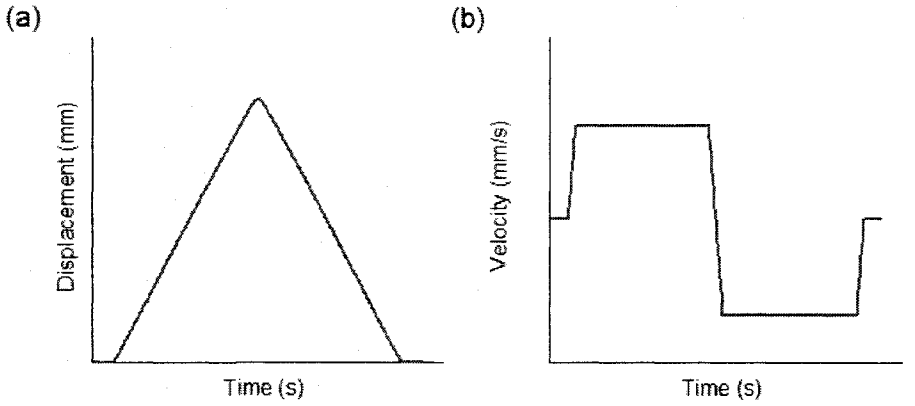

Figure 6.4: (a) Displacement pulse input used for test series 1.
(b) Velocity signal of test series 1.

6.3.3.2. Test series 2: Sinusoidal input (1 cycle)

A total of 9 tests were included in test series 2. These tests were sinusoidal displacement inputs with a range of displacement limited to 80 mm at a frequency determined to obtain a given set of maximum velocity values. Table 6.3 lists the parameters used for each of the 9 inputs. Similarly to test series 1, the selected velocity values were chosen in order to plot a representative curve for the force vs. velocity relationship for the viscous dampers. This test series was useful to evaluate the response of the viscous damper to a continuously varying velocity input as in the case of

earthquake shaking. Figure 6.5 (a) shows the sinusoidal displacement input used for the test series and Figure 6.5 (b) illustrates the velocity signal obtained for the displacement inputs.

Table 6.3: Description of the parameters used in test series 2.

Test name	Max Velocity (mm/s)	Max Displacement (mm)
S2.1	0.008	±2
S2.2	0.5	±10
S2.3	1	±10
S2.4	10	±40
S2.5	50	±40
S2.6	100	±40
S2.7	200	±40
S2.8	400	±40
S2.9	600	±40

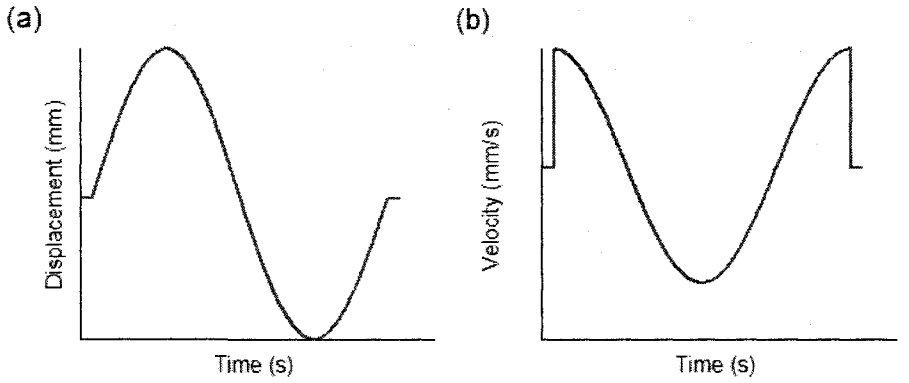

Figure 6.5: (a) Displacement sinusoidal input used for test series 2.
(b) Velocity signal of test series 2.

6.3.3.3. Test series 3: Sinusoidal input (10 cycle)

A total of three tests were included in test series 3. The signals in these tests were three of the sinusoidal displacement inputs from test series 2 that were extended in duration to last for 10 complete cycles. Test series 3 was useful to evaluate the performance of the viscous dampers over several cycles of use. Since most of the energy dissipated by the damper is converted into heat, the damper has a tendency to heat up.

This heat affects the viscosity of the silicone in the damper, thus modifying the properties of the damper over time. This test series was developed to determine whether the average earthquake input would have sufficient cycles to modify the response of the dampers. The average number of column base uplift cycles observed in the parametric study is around 10; therefore a sinusoidal input of 10 cycles was believed to be sufficient. This value was determined from the calculations performed to determine the rocking period of the structures, which was described in Chapter 4. Table 6.4 lists the three values of maximum velocity used in the test series 3. Figure 6.6 (a) shows the sinusoidal displacement input used for the test series and Figure 6.6 (b) illustrates the velocity signal obtained for each of the displacement inputs.

Table 6.4: Description of the parameters used in test series 3.

Test name	Max Velocity (mm/s)	Max Displacement (mm)
S3.1	50	±40
S3.2	200	±40
S3.3	400	±40

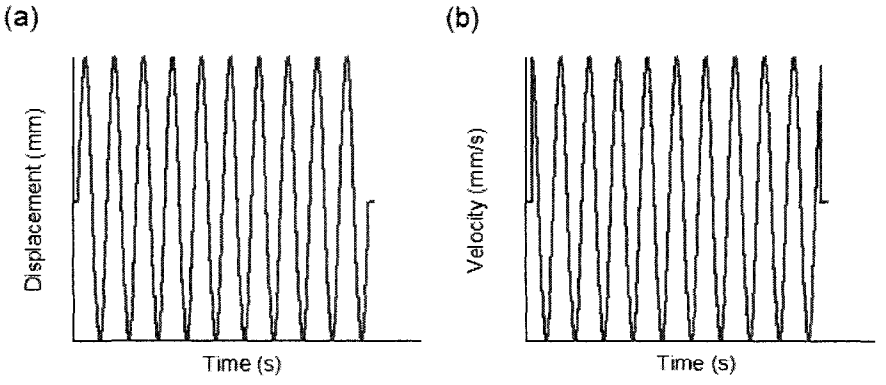

Figure 6.6: (a) Displacement sinusoidal input used for test series 3.
(b) Velocity signal of test series 3.

6.3.3.4. Test series 4: Time history displacement input

A total of six tests were included in test series 4. These tests were input displacement signals taken from the column base uplift displacement results obtained from the parametric study. Six time histories were selected for this test series. Two from analyses performed in Montreal, two from analyses performed in Vancouver and two from analyses performed in Los Angeles. The time histories selected cover the range of uplift periods observed in the parametric study (see Figure 4.24). Also, the displacement inputs were selected to cover the different building parameters used for the parametric study: 2-, 4- and 6-storey buildings, 5.625 m and 9 m wide frames, interior and exterior frames. Table 6.5 lists the description of the time histories used in the test series 4. Tests S4.4, S4.5 and S4.6 were scaled to respect the capacity limits of the seismic dampers in terms of displacement and velocity. Figure 6.7 illustrates the displacement inputs for each of time histories used for the test series.

Table 6.5: Description of the time histories used in test series 4.

Test name	Location	Earthquake	Building Parameters	Max Displ. (mm)	Max velocity (mm/s)	$T_{rocking}$ (s)
S4.1	MTL	E08	2 storeys, 9m exterior frame	16.1	212.6	0.66
S4.2	MTL	E10	6 storeys, 5.6 m exterior frame	19.5	82.9	3.13
S4.3	VAN	H06	2 storeys, 5.6 m exterior frame	54.1	162.5	1.37
S4.4	VAN	H09	6 storeys, 9 m exterior frame	82.6*	177.7*	2.48
S4.5	LA	LA28	2 storeys, 9 m interior frame	73.2*	229.8*	2.01
S4.6	LA	LA31	4 storeys, 5.6 m exterior frame	78.3*	205.7*	2.46

* Values adjusted to the limits of the viscous damper.

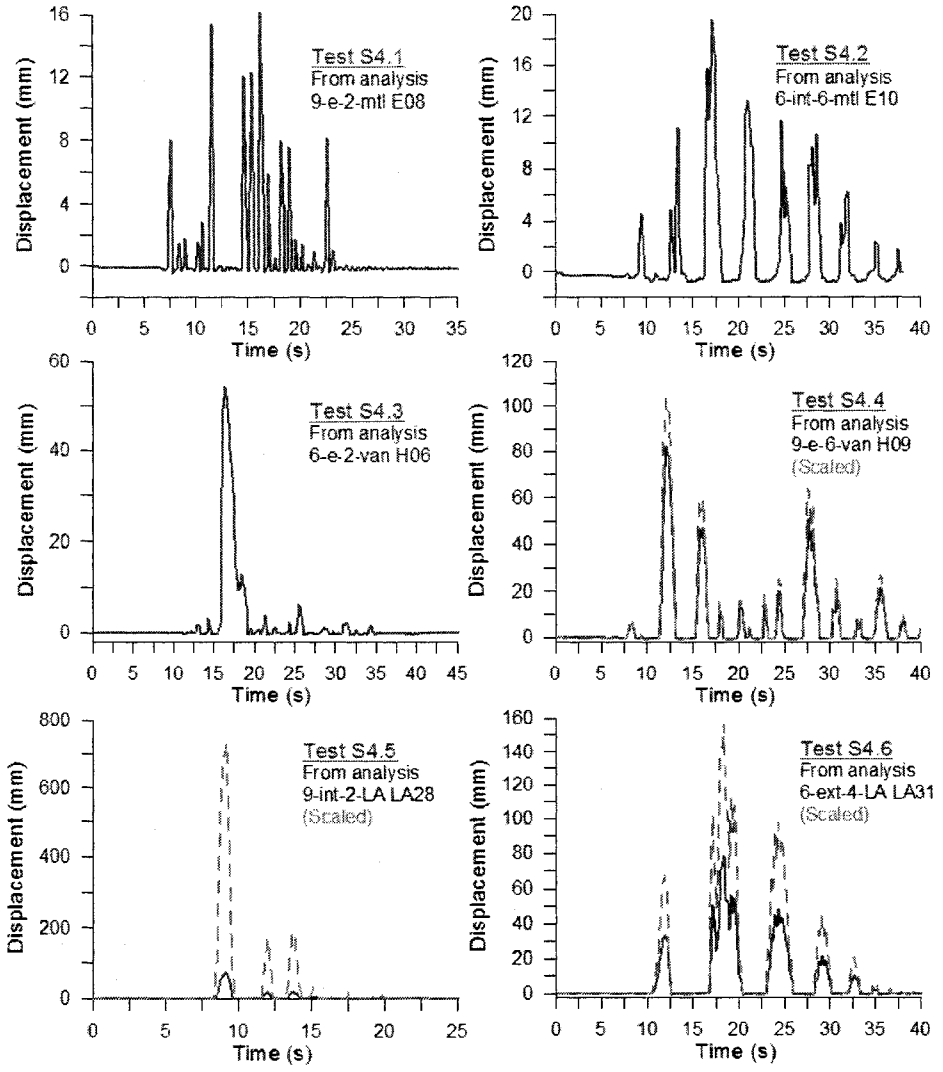

Figure 6.7: Displacement time history inputs used for test series 4.

6.4. Results of the experimental test program

The calibration of the seismic dampers to be used in the shake table test program, was a multi-step procedure. Two nearly identical shock damper units (SDU), damper specimens SDU-1 and SDU-2, were used for this procedure. The mechanical properties of the dampers were evaluated in alternation using the test program described above. The test results of one damper were used by the supplier to physically modify the characteristics of the other damper until both units reached the desired properties needed for the shake table tests. Table 6.6 lists the properties obtained for the damper units at

each of the steps in the calibration process. A total of 5 tests were performed. The first test was completed on the SDU-1 unit to evaluate the initial properties of the unit. The second test was completed on the SDU-2 unit to evaluate the performance of the damper with properties similar to the full scale prototype, thus representing typical damper properties that would be used in actual buildings. The third test was performed on the SDU-1 unit and was an intermediate step before attaining the final damping properties. The fourth and fifth test trials were the final tests required to fine tune the properties of both damper units to values similar to those of the scaled model. The final damper properties were not exactly equivalent to the target values, but were judge satisfactory to fulfill the objectives of the shake table test program.

Table 6.6: Properties of the dampers obtained from the different tests.

		Damper Properties	
Test Trial	Unit	Damping Coefficent, C (kNs/m)	Damping Exponant, γ
1	SDU-1	850	0.14
2 [1]	SDU-2	450	0.16
3	SDU-1	300	0.16
4 [2]	SDU-2	140	0.21
5 [2]	SDU-1	130	0.22

[1] Target damper properties (C=500kNs/m, γ=0.25) → Full scale Prototype.

[2] Target damper properties (C=119kNs/m, γ=0.25) → Scaled Model.

Final damper properties used for the shake table test trials

Using Equation 6.1, a trial and error procedure was used to determine the values for the damping coefficient (C) and the damping exponent (γ) to obtain the best match between the numerical predictions and test data for the damper forces. Figures 6.8 and 6.9 illustrate the results of the test trials 2 and 5 for a sinusoidal input and a time history input. The numerical results are plotted with the experimental results demonstrating the curve fitting procedure used to determine the properties of the damper units. As illustrated, a very good numerical prediction of the response of the damper was achieved. Similar results were obtained for the other test series.

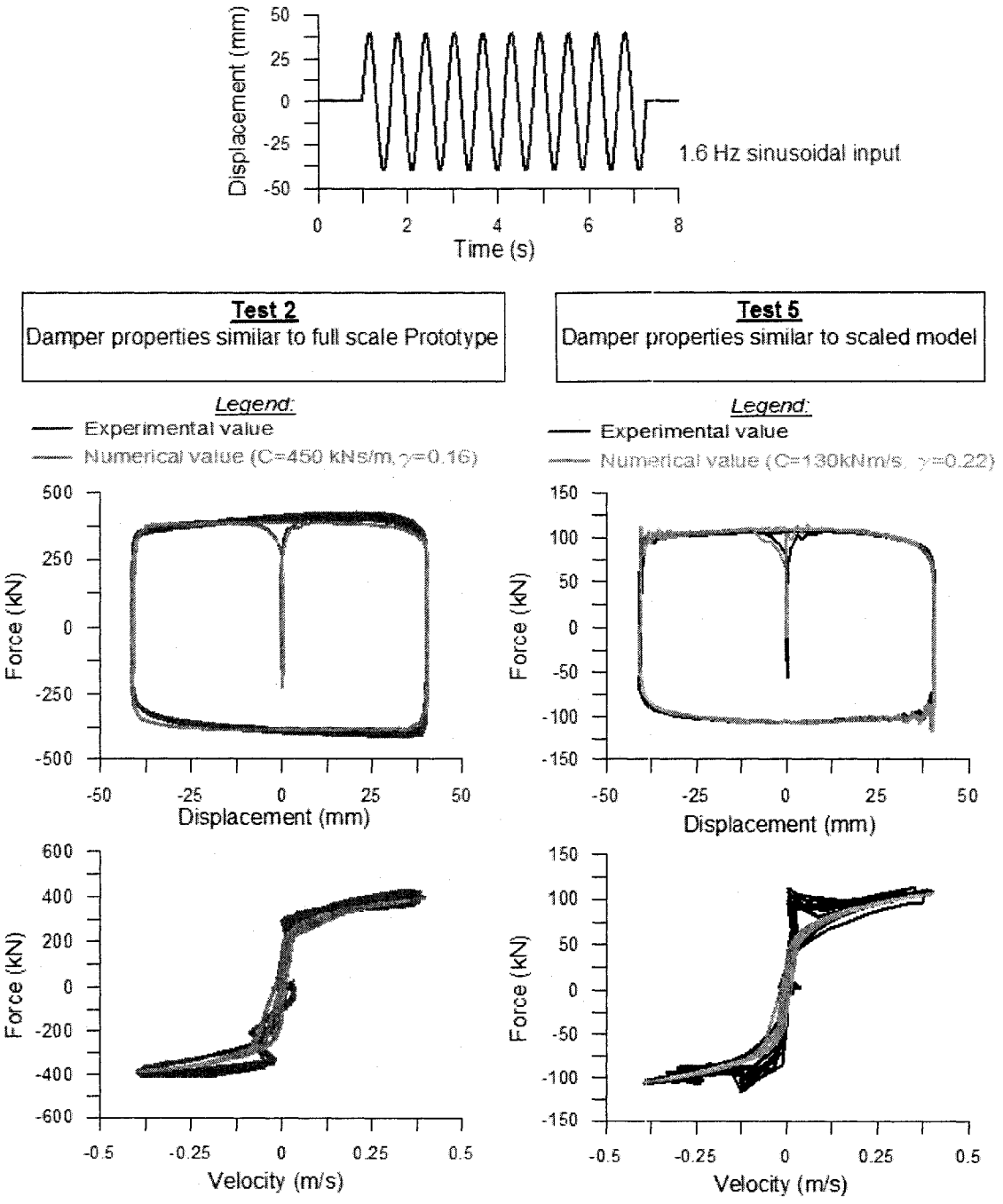

Figure 6.8: Input S3.3 – 1.6 Hz sinusoidal input of ten cycles.

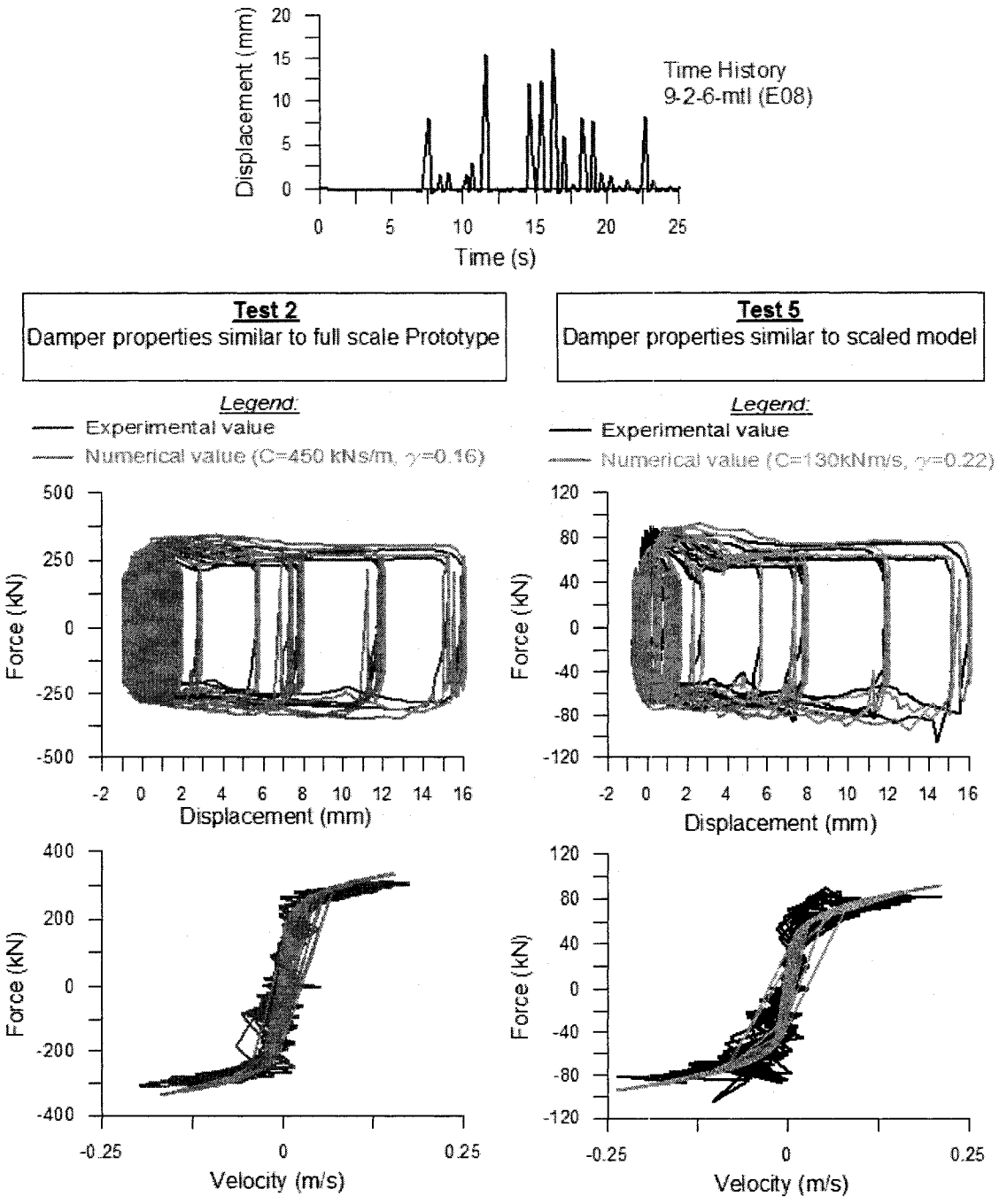

Figure 6.9: Input S4.1 – Time history displacement from parametric study
Analysis: 9-2-6-mtl, *Time history*: E08

6.5. Conclusion

Experimental tests were performed on two damper units to calibrate them for the shake table test program and to verify that the behaviour of the dampers could be reproduced numerically. A total of five (5) test trials were required for the calibration process. The behaviour of the units was reproduced numerically very well at each step of the experimental program. The final properties of the dampers were very similar to those required, according to the laws of similitude, for the laboratory model (Chapter 5). The following chapter presents the shake table test program.

CHAPTER 7

EXPERIMENTAL TEST PROGRAM - PART 2: SHAKE TABLE TEST PROGRAM

7.1. Introduction

The following chapter describes the shake table test program, which was the second test program performed in this study. The main objectives of this test program were: 1) to evaluate the real life performance of the Viscously Damped Controlled Seismic Rocking (VDCSR) system subjected to earthquakes and various other signals and 2) to validate the accuracy of the computer models used in the parametric study. This validation was very important to determine whether the numerical simulations could accurately reproduce the behaviour of the VDCSR system.

This chapter presents a description of the test setup used on the shake table, a description of the data acquisition setup and provides a description of the test signals used in the test program. Also, this chapter presents the results of the test program, followed by the results of identification and auxiliary tests performed on the specimen. The final sections of this chapter describe the numerical model used to replicate the experimental behaviour of the VDCSR system and the results of this comparison.

7.2. Test setup

As described in Chapter 5, the tests were performed on a large scale 2-storey rocking braced frame which was mounted on the earthquake simulator of the Hydro-Québec Structural Engineering Laboratory at Ecole Polytechnique of Montreal. The test model is illustrated in Figure 7.1. It was a 1:2 true replica of one of the braced frames from a 45 m x 45 m 2-storey building examined in the parametric study. Weights mounted on roller bearings were used at both levels of the test frame to simulate the actual tributary seismic weight of the building, resisted by the braced frame.

Concentrated weights were also attached at the beam-to-column joints at both levels to reproduce the tributary gravity loads supported by the bracing bent. The column bases were mounted on the seismic dampers, which were fixed to the shake table.

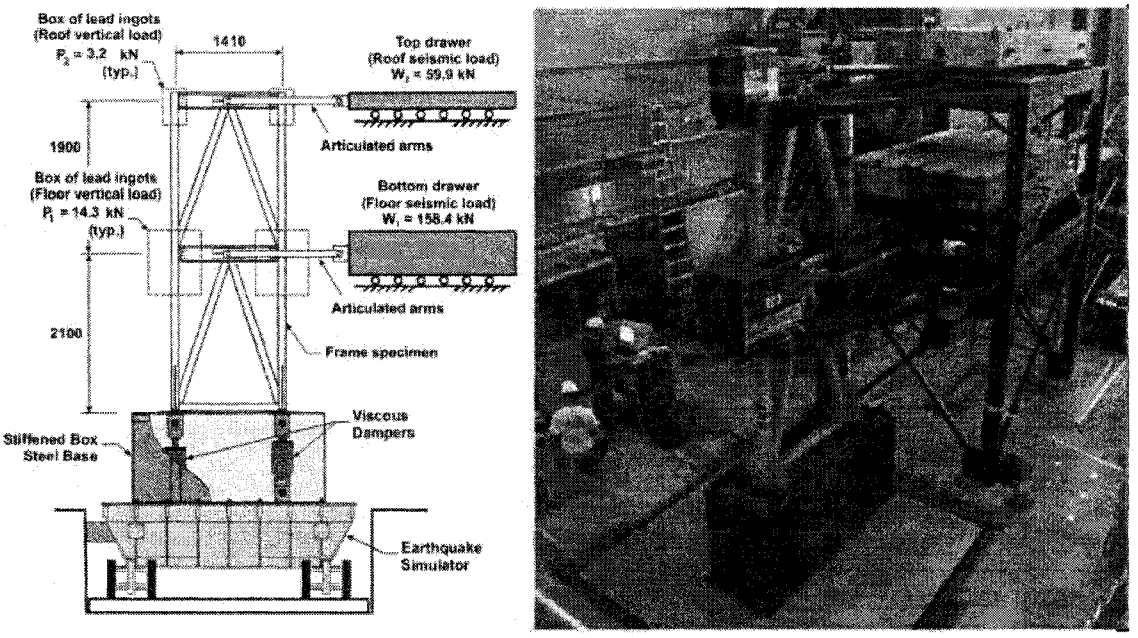

Figure 7.1: Experiment test setup used for the shake table test program.

The following is a description of the various components of the test setup. A complete set of the structural construction blueprints are presented in Appendix G.

7.2.1. Frame specimen

The frame specimen was a chevron concentric braced frame 1.41m wide by 4.0m tall. Figure 7.2 illustrates an isometric view of the frame specimen. The columns and the diagonal braces were HSS102x102x4.8 hollow square steel tubes welded together with full penetration welds. The roof and floor beams were W200x15 W-shape beams. Simple bolted shear connections were used between the beams and the columns. During preliminary testing, relative movement (slip) was observed between the beam ends and the angles connected to the columns. Short vertical welds were added between the angles and the beam webs to prevent this movement while allowing relative rotation

between the beam ends and the columns. A horizontal HSS 102x102x4.8 member was introduced at the base to maintain the column spacing. That bar was welded to the columns. The braces were welded to the beams at the beam mid-span connections. At the base, the braces were welded to gusset plates welded to the columns and the horizontal bar. At the floor level, the 2nd storey braces were welded to gusset plates welded to the beam only. At both levels, C shaped members were welded to the columns to support the lead ingot boxes that simulated the tributary vertical load on the columns. Two large base plates were welded to the columns. Pin-connected shear rods were attached to these base plates to provide the lateral restraint required for the shear forces at the base of specimen, without interfering with the rocking motion. The shear rods were connected to the stiffened steel box that was used to enclose the dampers at the base of the specimen. Articulated arms were connected on either side of the roof and floor beams with pinned connections. Figure 7.3 is a picture of the pinned connection on the roof beam. The articulated arms were attached to two drawers made of concrete and steel weights mounted on rollers which acted as the lateral seismic load tributary to the braced frame.

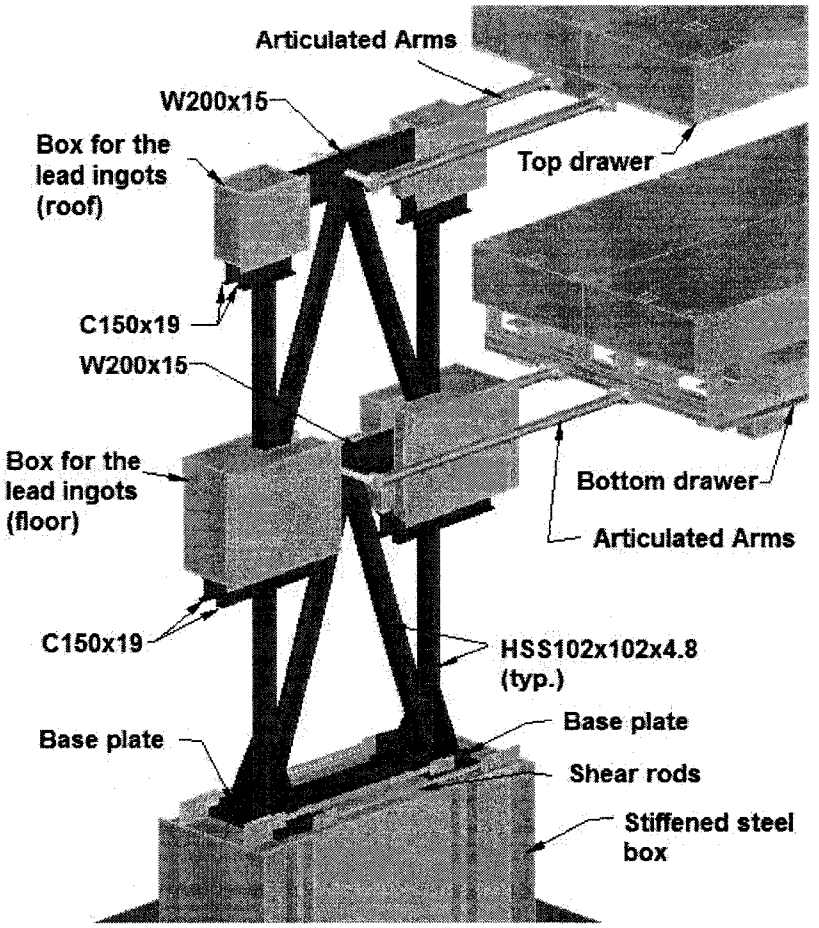

Figure 7.2: Components of the frame specimen.

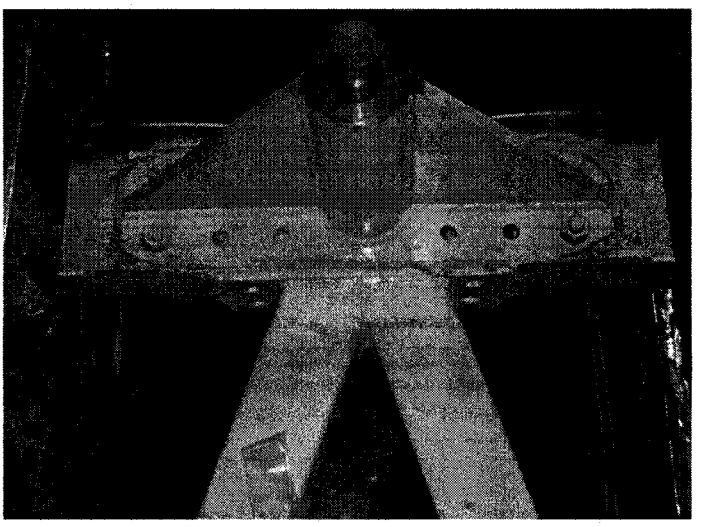

Figure 7.3: Picture of the pinned connection for the articulated arms.

7.2.2. The stiffened steel box

A stiffened steel box was assembled at the base of the frame specimen to enclose the seismic dampers, while providing enough rigidity to insure a synchronised horizontal movement for the table and the base of the frame. Figures 7.4 and 7.5 illustrate the stiffened steel casing. The box was an assembly of 12 mm thick steel plates. The four side panels were welded to the base plate. The top panel was bolted to the side plates, thus removable, to allow for the installation of the seismic dampers. Machined eyelets and 100 mm in diameter pins were fabricated and installed at either end of the dampers to obtain a true pinned connection. The pin connections were required to allow for the rocking motion. The bottom eyelets were welded to the base of the stiffened box. The top eyelets were bolted to the underside of the base plates of the frame specimen. Two openings 350 mm x 300 mm were provided in the top plate of the box, centered on the column base plates, to allow for the extension of the damper through the top of the casing and allow direct connection to the column base plates. The base plates of the frame specimen were designed to be large enough to rest on either side of the openings. Stiffeners were welded along the column sides to prevent bending of the base plates. Stiffeners were also installed along the front and the back side plates of the box to ensure direct transfer of the concentrated downward force from the columns to the shake table.

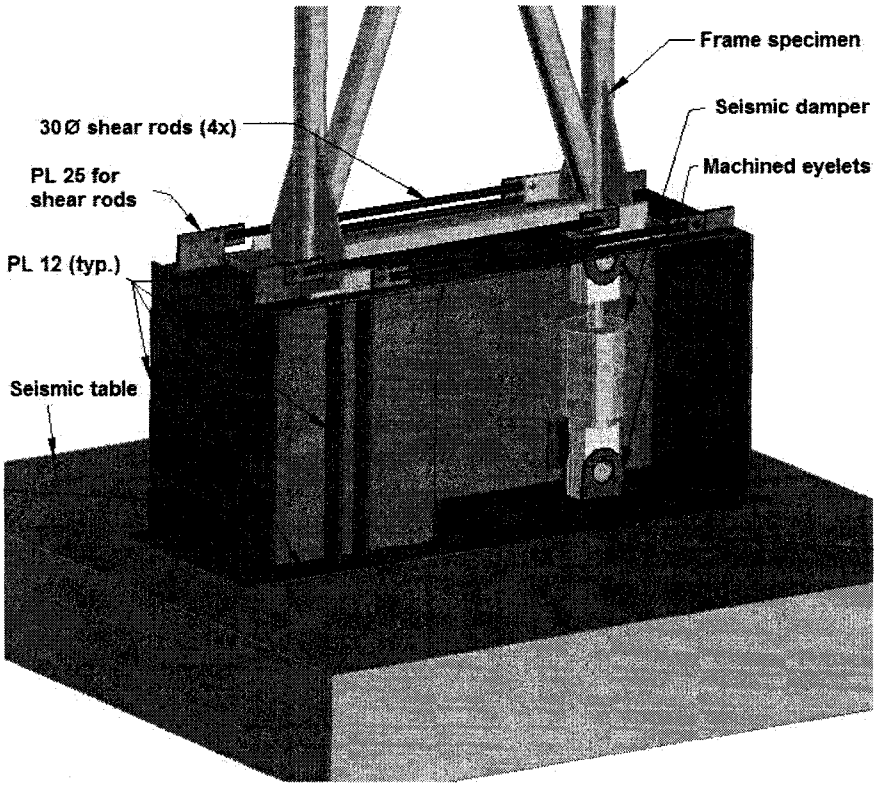

Figure 7.4: Components of the stiffened steel base box.

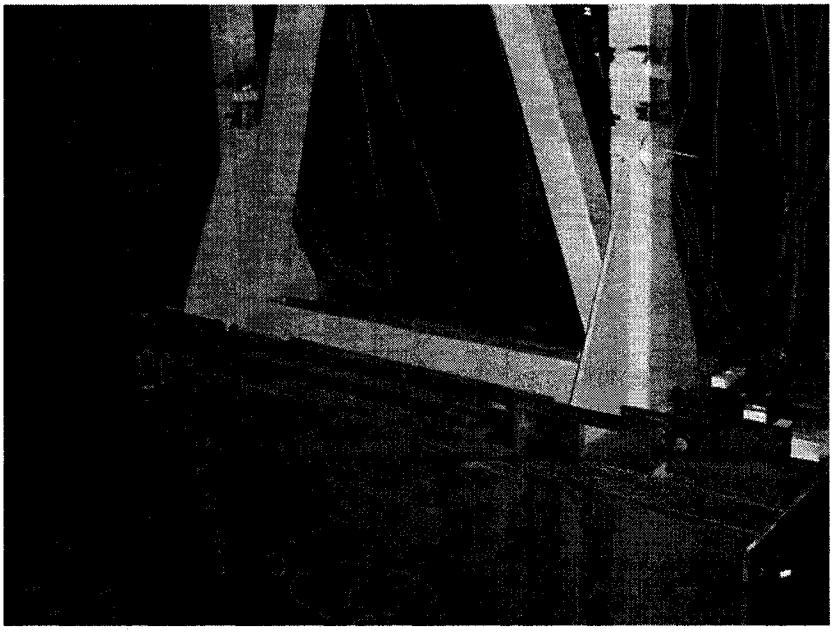

Figure 7.5: Picture of the stiffened steel box.

7.2.3. Gravity loads (vertical load boxes)

The vertical load in the braced frame comes from the dead load from the roof and the floors. The dead loads represent the weight of the structure and of the architectural finishes. For the frame specimen, these loads were simulated using lead ingots encased in steel boxes at the beam/column joints. Lead ingots were used for the vertical load due to the high density of lead (112 kN/m^3). The boxes were built out of 6 mm thick steel plates welded together. The front side plates and the top cover plates were connected using bolts so that they can be removed to simplify the placement the lead ingots in the boxes. Wood wedges were used to tightly secure the ingots inside the steel boxes and avoid any unwanted vibrations. The top boxes, simulating the tributary roof loads, were filled with 15 lead ingots each, for a total weight of 326 kg (3.2 kN) for each box. The bottom boxes, simulating the tributary floor loads, were filled with 72 lead ingots each, for a total of 1392 kg (13.66 kN) for each box. Figures 7.6 and 7.7 illustrate the vertical load boxes fixed onto the frame specimen.

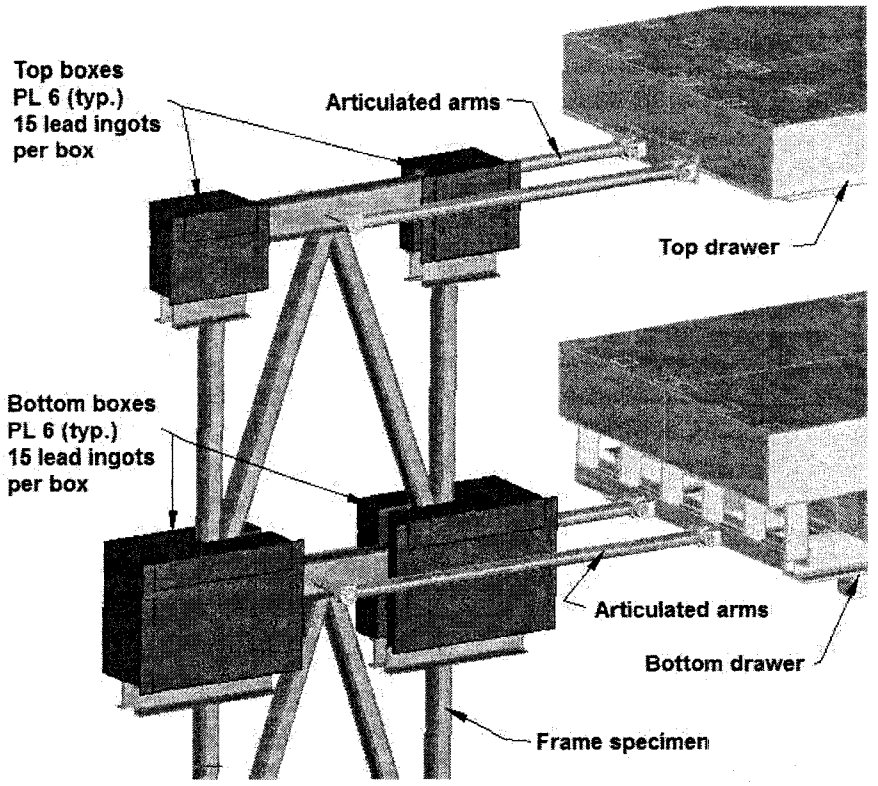

Figure 7.6: Vertical load boxes.

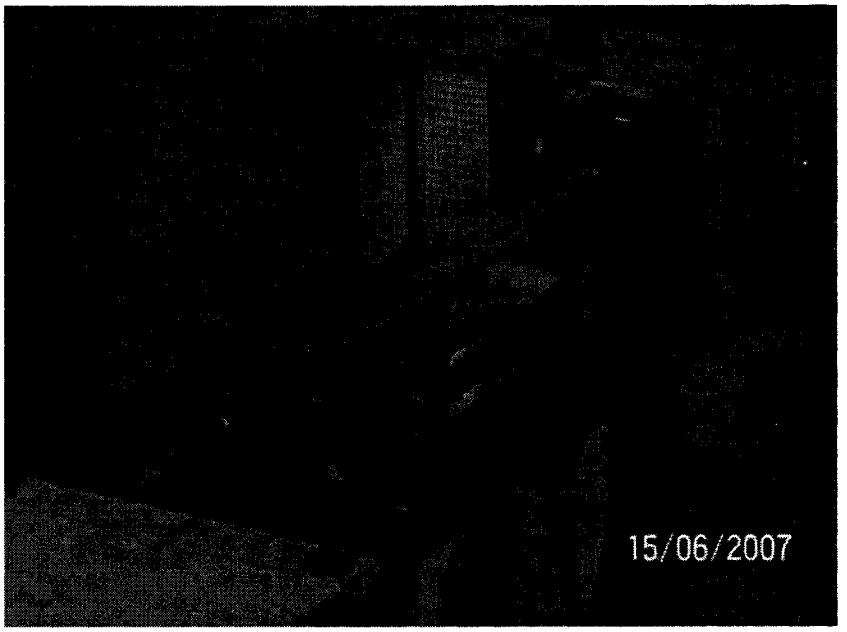

Figure 7.7: Picture of the vertical load boxes.

7.2.4. The seismic loads drawers

The tributary seismic weight of braced frames in a building is composed of the dead weight of the structure at all levels and of 25% of the snow load at the roof level. This seismic weight produces the horizontal inertia loads only. As illustrated on Figure 7.8, these loads were simulated using weights mounted on roller bearings. The top drawer had a total mass of 6106 kg (including the articulated arms) which resulted in a total lateral seismic weight of 66.3 kN when added to the weight of the two lead ingot boxes at the roof level. As illustrated on Figure 7.8, the top drawer was composed of two concrete masses and a set of steel plates. Bolts were used to connect the concrete masses together. The concrete blocks had a dimension of 3400mm x 960mm x 370mm and each weighed 2893 kg (28.38 kN). Two large 12 mm thick plates were placed at the bottom of the concrete blocks and were held in place by sixteen 32 mm diameter threaded rods with sixteen 6 mm x 100 mm x 100 mm top plates. A 12 mm thick front plate was welded to the bottom plate in order to attach the eyelets for the pin connections of the articulated arms. The total mass of the front and connecting plates, bolts, and the articulated arms was equal to 320 kg (included in the 6106 kg total mass of the top drawer).

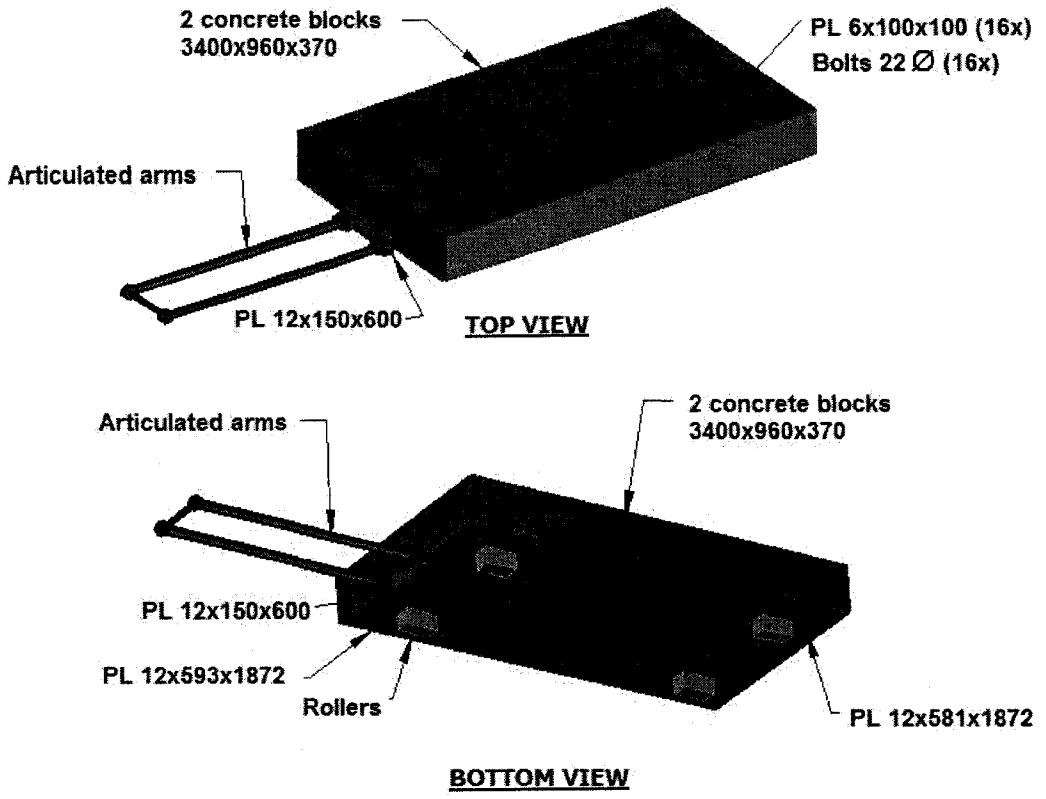

Figure 7.8: Components of the top drawer (roof seismic load).

The bottom drawer had a mass of 16 147 kg (including the articulated arms) which represented a total seismic weight of 187 kN when including the weight of the two lead ingot boxes at the floor level. As illustrated on Figure 7.9, the bottom drawer was composed of two concrete masses and sixteen 25 mm thick steel plates bolted onto a steel frame. The concrete blocks had a dimension of 3400 mm x 960 mm x 370 mm and each weighed 2893 kg (28.38 kN). The steel plates had a dimension of 25 mm x 1220 mm x 2440 mm and each weighed 594 kg (5.83 kN). The steel frame was composed of W-shaped beams and hollow square steel tubes weighing 530 kg (5.2 kN).

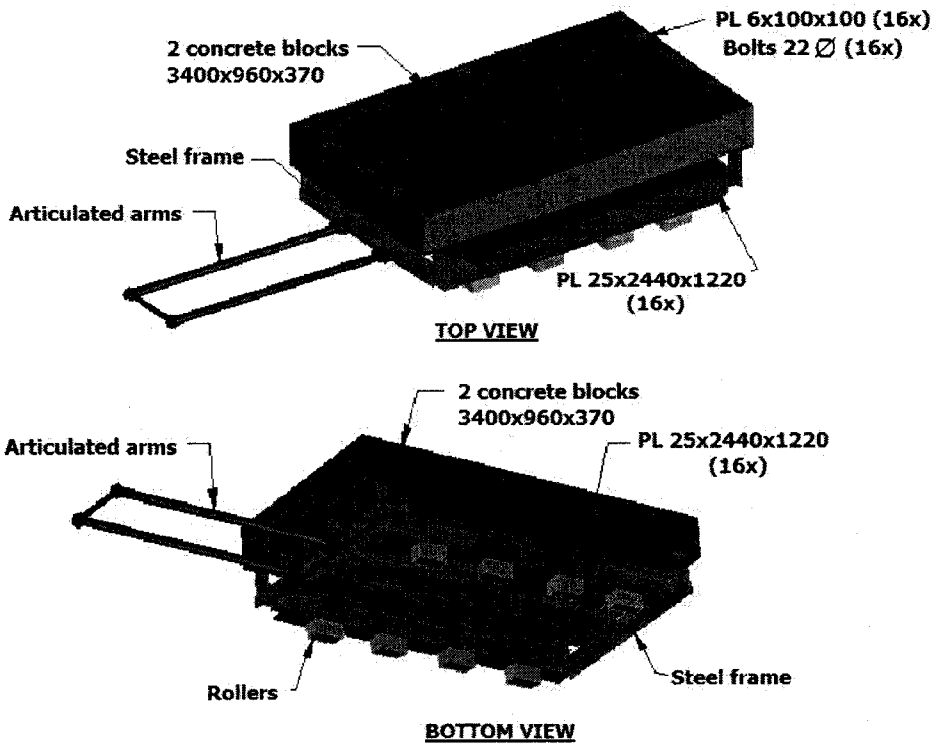

Figure 7.9: Components of the bottom drawer (floor seismic load).

The rollers used for the seismic drawers were 'Hilman Roller' which are bearing rollers typically used for moving heavy industrial equipment. Four 5 ton rollers were used for the top drawer and eight 30 ton rollers were used for the bottom drawer. Figure 7.10 is a picture of the bottom drawer mounted on the Hilman Rollers.

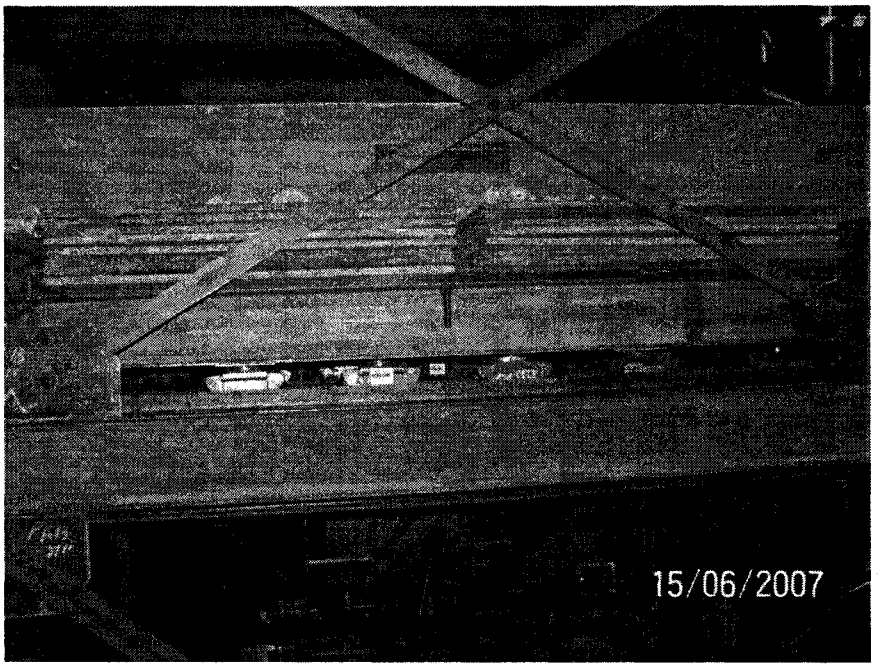

Figure 7.10: Bottom drawer mounted on Hillman Rollers.

7.2.5. 2-storey supporting frame

A 2-storey supporting frame was built next to the earthquake simulator to support the seismic weight drawers and to provide an out of plane lateral restraint to the frame specimen. This supporting frame was securely fastened to the strong floor of the laboratory with 25 mm diameter bolts and was braced using vertical X-bracings at both levels to provide a stable and stiff support system for the test setup. The two levels were framed using W250 steel beams with horizontal X-bracings. Rolling rails using C200 profiles laid out on their side were provided at each level for the seismic load drawers. Stainless steel plates were placed on the rails to provide a clean rolling interface for the rollers and minimize as much as possible horizontal frictional forces. Lateral restraining arms cantilevered from the supporting frame to provide lateral support to the test specimen. The arms were made of W250 beams attached to the front of the supporting frame. Lateral bracing was provided by HSS102x102x6.4 members. Teflon plates were inserted between the restraining arms and the frame specimen to ensure a frictionless horizontal and vertical (due to rocking) movement between these two components.

Figure 7.11 illustrates the various elements of the supporting frame. Figure 7.12 is a picture of the lateral restraining arms at the front of the support frame.

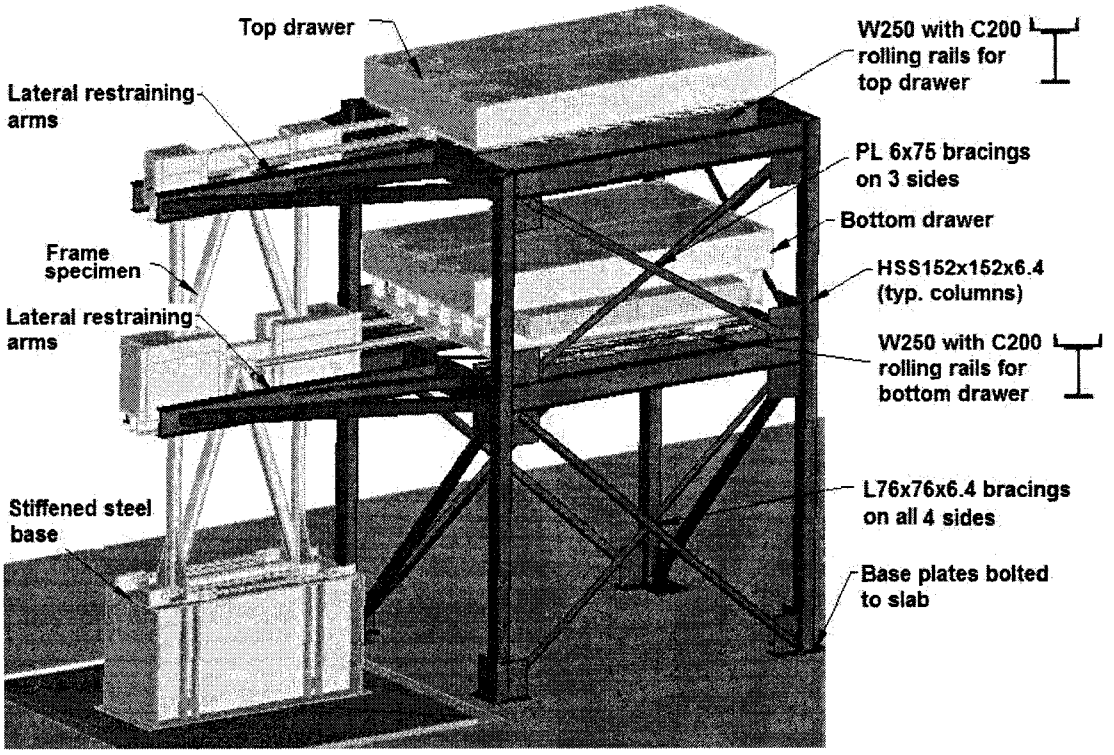

Figure 7.11: Components of the 2-storey support frame.

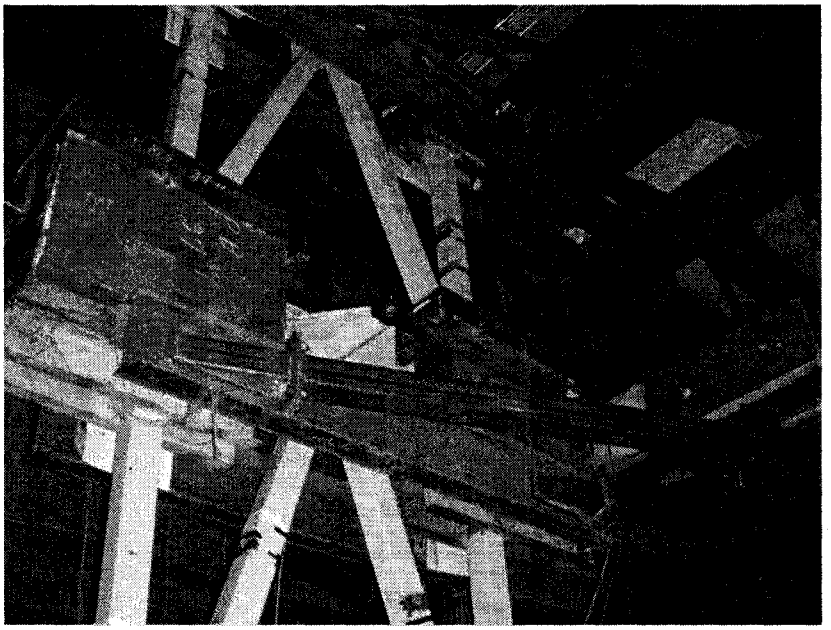

Figure 7.12: Lateral supporting arms.

7.3. Instrumentation and data acquisition system

Figure 7.13 illustrates the instrumentation used in the test program. Twelve accelerometers were used to measure the acceleration at various points of interest on the test setup: horizontal accelerations of the seismic weight and test frame at each level (A9 to A11) and vertical accelerations at the base and at each level along the two test frame columns (A3 to A8). Horizontal accelerations were also recorded at the base of the steel caisson and the base of the test frame (A1 and A2). Twenty-four strain gages were used to measure axial strains in braces and columns of the test frame (G1 to G16) as well as in the articulated arms (G17 to G24). Strain measurements were used to evaluate the forces in these members. Four linear variable displacement transformers (LVDT L1 to L4) were used to measure the vertical displacement of the column bases (uplift), and two contact gages (C1 & C2) were used to indicate when base uplift was occurring. Figure 7.14 is a picture of a LVDT fixed to the test specimen on the column base. Two cable position transducers (linear potentiometers) were used to measure the total horizontal displacement of the floor and the roof levels with respect to the strong floor of the laboratory. The total acceleration and displacement of the shake table were monitored by

the built-in instrumentation of the facility. To ensure synchronization, the signals from these two instruments were also recorded with the data acquisition system used for the test program.

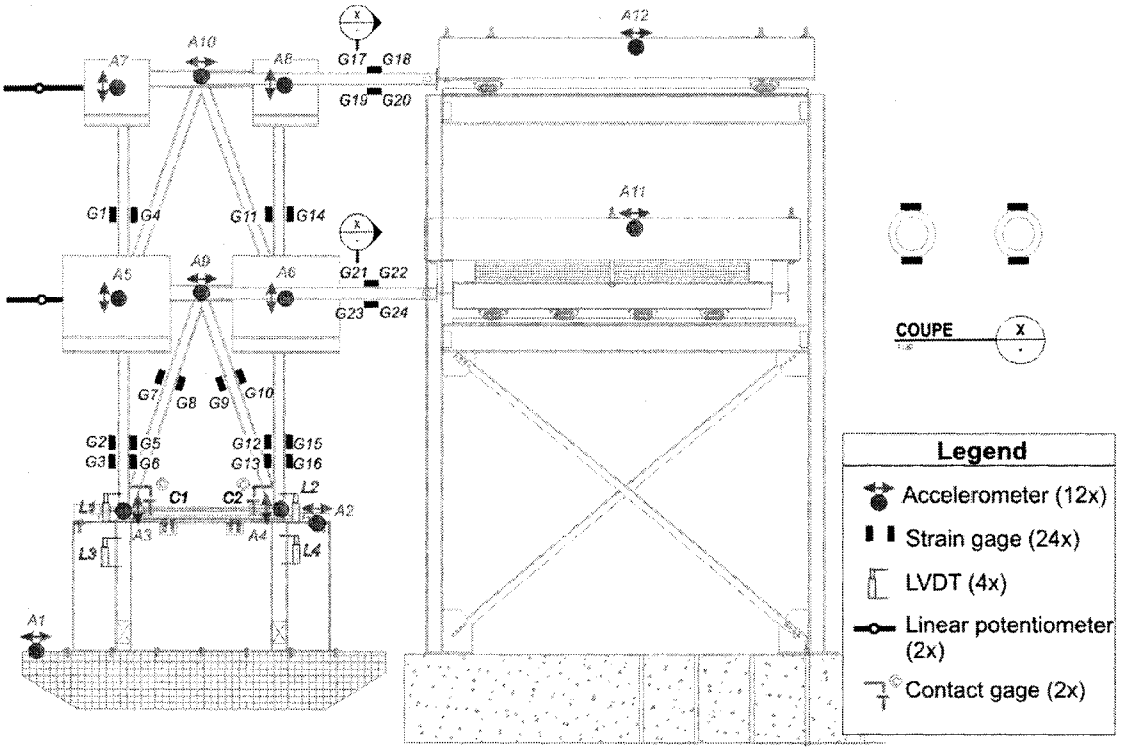

Figure 7.13: Instrumentation of the test setup.

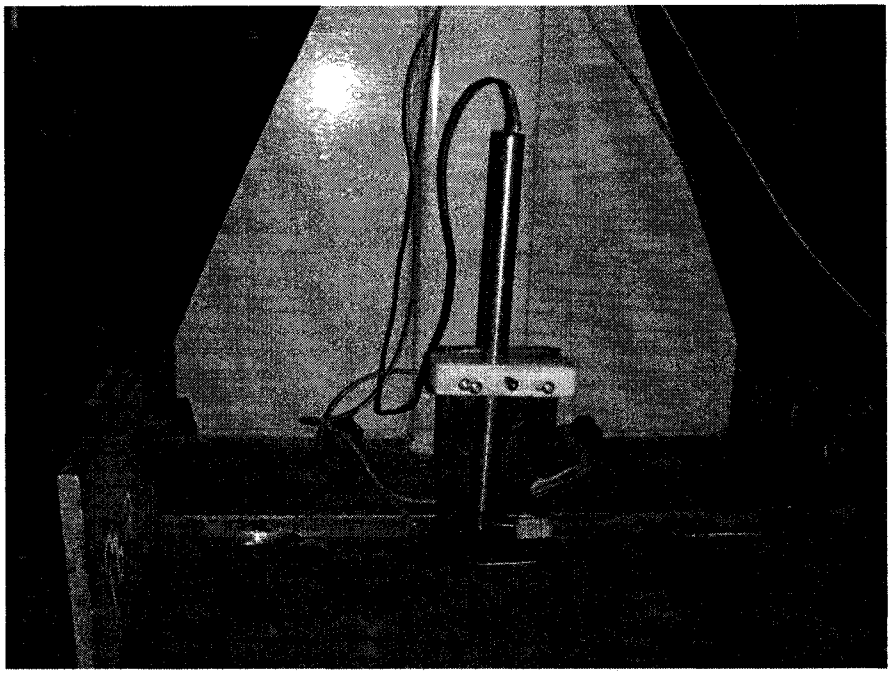

Figure 7.14: LVDT fixed to the column base of the test specimen.

7.4. Test (loading) signals

As described in section 5.6 of Chapter 5, nine historical earthquake ground motion records were selected from the parametric study for the shake table test program. These ground motions were modified to meet the similitude law requirements and were scaled according to the capacities of the earthquake simulator. In addition to these ground motions, a series of harmonic signals with various amplitudes and frequencies were selected for the test program. Table 7.1 presents a list of all the inputs used in the shake table test program and provides a description of the signals.

Table 7.1: Input signals used for the shake table test program.

ID	Test name	Description
STI.1	E08 modified	Time history ground motion E08 for Montreal, modified for the shake table program.
STI.2	E10 modified	Time history ground motion E10 for Montreal, modified for the shake table program.
STI.3	E12 modified	Time history ground motion E12 for Montreal, modified for the shake table program.
STI.4	A04 modified	Time history ground motion A04 for Vancouver, modified for the shake table program.
STI.5	H06 modified	Time history ground motion H06 for Vancouver, modified for the shake table program.
STI.6	H09 modified	Time history ground motion H09 for Vancouver, modified for the shake table program.
STI.7	LA28 modified	Time history ground motion LA28 for Los Angeles, modified for the shake table program.
STI.8	LA31 modified	Time history ground motion LA31 for Los Angeles, modified for the shake table program.
STI.9	LA37 modified	Time history ground motion LA37 for Los Angeles, modified for the shake table program.
STI.10	Sin1HZ_0.05g	Sinusoidal input with a frequency of 1Hz and a maximum amplitude of 0.05g.
STI.11	Sin1HZ_0.1g	Sinusoidal input with a frequency of 1Hz and a maximum amplitude of 0.1g.
STI.12	Sin1HZ_0.15g	Sinusoidal input with a frequency of 1Hz and a maximum amplitude of 0.15g.
STI.13	Sin1HZ_0.2g	Sinusoidal input with a frequency of 1Hz and a maximum amplitude of 0.2g.
STI.14	Sin2HZ_0.05g	Sinusoidal input with a frequency of 2Hz and a maximum amplitude of 0.05g.
STI.15	Sin2HZ_0.1g	Sinusoidal input with a frequency of 2Hz and a maximum amplitude of 0.1g.
STI.16	Sin2HZ_0.2g	Sinusoidal input with a frequency of 2Hz and a maximum amplitude of 0.2g.
STI.17	Sin2HZ_0.3g	Sinusoidal input with a frequency of 2Hz and a maximum amplitude of 0.3g.
STI.18	Sin2HZ_0.4g	Sinusoidal input with a frequency of 2Hz and a maximum amplitude of 0.4g.
STI.19	Sin2HZ_0.5g	Sinusoidal input with a frequency of 2Hz and a maximum amplitude of 0.5g.
STI.20	Sin3HZ_0.1g	Sinusoidal input with a frequency of 3Hz and a maximum amplitude of 0.1g.
STI.21	Sin3HZ_0.3g	Sinusoidal input with a frequency of 3Hz and a maximum amplitude of 0.3g.
STI.22	Sin3HZ_0.5g	Sinusoidal input with a frequency of 3Hz and a maximum amplitude of 0.5g.
STI.23	Triangle3Hz_0.05g	Triangular input with a frequency of 3Hz and a maximum amplitude of 0.05g.
STI.24	Triangle3Hz_0.1g	Triangular input with a frequency of 3Hz and a maximum amplitude of 0.1g.
STI.25	Triangle3Hz_0.3g	Triangular input with a frequency of 3Hz and a maximum amplitude of 0.3g.
STI.26	Triangle3Hz_0.5g	Triangular input with a frequency of 3Hz and a maximum amplitude of 0.5g.

7.5. System identification and auxiliary tests

7.5.1. Impact tests

Impact tests were performed on the frame specimen to determine its natural frequencies and mode shapes and to evaluate the damping values of the system. The properties are used for validation and adjustment of the numerical model, as will be discussed in Section 7.7. As illustrated in Figures 7.15 and 7.16, the tests were performed using a wooden battering ram, attached to an overhead crane at the height of the top level drawer. Manually, the battering ram was swung onto the drawer at an interval of 2 to 3 seconds. The data acquisition system used for the shake table test

program was activated during this process to measure the horizontal displacements and accelerations at both levels of the test frame. For these tests, the base plates of the columns were temporarily welded to the steel caisson in order to obtain the fixed base properties of the test specimen, without the effects of the seismic dampers. The measured natural frequencies were used to adjust the vertical and horizontal stiffness of the steel caisson in the numerical model.

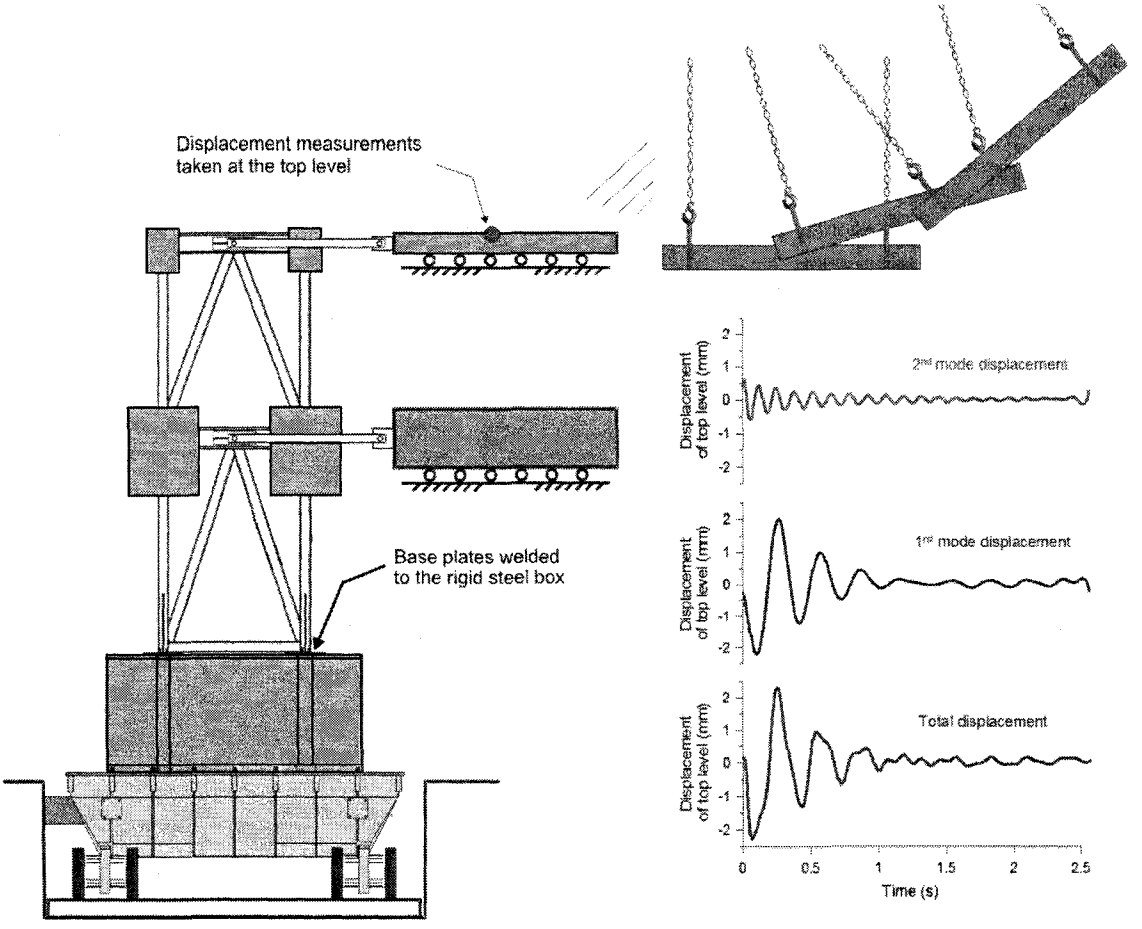

Figure 7.15: Setup for the impact tests and horizontal displacement time history recorded at the frame top level.

Figure 7.16: Picture of the impact test.

The natural frequencies were determined using the test results for the lateral displacement at the top level of the test specimen. The amplitude of the measured displacement was approximately ± 2 mm. As illustrated on Figure 7.15, the first and second mode displacements of the frame were isolated using the total displacement time history. Using these displacement values, a power spectrum was traced to determine the dominant frequencies of vibration. As illustrated on Figure 7.17 (a), the 1rst mode frequency was determined to be 3.5 Hz and the second mode frequency was determined to be 7.6 Hz.

The damping values of the system were determined using the Fast Fournier transform (FFT) algorithm using the displacement results at the top of the frame. As illustrated on Figure 7.17 (b), the first mode damping value was determine to be 12.9% and the second mode damping value was determined to be 5.4%.

These results are significantly higher than values that would be expected for a bare steel frame specimen (typically 1-2% damping) and it is suspected that the seismic dampers were in fact activated during the impact tests due to the flexibility of the top plate of the stiffened box, and provided most of the damping obtained from the impact test results. The fact that significantly higher damping is observed in the first (rocking) mode of the structure, the mode which is more likely to engage the seismic dampers, tends to confirm this assumption. This aspect is discussed further in the comparison between predicted and test data in Section 7.7.

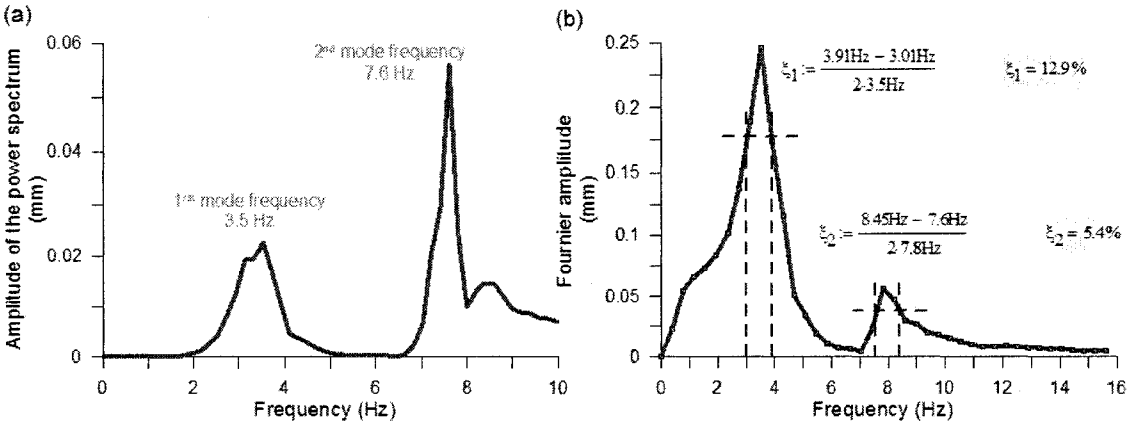

Figure 7.17 : (a) Power spectrum of the signals from impact tests;
(b) FFT algorithm of the signals from impact test.

7.5.2. Calibration of the strain gages

Tests were performed on individual components of the frame specimen to evaluate the gage factors of the strain gages mounted on the test frame members and articulated arms in order to convert the strain readings into axial force data. Twenty four strain gages were used in the shake table test program. These gages were piezoresistors, which are devices that exhibit a change in resistance when strained. The relationship between the change in resistance and the change in length (strain) is defined as the gage factor K. This relationship is given by Equation 7.1, where ε is the strain, L is the gage length and R_g is the gage resistance.

$$\varepsilon = \frac{\Delta L}{L} = \frac{\Delta R_g / R_g}{K} \qquad [7.1]$$

To determine the axial force F using the strain gage readings, the strain must be multiplied by the area A and the modulus of elasticity E of the member. Equation 7.2 defines the relationship between the axial force, the strain and the change in resistance.

$$F = \sigma A = EA\frac{\Delta L}{L} = \frac{EA}{K}\frac{\Delta R_g}{R_g} \qquad [7.2]$$

Axial load tests were conducted on the uni-axial load frame at the Hydro-Québec Structural Engineering Laboratory at Ecole Polytechnique of Montreal, on the four articulated arms (gages 17, 18, 19, 20, 21, 22, 23 and 24), the West side column of the test frame (gages 12, 13, 15 and 16) and the 1st-storey brace located on the west side of the test frame (gages 9 and 10). See Figure 7.13 for the location of the gages that were tested. The calibration tests on the column and brace elements were performed after completion of the shake table test programs. The column and brace segments that contained the strain gauges were cut off the frame and tested in the load frame.

A tension/compression trapezoidal load history of ± 100 kN was used to test the articulated arms. Figure 7.18 illustrates the test loading signal and the response output of the strain gages. The response output, given by the gages, was a measure of the modulus of elasticity (E) times the change in resistance ($\Delta R_g/R_g$). This data was used to determine the gage factors for each of the gages, which are presented in Table 7.2. These gage factors are used to determine the forces in the members. For example, the axial force in the 2nd-storey articulated arm is equal to *F = 200 x (2.17 G17 + 2.12 G18 + 2.085 G19 + 2.19 G20)/4* 1330 mm.*

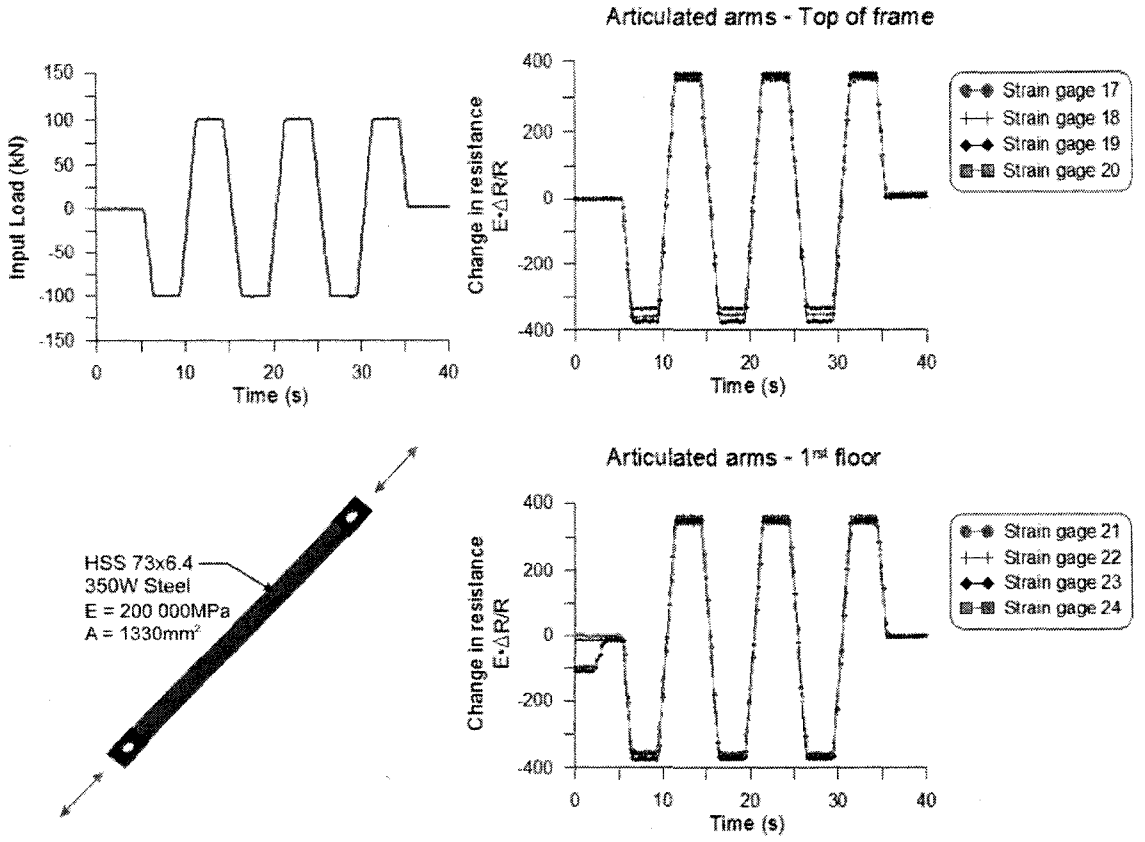

Figure 7.18: Test results for the strain gage tests performed on the articulated arms.

Cyclic compression loadings were used to test the column and brace samples. The amplitude was equal to of 430 kN for the column specimen and 400kN for the diagonal brace. Figure 7.19 illustrates the load inputs used for the tests, as well as the response output of the strain gages. Gages 13 and 16 had been damaged during the shake table test program; therefore their output responses were omitted. The gage factors for each of the gages are presented in Table 7.2.

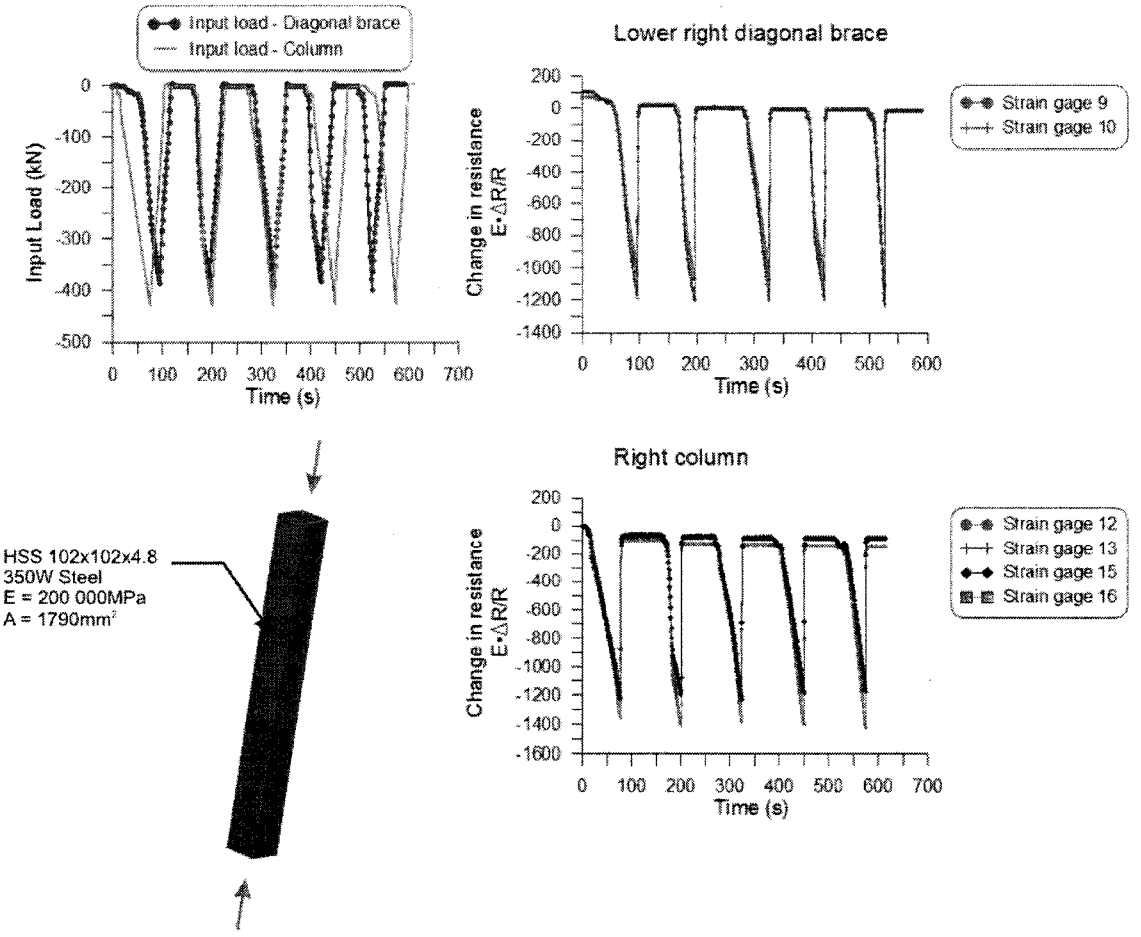

Figure 7.19: Test results for the strain gage tests performed on the column and the diagonal brace specimens.

Table 7.2: Gage factors.

Gage No.	Location	Gage factor (K)	Gage No.	Location	Gage factor (K)
9	Lower right diag. brace	*2.067*	17	Art. arm 1 (top of frame)	*2.170*
10	Lower right diag. brace	*1.888*	18	Art. arm 1 (top of frame)	*2.120*
12	Right column	*1.888*	19	Art. arm 2 (top of frame)	*2.085*
13	Right column	-	20	Art. arm 2 (top of frame)	*2.190*
15	Right column	*2.067*	21	Art. arm 3 (1^{rst} floor)	*2.200*
16	Right column	-	22	Art. arm 3 (1^{rst} floor)	*2.085*
			23	Art. arm 4 (1^{rst} floor)	*2.085*
			24	Art. arm 4 (1^{rst} floor)	*2.085*

7.6. Results from test trials

A three-month period was needed to construct and adjust the test setup prior to carry out the final tests. In particular, lengthy minor adjustments to the test setup were needed to ensure proper alignment of the test frame and the seismic weights so that secondary out-of-plane movements could be eliminated. Similarly, adjustments were needed at the base of the test frame to ensure proper contact between the test frame base plate and the stiffened steel box to achieve proper functioning of the shear rods designed to resist the base shear while allowing rocking to occur freely. This adjustment phase lasted for 2 to 3 weeks during which numerous tests were conducted using the various test signals. Once this was completed, the VDCSR system was tested successfully and performed very well under all 26 input signals. The following Figures illustrate the response of the test specimen to all seismic input signals for Montreal (7.20), for Vancouver (7.21), and for Los Angeles (7.22) as well as the response under four of the harmonic signal inputs (7.23). For each input signal, four response graphs are included. The first graph is a time history of the ground acceleration (a_g) of the input signals. The second graph is a time history of the lateral displacements of the shake table (u_g), the floor (u_1) and the roof (u_2). The third graph is a time history illustrating the rotation at the base of the frame and the inter-storey drifts at the floor and roof levels. The base rotation was obtained by dividing the algebraic difference between the uplift measurements at each column by the width of the frame. The floor and the roof inter-storey drifts were obtained from the ratio between the relative lateral displacement and the respective heights of each level.

The fourth graph is a time history illustrating the base shear (V) measured by the shake table hydraulic actuator, as a function of the seismic weight (W) of the test specimen. The horizontal reactions due to the self-weight of the shake table and the weight of the base steel caisson, including the dampers, have been removed in the calculations so that the base shear displayed correspond to the horizontal shear force at the base of the test frame.

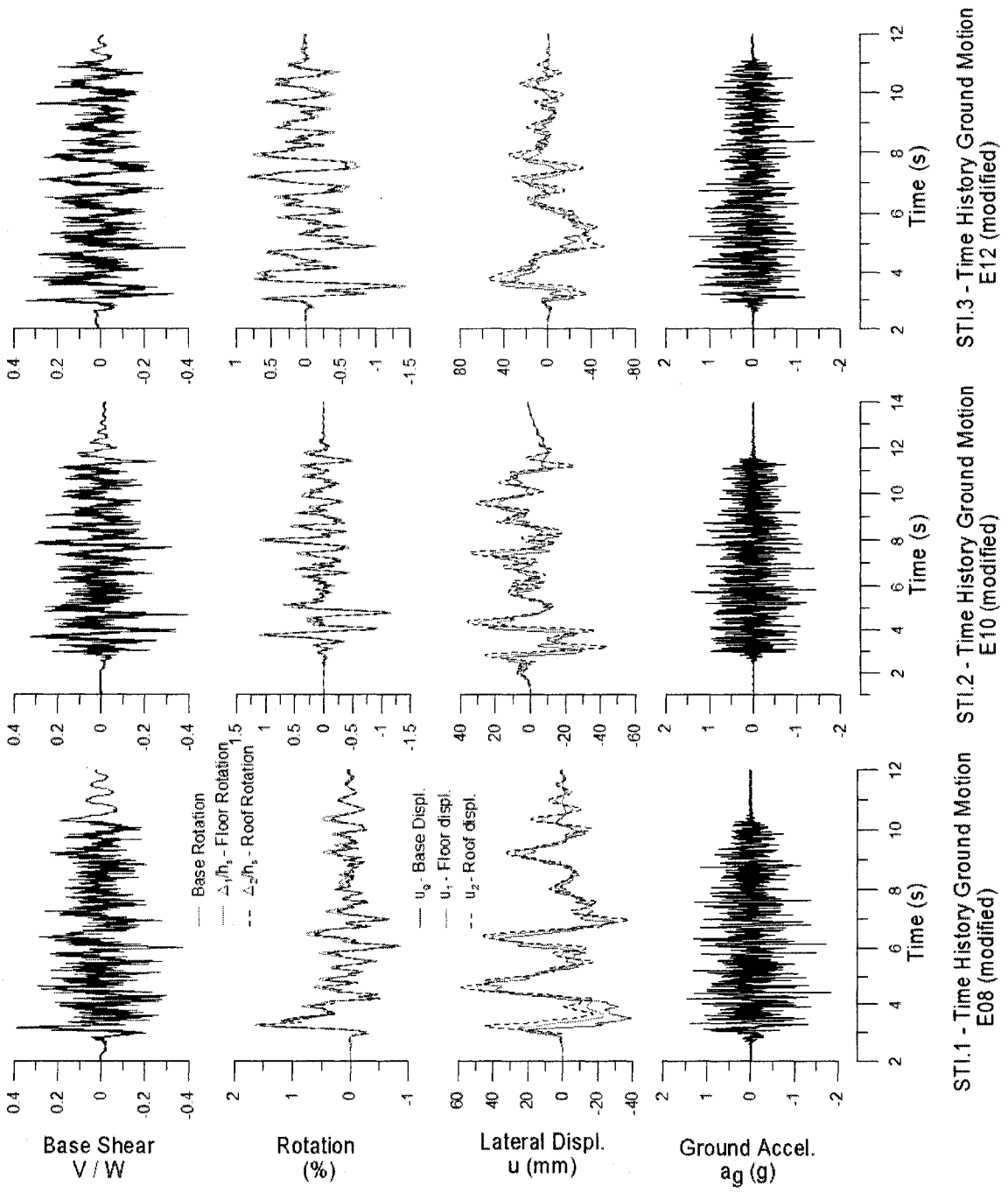

Figure 7.20: Test specimen response to the Montreal ground motion inputs.

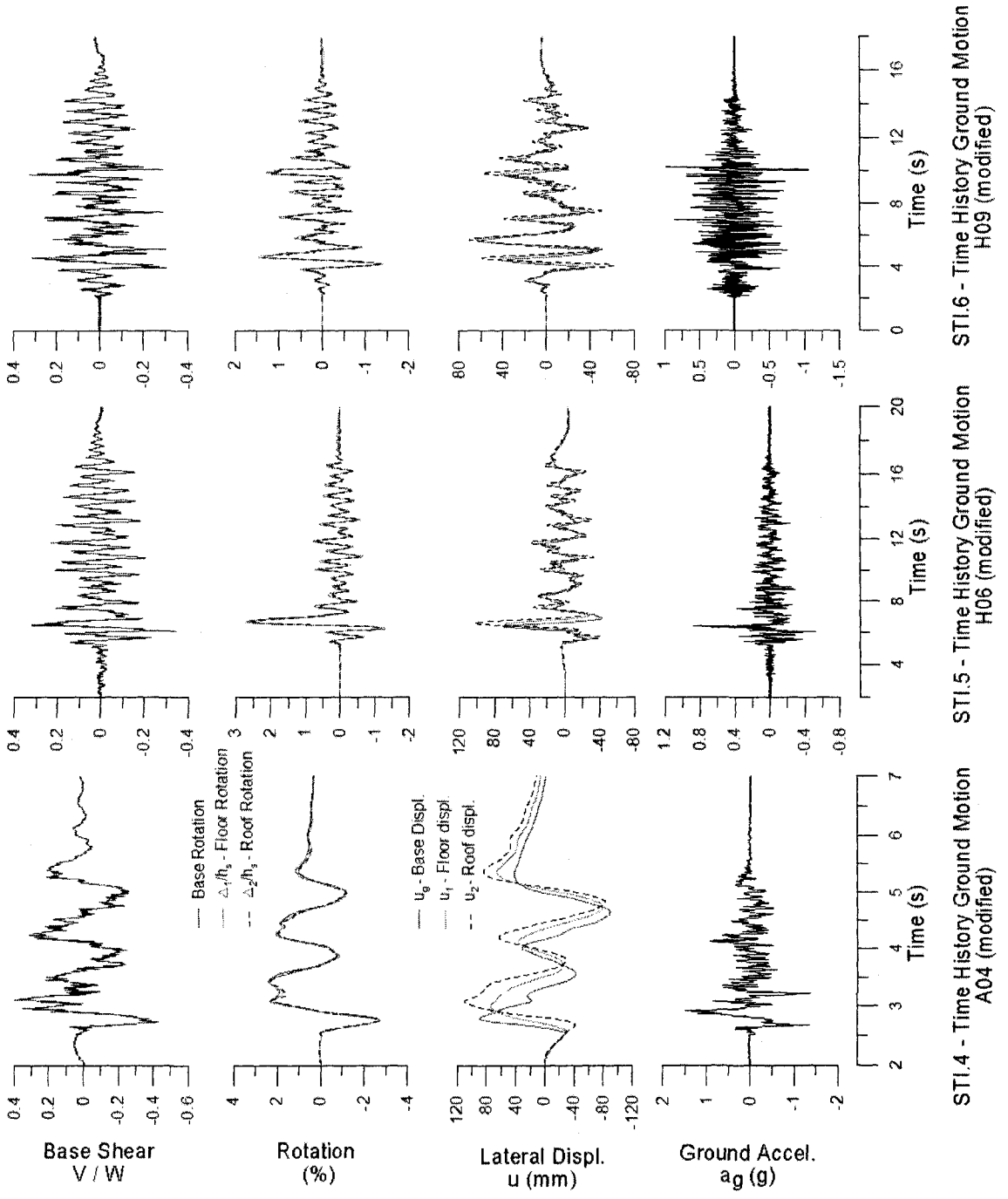

Figure 7.21: Test specimen response to the Vancouver ground motion inputs.

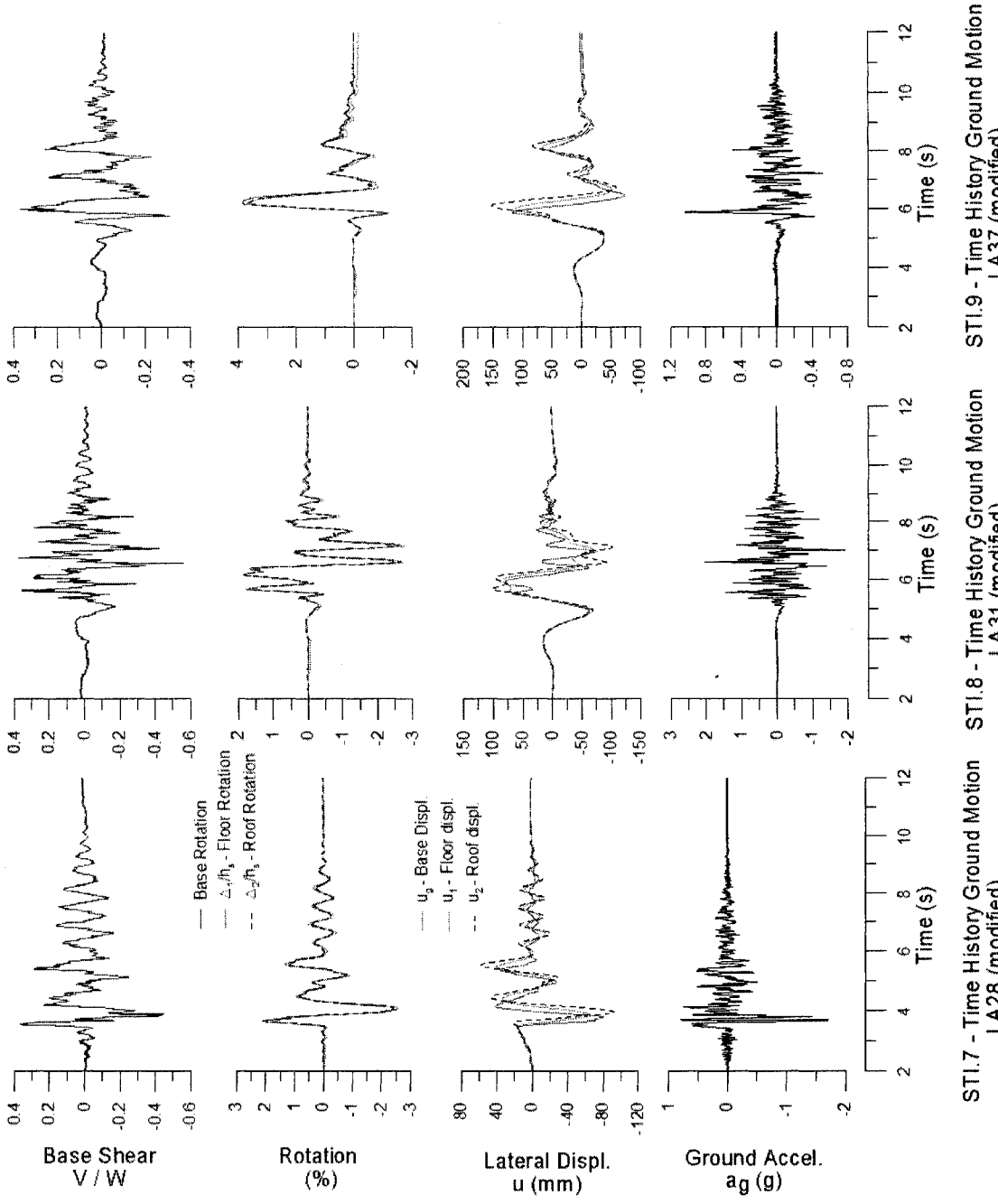

Figure 7.22: Test specimen response to the Los Angeles ground motion inputs.

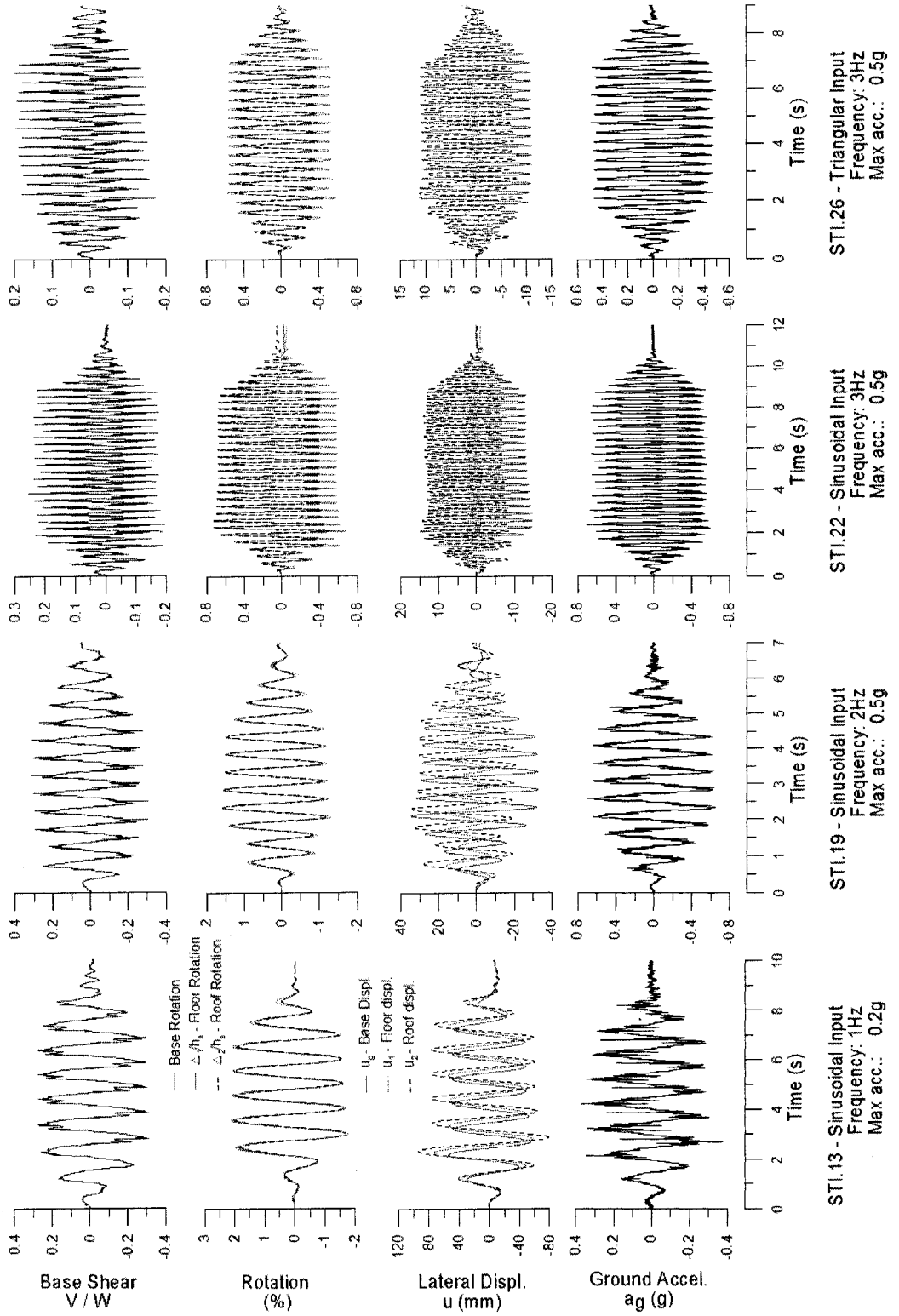

Figure 7.23: Test specimen response to the sinusoidal and triangular motion inputs.

Overall response

The results of the test trials demonstrate that the displacement (u) and the rotation of the two levels are in phase for most of the seismic inputs, which indicates that the motion of the frame is essentially resulting from rocking. The base rotation and inter-story drifts are also in phase under the higher frequency sinusoidal signals and triangular inputs, although the roof total displacements tend to lag behind the input base motion. Uplift displacements were measured for all the input motions indicating that the seismic dampers were active and participated in the rocking motion. Uplift displacements at the base of the columns reached between 18 mm and 28 mm for the Montreal ground motions, between 24 mm and 50 mm for the Vancouver ground motions, between 42 mm and 58 mm for the Los Angeles ground motions and between 8 mm et 36 mm for the sinusoidal and triangular input motions. In all tests, the frame returned to its initial position, without residual deformations and structural damage, as was anticipated.

7.7. Numerical Analyses

7.7.1. Numerical model

A numerical model was developed using SAP2000 to replicate the measured response of the VDCSR system as obtained from the shake table test program. The objective of this procedure was to determine if the behaviour of the VDCSR system could be predicted with a simplified two-dimensional model, similar to the ones used in the parametric study. Figure 7.24 illustrates the numerical model used for the comparison.

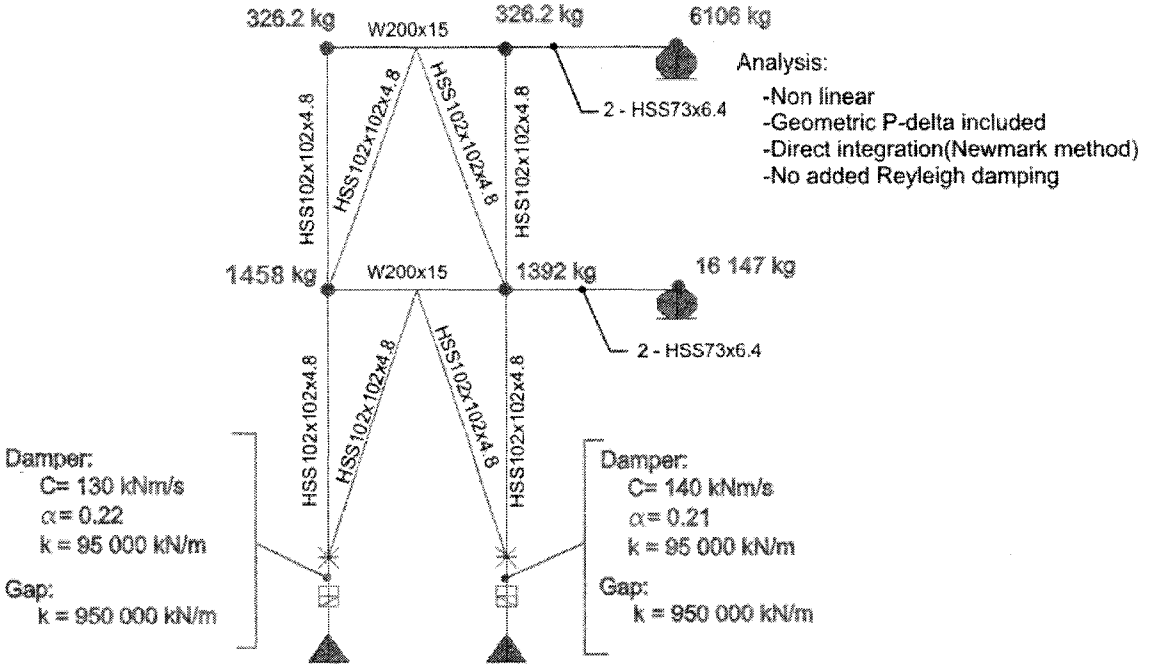

Figure 7.24: Numerical model of the shake table test program.

The element and mass properties specified in the numerical model replicated exactly those of the test specimen. The joint masses at the beam-to-column joints were specified in the horizontal and vertical directions. All connections between the members were fixed except that pinned connections were specified between the beams and the columns (the braces were rigidly connected to the beams at the first and second levels and to the columns at the base). The type of analysis used for the numerical model was a nonlinear, direct integration analysis, using the Newmark method, with the P-delta effects included. The output time step used was 0.05 seconds.

The base conditions were modelized using the same simplified concept developed for the parametric study. A damper element and a gap element were used in parallel to replicate the vertical support conditions of the seismic dampers. The damper properties used for the numerical model were those measured experimentally; these were described in the previous chapter. The rigidity (k) of the damper and the gap elements were selected in order to obtain a first mode of frequency equal to 3.5 Hz, as determined from

the impact tests. Initially, the damping values from the impact tests, illustrated in Figure 7.17, were included into the numerical mode (mode specified damping), but it was found that the numerical predictions better matched the experimental data when this damping was omitted. As discussed in Section 7.5, it is very likely that the damping measured during the impact tests was actually essentially induced by the seismic dampers. Hence, specifying modal damping and including the seismic dampers in the numerical model would therefore overestimate the actual damping available in the test frame and the decision was made to omit modal damping.

All 26 input signals used for the shake table test program were applied to the numerical model for comparison purposes. However, the input signals used for the numerical analyses were the measured acceleration output from the built-in accelerometer of the earthquake simulator, so that the exact same excitation was applied to the numerical model and the test specimen.

7.7.2. Comparison between the numerical and experimental results

Figures 7.25 to 7.29 illustrate the typical response of the numerical model to five of the twenty six input ground motions. These results were plotted against the measured results from the shake table test program. The five selected input signals were representative of the five types of input signals imposed onto the test specimen and the numerical model; a ground motion from Montreal (E08), a ground motion from Vancouver (H09), a ground motion from Los Angeles (LA28), a sinusoidal input signal (2Hz, 0.5g) and a triangular input signal (3Hz, 0.5g). Plotted are the graphs for the total lateral displacement at the top and 1st floor of the frame, the vertical (uplift) displacement of the East and West column bases, the axial forces in the West column and the 1st-storey brace on the West side, and, finally, the axial forces in the articulated arms at the top and 1st level of the frame. The displacement results were taken directly from the experimental and numerical data, while the axial forces were computed using

the readings from the strain gages and applying the appropriate gage factors, as described above.

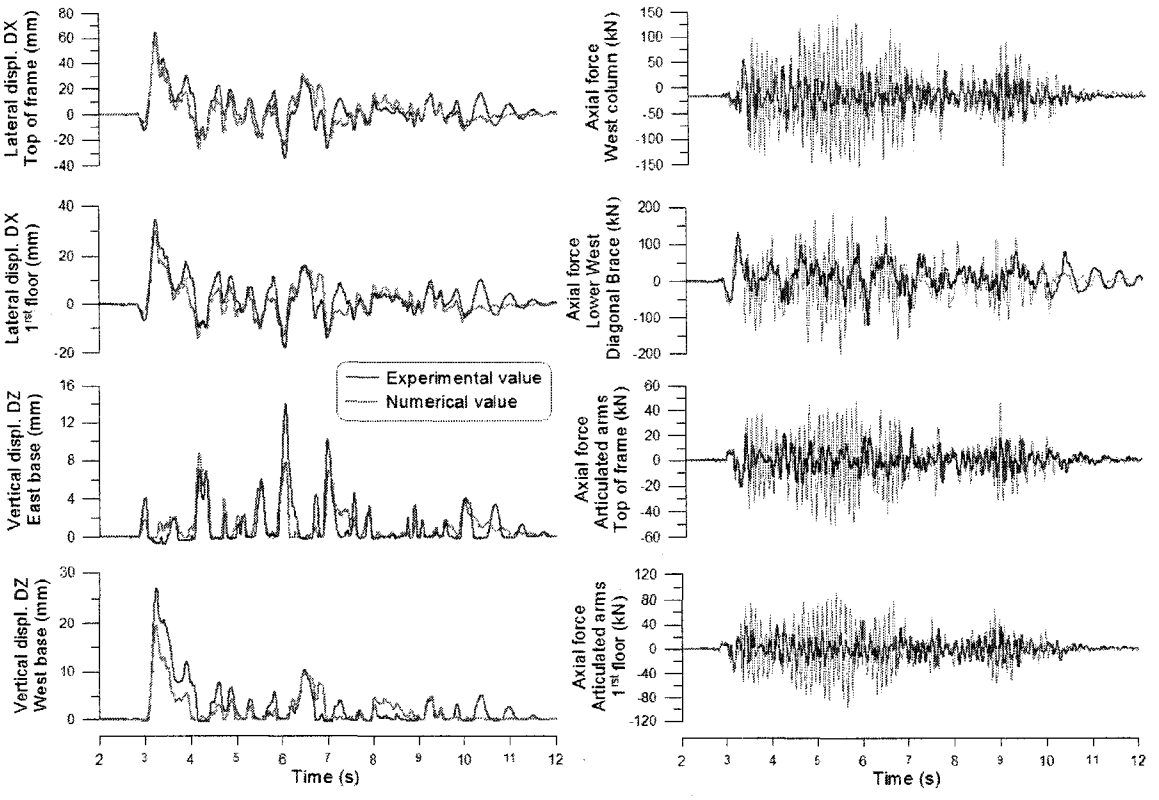

Figure 7.25: Comparison of the results for the STI.1 input signal (Montreal, E08).

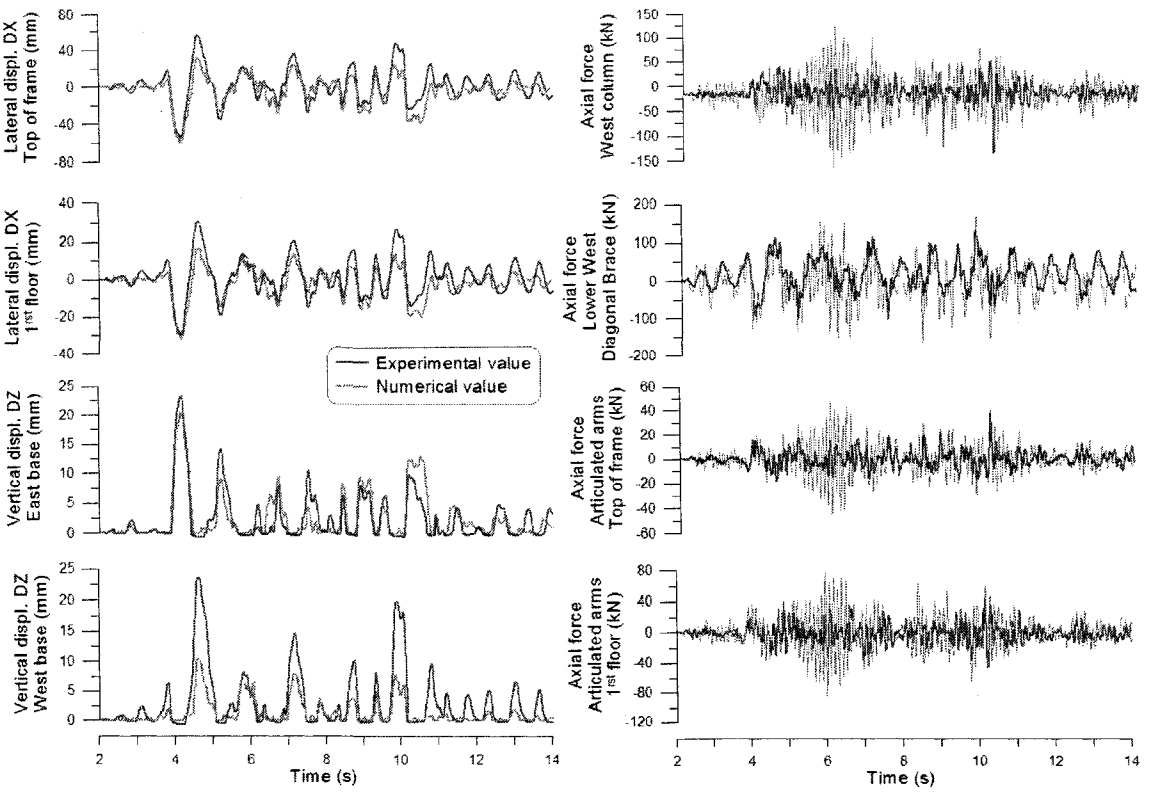

Figure 7.26: Comparison of the results for the STI.6 input signal (Vancouver, H09).

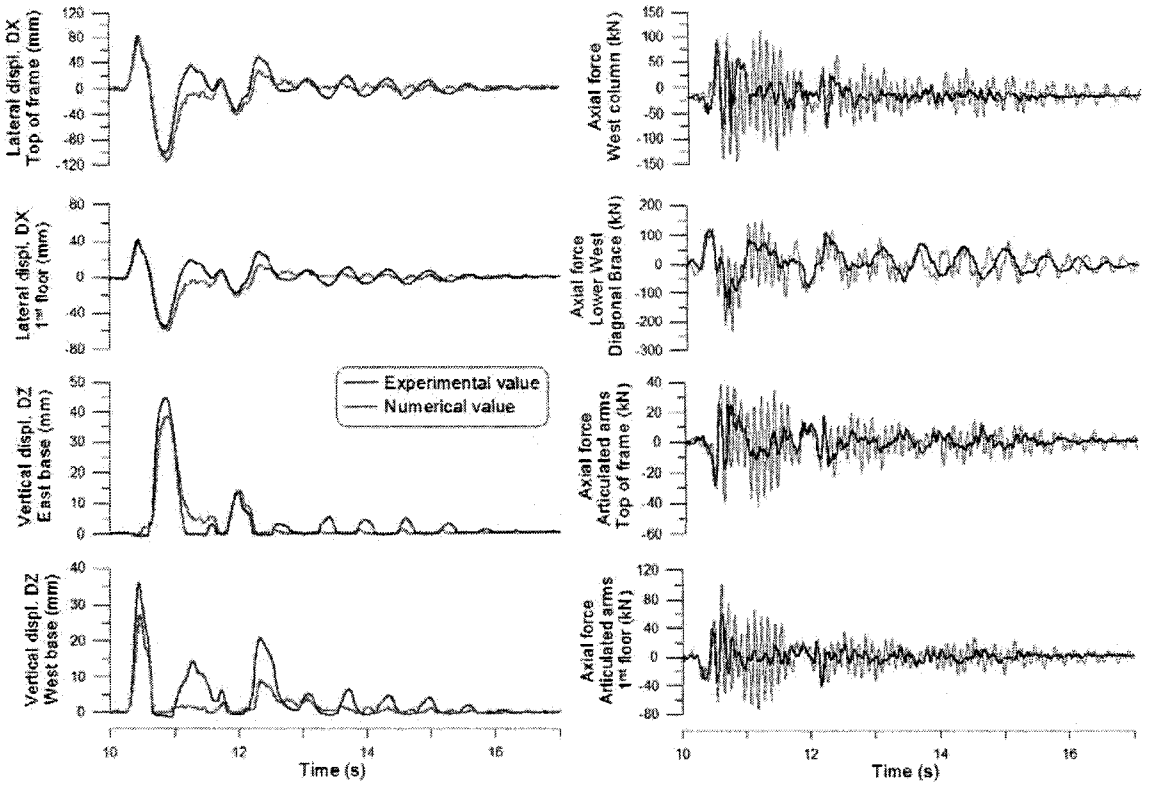

Figure 7.27: Comparison of the results for the STI.7 input signal (Los Angeles, LA28).

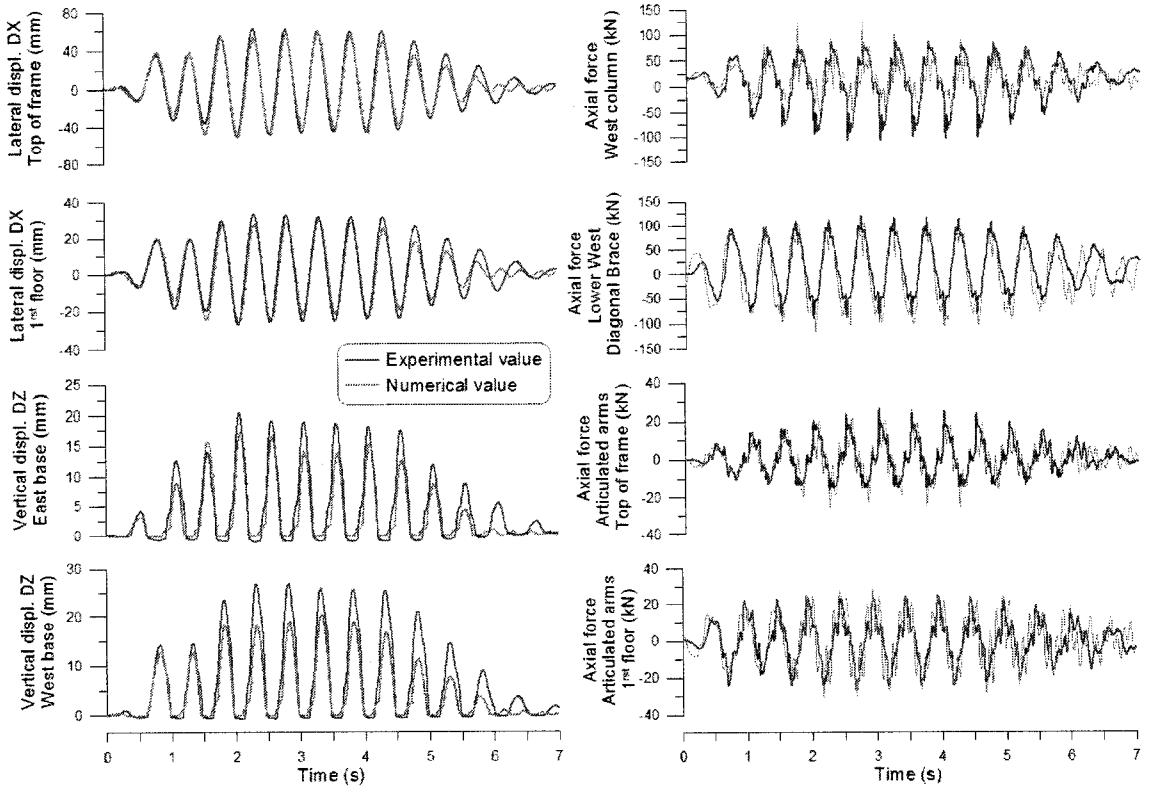

Figure 7.28: Comparison of the results for the STI.19 input signal (Sinusoidal 2Hz, 0.5g).

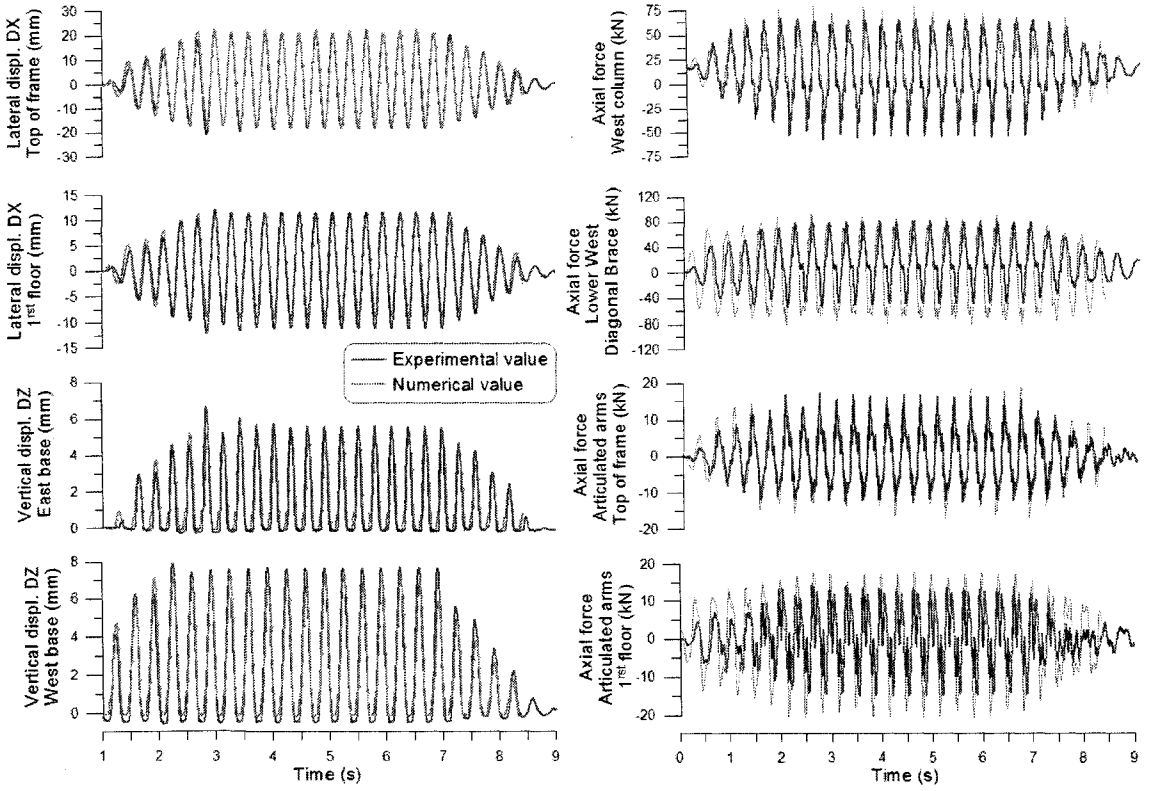

Figure 7.29: Comparison of the results for the STI.26 input signal (Triangular 3Hz, 0.5g).

The simplified numerical model used to replicate the behaviour of the VDCSR system is found to be very accurate in predicting the horizontal and base uplift displacement responses of the VDCSR system to all ground motion types. In some cases, the peak displacement amplitudes were not fully attained with the numerical model, but in general, the numerical predictions are very precise.

The numerical predictions of the member forces were however over-estimated in comparison to the values measured experimentally for all earthquake ground motions. The general trends associated to the rocking response of the frames were well reproduced by the simulation model but a significant high frequency response was also predicted by the analysis that was not measured in the experimental program. This phenomenom is not observed in the tests with a sinusoidal and triangular input applied at a given frequency. In these tests, the force outputs were nearly perfectly predicted by the

numerical model. This suggests that the numerical model could be likely enhanced by introducing damping for higher mode response.

Figure 7.30 illustrates the reason why confidence is given to the readings of the strain gages from the experimental tests over the axial force output of the finite element program. This figure compares the axial force in one of the articulated arms at the top of the frame measured by the strain gages G17 and G18, and measured by the acceleration of the top drawer A12 multiplied by half the weight of the drawer (6106 kg / 2 = 3053 kg). The comparison is performed for the ground motion H09; however, the same results are obtained for the other input signals: A perfect match. This validated the readings of the strain gages. Also, the behaviour of the gages observed in the tests performed on the individual frame elements (Section 7.5.2) helps strengthen our confidence.

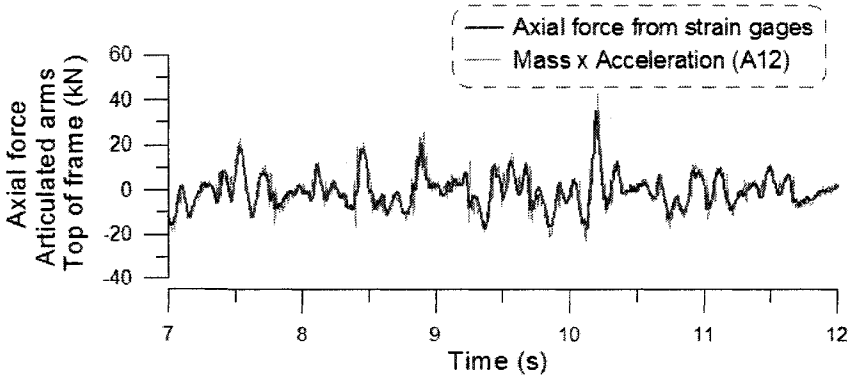

Figure 7.30: Validation of the strain gage readings (ground motion H09).

7.8. Conclusion

A shake table test program was developed using one of the braced frames from a 2-storey building examined in the parametric study. The test program was conducted on a half-scale model mounted on vertical viscous dampers. The test frame was subjected to nine earthquake ground motion records exhibiting different characteristics, i.e. three records for each of the three seismic locations considered: Montreal, Vancouver, and Los Angeles. In addition, the test model was subjected to harmonic signals with various amplitudes and frequencies. The objectives of the test program were to evaluate the real life performance of the Viscously Damped Controlled Seismic Rocking (VDCSR) system subjected to earthquakes and various other signals, and to validate the accuracy of the computer models used in the parametric study.

The test program was completed successfully. The VDSCR system behaved as intended in design, without structural damage. Uplift displacements were measured for all the input ground motions indicating that the seismic dampers were active and participated in the rocking motion. Numerical simulations were performed using the SAP2000 finite element analysis program to replicate the response of the test frame measured in the shake table test program. The comparison results demonstrated that the analytical model can predict very accurately the displacement and uplift responses of the test frame under all the loading signals that were considered. However, it was found that the brace and column axial loads predicted under the seismic motions were overestimated by the numerical models. This was not true for the harmonic signals applied at a constant frequency. This suggests that the numerical model could be likely enhanced by introducing damping for higher mode response. Further investigation is required to fully explain this problem.

CHAPTER 8

CONCLUSION

The Viscously Damped Controlled Seismic Rocking (VDCSR) system is an innovative self-centering base isolation system, proposed for steel braced frames as a cost-effective method for enhanced seismic performance against strong earthquake ground motions. The system includes viscous dampers that are vertically mounted between the foundation and the column bases to dissipate energy and control the lateral displacements of the structure during the rocking motion, while limiting the impact forces induced in the columns. The two beneficial components of this mechanism are the rocking motion, which increases the fundamental period of vibration of the braced frame thus reducing the seismic loads imposed onto the structure, and the viscous dampers, which provide additional damping to the system thus decreasing the seismic loads and the lateral displacements of the structure. Braced frames with the VDCSR system remain elastic during design level earthquakes; therefore they do not experience structural damage. Also, the vertical force demand on the foundations is reduced compared to the forces that would develop in conventional braced steel frames designed according to current seismic provisions.

The main objective of this project was to study the performance of the VDCSR system and to verify its applicability to low-rise buildings through analytical and experimental studies. Initially, simplified methods were evaluated to find a preliminary design procedure to predict the properties needed for the system. This was followed by a parametric study to evaluate the structural parameters that influence most the performance of the VDCSR system and identify the seismic regions that would benefit more significantly from such a system. This study led to an experimental test program that was conducted to verify the response the foundation/fluid damper/column assembly under cyclic loading. The test program also aimed at validating the adequacy of the

numerical models used in the parametric study to accurately reproduce the response of the system. Following are the conclusions of the various analyses and experimental work completed.

Three simplified methods developed to predict the maximum displacement of rocking structures under seismic loadings were evaluated. The three methods are the Substitute Substructure technique (Preisley et al., 1996), the Energy Balance method and the Equal Energy method (Anderson, 1993). Example problems using rigid blocks and single-degree-of-freedom (SDOF) structures were performed to evaluate the effectiveness of these simplified methods. Nonlinear finite element models using SAP2000 were used to validate the simplified methods. This program demonstrated itself as being capable of correctly reproducing the rocking response of SDOF structures. Its results were successfully compared to the dimensionless analytical method proposed by Yim and Chopra (1983). This study demonstrated that the effectiveness of the simplified methods were dependant on the structure and the ground motion properties. None of the techniques was predominantly more accurate than the others, although all of them predicted very accurately the displacement of the structure in certain cases. It is the author's opinion that the evaluations performed are not conclusive. In design circumstances, a more complete nonlinear dynamic analysis should be performed with a finite element program such as SAP2000.

A parametric study was conducted to evaluate the seismic performance of the VDCSR system for various 2-, 4- and 6-storey building applications located in three seismic locations (Montreal, Vancouver, and Los Angeles). The structures studied had 45 m x 45 m plan dimensions. The influence of the width of the rocking bracing bents (5.625 and 9.0 m) as well as their location in the building structures (along the exterior or interior column lines) was examined. For all buildings, the results of the study demonstrate that the column uplift loads with the VDCSR system are nearly entirely annihilated. The downwards forces on the foundations are also greatly reduced

compared to conventional fixed base seismic force resisting systems (SFRS). During the rocking process, one column of the braced frame must carry the total gravity loads supported by the bracing bay. In spite of this penalty, the peak axial loads in the columns are not considerably greater than the forces that must be considered in the design of conventional fixed base steel braced frames. Increased shear forces at the base of the frame are expected however with the VDCSR system, especially for structures located along the western part of North America. For these structures, the base shear forces increase is more pronounced for the taller frames. As the height of the building increases, the overturning moment response tends to lag behind the horizontal shear force demand and the capacity of controlling base shear forces by reducing the base overturning moment reaction through rocking gradually diminishes. The shear forces become greater than those of a conventional fixed base designs. Similarly, axial loads in the diagonal bracing members of the VDCSR system are also larger than the design loads for a conventional chevron frame. The increase in brace axial forces is more pronounced as the slenderness ratio of the braced frame is decreased and the vertical weight to seismic mass ratio is decreased. Cost comparisons should be carried out for the sample frames studied herein to identify building applications where the highest overall cost savings can be achieved (where savings on column and foundation costs exceed most the additional costs due to the increased storey shears). The study also showed that the structures can be designed to avoid any residual deformation and structural damage after strong ground motion, thus reducing considerably the repair costs and disruption periods after a severe earthquake event. This represents a significant advantage compared to conventional SFRS that are designed to undergo inelastic deformations under design level earthquakes.

The parametric study demonstrated that the VDCSR system performed very well in low and moderate seismic regions, such as the Montreal and Vancouver sites. For these two sites, the inter-storey drifts remained well below code imposed limits. However, relatively higher brace forces are expected at the Montreal site, and VDCSR buildings in

Vancouver are likely to experience relatively higher base shear forces. The results for the Los Angles site indicate that the VDCSR system in high seismic regions where impulsive type ground motions are expected may result in excessive inter-storey drift demand, even if high capacity viscous dampers are used. This reduces the advantage of the system as these large deformations may lead to structural and non-structural damage. It is believed that increasing the restoring or self-centering capability of the system would enhance the response of the system in high seismic zones. Adding vertical post-tensioned cables is one approach to achieve this.

A shake table test program was developed using one of the braced frames from a 2-storey building examined in the parametric study. The test program was conducted on a half-scale model mounted on vertical viscous dampers. The test model was designed following strict similitude requirements to fully exploit the capacity of the earthquake simulation facility. The viscous dampers used were calibrated to meet the applicable similitude requirements through a series of dynamic cyclic tests conducted on individual damper units. The shake table test setup was composed of seismic weights mounted on roller bearings at both levels of the test frame to simulate the actual braced frame tributary seismic weight in the prototype building. Concentrated weights were applied at the beam-to-column joints at both levels to reproduce the tributary gravity loads supported by the bracing bent. The test frame was subjected to nine earthquake ground motion records exhibiting different characteristics, i.e. three records for each of the three seismic locations considered: Montreal, Vancouver, and Los Angeles. In addition, the test model was subjected to harmonic signals with various amplitudes and frequencies. The test program was completed successfully. The VDCSR system behaved as intended in design, without structural damage. Uplift displacements were measured for all the input ground motions indicating that the seismic dampers were active and participated in the rocking motion. One of the main objectives of the test program was to validate the numerical models used to predict the response of building structures equipped with the VDCSR system, so that the results obtained from the parametric study could be

supported and the model used for future design applications. Numerical simulations were performed using the SAP2000 finite element analysis program to replicate the response of the test frame measured in the shake table test program. The comparison results demonstrated that the numerical model can predict very accurately the displacement and uplift responses of the test frame under all the loading signals that were considered. However, it was found that the brace and column axial loads predicted under the seismic motions were overestimated by the numerical models. This was due to high frequency numerical response that was not observed in the tests. Conversely, the member force demand was very well predicted under harmonic signals applied at a constant frequency. Further investigation is required to fully explain this problem. Nevertheless, these findings suggest that currently available simple numerical models can be used with confidence to predict the deformation demand on rocking braced frames equipped with nonlinear viscous dampers. Caution must be exercised in the interpretation of the axial force outputs provided by the numerical models. This also applies to the results of the parametric study.

This project addressed several aspects of an innovative seismic force resisting system exhibiting interesting features. The results of this study are promising and suggest that this system has excellent potential to become a cost-effective solution for enhanced seismic performance in low and moderate seismic regions. Further investigations are needed however to evaluate the effects of the vertical component of earthquakes on the performance of the system, the impact forces generated in the frame when the column bases come in renewed contact with the foundations and the effects the type of soil has on the behaviour of the system.

REFERENCES

Anderson, D.L. (2003). Effect of foundation rocking on the seismic response of shear walls, *Canadian Journal of Civil Engineering, 30*(2), 360-365.

Anderson, D.L. (1993). Buildings with Rocking Foundations", *Proceedings of the Seismic Soil/Structure Interaction Seminar, Vancouver, B.C.*, May 29.

ATC. (2008). *Quantification of Building Seismic Performance Factors ATC-63 Project Report - 90% Draft FEMA P695 / April 2008.* Applied Technology Council, Redwood City, California.

Buckingham, E., (1914). On Physically Similar Systems; Illustrations of the Use of Dimensional Equations, *Physics Review, 4*(4), 345-376.

Canadian Standard Association. (2001). *Limits States Design of Steel Structures*, Canadian Standard Association, CAN/CSA-S16-01.

Canadian Standard Association. (2005). *Supplement No. 1 to CAN/CSA-S16-01 Limits States Design of Steel Structures*, Canadian Standard Association, CAN/CSA-S16S1-05.

Computer & Structures inc. CSI (2007). *SAP2000 – Integrated Software for Structural Analysis and Design, Version 10* [Computer program]. Berkley, CA: CSI.

Clough, R.W. and HuckelBridge, A.A. (1977). *Preliminary Experimental Study of Seismic Uplift of a Steel Frame*, (UBC/EERC-77/22), Earthquake Engineering Research Center, College of Engineering, University of California, Berkeley, CA.

Dowdell, D. and Hamersley, B. (2001). Lions' Gate Bridge North Approach: Seismic Retrofit, *Behaviour of Steel Structures in Seismic Areas: Proceedings of the Third International Conference: STESSA 2000; Montreal, Canada, August 21-24 2000* (pp. 319-326). Rotterdam, The Netherlands: A.A. Balkema.

Federal Emergency Management Agency. (2000). *Prestandard and Commentary for the Seismic Rehabilitation of Buildings.* Prepared by the American Society of Civil Engineers for the Federal Emergency Management Agency, FEMA 356.

Filiatrault, A., Anderson, D.L., and DeVall, R.H. (1992). Effect of a weak foundation on the seismic response of core wall type buildings, *Canadian Journal of Civil Engineering, 19*(3), 530-539.

Filiatrault, A., Restrepo, J. and Christopoulos (2004). Development of Self-Centering Earthquake Resisting Systems, *Paper No. 3393, 13th World Conference on Earthquake Engineering, Vancouver, Canada, August 2004.*

Griffith, M.C., Kelly, J.M., Coveney, V.A. and Koh, C.G. (1988). *Experimental Evaluation of Seismic Isolation Medium-Rise Structures Subject to Uplift* (UBC/EERC-88/02). Earthquake Engineering Research Center, College of Engineering, University of California, Berkeley, CA.

Griffith, M.C., Aiken, I.D. and Kelly, J.M. (1988). *Experimental Evaluation of Seismic Isolation of a 9-Story Braced Frame Subject to Uplift* (UBC/EERC-88/05). Earthquake Engineering Research Center, College of Engineering, University of California, Berkeley, CA.

Gupta, A. and Krawinkler H. (2000). Eehaviour of Ductile SMRFs at Various Seismic Hazard Levels. *American Society of Civil Engineers Journal of Structural Engineering.*, 126 (1), 98-107.

Huckelbridge, AA. (1977), *Earthquake simulation tests of a nine story steel frame with columns allowed to uplift* (UBC/EERC-77/23). Earthquake Engineering Research Center, College of Engineering, University of California, Berkeley, CA.

Humar, J.L. (2002). *Dynamics of Structures* (2nd Edition). Lisse: A.A. Balkema Publishers. 957p.

Housner, G.W. (1963). The Behaviour of Inverted Pendulums Structures during Earthquakes, *Bulletin of the Seismological Society of America, 53*(2), 403-417.

Izvernari, C., Lacerte, M., and Tremblay, R. (2007). Seismic performance of multi-storey concentrically braced steel frames designed according to the 2005 Canadian seismic provisions. *Paper No. 1419. Proceedings of the 9th Canadian Conference on Earthquake Engineering, Ottawa, ON.*

International Code Council and the California Building Standards Commission. (2001). *2001California Building Code.* International Code Council and the California Building Standards Commission. CBC 2001.

Kelly, J.M. and Tsztoo, D.F. (1977). *Earthquake Simulation Testing of a Stepping Frame with Energy-Absorbing Devices* (UBC/EERC-77/17). Earthquake Engineering Research Center, College of Engineering, University of California, Berkeley, CA.

Makris, N. and Konstantinidis (2001). *The Rocking Spectrum and the Shortcomings of the Design Guidelines* (PEER Report 2001/07). Pacific Earthquake Engineering Research Center, College of Engineering, University of California, Berkeley, CA.

Meek, J.W. (1975). Effects of Foundation Tipping on Dynamic Responce, *Journal of Structural Division, 101*(7), 1297-1311.

Midorikawa, M., Azuhata, T., Ishihara, T., and Wada, A. (2003). Shaking table tests on rocking structural systems installed yielding base plates in steel frames, *Proceedings of the conference on behaviour of steel structures in seismic areas, 9-12 June 2003, Naples, Italy: STESSA 2003* (pp.449-454). Lisse, The Netherlands: Swets and Zeitlinger B.V.

Mitchell, D., Tremblay, R., Karacabeyli, E., Paultre, P., Saatcioglu, M., and Anderson, D. (2003). Seismic Force Modification Factors for the Proposed 2005 NBCC. *Canadian Journal of Civil Engineering, 30*(2), 308-327.

Merzouq, S. (2006). *Le dual-BRB : une alternative pour un comportement sismique amélioré.* M.Sc.A. Dissertation. Ecole Polytechnique de Montreal, Montreal,Qc.

Moncarz, P.D. (1981). *Theory and Application of Experimental Model Analysis in Earthquake Engineering.* Ph.D. Dissertation. Stanford University, Palo Alto, CA.

Naeim, F. (2001). *The Seismic Design Handbook* (2nd Edition). New York: Springer. 830p.

National Research Council of Canada. (2005). *National Building Code of Canada 2005.* National Research Council of Canada, NBCC 2005.

Palermo, A., Pampanin, S. and Calvi, G.M. (2004). Use of Controlled Rocking in the Seismic Design of Bridges, *Paper No. 4006, 13th World Conference on Earthquake Engineering, Vancouver, Canada, August 2004.*

Pollino, M. and Bruno, M. (2007). Seismic Retrofit of Bridge Steel Truss Piers Using a Controlled Rocking Approach, *ASCE Journal of Bridge Engineering, 12*(5), 600-610.

Poirier, L.-P. , Tremblay, R. and Bouaanani, N. 2008. Parametric Study on the Use of the Viscously Damped Controlled Seismic Rocking Braced Frame System for building applications. *Research Report No. SR08-06, Group for Research in Structural Engineering, Dept. of Civil, Geological and Mining Eng., Ecole Polytechnique, Montreal, QC*

Priestley, M.J.N., Evison, R.J., and Carr, A. (1978). Seismic Response of Structures Free to Rock on their Foundations, *Bulletin New Zealand Society for Earthquake Engineering, 11* (3), 141-150.

Priestley, M.J.N., Seible, F. and Calvi, G.M. (1996). *Seismic Design and Retrofit of Bridges.* New York: John Wiley and Sons. 686p.

Psycharis, I.N. (1982). *Dynamic Behaviour of Rocking Structures Allowed to Uplift.* Ph.D. Dissertation. California Institute of Technology, Pasadena, CA.

Psycharis, I.N. and Jennings, P.C. (1983). Rocking of Slender Rigid Bodies Allowed to Uplift, *Earthquake Engineering and Structural Dynamics, 11*, 57-76.

Somerville, P., Smith, N., Punyamurthula, S. and Sun, J. (1997). *Development of Ground Motion Time Histories for Phases 2 of the FEMA/SAC Steel Project* (SAC/BD-97/04). SAC Joint Venture, October 1997.

Rodriguez, S. and Ingham, T.J. (1996). "Nonlinear Dynamic Analysis of the Golden Gate Bridge", *Report UBC/CEE-96/09, Seismic Design, Evaluation and Retrofit of Steel Bridges: Proceedings of the Second US Seminar, San Francisco, University of California, Berkeley, CA, November 20-21, 1996.*

Rutenberg, A., Jennings, P.C. and Housner, G.W. (1982). The Response of Veterans Hospital Building 41 in the San Fernando Earthquake, *Earthquake Engineering and Structural Dynamics, 10*, 359-379.

Sabelli, R., Mahin, S., and Chang, C. (2003). Seismic demands on steel braced frame buildings with buckling restrained braces. *Engineering Structures*, 25, 655-666.

Sause, R., Ricles, J., Roke, D., Seo, C.-Y., Wolski, M. (2007). *Self-Centering Steel Frame Systems*. Network for Earthquake Engineering Simulations (NEES). Consulted August 14th 2007, taken from the following web site: http://www.nees.org/About_NEES/Announcements/NEES4AM/Thursday/NEESRActiveProjectsSpotlight1/R_Sause_abstract.pdf

Taylor, D.P. (1999). *History, Design, and Applications of Fluid Dampers in Structural Engineering*. Taylor Devices inc., North Tonawanda, NY

Toranzo, L.A., Restrepo, J.I., Carr, A.J., and Mander, J.B. (2004). Rocking Confined Masonry Walls with Hysteretic Energy Dissipaters and Shake-Table Validation, *Paper No. 248, 13th World Conference on Earthquake Engineering, Vancouver, Canada, August 2004.*

Tremblay, R. and Atkinson, G.-M. (2001). Comparative Study of the Inelastic Seismic Demand of Eastern and Western Sites. *Earthquake Spectra* 2001, 17 (2), 333-358.

Tremblay, R., Velev, N., Merzouq, S., Blais, C., Leclerc, M., Léger, P., Massicotte, B., Rogers, C.A., (2005). Multi-purpose earthquake simulation testing set-up for seismic force resisting systems of multi-storey buildings, *1st International Conference on Advances in Experimental Structural Engineering, Nagoya, Japan July 18-21, 2005* (pp. 533-540).

Tremblay, R. (2005). Canadian Seismic Design Provisions for Steel Structures. *Proceedings of the North American Steel Conference 2005, Montreal, Canada, April 5-7,* (12p.).

Tremblay, R., Lacerte, M., and Christopoulos, C. (2008). Seismic Response of Multi-Storey Buildings with Self-Centering Energy Dissipative Steel Braces. *ASCE J. of Struct. Eng.*, 134 (1), 108-120.

Tremblay, R., Poirier, L.-P., Bouaanani, N., Leclerc, M., Fronteddu, L. and Rivest, S. (2008). Seismic Response of Viscously Damped Controlled Rocking Braced Steel Frames for Building Structures. *Proceedings of the CSCE 2008 Annual Conference, Quebec, Canada, June 10-13* (10p.).

Yim, C.-S., Chopra, A.K. and Penzien, J. (1980). *Rocking Response of Rigid Blocks to Earthquakes* (UBC/EERC-80/02). Earthquake Engineering Research Center, College of Engineering, University of California, Berkeley, CA.

Yim, C.-S. and Chopra, A.K. (1983). *Effects of Transient Uplift on Earthquake Response of Structures* (UBC/EERC 83/09). Earthquake Engineering Research Center, College of Engineering, University of California, Berkeley, CA.

Yoshioka, H., Ramallo, J.C. and Spencer, B.F. Jr. (2002). Smart Base Isolation Employing Magnetorheological Dampers, *Journal of Engineering Mechanics, 128*(5), 540-551.

Zang, J. and Makris, N. (2001). Rocking Response of Free-Standing Blocks under Cycloidal Pulses, *Journal of Engineering Mechanics, 127*(5), 473-483.

APPENDIX A

GROUND MOTIONS USED FOR THE SIMPLIFIED METHODS

GROUND MOTION – IMPERIAL VALLEY EARTHQUAKE (EL CENTRO, 1940)

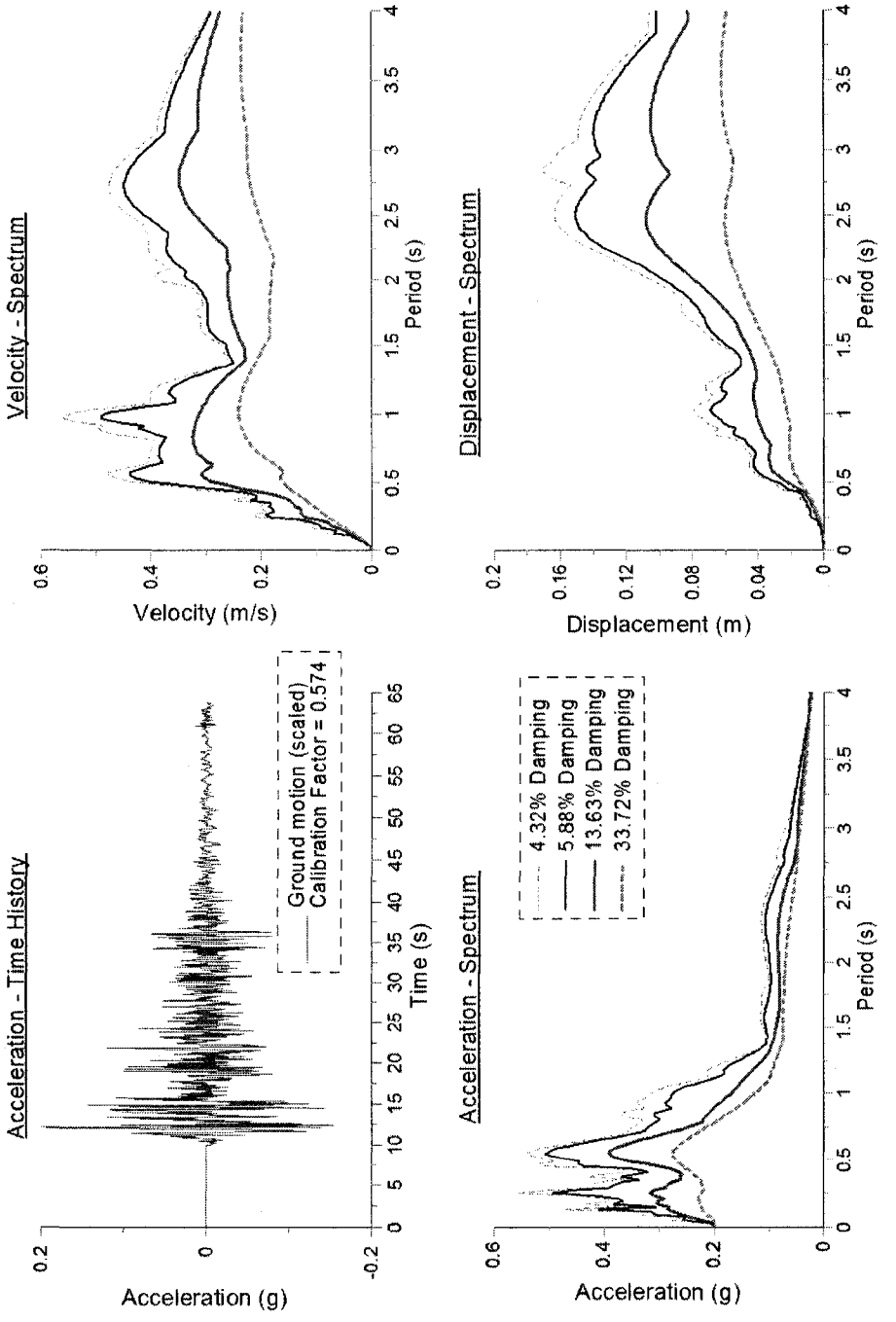

GROUND MOTION – KERN COUNTY EARTHQUAKE (TAFT, 1952)

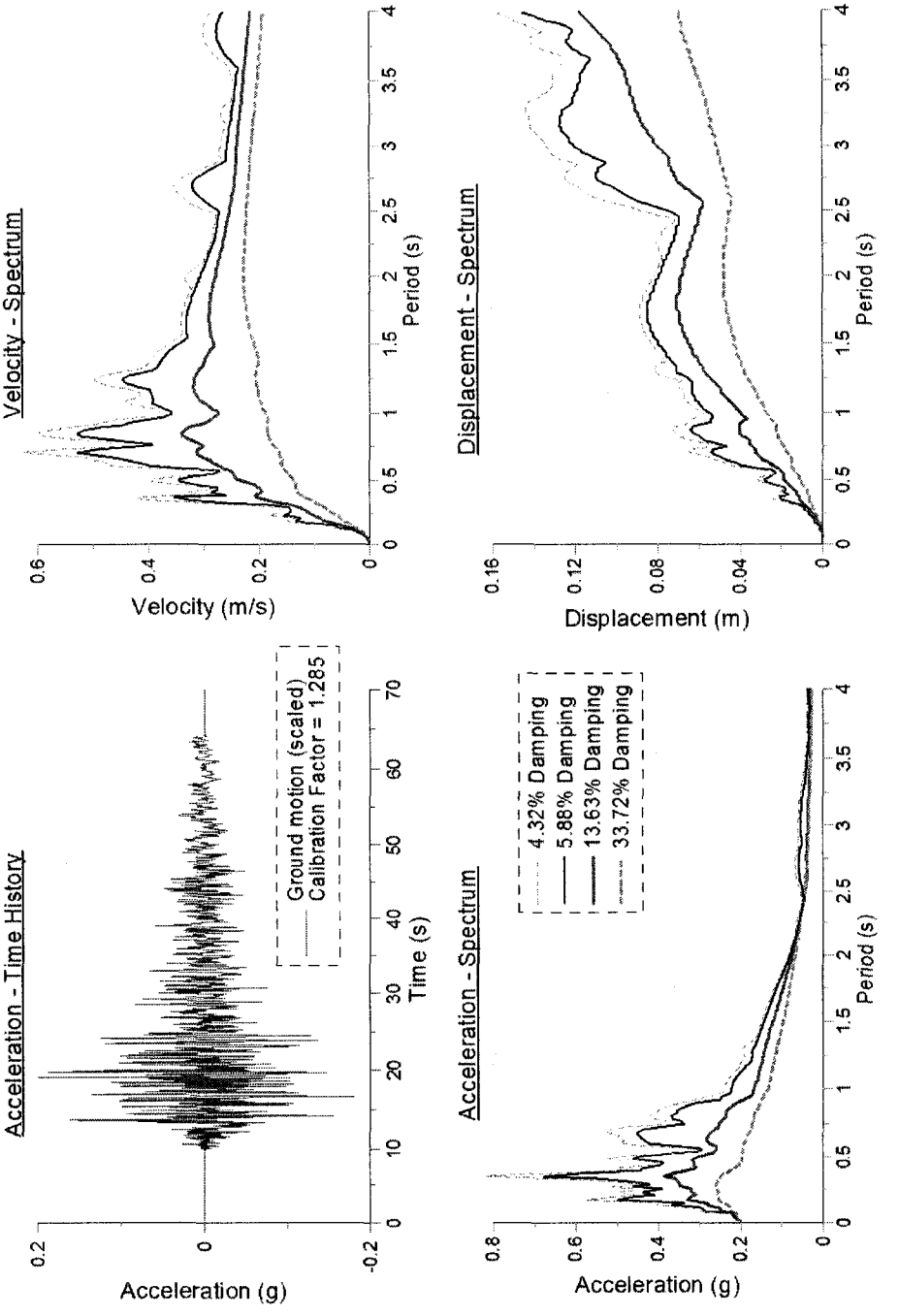

GROUND MOTION – SIMULATED EARTHQUAKE M701001

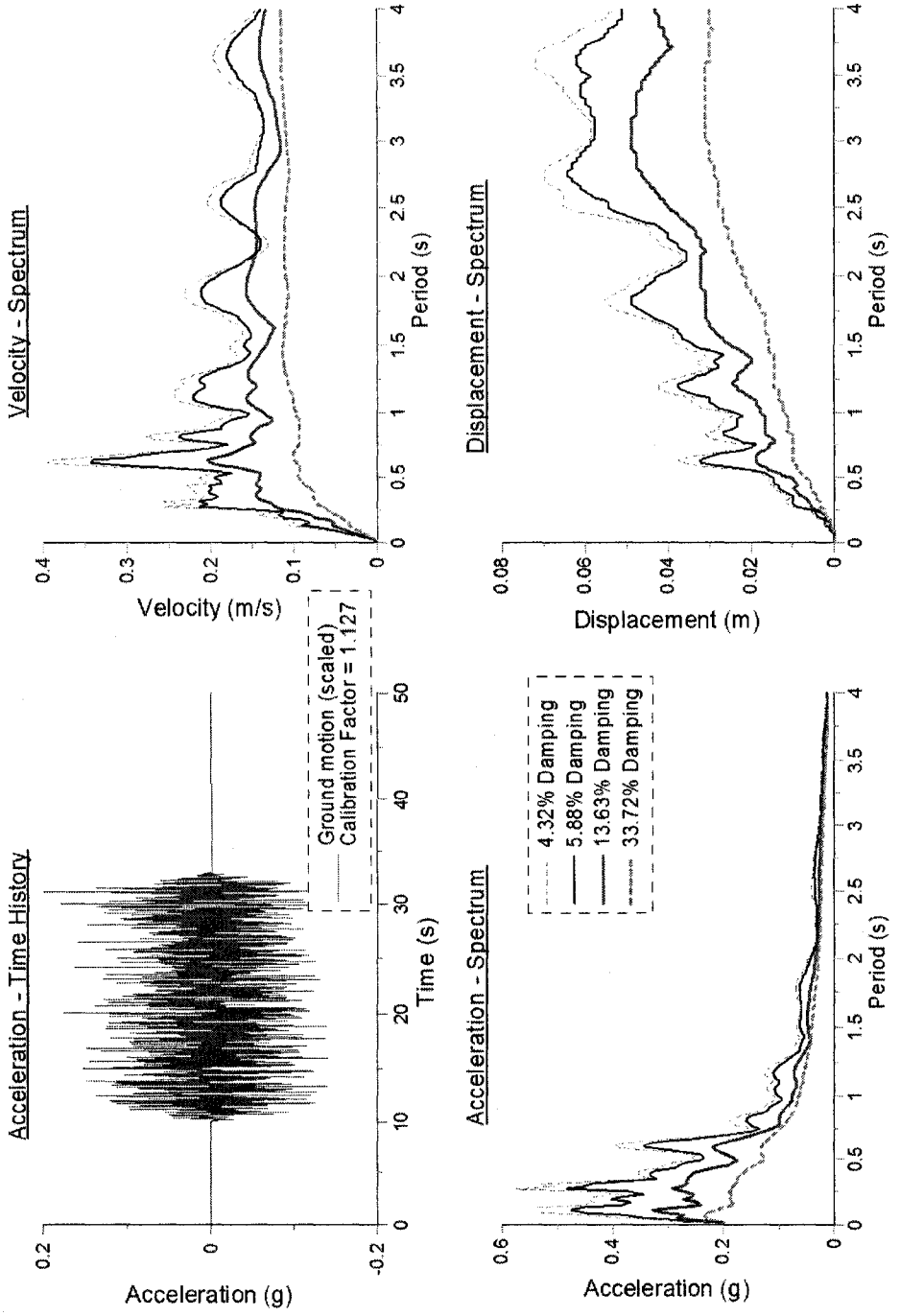

GROUND MOTION – SINUSOIDAL WAVE
(T = 0.6s)

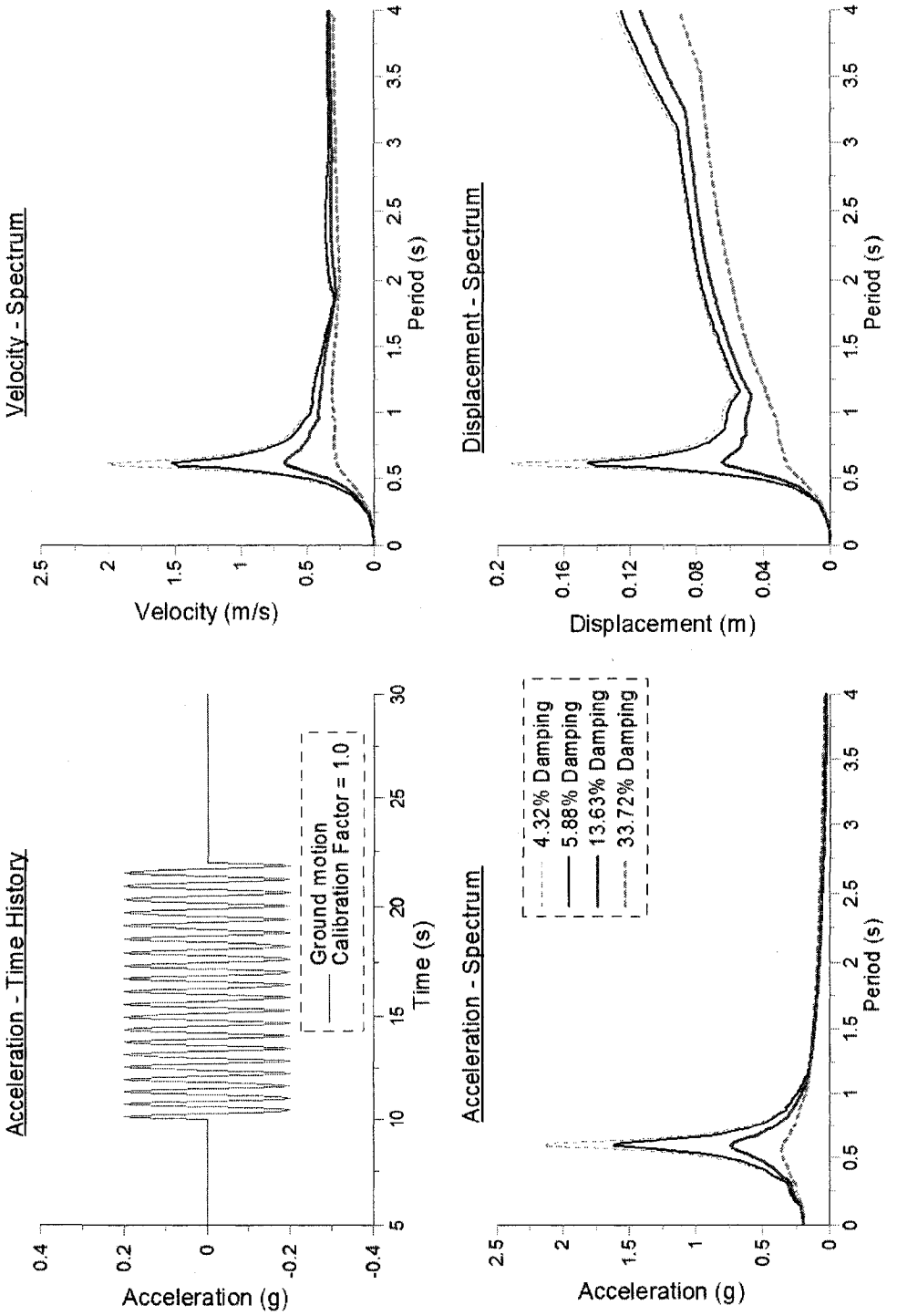

APPENDIX B

CALCULATIONS USING THE SIMPLIFIED METHODS

Example 1 - Rigid Block Structures

Table 1 : Calculations using the Substitute Substructure Technique

H = 3m

		TH ElCentro	TH Taft	TH MV01001	TH Sin Wave
		W = 2000 kN; l = 3 m; H = 3 m; Mr = 3000 kNm; A_{max} = 0.5 g; α = 28.6; cos2α = 0.60; r = 0.56; $ξ_c$ = 30.72 %; $ξ_{struct}$ = 3.00 %; $ξ_{tot}$ = 33.72 %			
1	$Δ_1$ =	0 m	0 m	0 m	0 m
	V_{b1} =	1000 kN	1000 kN	1000 kN	1000 kN
	K_{e1} =	— kN/m	— kN/m	— kN/m	— kN/m
	T_{e1} =	— s	— s	— s	— s

H = 6m

		TH ElCentro	TH Taft	TH MV01001	TH Sin Wave
		W = 2000 kN; l = 3 m; H = 6 m; Mr = 3000 kNm; A_{max} = 0.25 g; α = 14.5; cos2α = 0.88; r = 0.75; $ξ_c$ = 10.63 %; $ξ_{struct}$ = 3.00 %; $ξ_{tot}$ = 13.63 %			
1	$Δ_1$ =	0.001 m	0.001 m	0.001 m	0 m
	V_{b1} =	499.85 kN	499.85 kN	499.85 kN	1000 kN
	K_{e1} =	439646 kN/m	499848 kN/m	499848 kN/m	— kN/m
	T_{e1} =	0.13 s	0.13 s	0.13 s	— s
2	$Δ_2$ =	0.0017 m	0.001 m	0.001 m	
	V_{b2} =	499.41 kN			
	K_{e2} =	293772 kN/m			
	T_{e2} =	0.17 s			
3	$Δ_3$ =	0.0023 m			
	V_{b3} =	499.21 kN			
	K_{e3} =	217049 kN/m			
	T_{e3} =	0.19 s			
4	$Δ_4$ =	0.0028 m			
	V_{b4} =	499.05 kN			
	K_{e4} =	178232.87 kN/m			
	T_{e4} =	0.21 s			
5	$Δ_5$ =	0.0028 m			

H = 12m

		TH ElCentro	TH Taft	TH MV01001	TH Sin Wave
		W = 2000 kN; l = 3 m; H = 12 m; Mr = 3000 kNm; A_{max} = 0.125 g; α = 7.1; cos2α = 0.97; r = 0.94; $ξ_c$ = 2.91 %; $ξ_{struct}$ = 3.00 %; $ξ_{tot}$ = 5.91 %			
1	$Δ_1$ =	0.001 m	0.001 m	0.001 m	0.001 m
	V_{b1} =	249.83 kN	249.83 kN	249.83 kN	249.83 kN
	K_{e1} =	249831 kN/m	249831 kN/m	249831 kN/m	249831 kN/m
	T_{e1} =	0.18 s	0.18 s	0.18 s	0.18 s
2	$Δ_2$ =	0.0028 m	0.0038 m	0.003 m	0.002 m
	V_{b2} =	249.53 kN	249.38 kN	249.50 kN	249.66 kN
	K_{e2} =	89118 kN/m	65652 kN/m	83166 kN/m	124832 kN/m
	T_{e2} =	0.30 s	0.36 s	0.31 s	0.25 s
3	$Δ_3$ =	0.009 m	0.02 m	0.01 m	0.0047 m
	V_{b3} =	248.50 kN	246.66 kN	248.33 kN	249.21 kN
	K_{e3} =	27611 kN/m	12333 kN/m	24833 kN/m	53024 kN/m
	T_{e3} =	0.54 s	0.81 s	0.57 s	0.39 s
4	$Δ_4$ =	0.0273 m	0.059 m	0.024 m	0.018 m
	V_{b4} =	243.78 kN	240.16 kN	246.00 kN	247.00 kN
	K_{e4} =	8929.67 kN/m	4070.58 kN/m	10249.80 kN/m	13722 kN/m
	T_{e4} =	1.11 s	1.41 s	0.89 s	0.77 s
5	$Δ_5$ =	0.061 m	0.076 m	0.023 m	0.072 m
	V_{b5} =	239.83 kN	237.33 kN	246.16 kN	236.00 kN
	K_{e5} =	3932 kN/m	3123 kN/m	10702 kN/m	3278 kN/m
	T_{e5} =	1.43 s	1.61 s	0.87 s	1.55 s
6	$Δ_6$ =	0.052 m	0.083 m	0.023 m	0.068 m
	V_{b6} =	241.33 kN	236.10 kN		238.86 kN
	K_{e6} =	4641 kN/m	2845 kN/m		3512 kN/m
	T_{e6} =	1.32 s	1.68 s		1.51 s
7	$Δ_7$ =	0.054 m	0.084 m		0.067 m
	V_{b7} =	241.00 kN	236.00 kN		238.83 kN
	K_{e7} =	4463 kN/m	2809 kN/m		3565 kN/m
	T_{e7} =	1.34 s	1.69 s		1.50 s
8	$Δ_8$ =	0.053 m	0.084 m		0.067 m
	V_{b8} =	241.18 kN			
	K_{e8} =	4550 kN/m			
	T_{e8} =	1.33 s			
9	$Δ_9$ =	0.053 m			

H = 18m

		TH ElCentro	TH Taft	TH MV01001	TH Sin Wave
		W = 2000 kN; l = 3 m; H = 18 m; Mr = 3000 kNm; A_{max} = 0.083 g; α = 4.8; cos2α = 0.99; r = 0.97; $ξ_c$ = 1.32 %; $ξ_{struct}$ = 3.00 %; $ξ_{tot}$ = 4.32 %			
1	$Δ_1$ =	0.001 m	0.001 m	0.001 m	0.001 m
	V_{b1} =	166.65 kN	166.56 kN	166.55 kN	166.55 kN
	K_{e1} =	166650 kN/m	166565 kN/m	166555 kN/m	166555 kN/m
	T_{e1} =	0.22 s	0.22 s	0.22 s	0.22 s
2	$Δ_2$ =	0.0045 m	0.005 m	0.0045 m	0.004 m
	V_{b2} =	166.17 kN	166.11 kN	166.17 kN	166.22 kN
	K_{e2} =	36926 kN/m	33222 kN/m	36926 kN/m	41555 kN/m
	T_{e2} =	0.47 s	0.49 s	0.47 s	0.44 s
3	$Δ_3$ =	0.028 m	0.028 m	0.0155 m	0.026 m
	V_{b3} =	163.56 kN	163.56 kN	164.94 kN	163.78 kN
	K_{e3} =	5841 kN/m	5841 kN/m	10642 kN/m	6299 kN/m
	T_{e3} =	1.17 s	1.17 s	0.87 s	1.13 s
4	$Δ_4$ =	0.0715 m	0.068 m	0.028 m	0.058 m
	V_{b4} =	158.72 kN	159.11 kN	163.55 kN	160.22 kN
	K_{e4} =	2219.86 kN/m	2339.86 kN/m	5841.24 kN/m	2762 kN/m
	T_{e4} =	1.90 s	1.55 s	1.17 s	1.71 s
5	$Δ_5$ =	0.0902 m	0.083 m	0.042 m	0.073 m
	V_{b5} =	156.44 kN	157.44 kN	162.03 kN	158.55 kN
	K_{e5} =	1730.48 kN/m	1896.91 kN/m	3857 kN/m	2172 kN/m
	T_{e5} =	2.16 s	2.06 s	1.44 s	1.93 s
6	$Δ_6$ =	0.129 m	0.081 m	0.031 m	0.078 m
	V_{b6} =	152.33 kN	157.67 kN	163.22 kN	158.00 kN
	K_{e6} =	1180.87 kN/m	1946.49 kN/m	5265 kN/m	2026 kN/m
	T_{e6} =	2.61 s	2.05 s	1.24 s	1.98 s
7	$Δ_7$ =	0.161 m	0.081 m	0.038 m	0.078 m
	V_{b7} =	148.78 kN		162.33 kN	157.39 kN
	K_{e7} =	924.09 kN/m		4272 kN/m	1992 kN/m
	T_{e7} =	2.95 s		1.39 s	2.01 s
8	$Δ_8$ =	0.161 m		0.032 m	0.078 m
	V_{b8} =			163.11 kN	
	K_{e8} =			5097 kN/m	
	T_{e8} =			1.28 s	
9	$Δ_9$ =			0.035 m	
	V_{b9} =			162.78 kN	
	K_{e9} =			4651 kN/m	
	T_{e9} =			1.32 s	
10	$Δ_{10}$ =			0.035 m	

(Rows grouped under "Iterations".)

Table 2 : Calculations using the Energy Balance Method

	H = 3m				H = 6m				H = 12m				H = 18m			
	P = 2000 kN W = 2000 kN L = 3 m H = 3 m T= 0.033 sec $\zeta_{desired}$ = 3.00 %				P = 2000 kN W = 2000 kN L = 3 m H = 6 m T= 0.08 sec $\zeta_{desired}$ = 3.00 %				P = 2000 kN W = 2000 kN L = 3 m H = 12 m T= 0.21 sec $\zeta_{desired}$ = 3.00 %				P = 2000 kN W = 2000 kN L = 3 m H = 18 m T= 0.37 sec $\zeta_{desired}$ = 3.00 %			
	TH 'ElCentro'	TH 'Taft'	TH 'M7D1001'	TH 'Sin Wave'	TH 'ElCentro'	TH 'Taft'	TH 'M7D1001'	TH 'Sin Wave'	TH 'ElCentro'	TH 'Taft'	TH 'M7D1001'	TH 'Sin Wave'	TH 'ElCentro'	TH 'Taft'	TH 'M7D1001'	TH 'Sin Wave'
$\dot{S}_e$ =	0.341 m/s	0.228 m/s	0.11 m/s	0.31 m/s	0.341 m/s	0.228 m/s	0.11 m/s	0.31 m/s	0.341 m/s	0.228 m/s	0.11 m/s	0.31 m/s	0.341 m/s	0.228 m/s	0.11 m/s	0.31 m/s
KE =	5.821 kN'm	5.299 kN'm	1.233 kN'm	9.796 kN'm	5.82059 kN'm	5.299 kN'm	1.233436 kN'm	9.796 kN'm	5.821 kN'm	5.299 kN'm	1.233 kN'm	9.796 kN'm	5.821 kN'm	5.299 kN'm	1.233 kN'm	9.796 kN'm
Ø =	0.00 rads	0.00 rads	0.001 rads	0.01 rads	0.00 rads	0.00 rads	0.001 rads	0.01 rads	0.00 rads	0.00 rads	0.001 rads	0.01 rads	0.00 rads	0.00 rads	0.001 rads	0.01 rads
Δ_d =	0.0116 m	0.0106 m	0.0025 m	0.0198 m	0.0237 m	0.0212 m	0.0049 m	0.0392 m	0.0474 m	0.0424 m	0.0098 m	0.0784 m	0.0710 m	0.0636 m	0.0148 m	0.1176 m

Table 3 : Calculations using the Equal Energy Method

	H = 3m				H = 6m				H = 12m				H = 18m			
	P = 2000 kN L = 3 m H = 3 m V_b = 1000 kN T= 0.033 sec k = 7513148.0 kN/m $\zeta_{desired}$ = 3.00 %				P = 2000 kN L = 3 m H = 6 m V_b = 500 kN T= 0.08 sec k = 1333333.0 kN/m $\zeta_{desired}$ = 3.00 %				P = 2000 kN L = 3 m H = 12 m V_b = 250 kN T= 0.21 sec k = 197628.5 kN/m $\zeta_{desired}$ = 3.00 %				P = 2000 kN L = 3 m H = 18 m V_b = 166.7 kN T= 0.37 sec k = 61804.7 kN/m $\zeta_{desired}$ = 3.00 %			
	TH 'ElCentro'	TH 'Taft'	TH 'M7D1001'	TH 'Sin Wave'	TH 'ElCentro'	TH 'Taft'	TH 'M7D1001'	TH 'Sin Wave'	TH 'ElCentro'	TH 'Taft'	TH 'M7D1001'	TH 'Sin Wave'	TH 'ElCentro'	TH 'Taft'	TH 'M7D1001'	TH 'Sin Wave'
S_d =	0 m	0 m	0 m	0 m	0.0006 m	0 m	0.001000 m	0 m	0.0046 m	0.0060 m	0.0044 m	0.0032 m	0.0145 m	0.0240 m	0.0120 m	0.0150 m
V_s =	0 kN	0 kN	0 kN	0 kN	800 kN	0 kN	1333.333 kN	0 kN	899.3 kN	968.1 kN	869.6 kN	632.4 kN	902.3 kN	1483 kN	741.7 kN	927.1 kN
E_s =	0 kN'm	0 kN'm	0 kN'm	0 kN'm	0.48 kN'm	0.00 kN'm	1.33 kN'm	0.00 kN'm	4.00 kN'm	4.94 kN'm	3.83 kN'm	2.02 kN'm	13.17 kN'm	35.60 kN'm	8.90 kN'm	13.91 kN'm
E_s =	0 kN'm	0 kN'm	0 kN'm	0 kN'm	0.48 kN'm	0.00 kN'm	1.33 kN'm	0.00 kN'm	4.00 kN'm	4.94 kN'm	3.83 kN'm	2.02 kN'm	13.17 kN'm	35.60 kN'm	8.90 kN'm	13.91 kN'm
Δ_d =	0 m	0 m	0 m	0 m	0.0011 m	0 m	0.0029 m	0 m	0.0198 m	0.0204 m	0.0169 m	0.0097 m	0.0504 m	0.2148 m	0.0647 m	0.0548 m

Example 2 - Single Degree of Freedom Structures

Table 1 : Results for the Substitute Substructure Technique

2 storey frame (T = 0.6s)	
W_{tot} =	490.5 kN
W_{eq} =	4905 kN
l =	5 m
H =	8 m
Mr =	1471.5 kNm
A_{max} =	0.05 g
α =	28.8
cos2α =	0.50
r =	0.35
ξc =	30.72 %
ξstruct =	3.00 %
ξtot =	33.72 %

Iterations		TH 'ElCentro'	TH 'Taft'	TH 'MEX01001'	TH 'Sin Wave'
1	Δ_1 =	0.001 m	0.001 m	0.001 m	0.001 m
	V_{b1} =	245.15 kN	245.15 kN	245.15 kN	245.15 kN
	K_{e1} =	245148 kN/m	245148 kN/m	245148 kN/m	245148 kN/m
	T_{e1} =	0.28 s	0.28 s	0.28 s	0.28 s
2	Δ_2 =	0.0051 m	0.005 m	0.0033 m	0.0055 m
	V_{b2} =	244.73 kN	244.82 kN	244.96 kN	244.78 kN
	K_{e2} =	47986 kN/m	48664 kN/m	74230 kN/m	44505 kN/m
	T_{e2} =	0.44 s	0.43 s	0.52 s	0.47 s
3	Δ_3 =	0.02 m	0.0151 m	0.0077 m	0.0273 m
	V_{b3} =	243.53 kN	244.02 kN	244.00 kN	243.00 kN
	K_{e3} =	12192 kN/m	16158 kN/m	31706 kN/m	8901 kN/m
	T_{e3} =	1.27 s	1.11 s	0.79 s	1.49 s
4	Δ_4 =	0.0265 m	0.0315 m	0.01 m	0.0499 m
	V_{b4} =	243.06 kN	242.85 kN	244.41 kN	241.25 kN
	K_{e4} =	9172 kN/m	7703 kN/m	24441 kN/m	4833 kN/m
	T_{e4} =	1.47 s	1.63 s	0.90 s	2.00 s
5	Δ_5 =	0.0332 m	0.0441 m	0.011 m	0.0589 m
	V_{b5} =	242.52 kN	241.82 kN	244.33 kN	240.41 kN
	K_{e5} =	7305 kN/m	5479 kN/m	22212 kN/m	4082 kN/m
	T_{e5} =	1.64 s	1.92 s	0.96 s	2.20 s
6	Δ_6 =	0.0395 m	0.0479 m	0.011 m	0.063 m
	V_{b6} =	242.00 kN	241.35 kN		240.06 kN
	K_{e6} =	6127 kN/m	5038 kN/m		3811 kN/m
	T_{e6} =	1.79 s	1.98 s		2.28 s
7	Δ_7 =	0.045 m	0.0479 m		0.064 m
	V_{b7} =	241.55 kN			240.00 kN
	K_{e7} =	5368 kN/m			3750 kN/m
	T_{e7} =	1.92 s			2.29 s
8	Δ_8 =	0.049 m			0.064 m
	V_{b8} =	241.22 kN			
	K_{e8} =	4923 kN/m			
	T_{e8} =	2.00 s			
9	Δ_9 =	0.0524 m			
	V_{b9} =	240.95 kN			
	K_{e9} =	4598 kN/m			
	T_{e9} =	2.07 s			
10	Δ_{10} =	0.0541 m			
	V_{b10} =	240.81 kN			
	K_{e10} =	4451 kN/m			
	T_{e10} =	2.11 s			
11	Δ_{11} =	0.0552 m			
	V_{b11} =	240.72 kN			
	K_{e11} =	4361 kN/m			
	T_{e11} =	2.13 s			
12	Δ_{12} =	0.0557 m			
	V_{b12} =	240.68 kN			
	K_{e12} =	4321 kN/m			
	T_{e12} =	2.14 s			
13	Δ_{13} =	0.0557 m			

4 storey frame (T = 0.9s)	
W_{tot} =	1128 kN
W_{eq} =	11282 kN
l =	6 m
H =	12 m
Mr =	3384 kNm
A_{max} =	0.025 g
α =	34.0
cos2α =	0.66
r =	0.78
ξc =	10.63 %
ξstruct =	3.00 %
ξtot =	13.63 %

Iterations		TH 'ElCentro'	TH 'Taft'	TH 'MEX01001'	TH 'Sin Wave'
1	Δ_1 =	0.001 m	0.001 m	0.001 m	0.001 m
	V_{b1} =	281.90 kN	281.90 kN	281.90 kN	281.90 kN
	K_{e1} =	281900 kN/m	281900 kN/m	281900 kN/m	281900 kN/m
	T_{e1} =	0.40 s	0.40 s	0.40 s	0.40 s
2	Δ_2 =	0.0107 m	0.0126 m	0.009 m	0.0167 m
	V_{b2} =	280.99 kN	280.51 kN	281.15 kN	280.42 kN
	K_{e2} =	26261 kN/m	22280 kN/m	31239 kN/m	16792 kN/m
	T_{e2} =	1.31 s	1.43 s	1.21 s	1.64 s
3	Δ_3 =	0.0417 m	0.063 m	0.024 m	0.0632 m
	V_{b3} =	278.07 kN	276.27 kN	279.74 kN	276.05 kN
	K_{e3} =	6668 kN/m	4382 kN/m	11656 kN/m	4368 kN/m
	T_{e3} =	2.61 s	3.22 s	1.97 s	3.22 s
4	Δ_4 =	0.105 m	0.0686 m	0.032 m	0.064 m
	V_{b4} =	272.12 kN		278.99 kN	
	K_{e4} =	2592 kN/m		8718 kN/m	
	T_{e4} =	4.19 s		2.28 s	
5	Δ_5 =	0.183 m		0.032 m	

8 storey frame (T = 2.2s)	
W_{tot} =	2403.5 kN
W_{eq} =	24040 kN
l =	6 m
H =	24 m
Mr =	7210.5 kNm
A_{max} =	0.0125 g
α =	7.1
cos2α =	0.97
r =	0.34
ξc =	2.81 %
ξstruct =	3.00 %
ξtot =	5.81 %

Iterations		TH 'ElCentro'	TH 'Taft'	TH 'MEX01001'	TH 'Sin Wave'
1	Δ_1 =	0.001 m	0.001 m	0.001 m	0.001 m
	V_{b1} =	300.34 kN	300.34 kN	300.34 kN	300.34 kN
	K_{e1} =	300336 kN/m	300336 kN/m	300336 kN/m	300336 kN/m
	T_{e1} =	0.57 s	0.57 s	0.57 s	0.57 s
2	Δ_2 =	0.04 m	0.0252 m	0.0243 m	0.11 m
	V_{b2} =	298.43 kN	297.91 kN	298.20 kN	289.42 kN
	K_{e2} =	7411 kN/m	11822 kN/m	12283 kN/m	2631 kN/m
	T_{e2} =	3.81 s	2.86 s	2.81 s	5.96 s
3	Δ_3 =	0.138 m	0.105 m	0.063 m	0.09 m
	V_{b3} =		293.97 kN	294.73 kN	
	K_{e3} =		2791 kN/m	4669 kN/m	
	T_{e3} =		5.92 s	4.55 s	
4	Δ_4 =		0.12 m	0.0598 m	

12 storey frame (T = 3.4s)	
W_{tot} =	3578 kN
W_{eq} =	35780 kN
l =	8 m
H =	35 m
Mr =	11234 kNm
A_{max} =	0.028 g
α =	4.8
cos2α =	0.99
r =	0.97
ξc =	1.32 %
ξstruct =	3.00 %
ξtot =	4.32 %

Iterations		TH 'ElCentro'	TH 'Taft'	TH 'MEX01001'	TH 'Sin Wave'
1	Δ_1 =	0.001 m	0.001 m	0.001 m	0.001 m
	V_{b1} =	308.40 kN	308.40 kN	308.40 kN	308.40 kN
	K_{e1} =	308387 kN/m	308387 kN/m	308387 kN/m	308387 kN/m
	T_{e1} =	0.70 s	0.70 s	0.72 s	0.70 s
2	Δ_2 =	0.0456 m	0.0315 m	0.0254 m	0.094 m
	V_{b2} =	301.84 kN	303.29 kN	303.90 kN	298.50 kN
	K_{e2} =	6619 kN/m	9628 kN/m	11965 kN/m	3158 kN/m
	T_{e2} =	4.73 s	3.92 s	3.52 s	6.85 s
3	Δ_3 =	0.16 m	0.125 m	0.0999 m	0.091 m

Table 2 : Results for the Energy Balance Method

	2 storey frame (T =0.6s)				4 storey frame (T =0.9s)				6 storey frame (T =2.0s)				8 storey frame (T =3.4s)			
	P = 490.4 kN W = 4904 kN L = 6 m H = 6 m T= 0.6 sec ξ_{assu} = 3.00 %				P = 1128 kN W = 11280 kN L = 6 m H = 12 m T= 0.9 sec ξ_{assu} = 3.00 %				P = 2404 kN W = 24040 kN L = 6 m H = 24 m T= 2 sec ξ_{assu} = 3.00 %				P = 3678 kN W = 36780 kN L = 6 m H = 36 m T= 3.4 sec ξ_{assu} = 3.00 %			
	TH 'ElCentro'	TH 'Taft'	TH 'M7010001'	TH 'Sin Wave'	TH 'ElCentro'	TH 'Taft'	TH 'M7010001'	TH 'Sin Wave'	TH 'ElCentro'	TH 'Taft'	TH 'M7010001'	TH 'Sin Wave'	TH 'ElCentro'	TH 'Taft'	TH 'M7010001'	TH 'Sin Wave'
E_k =	0.241 m/s	0.228 m/s	0.11 m/s	0.31 m/s	0.241 m/s	0.228 m/s	0.11 m/s	0.31 m/s	0.241 m/s	0.228 m/s	0.11 m/s	0.31 m/s	0.241 m/s	0.228 m/s	0.11 m/s	0.31 m/s
KE =	14.52 kN*m	12.99 kN*m	3.024 kN*m	24.02 kN*m	33.3921 kN*m	29.89 kN*m	6.96657 kN*m	55.26 kN*m	71.17 kN*m	63.69 kN*m	14.83 kN*m	117.75 kN*m	108.9 kN*m	97.45 kN*m	22.68 kN*m	180.15 kN*m
Ø =	0.02 rads	0.02 rads	0.004 rads	0.03 rads	0.02 rads	0.02 rads	0.004 rads	0.03 rads	0.02 rads	0.02 rads	0.004 rads	0.03 rads	0.02 rads	0.02 rads	0.004 rads	0.03 rads
Δ_d =	**0.1184 m**	**0.1060 m**	**0.0247 m**	**0.1960 m**	**0.2369 m**	**0.2120 m**	**0.0493 m**	**0.3920 m**	**0.4737 m**	**0.4240 m**	**0.0987 m**	**0.7840 m**	**0.7106 m**	**0.6360 m**	**0.1480 m**	**1.1760 m**

Table 3 : Results for the Equal Energy Method

	2 storey frame (T =0.6s)				4 storey frame (T =0.9s)				6 storey frame (T =2.0s)				8 storey frame (T =3.4s)			
	P = 490.4 kN I = 6 m H = 6 m V_b = 245.2 kN T= 0.6 sec k = 54831.1 kN/m ξ_{assu} = 3.00 %				P = 1128 kN I = 6 m H = 12 m V_b = 282 kN T= 0.9 sec k = 99049.6 kN/m ξ_{assu} = 3.00 %				P = 2404 kN I = 6 m H = 24 m V_b = 300.4 kN T= 2 sec k = 24181.0 kN/m ξ_{assu} = 3.00 %				P = 3678 kN I = 6 m H = 36 m V_b = 306.5 kN T= 3.4 sec k = 12606.6 kN/m ξ_{assu} = 3.00 %			
	TH 'ElCentro'	TH 'Taft'	TH 'M7010001'	TH 'Sin Wave'	TH 'ElCentro'	TH 'Taft'	TH 'M7010001'	TH 'Sin Wave'	TH 'ElCentro'	TH 'Taft'	TH 'M7010001'	TH 'Sin Wave'	TH 'ElCentro'	TH 'Taft'	TH 'M7010001'	TH 'Sin Wave'
Φ_d =	0.019 m	0.014 m	0.01 m	0.026 m	0.021 m	0.023 m	0.011 m	0.0315 m	0.0520 m	0.0479 m	0.0210 m	0.0593 m	0.0520 m	0.0517 m	0.0310 m	0.0765 m
V_b =	1047 kN	797.6 kN	548.3 kN	1358 kN	1177.04 kN	1289 kN	616.546 kN	1765.6 kN	1257 kN	1158 kN	507.8 kN	1433.9 kN	794 kN	662.1 kN	397 kN	979.7 kN
E_k =	10.00 kN*m	5.37 kN*m	2.74 kN*m	17.83 kN*m	12.36 kN*m	14.83 kN*m	3.39 kN*m	27.81 kN*m	65.39 kN*m	55.48 kN*m	10.66 kN*m	85.03 kN*m	49.23 kN*m	34.23 kN*m	12.31 kN*m	74.95 kN*m
E_k =	10.00 kN*m	5.37 kN*m	2.74 kN*m	17.83 kN*m	12.36 kN*m	14.83 kN*m	3.39 kN*m	27.81 kN*m	65.39 kN*m	55.48 kN*m	10.66 kN*m	85.03 kN*m	49.23 kN*m	34.23 kN*m	12.31 kN*m	74.95 kN*m
Δ_d =	**0.0430 m**	**0.0342 m**	**0.0134 m**	**0.0749 m**	**0.0468 m**	**0.0561 m**	**0.0146 m**	**0.1011 m**	**0.1169 m**	**0.0998 m**	**0.0249 m**	**0.1477 m**	**0.0928 m**	**0.0878 m**	**0.0320 m**	**0.1942 m**

APPENDIX C

GROUND MOTIONS USED FOR MONTREAL

GROUND MOTION E01

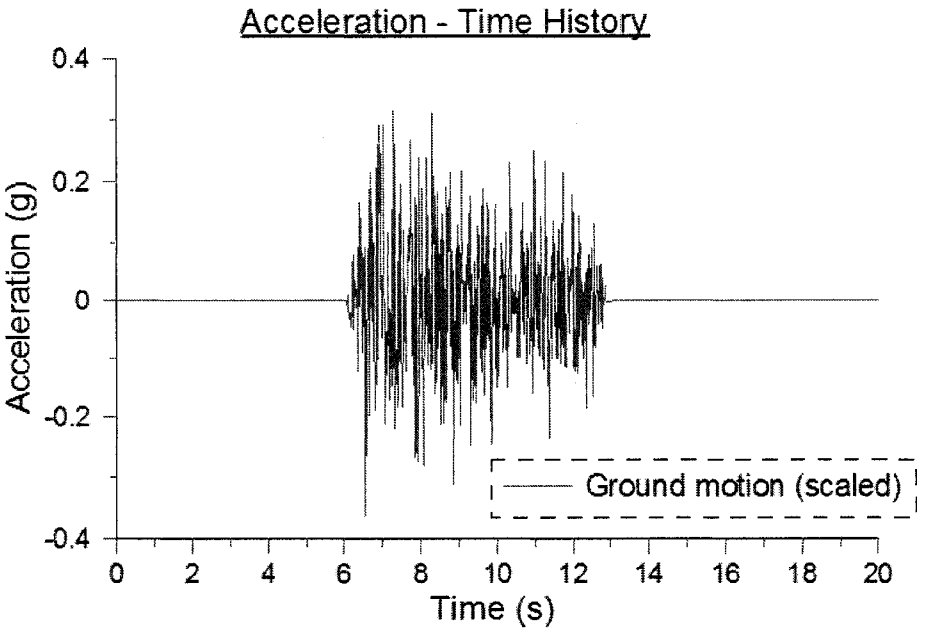

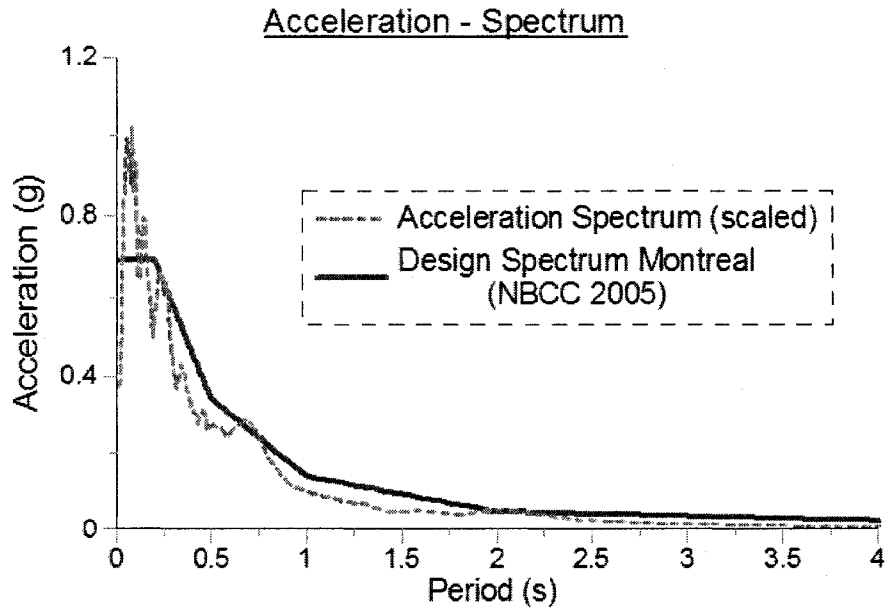

GROUND MOTION E02

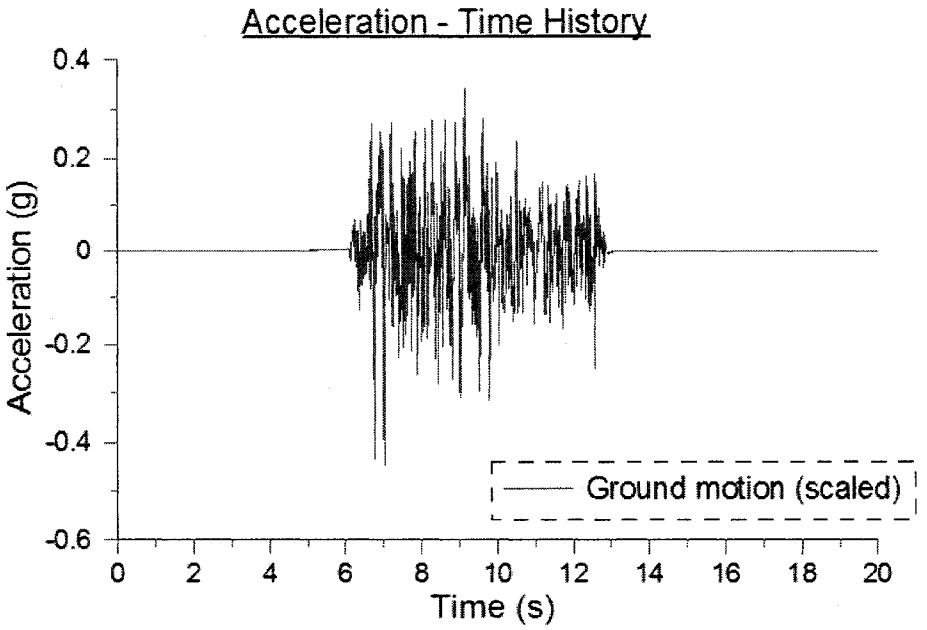

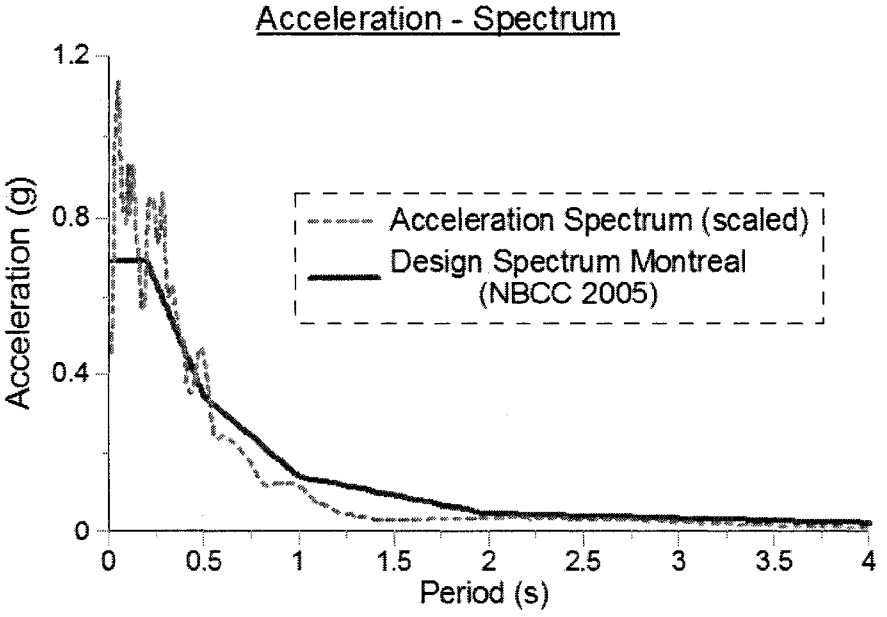

GROUND MOTION E03

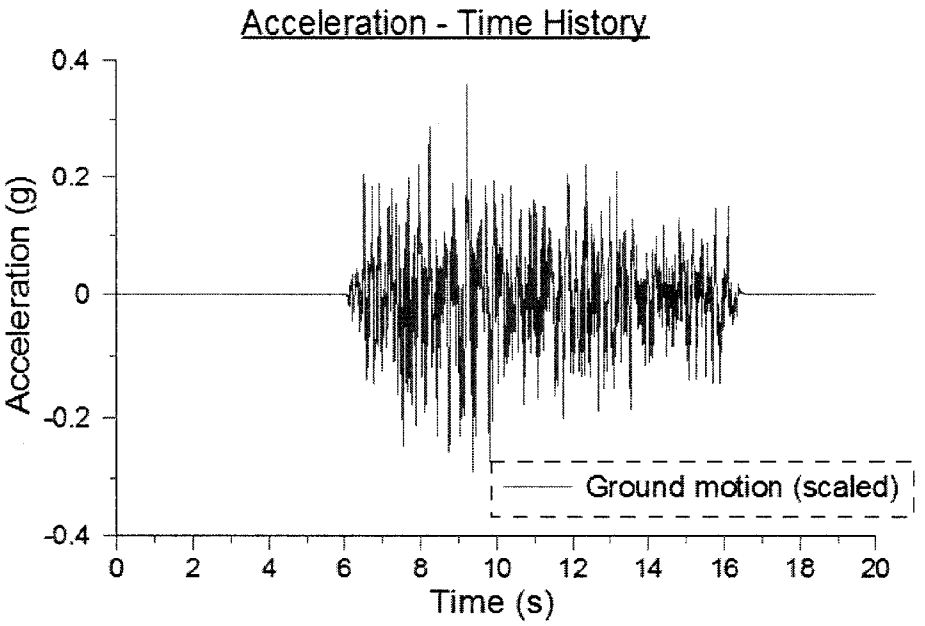

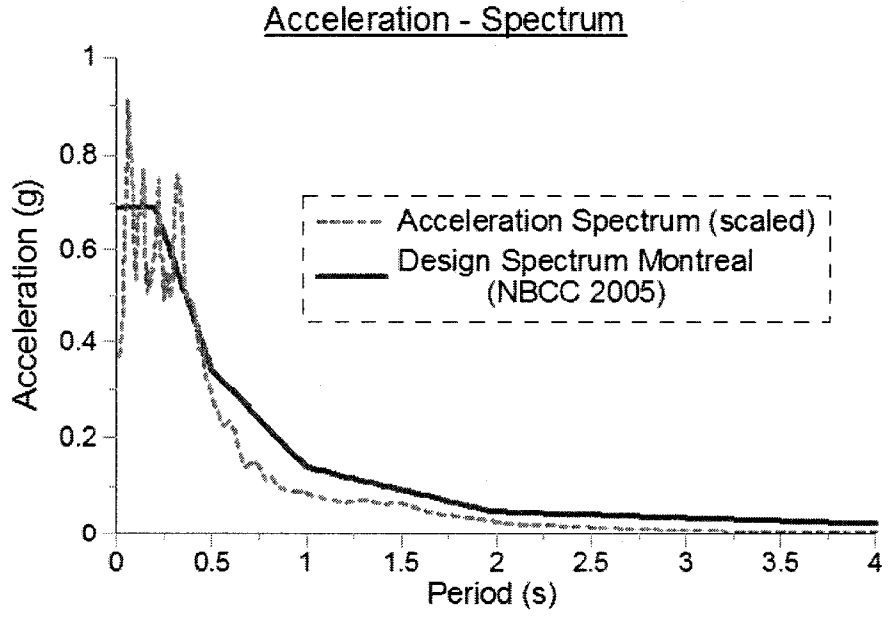

GROUND MOTION E04

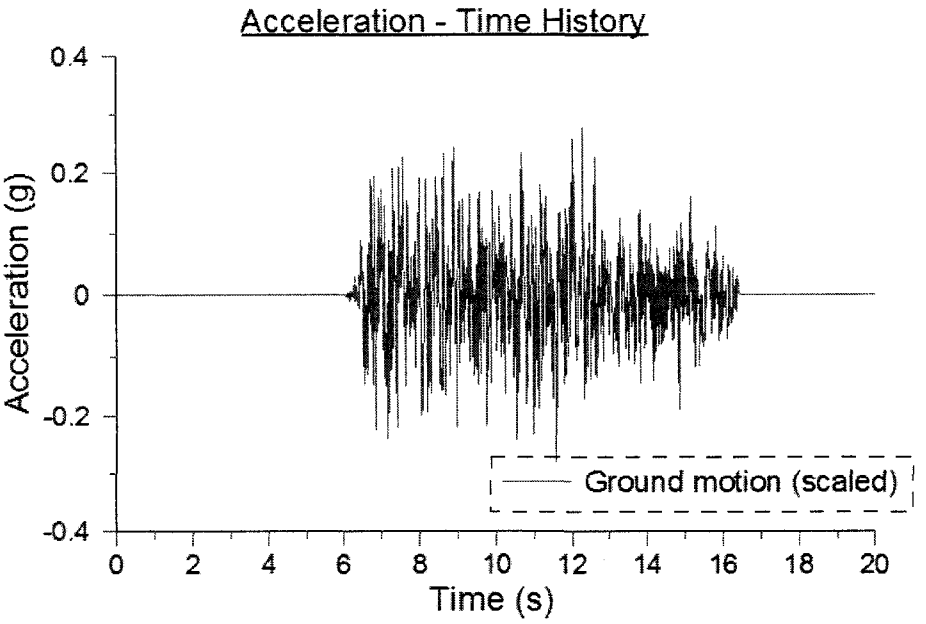

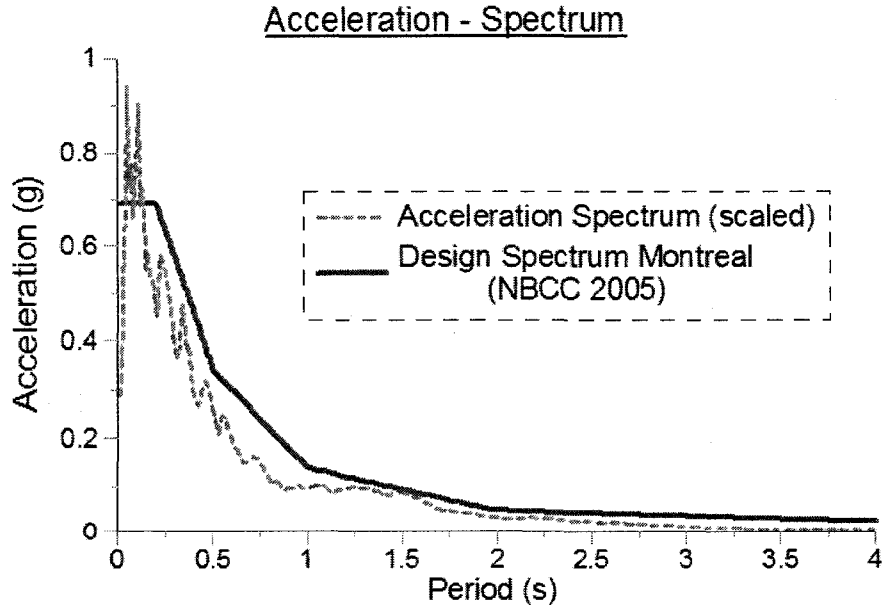

GROUND MOTION E05

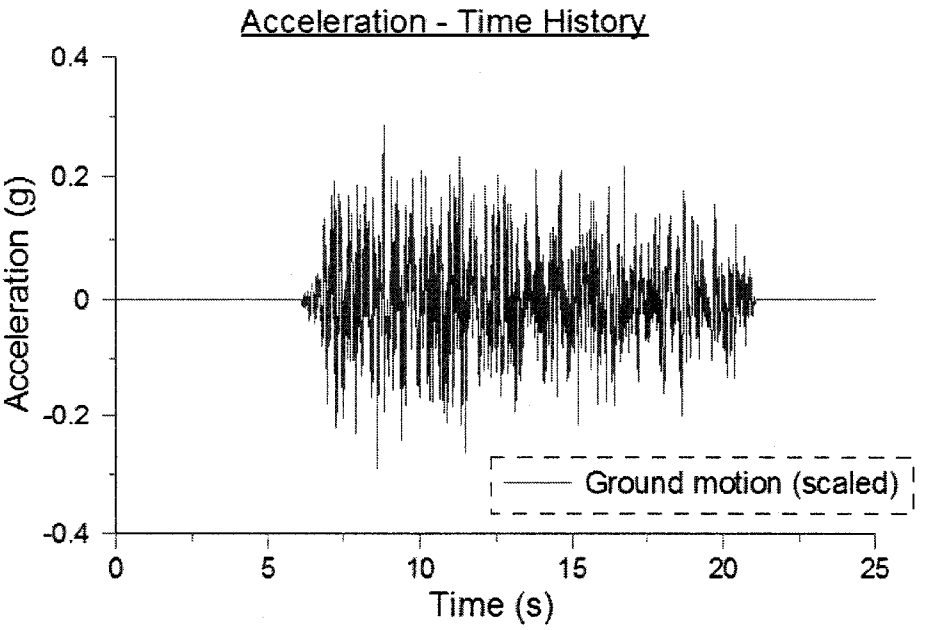

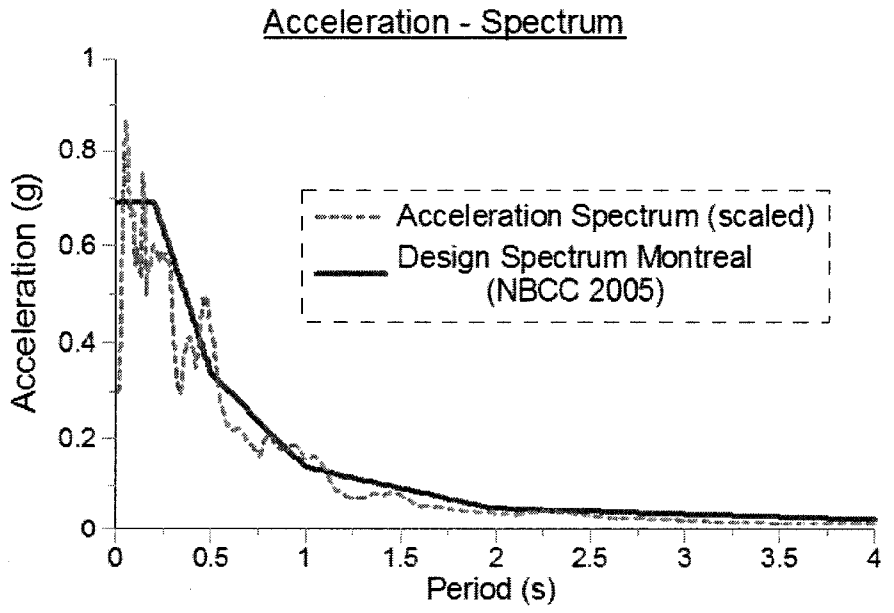

GROUND MOTION E06

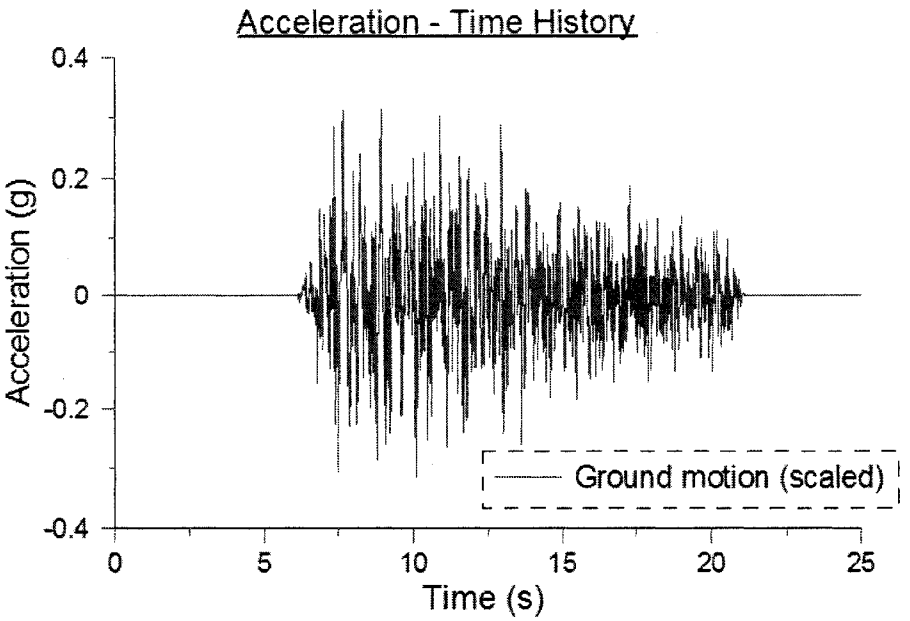

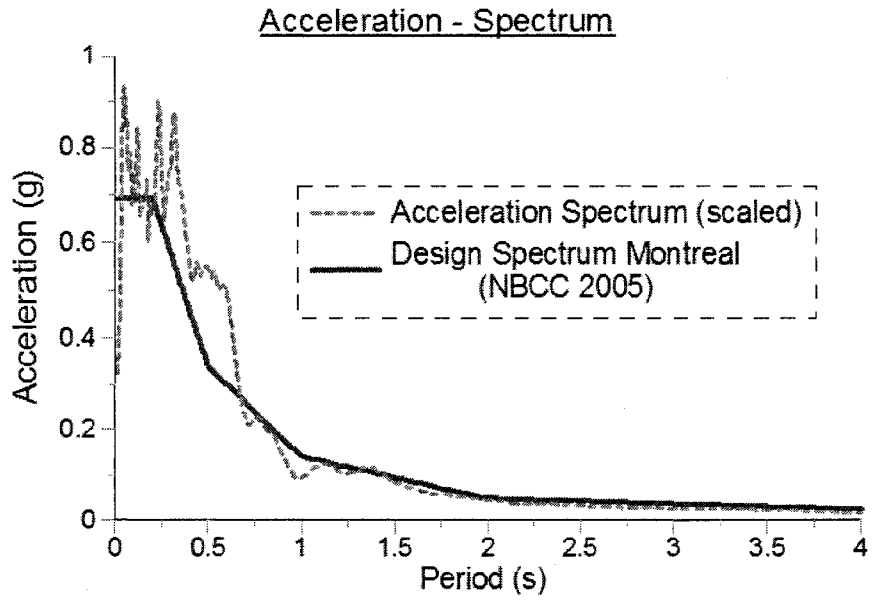

GROUND MOTION E07

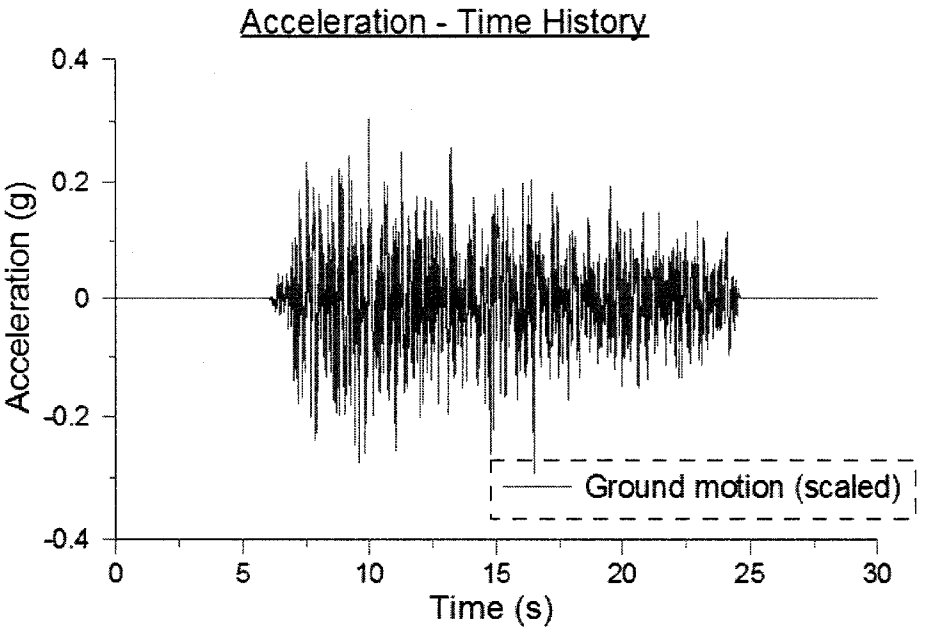

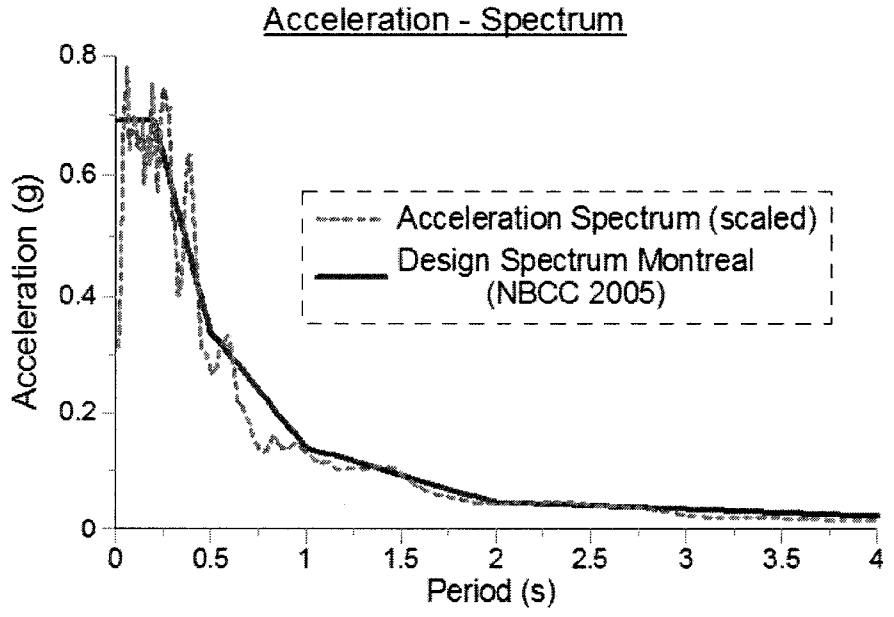

GROUND MOTION E08

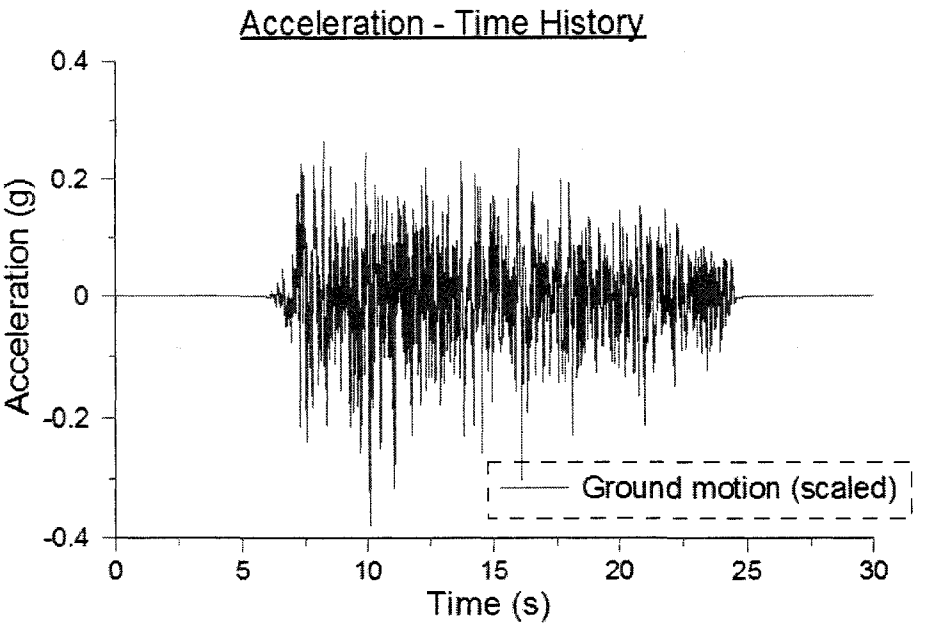

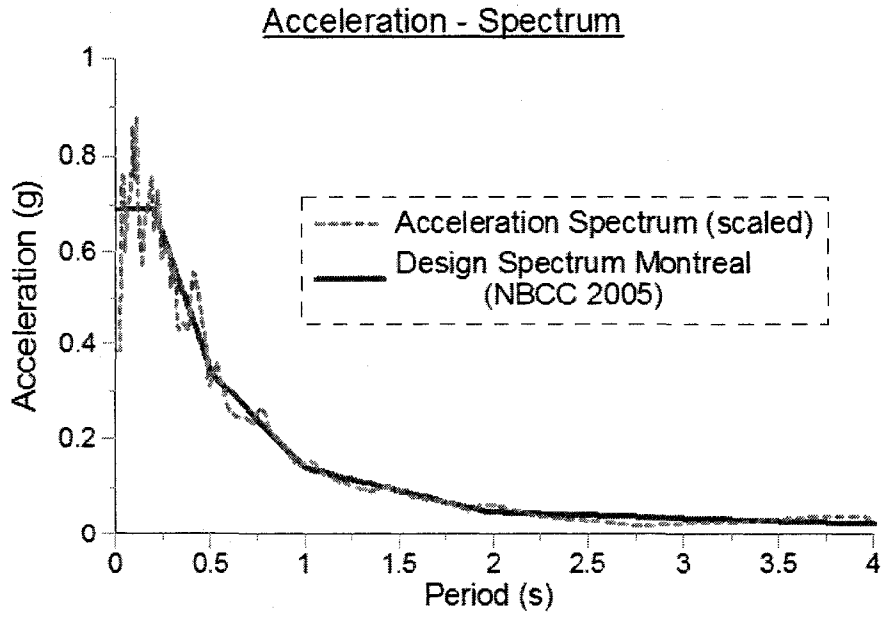

GROUND MOTION E09

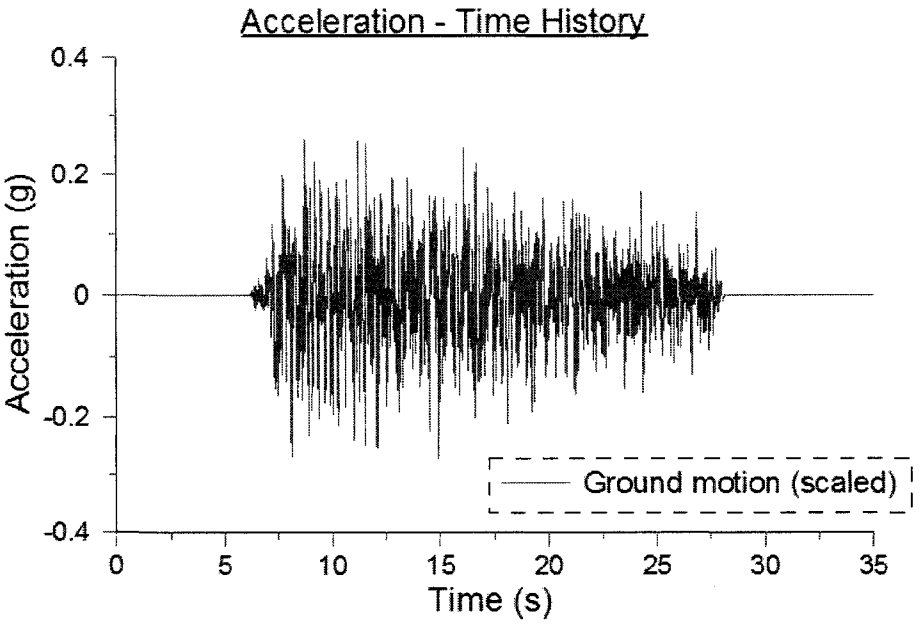

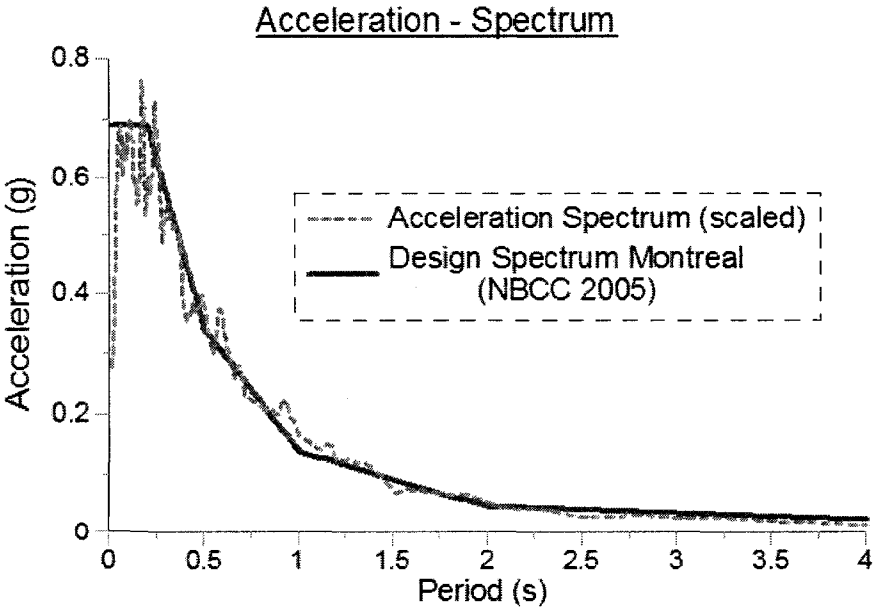

GROUND MOTION E10

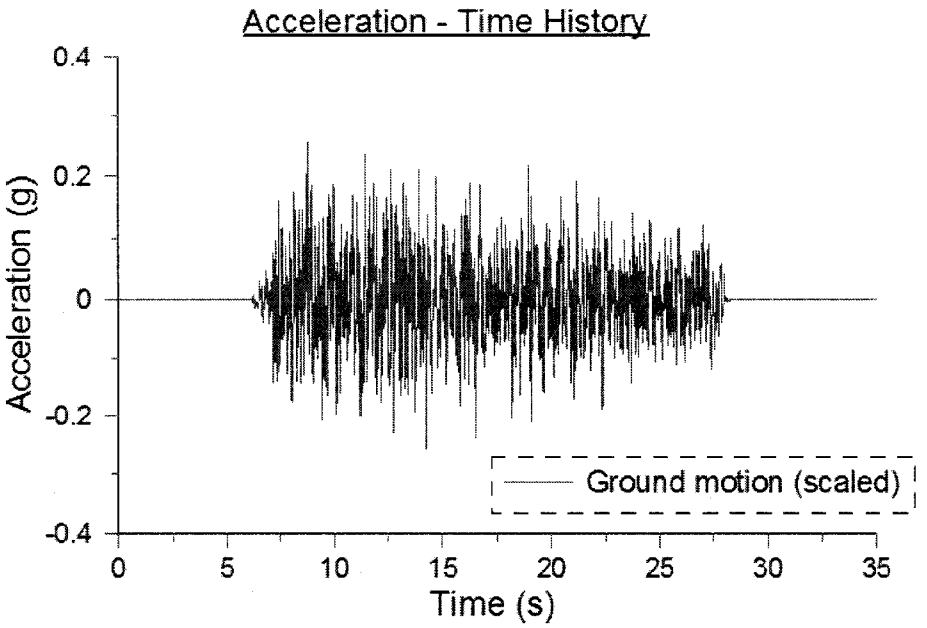

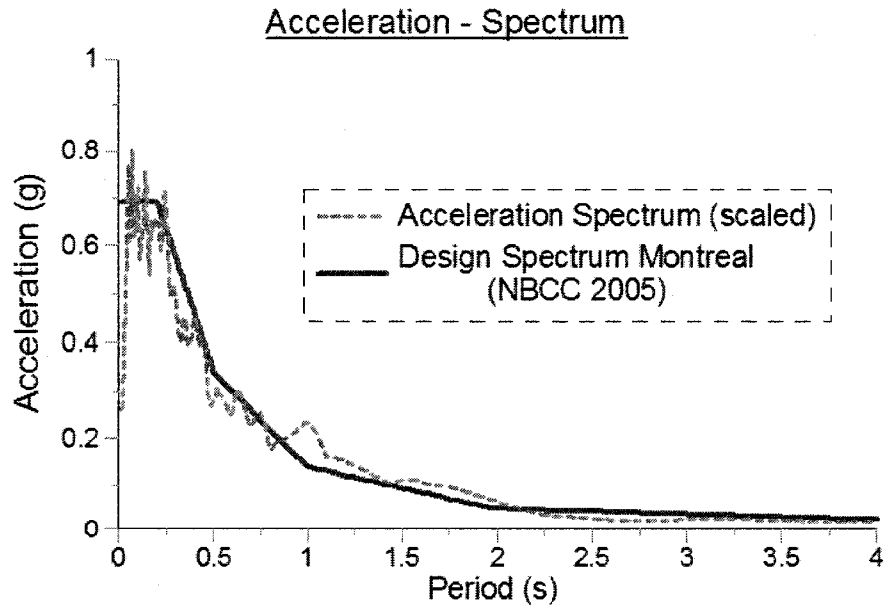

GROUND MOTION E11

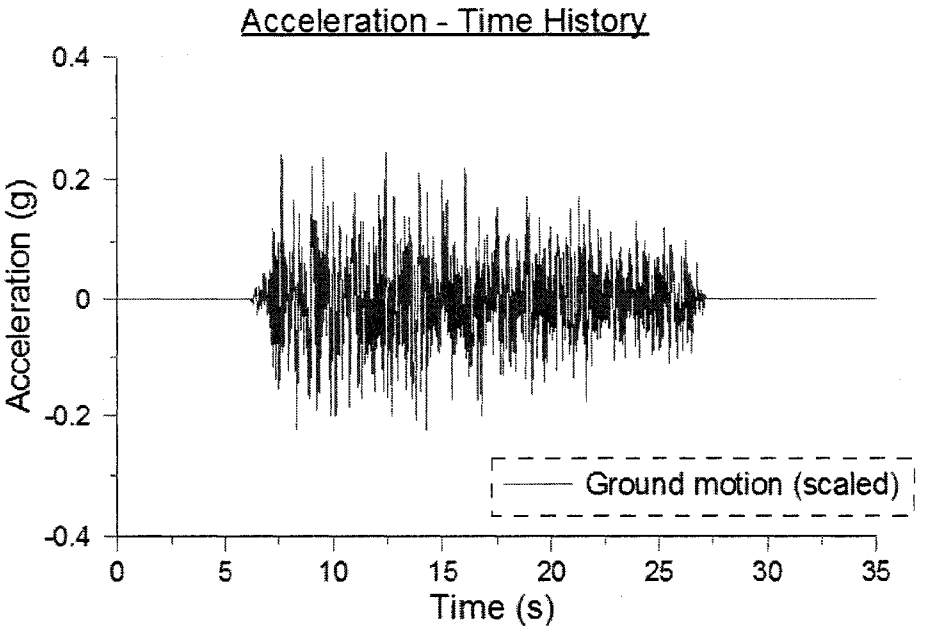

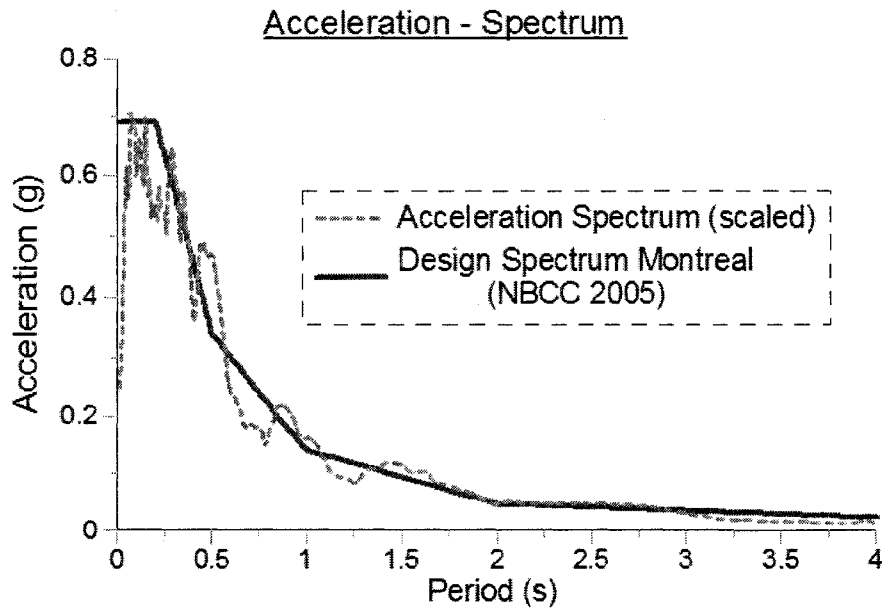

GROUND MOTION E12

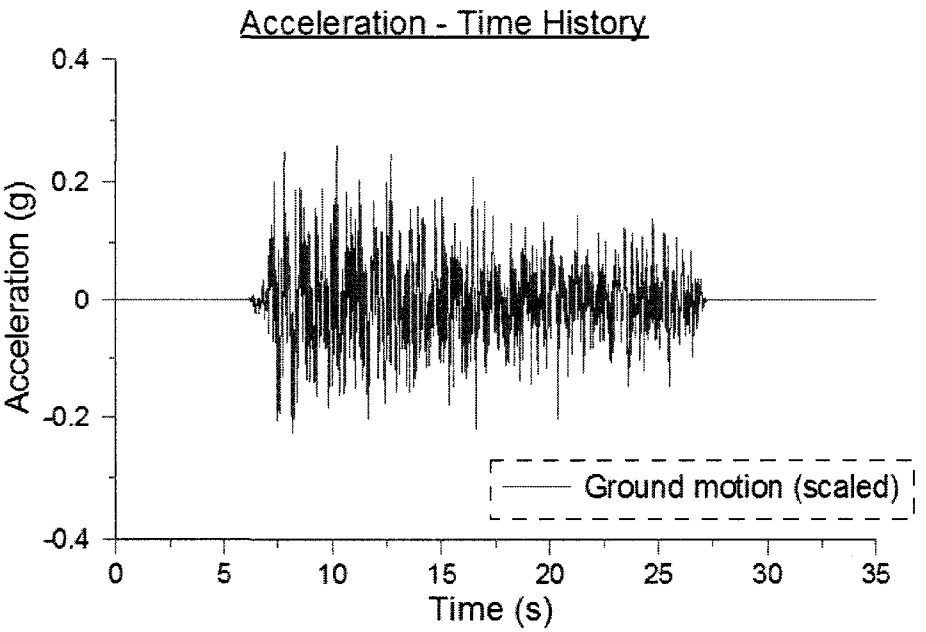

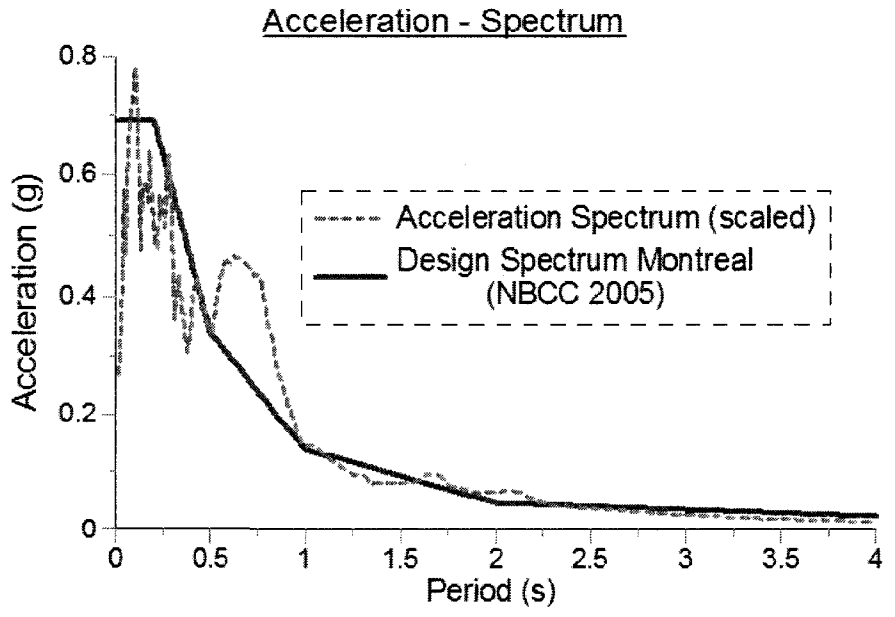

APPENDIX D

GROUND MOTIONS USED FOR VANCOUVER

GROUND MOTION H01

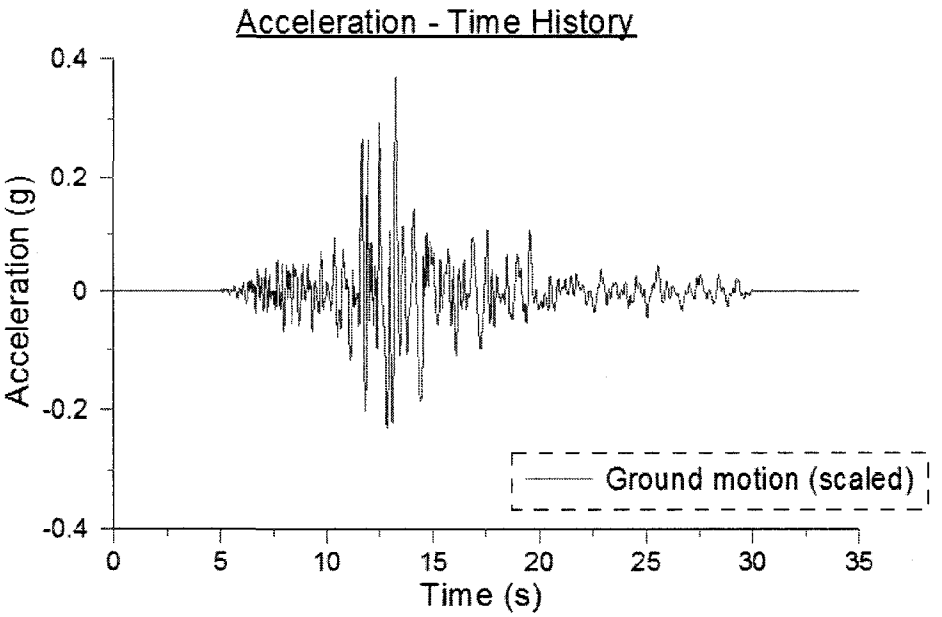

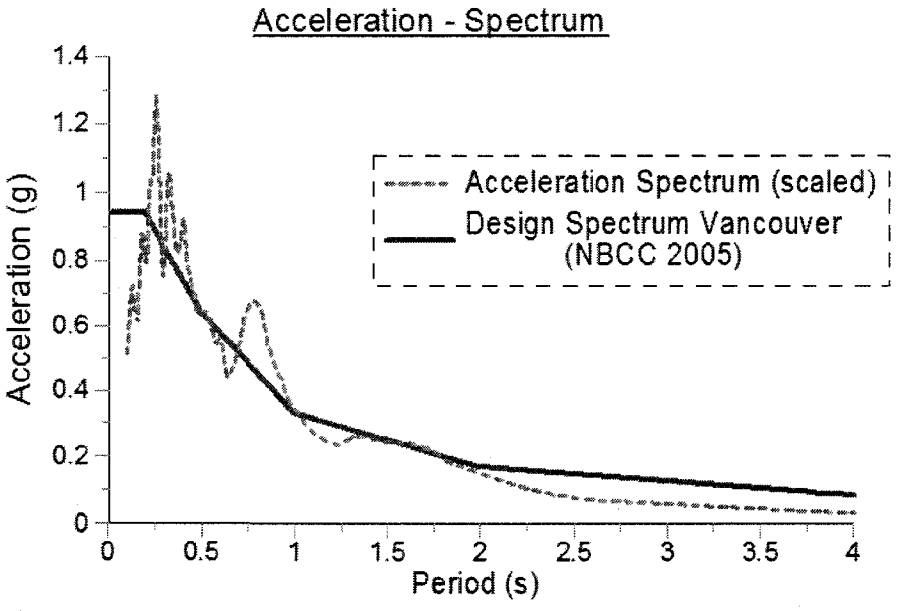

GROUND MOTION H02

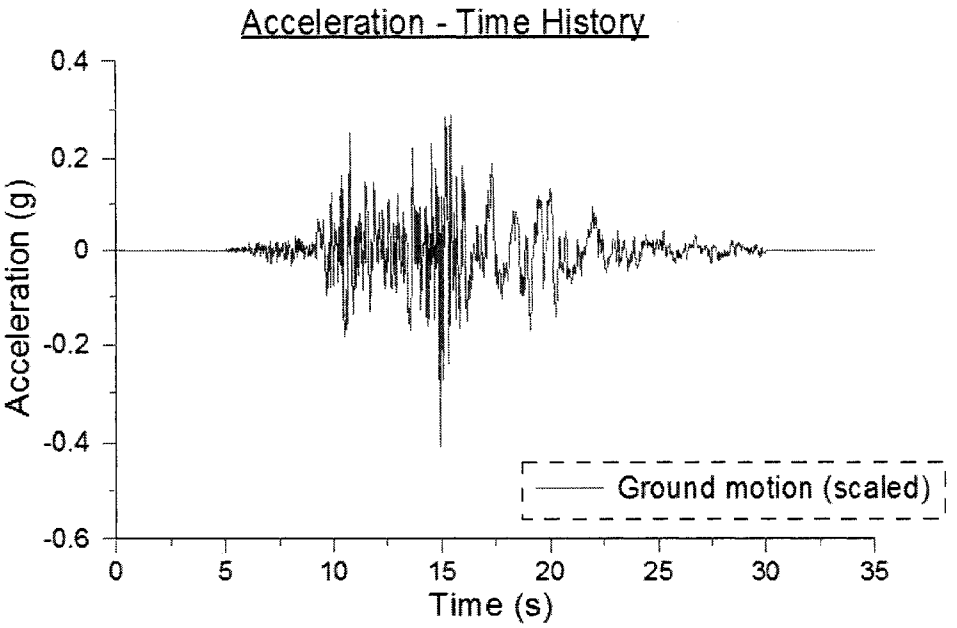

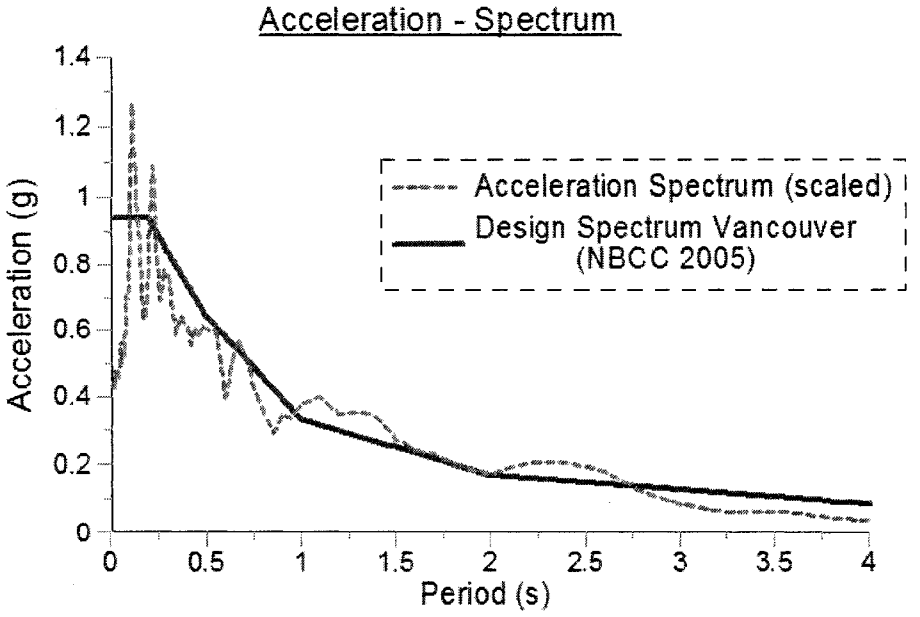

GROUND MOTION H03

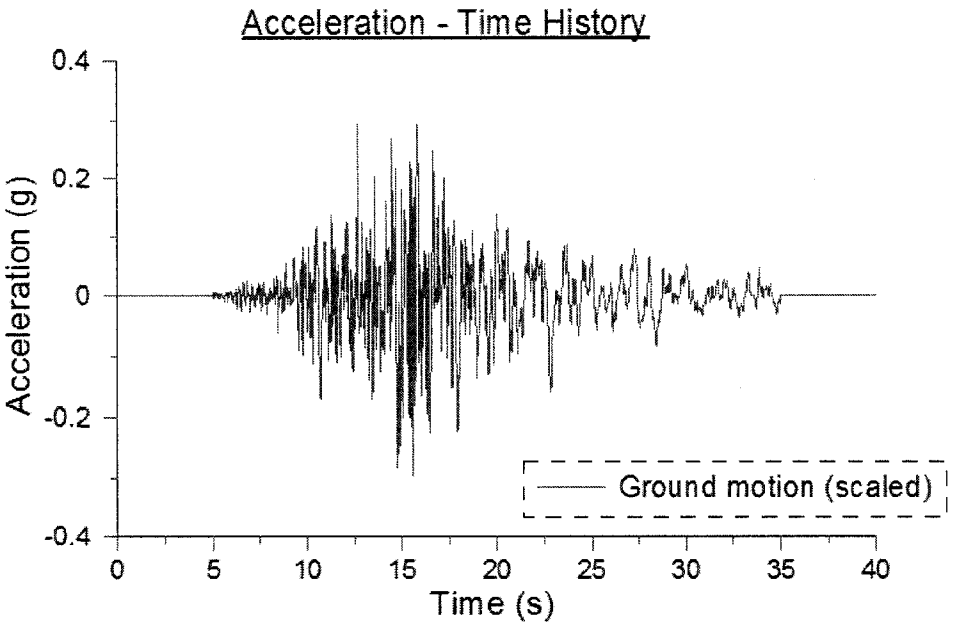

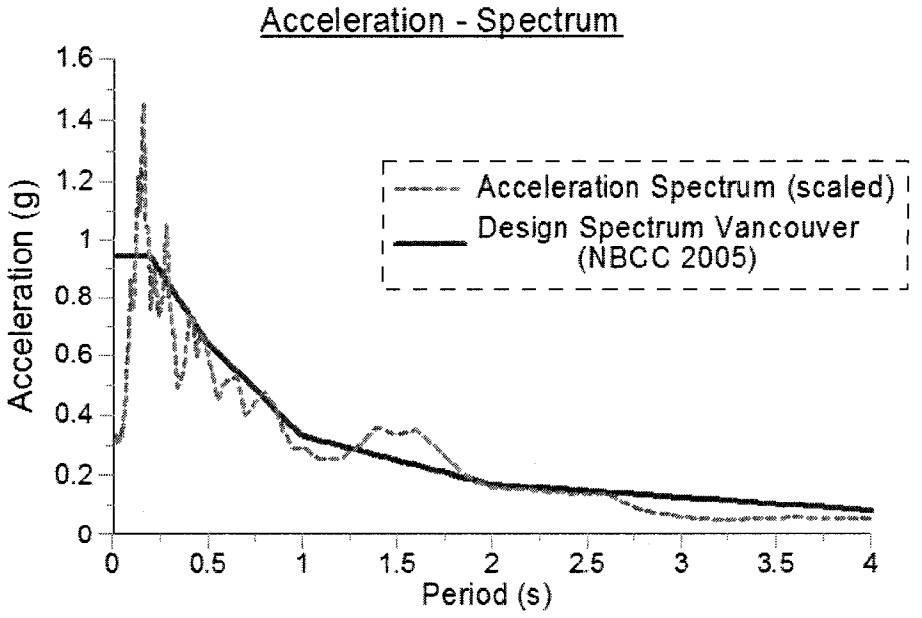

GROUND MOTION H04

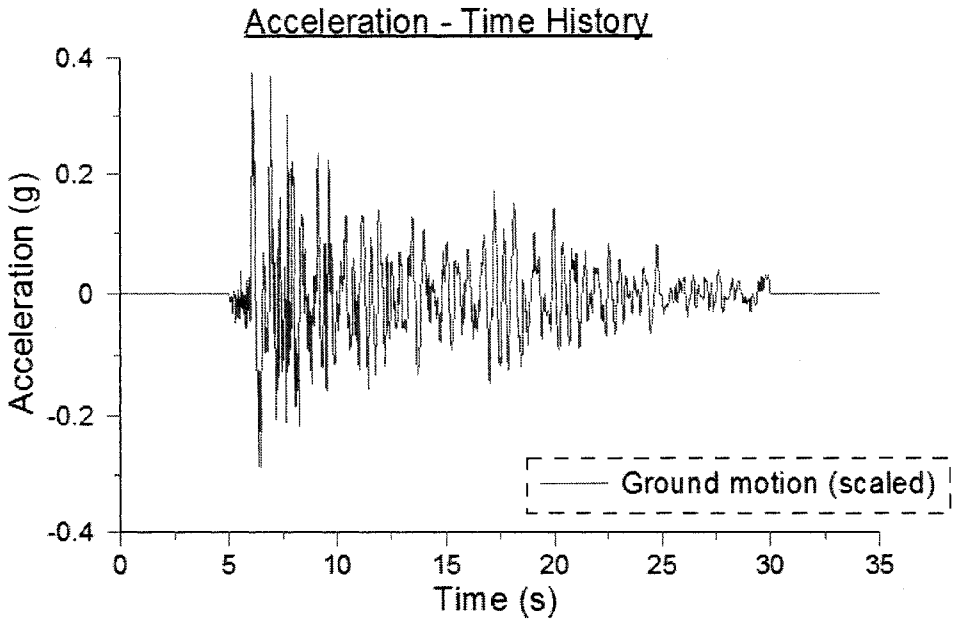

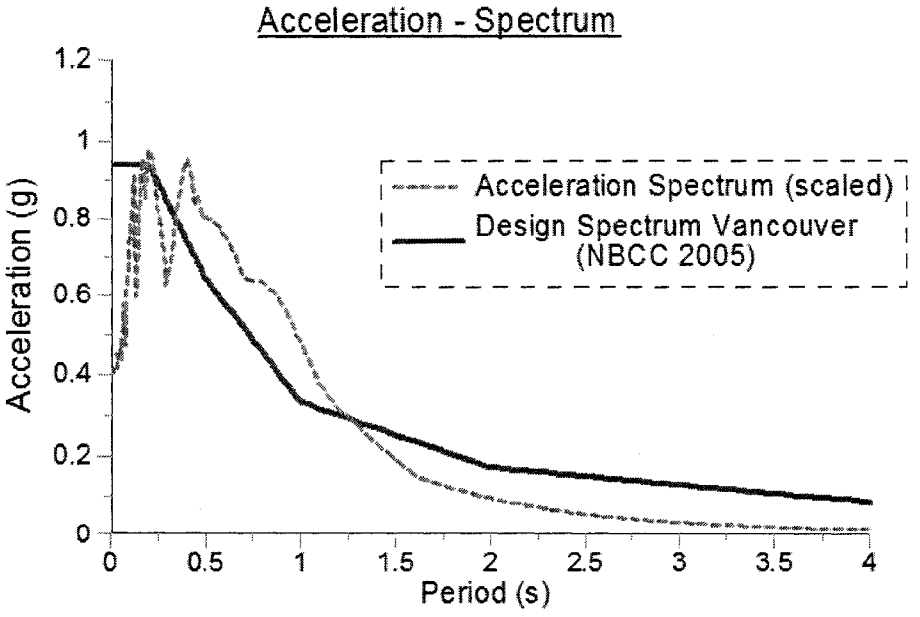

GROUND MOTION H05

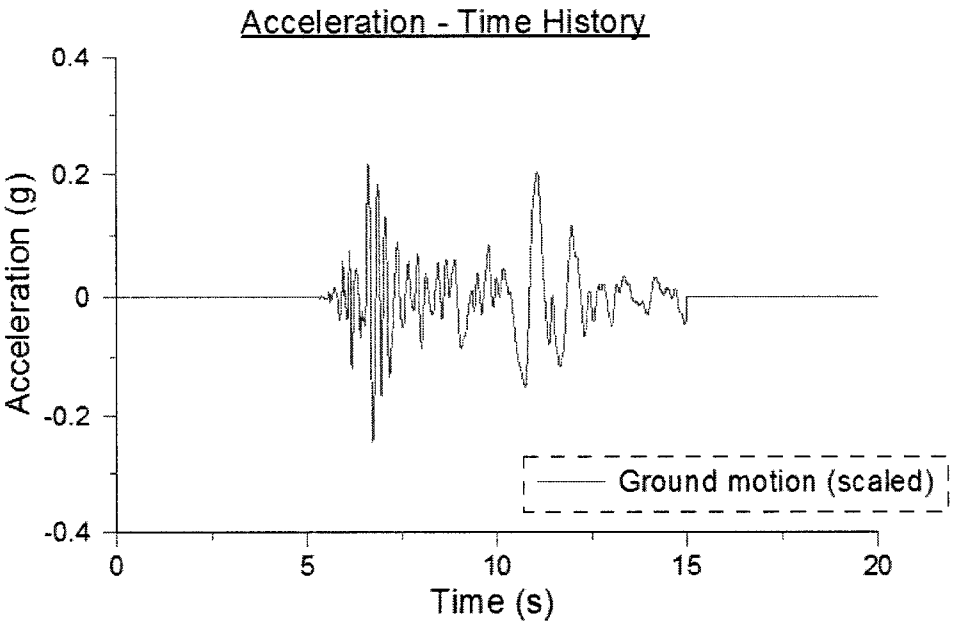

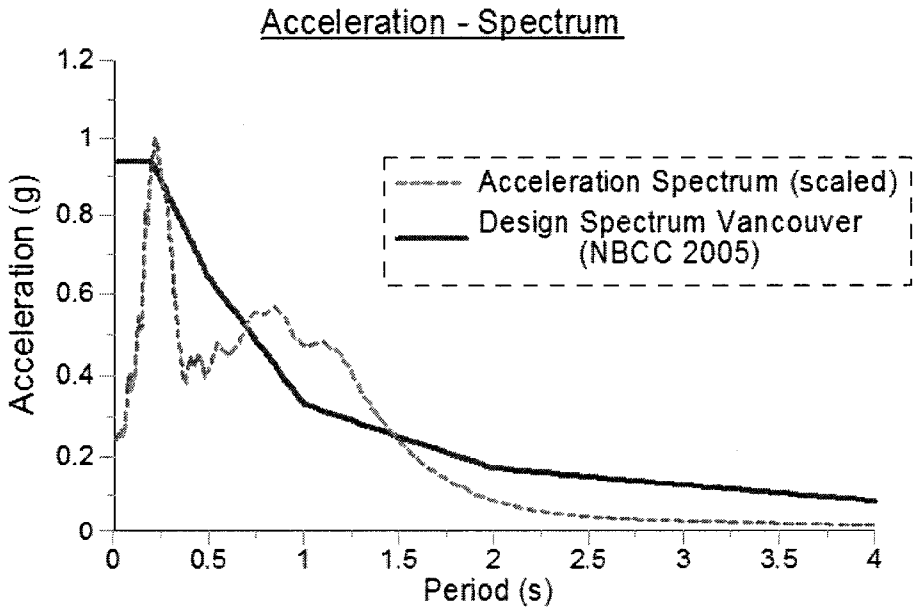

GROUND MOTION H06

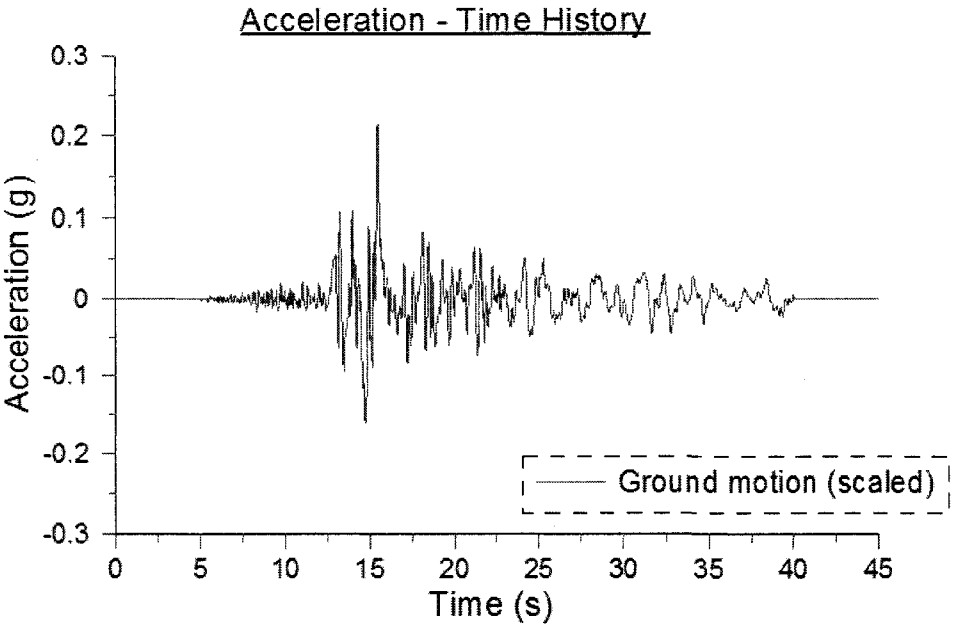

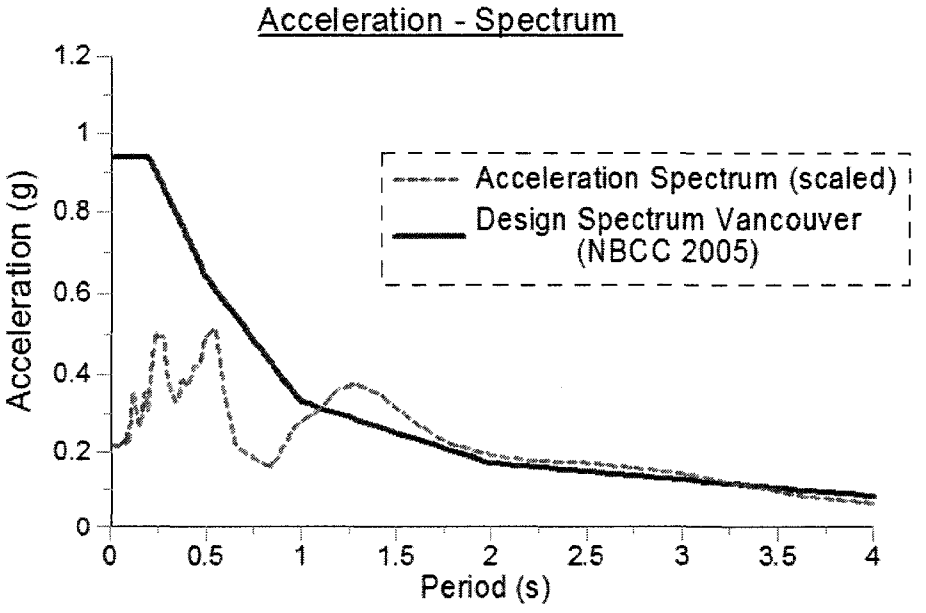

GROUND MOTION H07

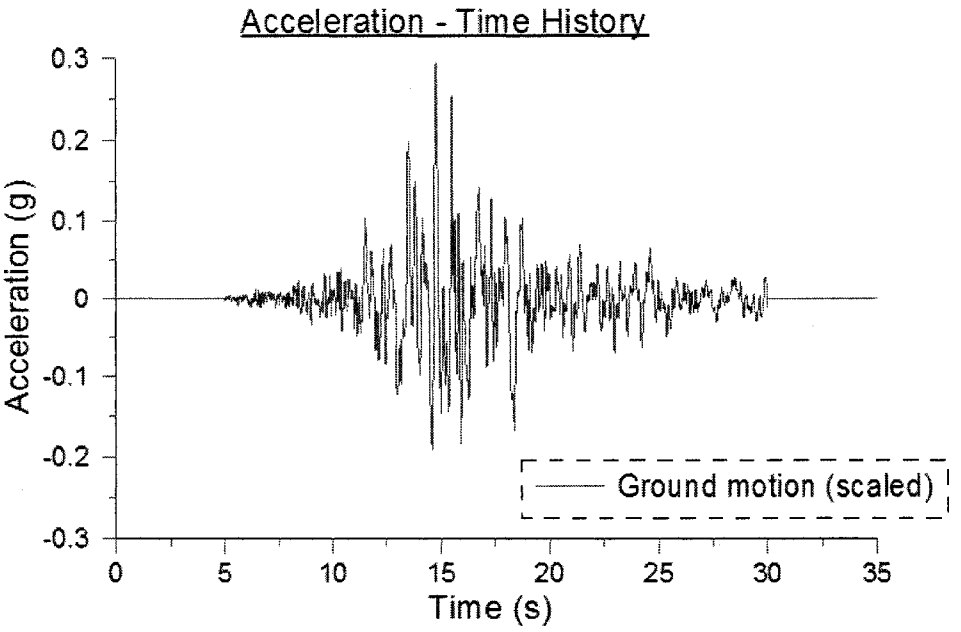

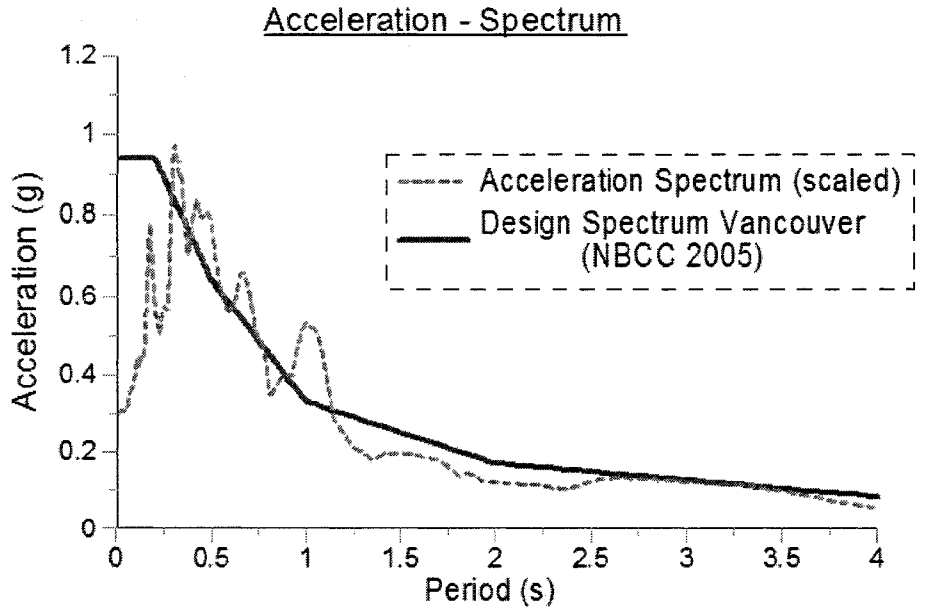

GROUND MOTION H08

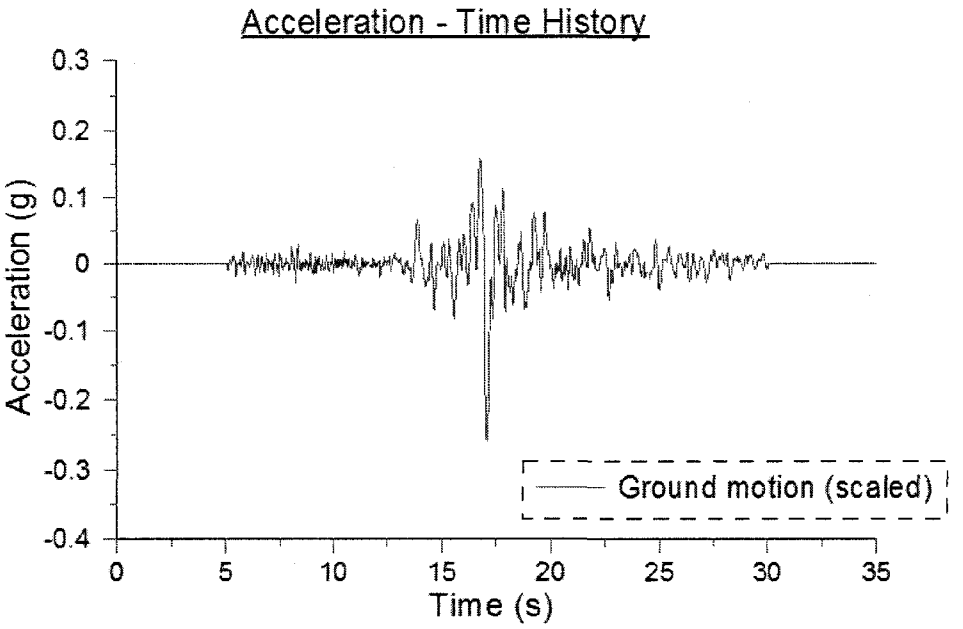

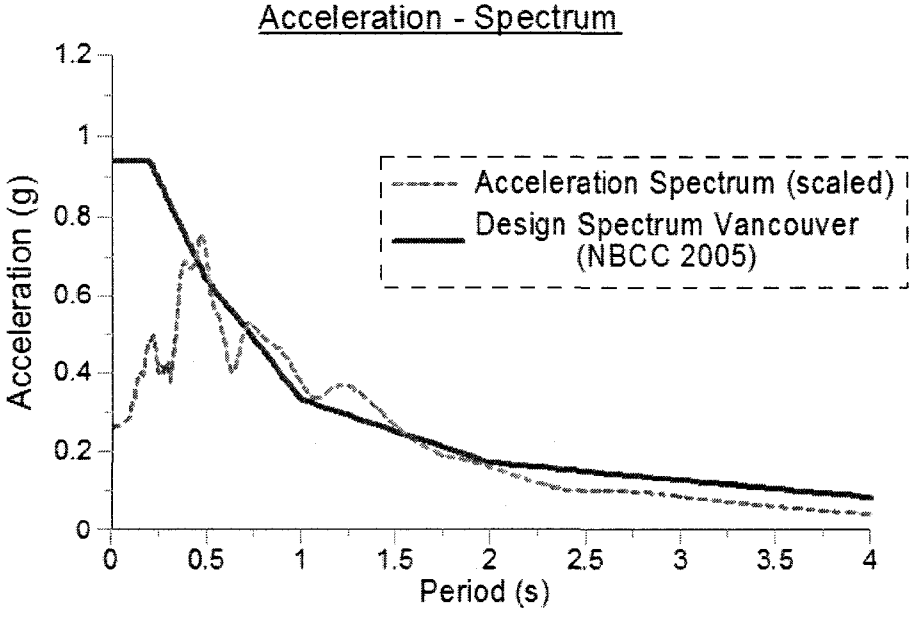

GROUND MOTION H09

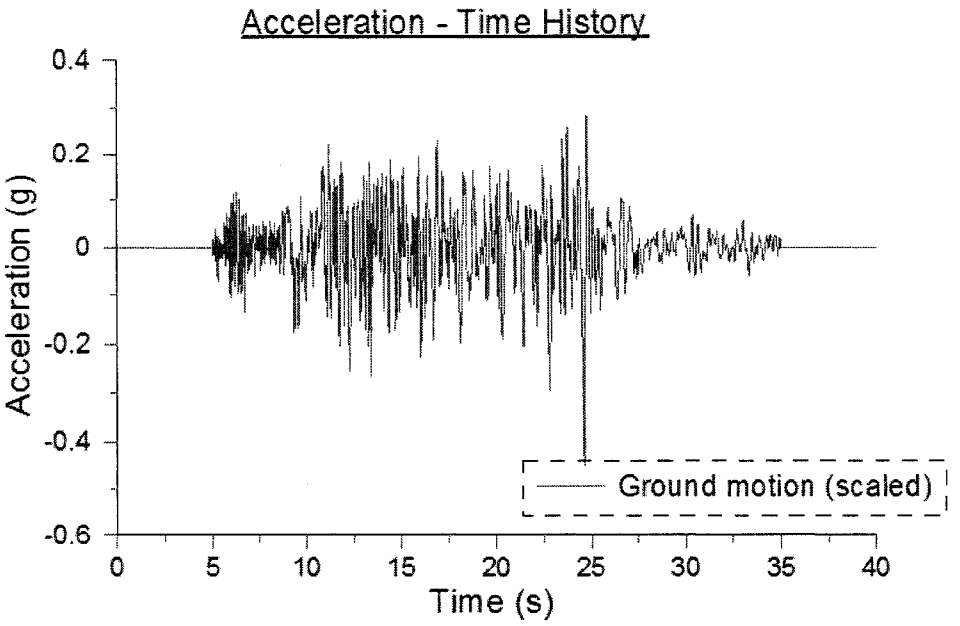

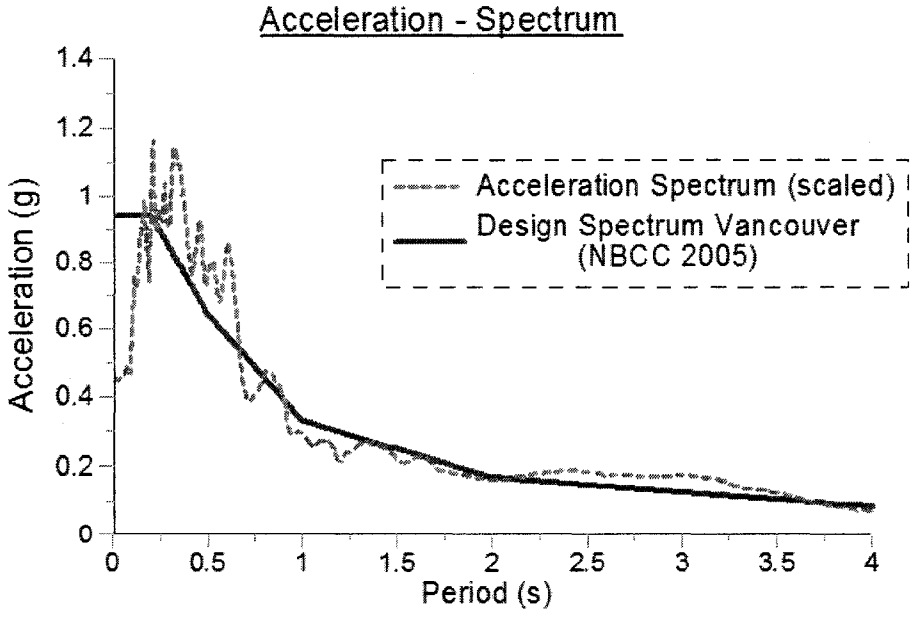

GROUND MOTION H10

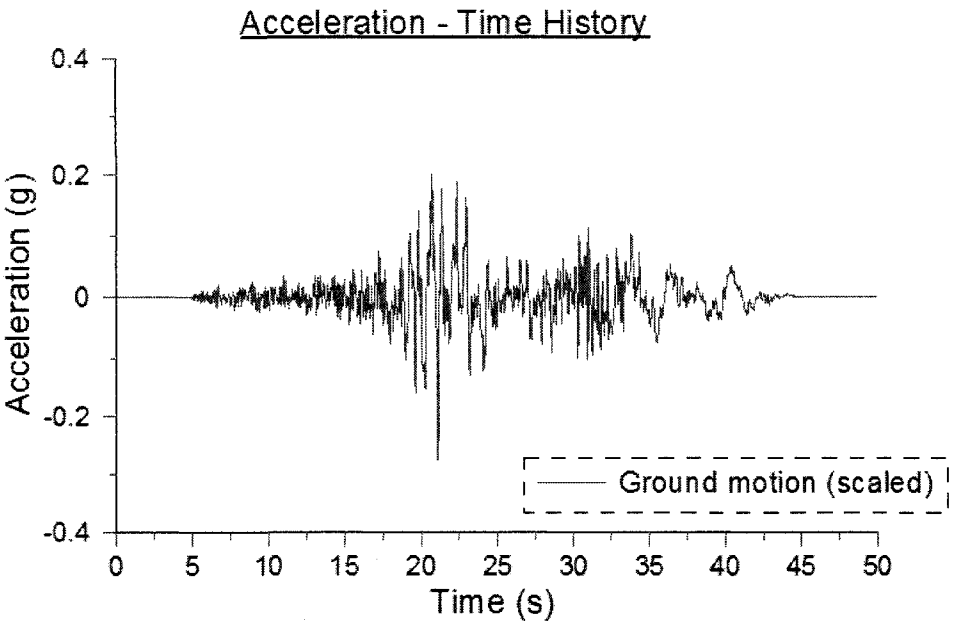

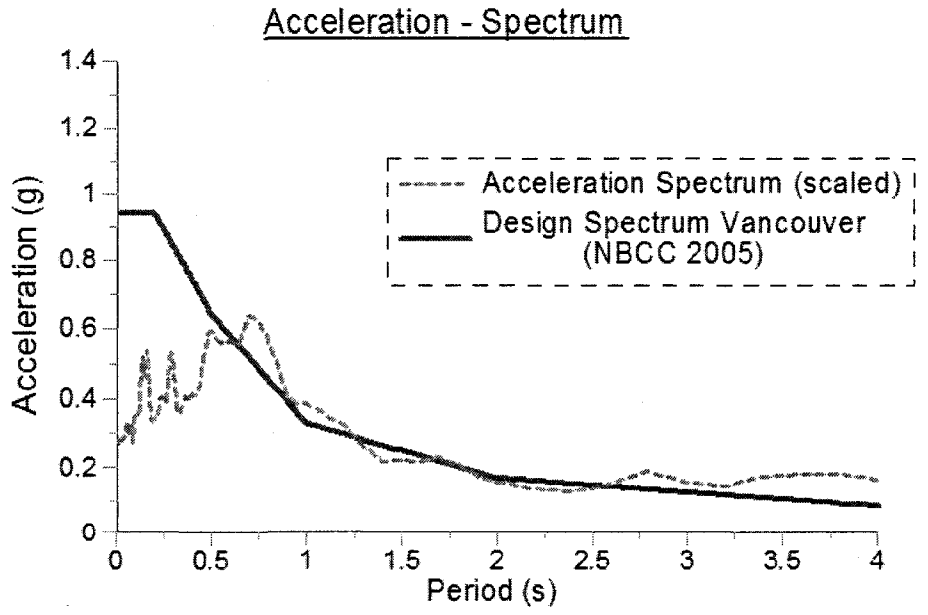

GROUND MOTION A01

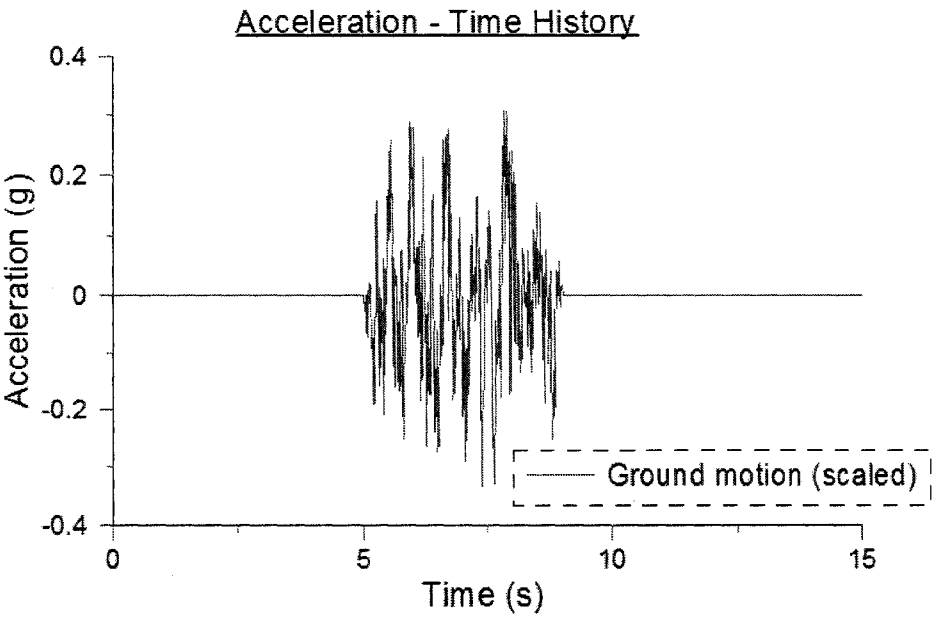

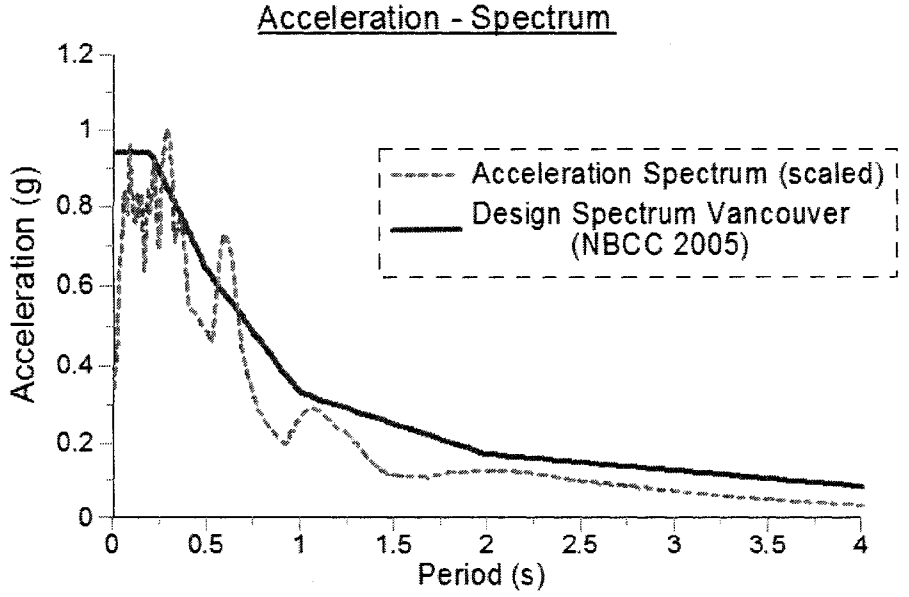

GROUND MOTION A02

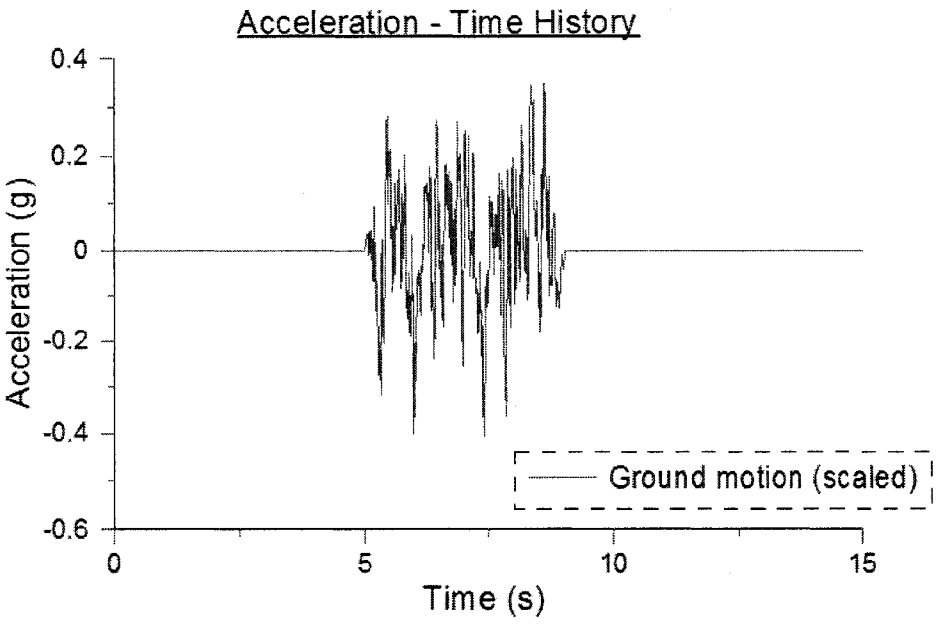

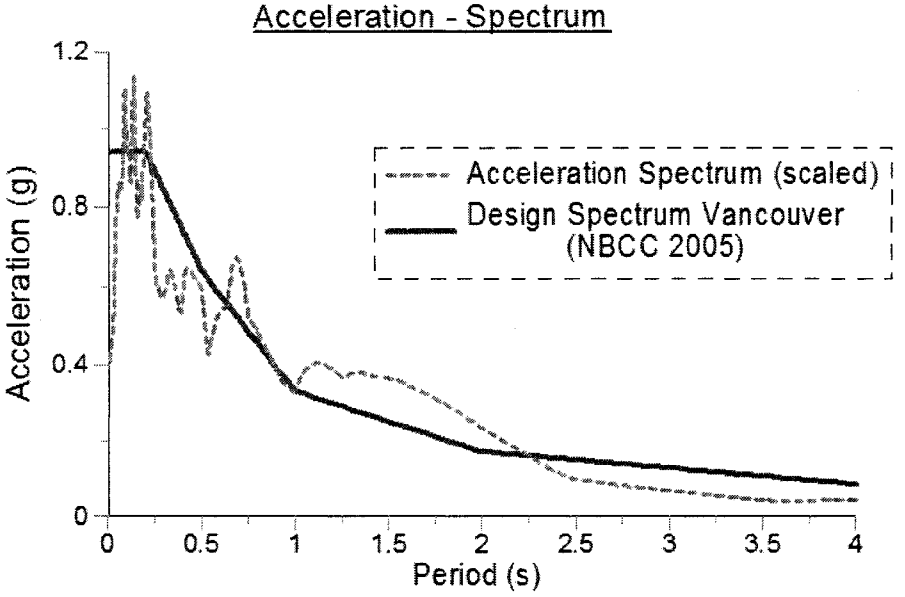

GROUND MOTION A03

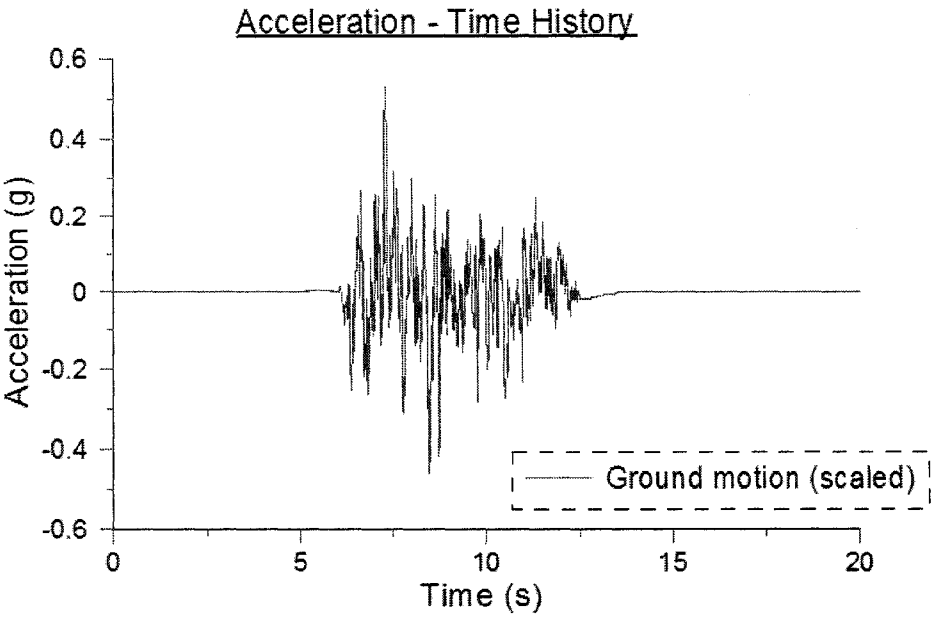

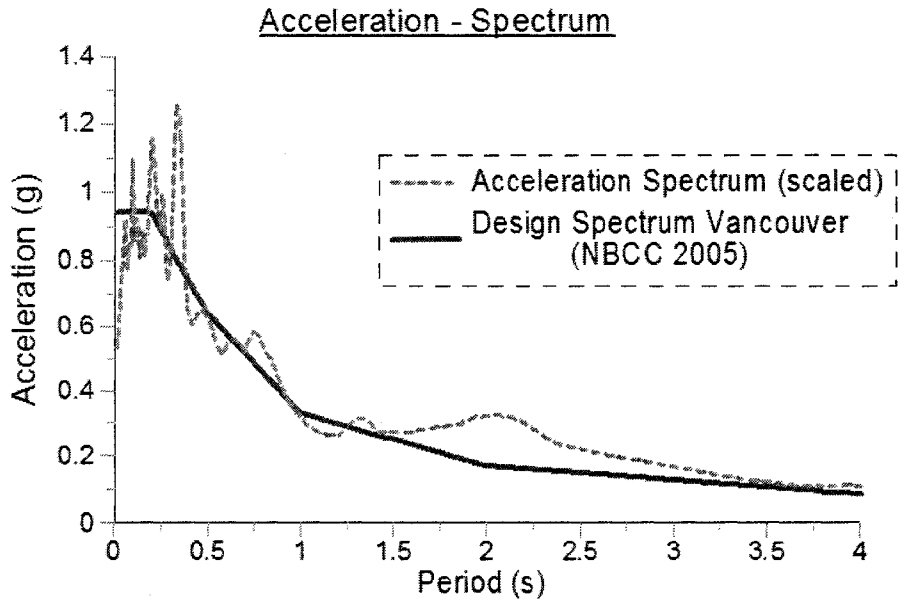

GROUND MOTION A04

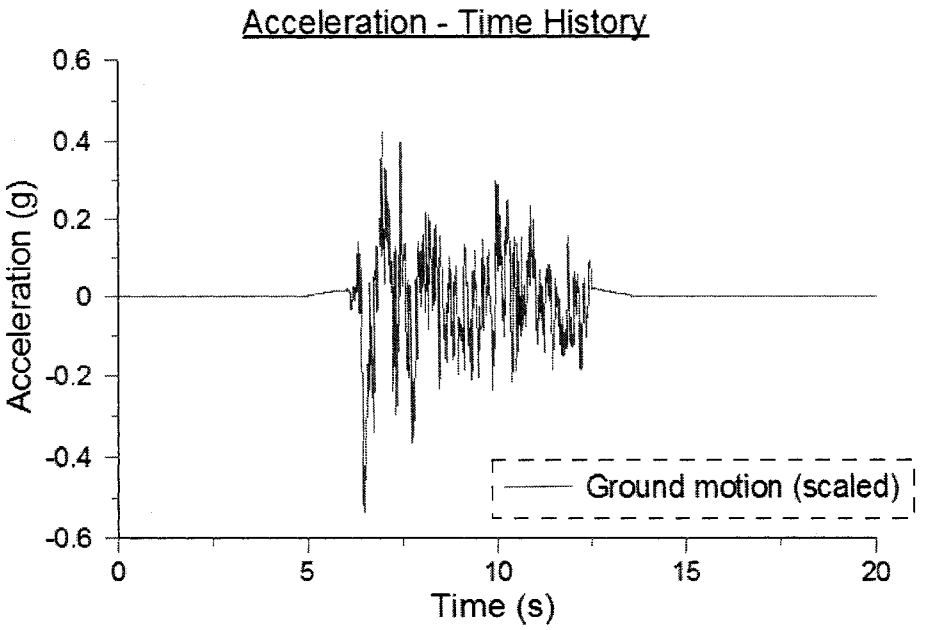

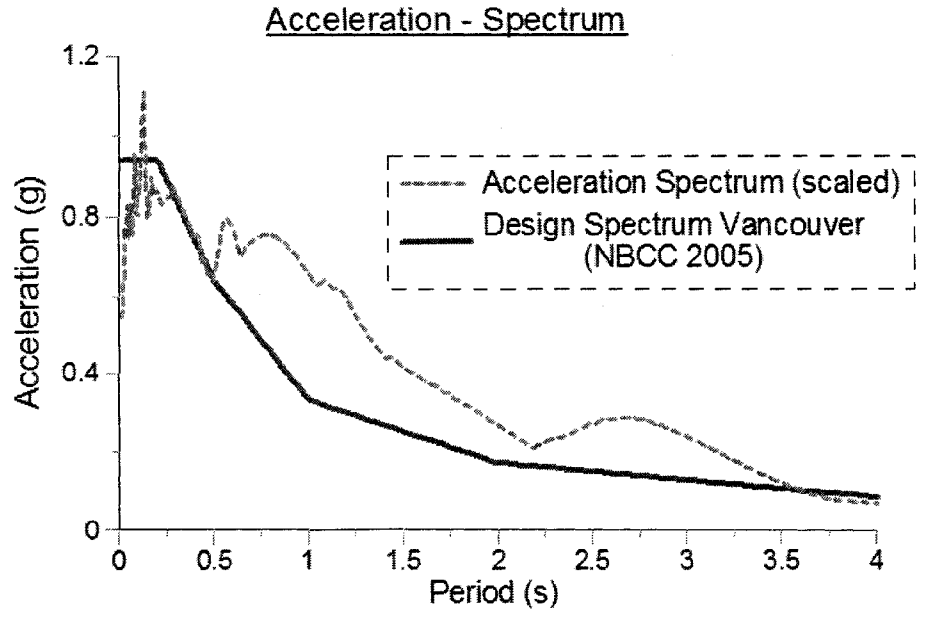

GROUND MOTION A05

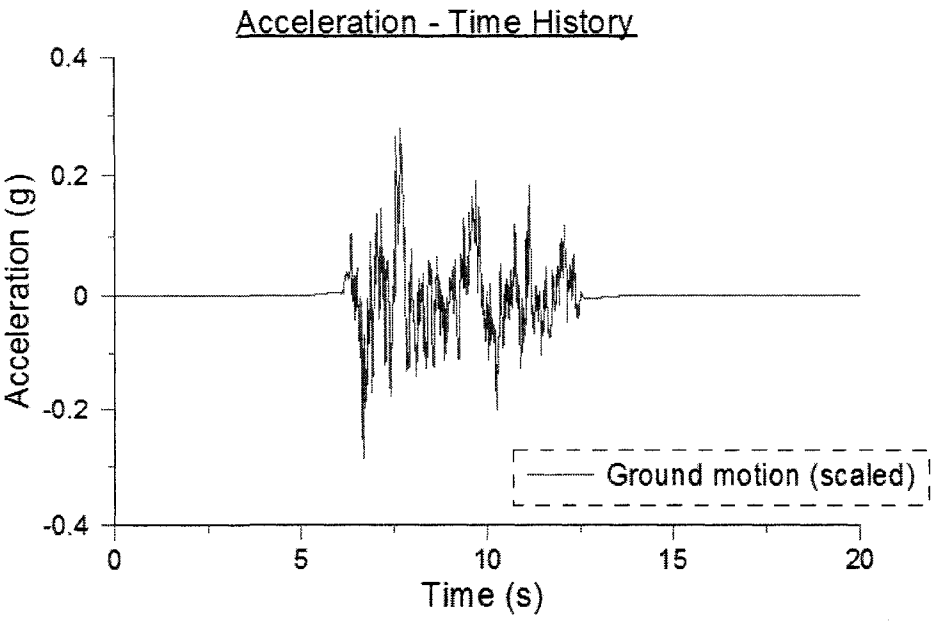

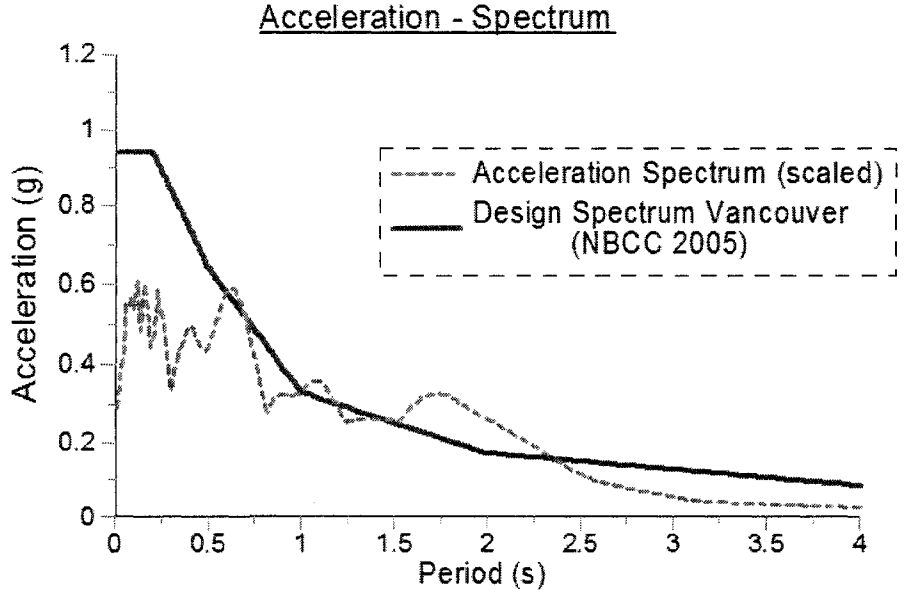

GROUND MOTION A06

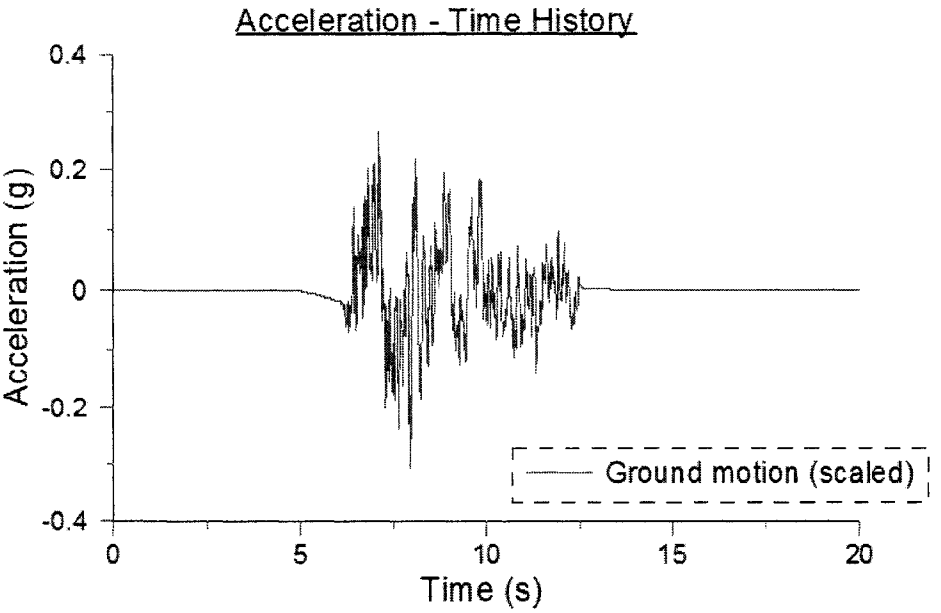

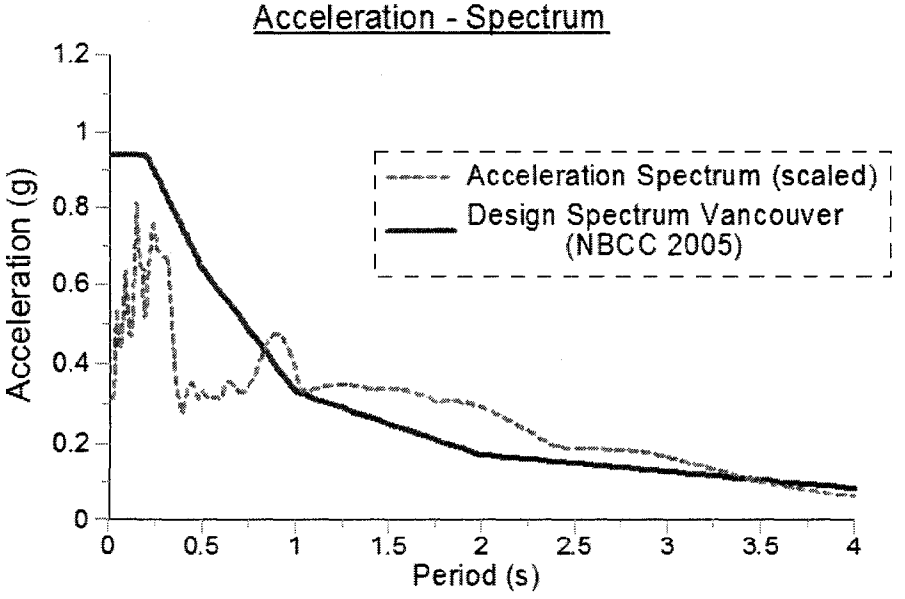

GROUND MOTION A07

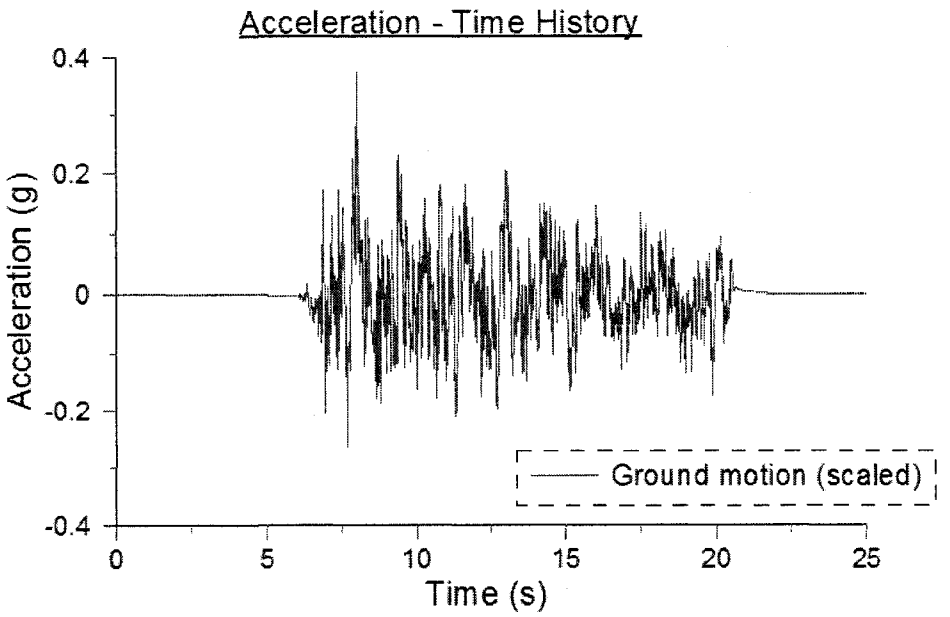

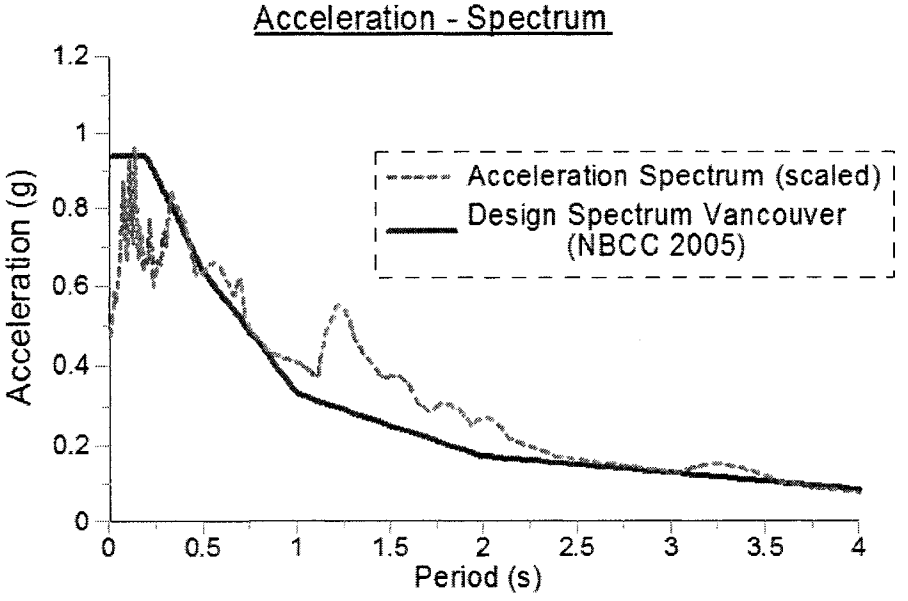

GROUND MOTION A08

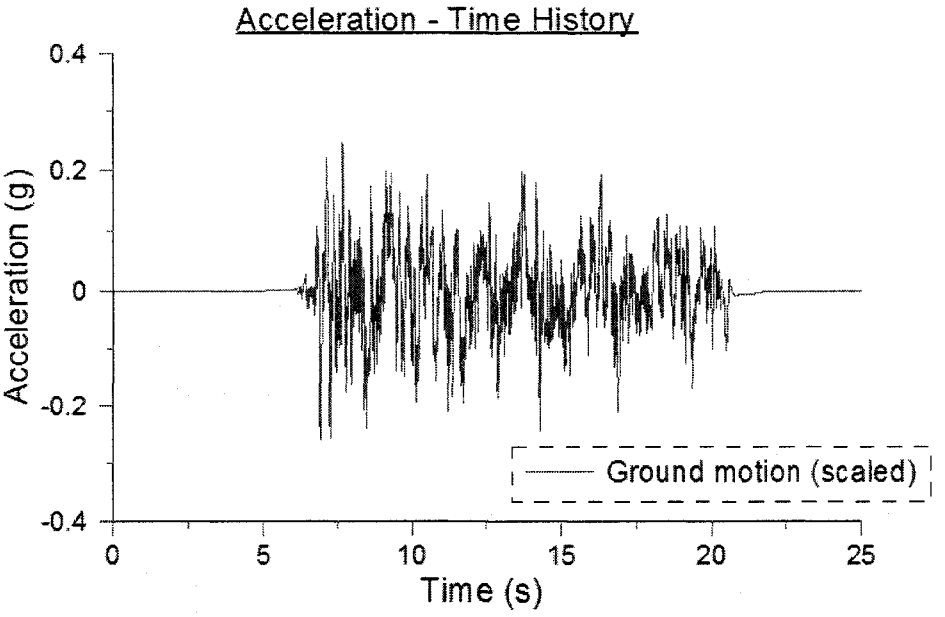

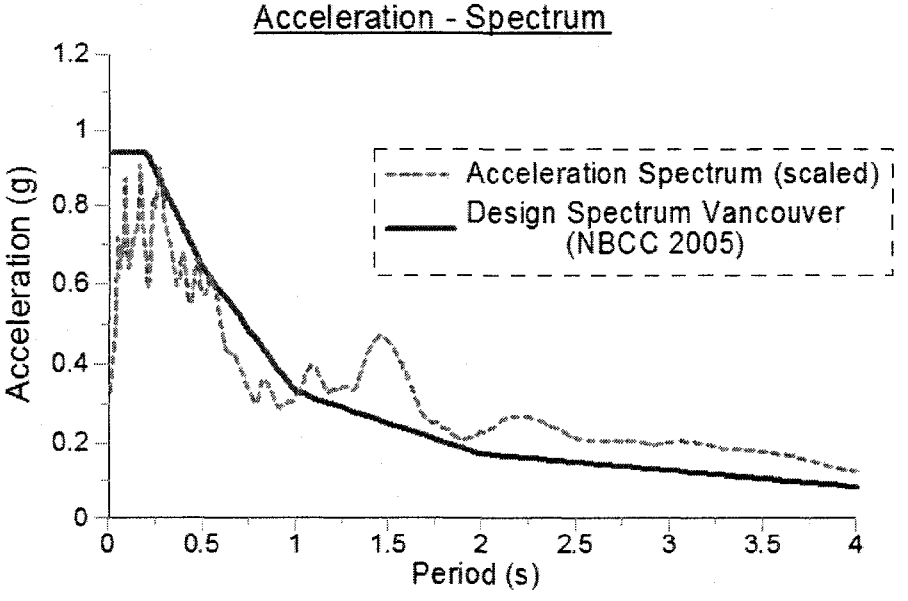

GROUND MOTION A09

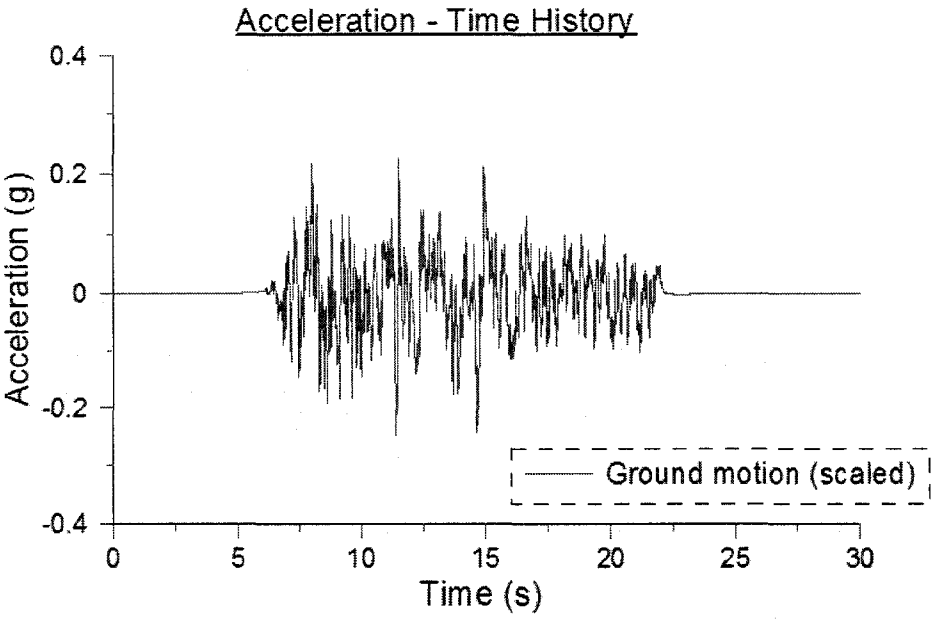

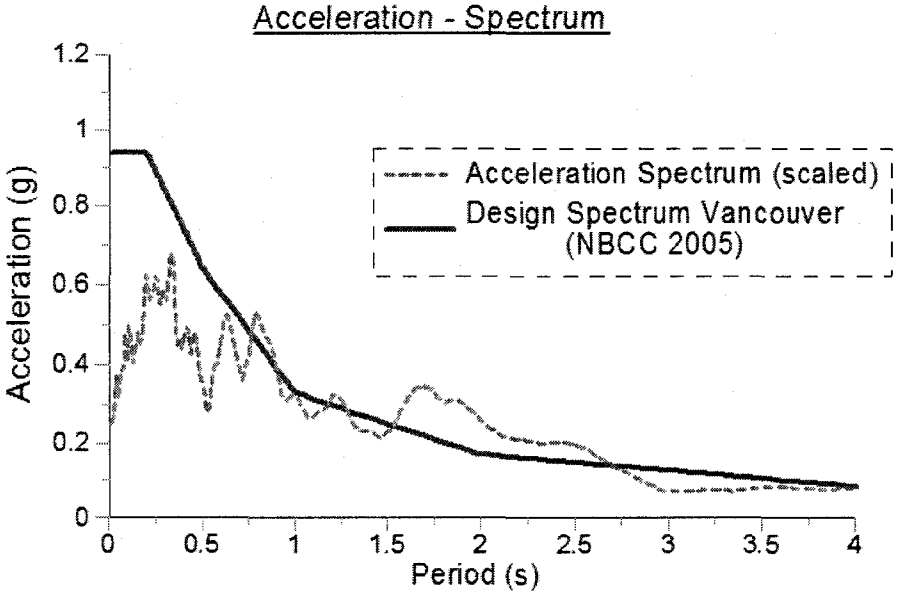

GROUND MOTION A10

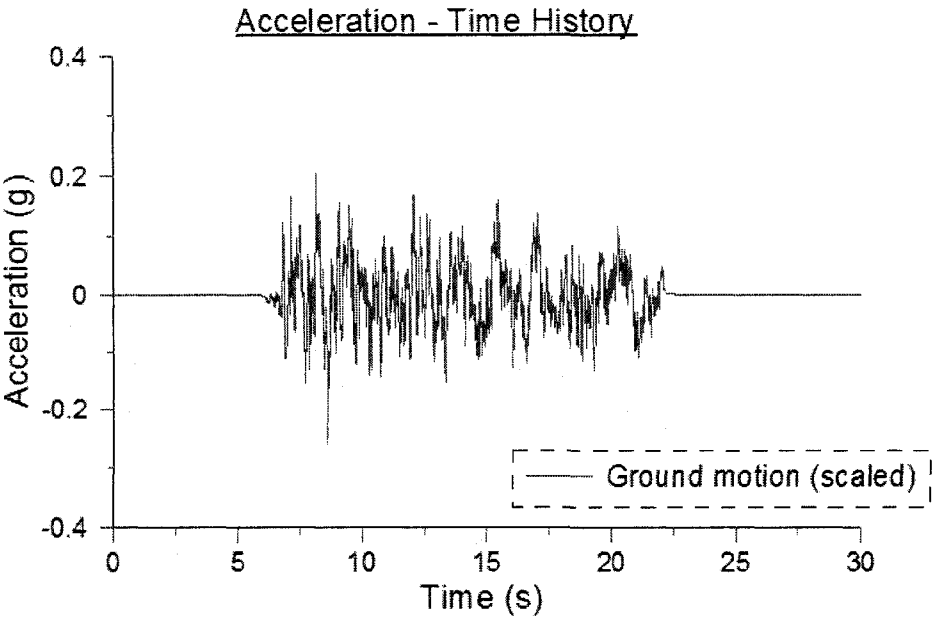

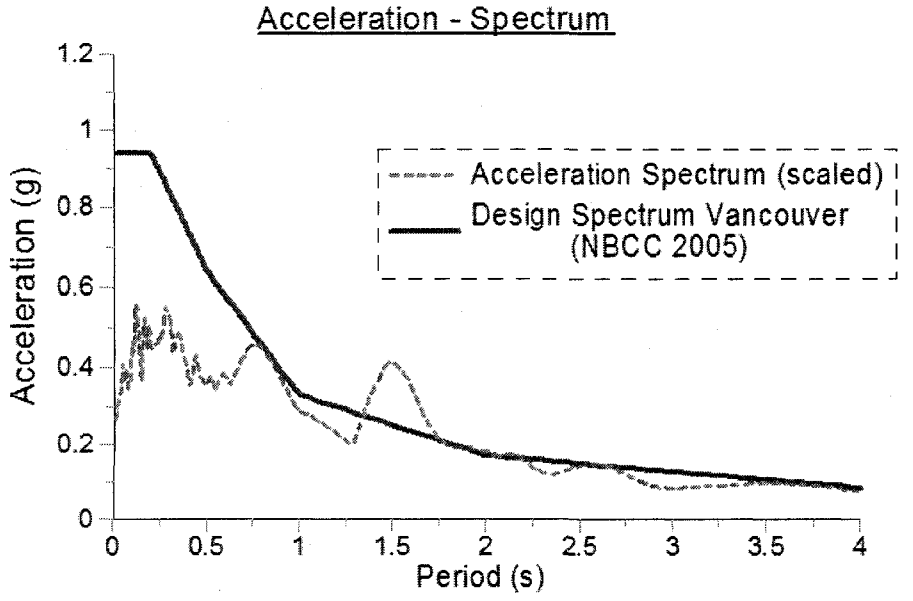

APPENDIX E

GROUND MOTIONS USED FOR LOS ANGELES

GROUND MOTION LA23

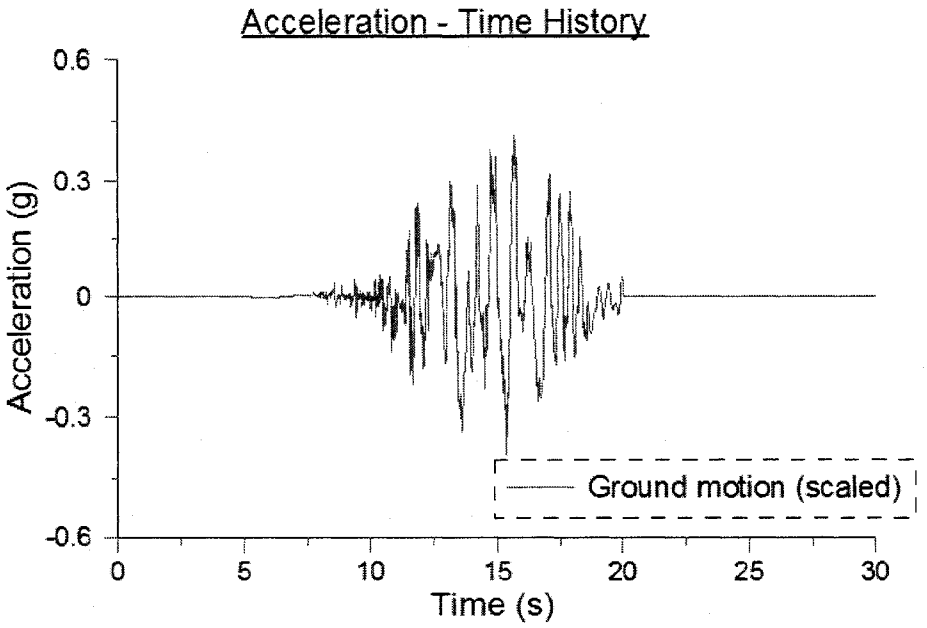

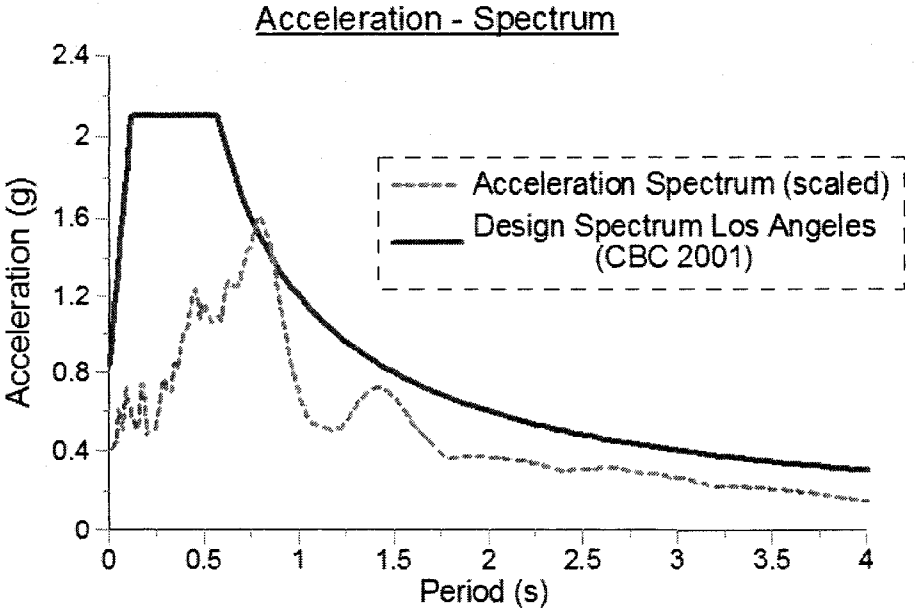

GROUND MOTION LA24

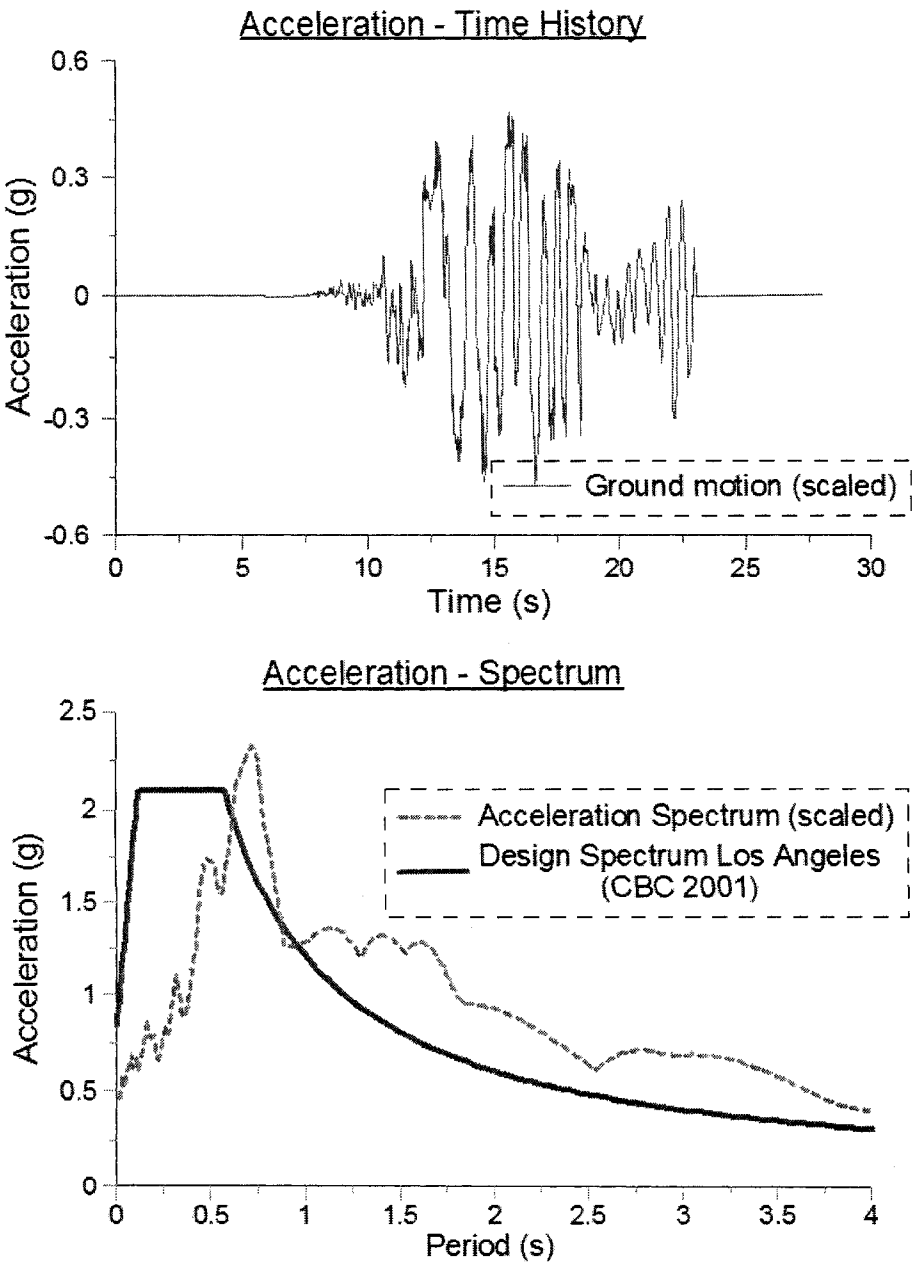

GROUND MOTION LA25

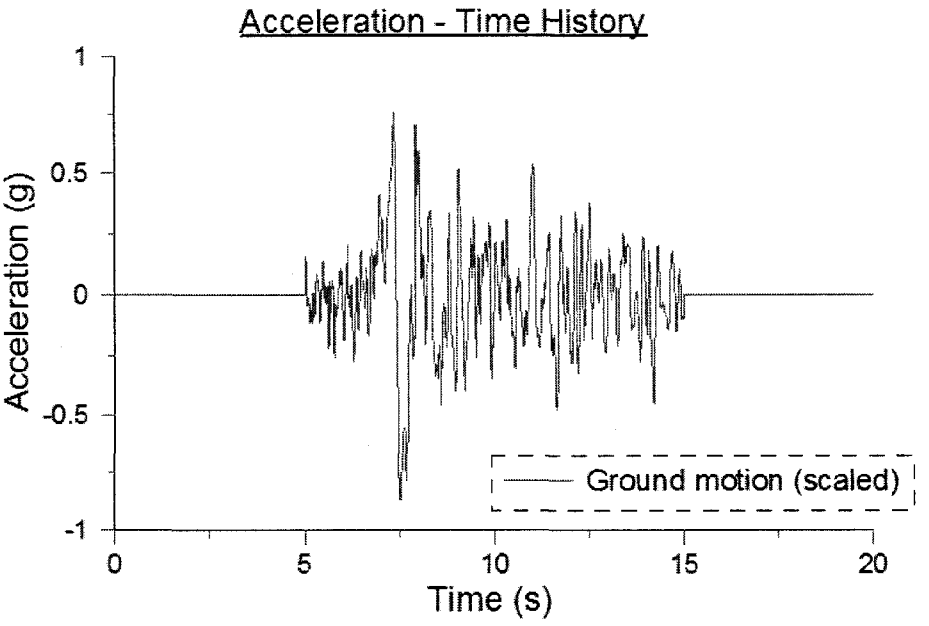

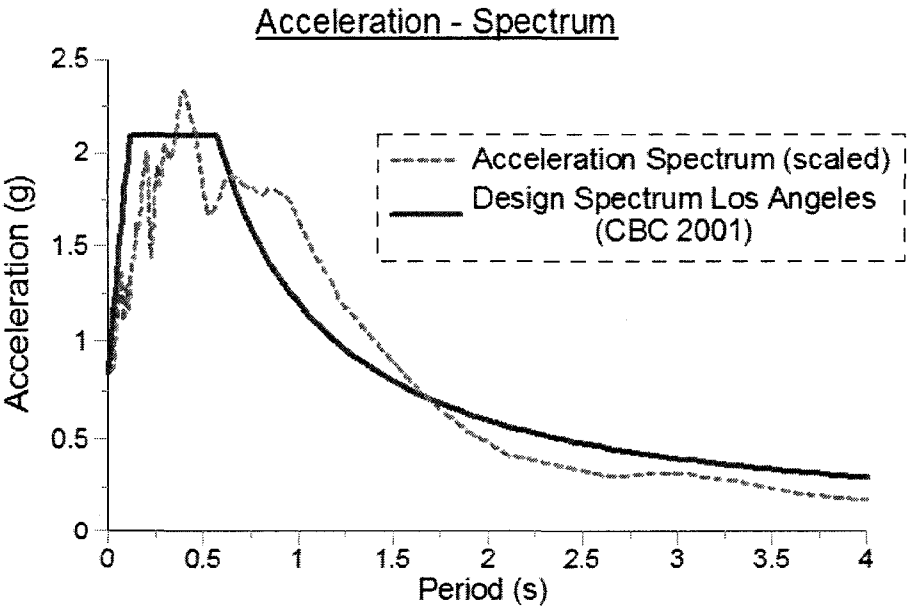

GROUND MOTION LA26

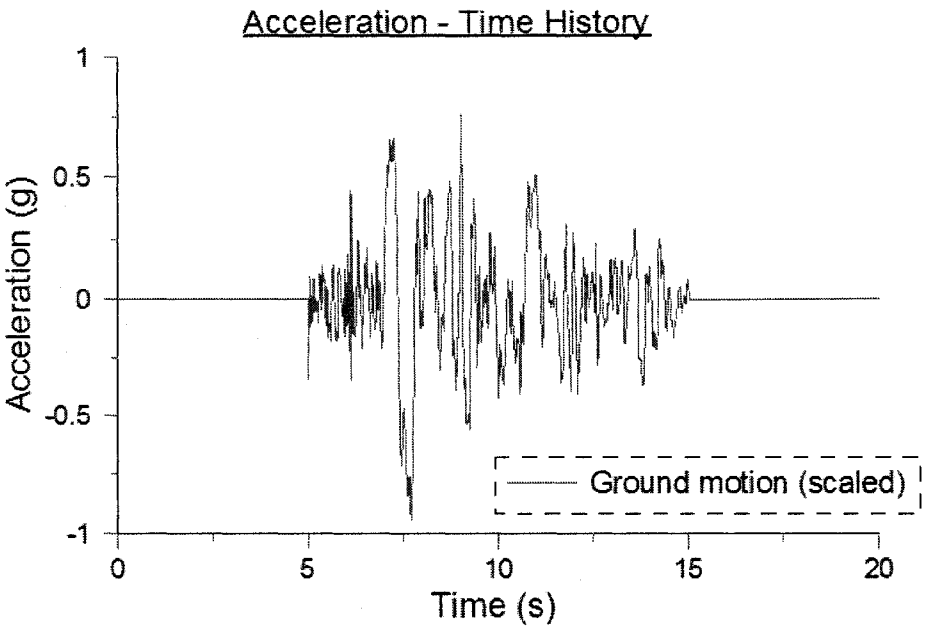

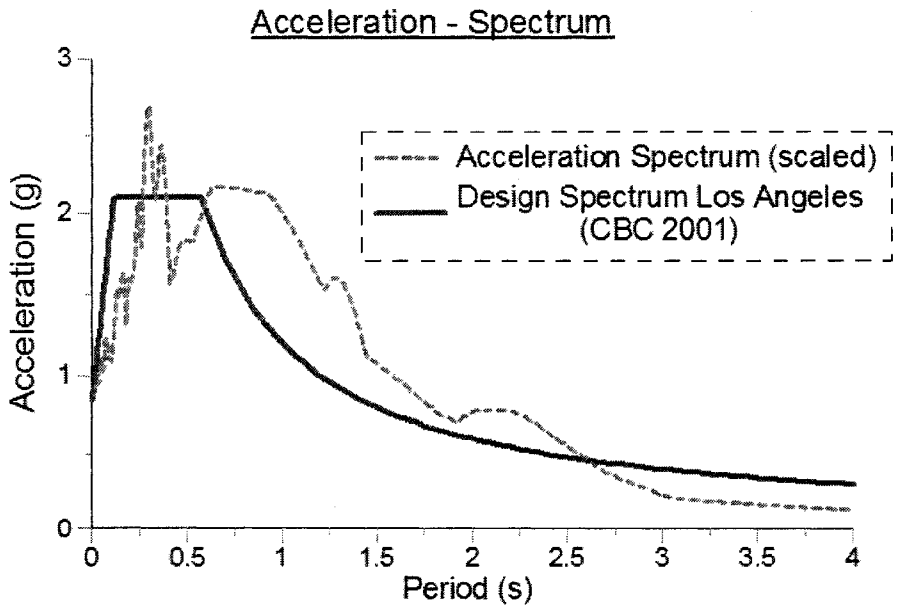

GROUND MOTION LA27

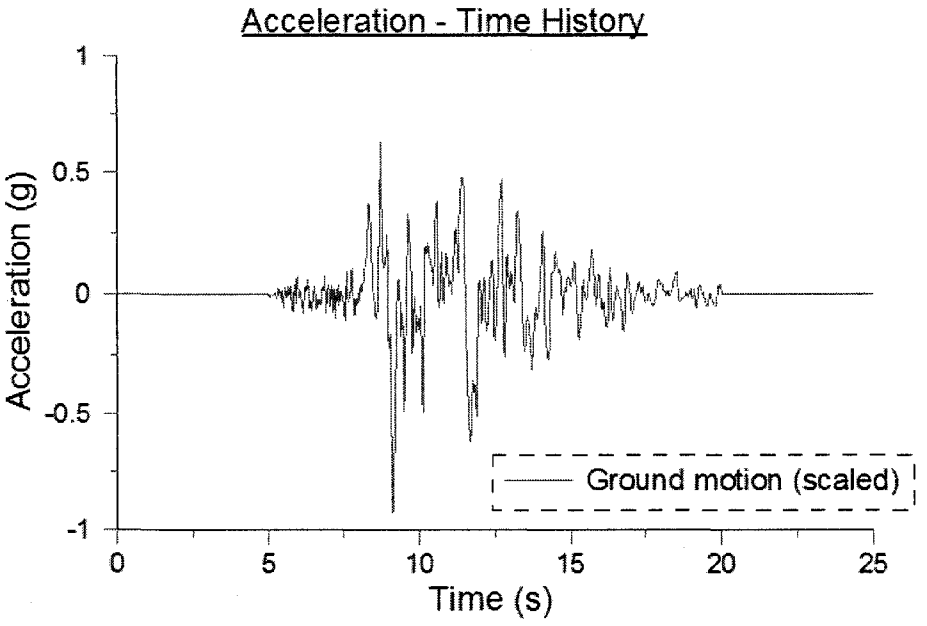

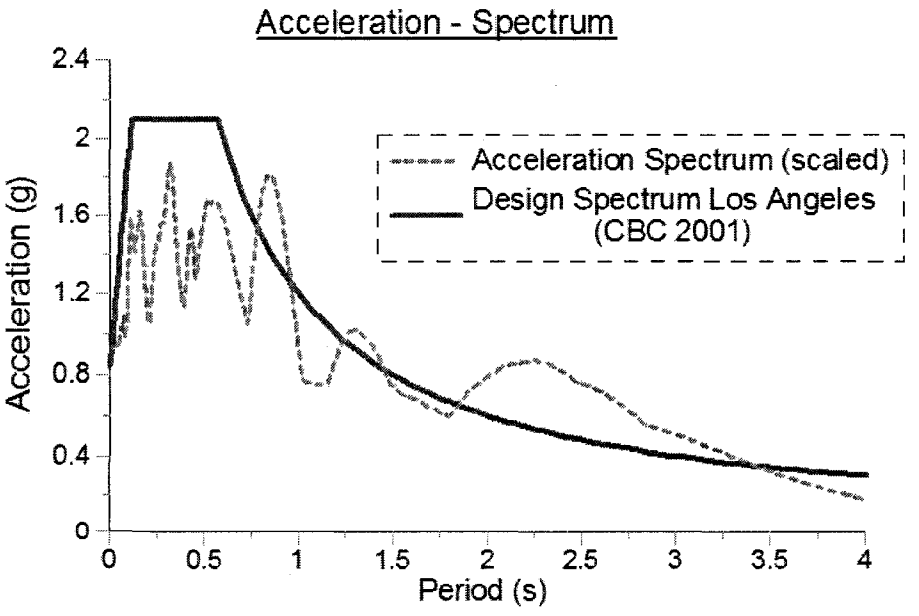

GROUND MOTION LA28

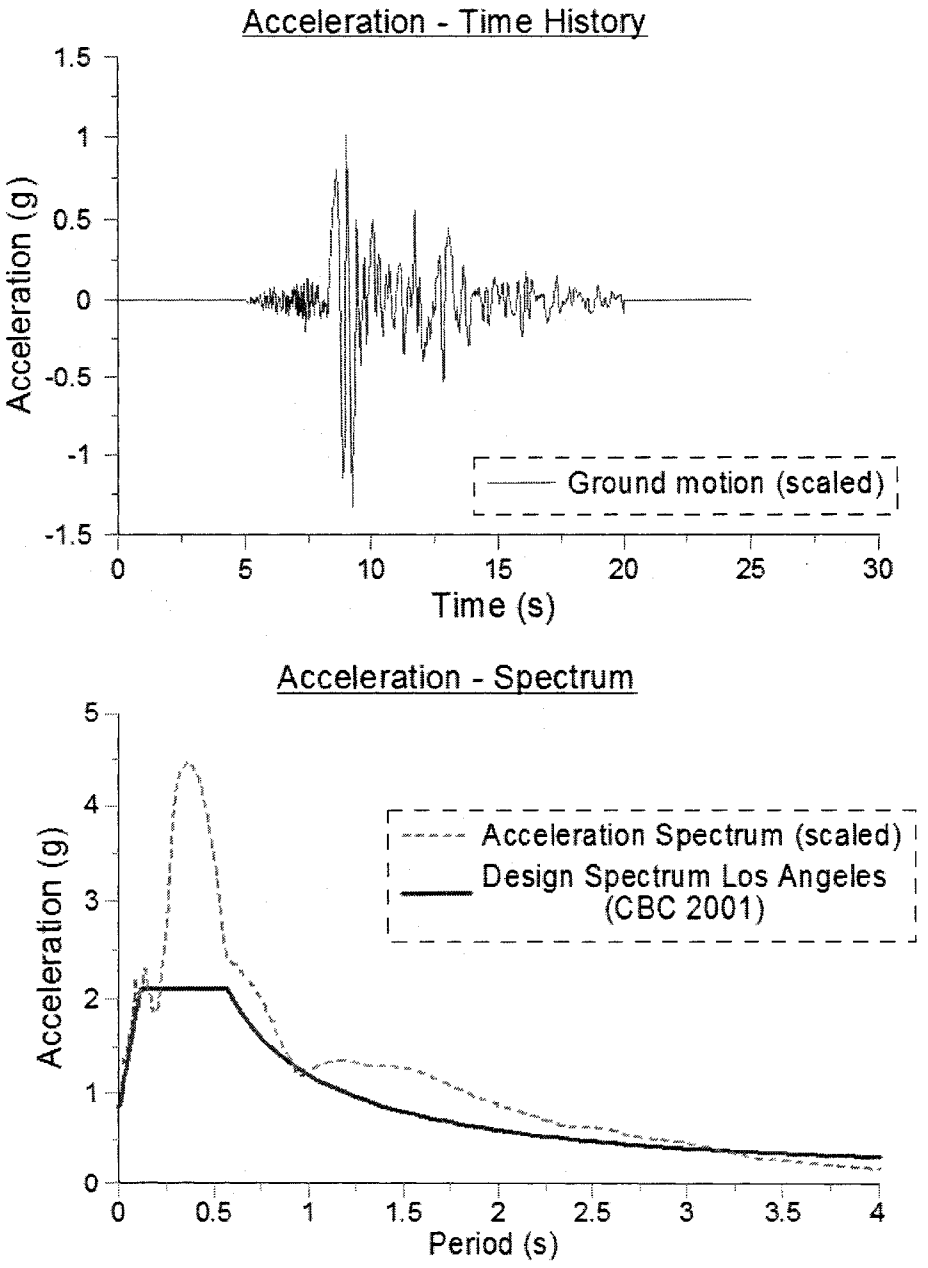

GROUND MOTION LA31

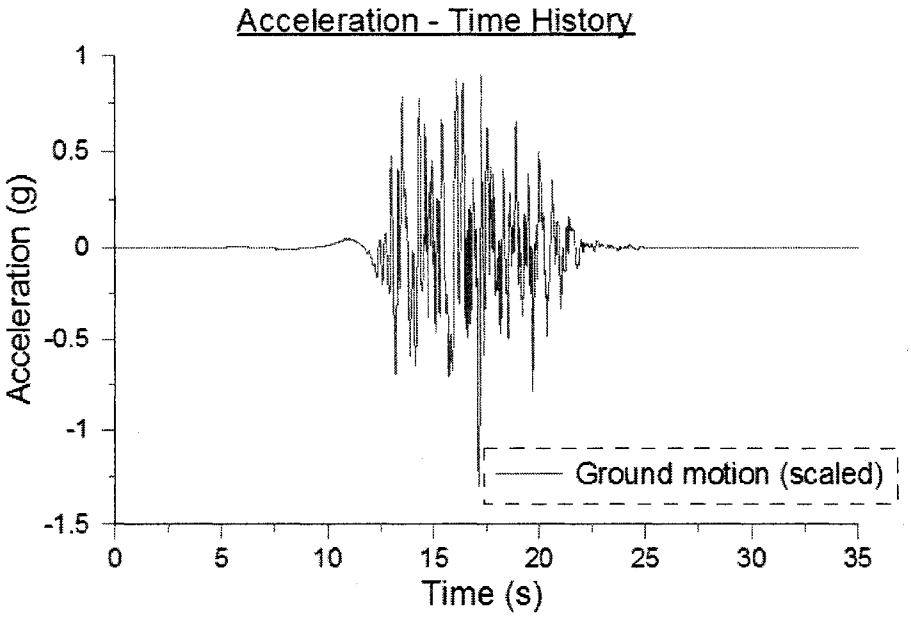

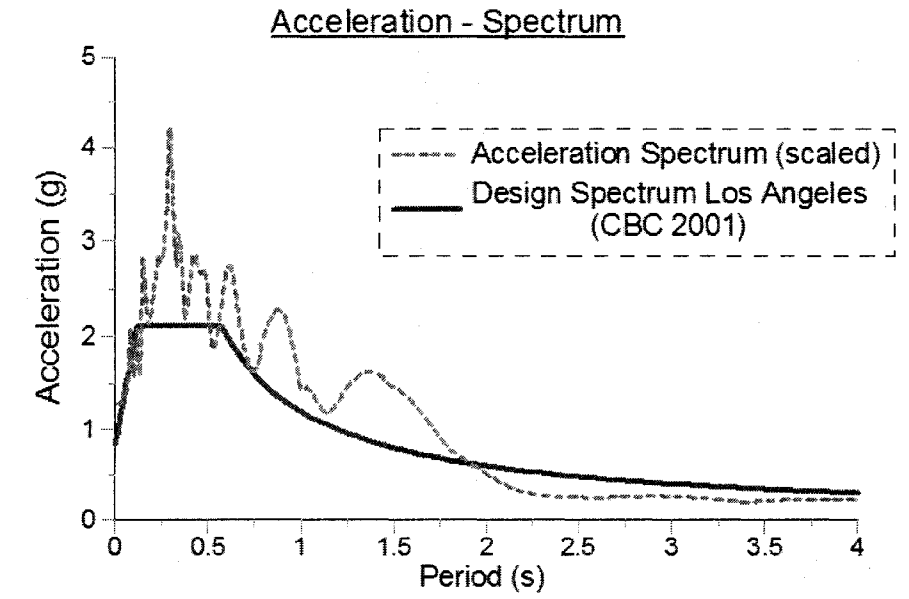

GROUND MOTION LA32

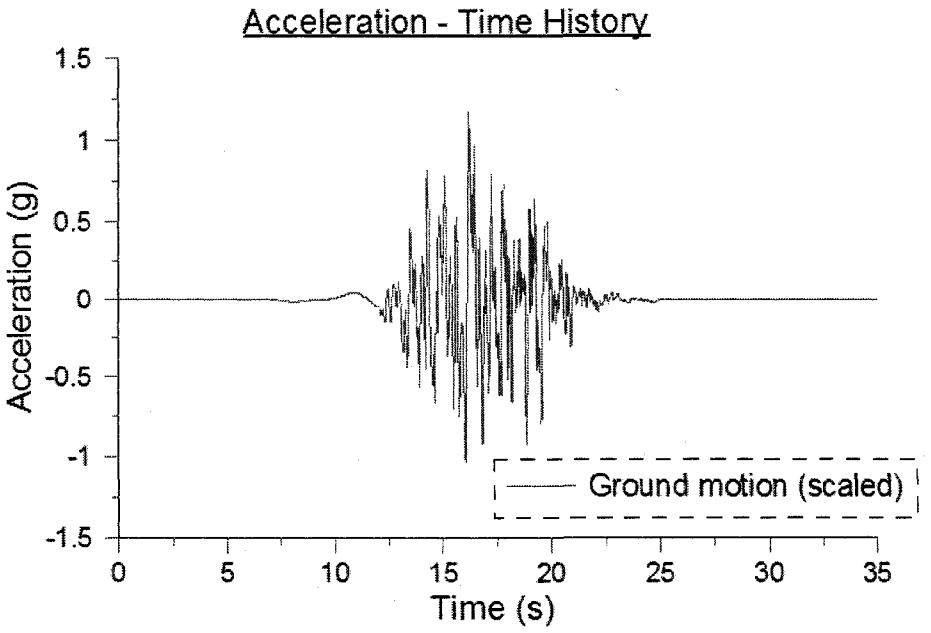

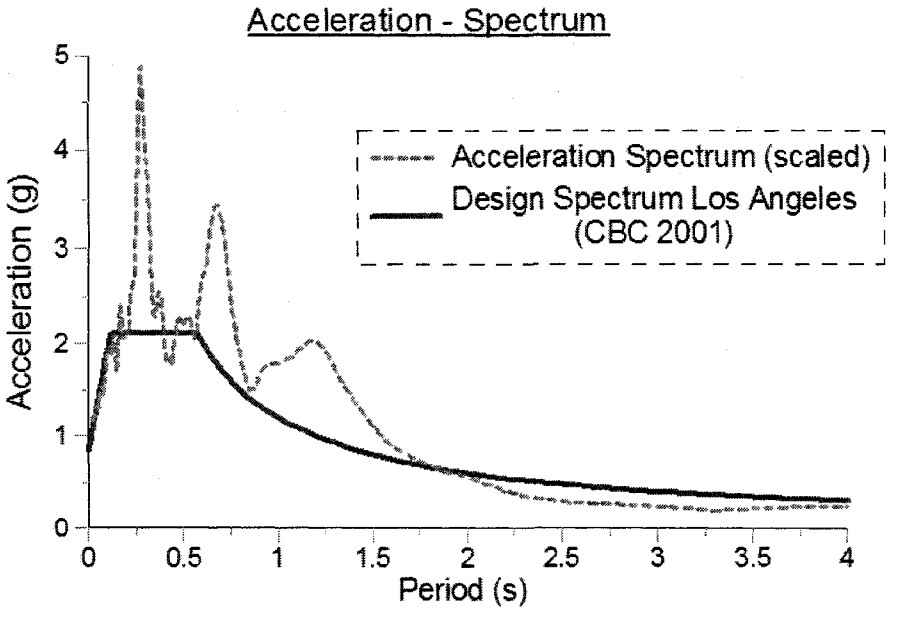

GROUND MOTION LA37

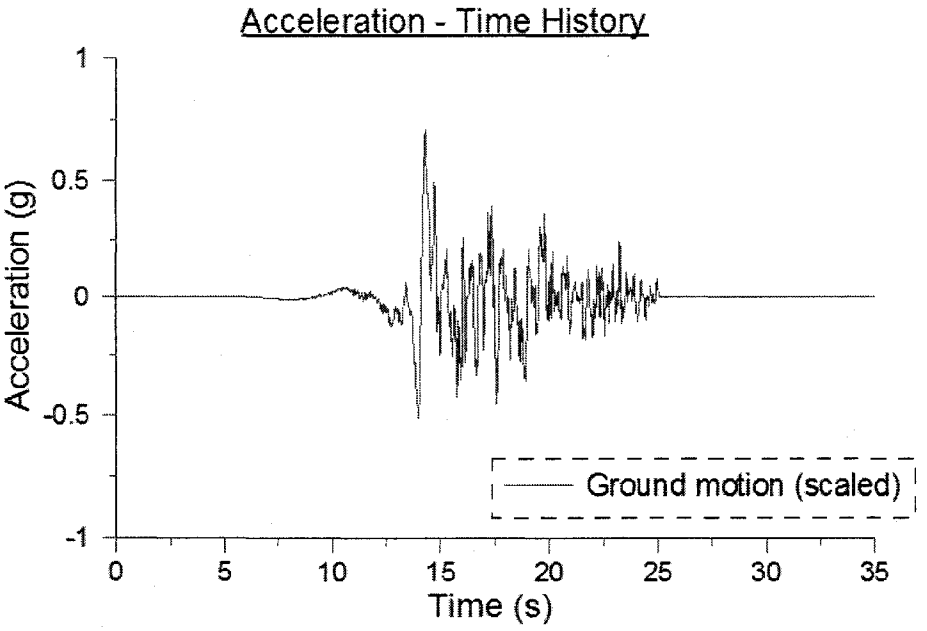

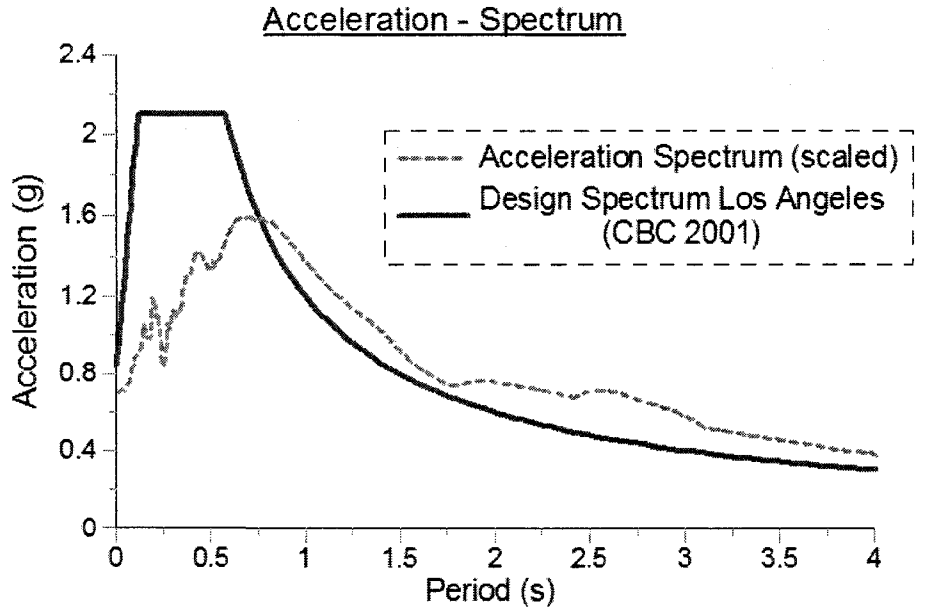

GROUND MOTION LA38

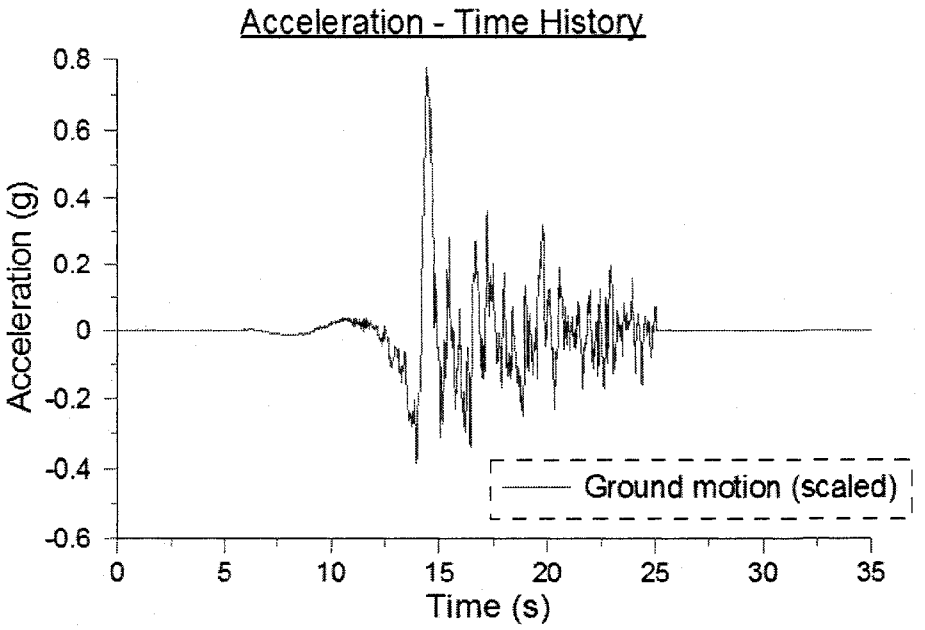

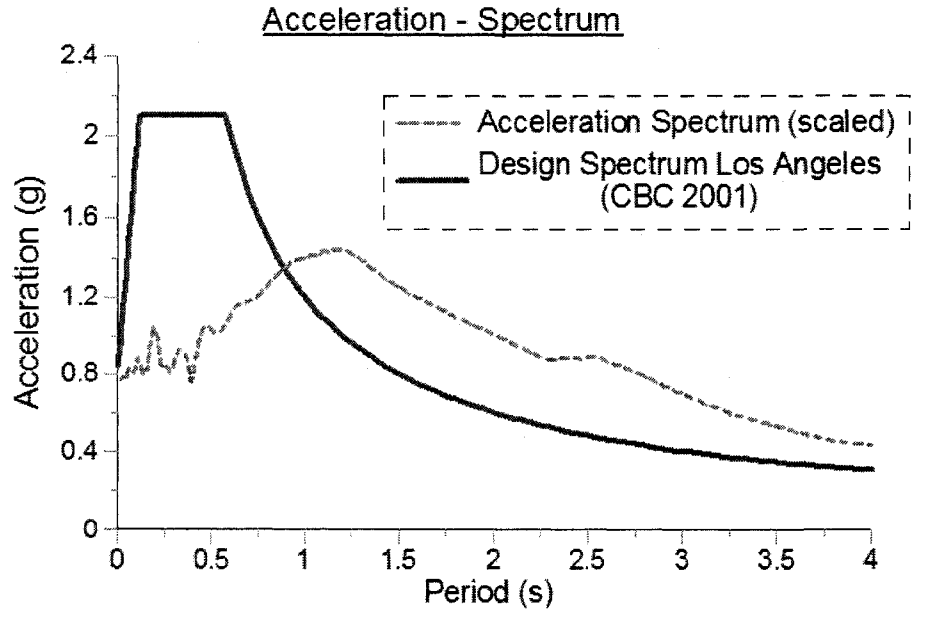

APPENDIX F

DESCRIPTION OF THE BRACED FRAMES USED IN THE PARAMETRIC STUDY

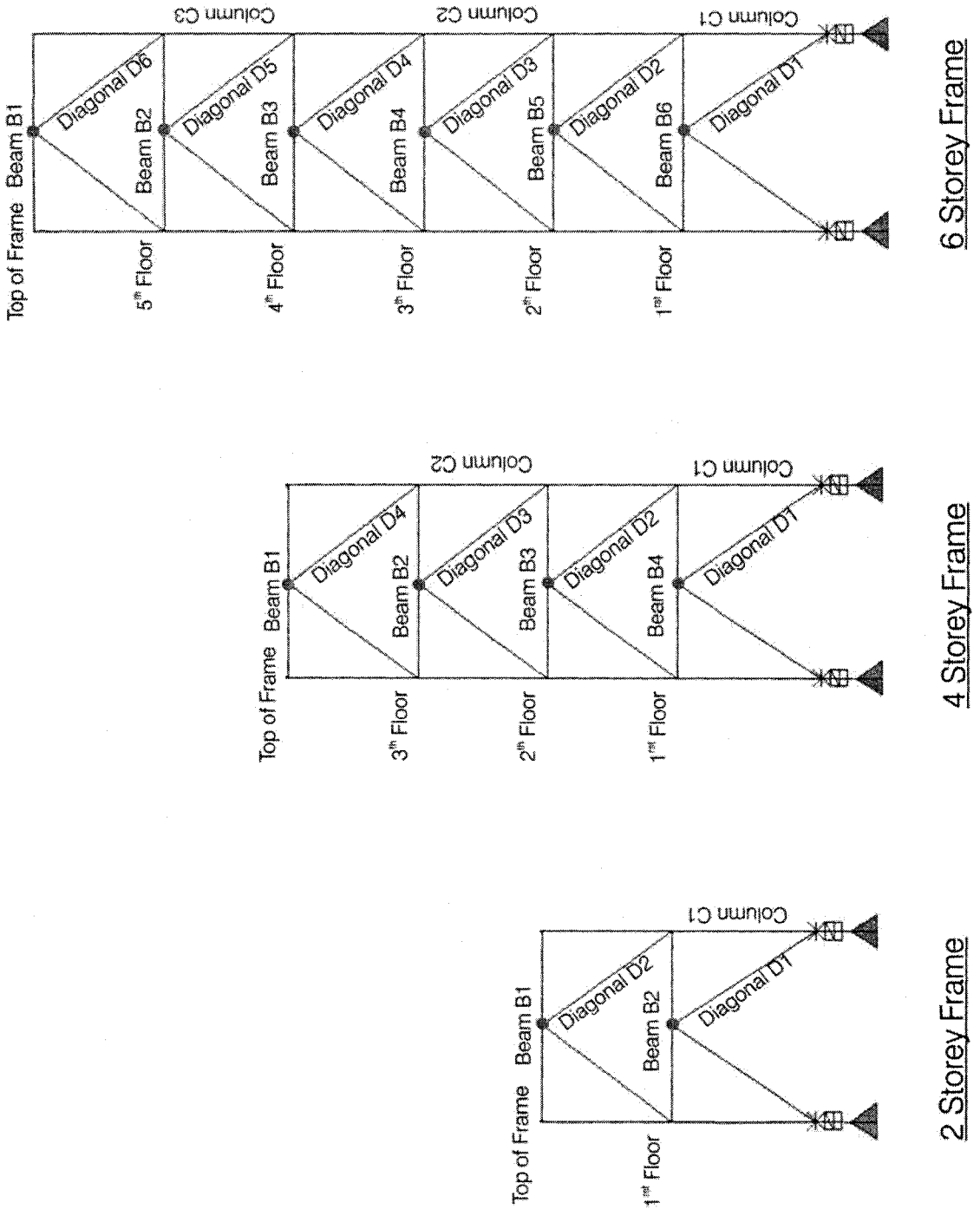

Figure F.1 Element identification used for the braced frames

1. Montreal (QC)

1.1 *2-storey building, exterior bracing, 2.81m span (3-e-2-mtl)*

Seismic masses (kg)		Steel sections					
		Diagonals		Columns		Beams	
Roof	780,825.7	D2	HSS127x127x13			B1	W200x15
1rst floor	913,761.5	D1	HSS178x178x9.5	C1	W200x46	B2	W300x21
Spring rigidity *k* (kN/m)							
Damper	1,500,000.00						
Gap	1,500,000.00						

1.2 *2-storey building, exterior bracing, 5.625m span (6-e-2-mtl)*

Seismic masses (kg)		Steel sections					
		Diagonals		Columns		Beams	
Roof	780,825.7	D2	HSS127x127x8.0			B1	W360x33
1rst floor	913,761.5	D1	HSS152x152x8.0	C1	W200x42	B2	W410x39
Spring rigidity *k* (kN/m)							
Damper	1,500,000.00						
Gap	1,500,000.00						

1.3 *2-storey building, interior bracing, 5.625m span (6-int-2-mtl)*

Seismic masses (kg)		Steel sections					
		Diagonals		Columns		Beams	
Roof	780,825.7	D2	HSS127x127x8.0			B1	W410x46
1rst floor	913,761.5	D1	HSS152x152x8.0	C1	W200x46	B2	W530x66
Spring rigidity *k* (kN/m)							
Damper	1,500,000.00						
Gap	1,500,000.00						

1.4 *2-storey building, exterior bracing, 9m span (9-e-2-mtl)*

Seismic masses (kg)		Steel sections					
		Diagonals		Columns		Beams	
Roof	780,825.7	D2	HSS127x127x8.0			B1	W410x39
1rst floor	913,761.5	D1	HSS152x152x9.5	C1	W200x36	B2	W460x52
Spring rigidity *k* (kN/m)							
Damper	1,500,000.00						
Gap	1,500,000.00						

1.5 *2-storey building, interior bracing, 9m span (9-int-2-mtl)*

Seismic masses (kg)		Steel sections					
		Diagonals		Columns		Beams	
Roof	780,825.7	D2	HSS127x127x8.0			B1	W530x66
1rst floor	913,761.5	D1	HSS152x152x9.5	C1	W200x46	B2	W610x82

Spring rigidity *k* (kN/m)	
Damper	1,500,000.00
Gap	1,500,000.00

1.6 *4-storey building, exterior bracing, 5.625m span (6-e-4-mtl)*

Seismic masses (kg)		Steel sections					
		Diagonals		Columns		Beams	
Roof	780,825.7	D4	HSS102x102x13			B1	W360x33
3rd floor	909,357.8	D3	HSS127x127x8.0	C2	W200x36	B2	W410x39
2nd floor	909,357.8	D2	HSS127x127x9.5			B3	W410x39
1rst floor	913,761.5	D1	HSS152x152x9.5	C1	W250x73	B4	W410x39

Spring rigidity *k* (kN/m)	
Damper	1,500,000.00
Gap	1,500,000.00

1.7 *4-storey building, interior bracing, 5.625m span (6-int-4-mtl)*

Seismic masses (kg)		Steel sections					
		Diagonals		Columns		Beams	
Roof	780,825.7	D4	HSS102x102x13			B1	W410x46
3rd floor	909,357.8	D3	HSS127x127x8.0	C2	W200x52	B2	W530x66
2nd floor	909,357.8	D2	HSS127x127x9.5			B3	W530x66
1rst floor	913,761.5	D1	HSS152x152x9.5	C1	W310x97	B4	W530x66

Spring rigidity *k* (kN/m)	
Damper	1,500,000.00
Gap	1,500,000.00

1.8 *4-storey building, exterior bracing, 9m span (9-e-4-mtl)*

Seismic masses (kg)		Steel sections					
		Diagonals		Columns		Beams	
Roof	780,825.7	D4	HSS127x127x6.4			B1	W410x39
3rd floor	909,357.8	D3	HSS127x127x8.0	C2	W200x36	B2	W460x52
2nd floor	909,357.8	D2	HSS152x152x6.4			B3	W460x52
1rst floor	913,761.5	D1	HSS152x152x9.5	C1	W250x58	B4	W460x52

Spring rigidity *k* (kN/m)	
Damper	1,500,000.00
Gap	1,500,000.00

1.9 *4-storey building, interior bracing, 9m span (9-int-4-mtl)*

Seismic masses (kg)		Steel sections					
		Diagonals		Columns		Beams	
Roof	780,825.7	D4	HSS127x127x6.4			B1	W530x66
3rd floor	909,357.8	D3	HSS127x127x8.0	C2	W200x46	B2	W610x82
2nd floor	909,357.8	D2	HSS152x152x6.4			B3	W610x82
1rst floor	913,761.5	D1	HSS152x152x9.5	C1	W250x73	B4	W610x82

Spring rigidity *k* (kN/m)	
Damper	1,500,000.00
Gap	1,500,000.00

1.10 *6-storey building, exterior bracing, 5.625m span (6-e-6-mtl)*

Seismic masses (kg)		Steel sections					
		Diagonals		Columns		Beams	
Roof	780,825.7	D6	HSS102x102x9.5			B1	W360x33
5th floor	909,357.8	D5	HSS102x102x13	C3	W200x36	B2	W410x39
4th floor	909,357.8	D4	HSS102x102x13			B3	W410x39
3rd floor	909,357.8	D3	HSS127x127x6.4	C2	W200x59	B4	W410x39
2nd floor	909,357.8	D2	HSS127x127x8.0			B5	W410x39
1rst floor	913,761.5	D1	HSS152x152x8.0	C1	W250x73	B6	W410x39

Spring rigidity *k* (kN/m)	
Damper	2,000,000.00
Gap	2,000,000.00

1.11 *6-storey building, interior bracing, 5.625m span (6-int-6-mtl)*

Seismic masses (kg)		Steel sections					
		Diagonals		Columns		Beams	
Roof	780,825.7	D6	HSS102x102x9.5			B1	W410x46
5th floor	909,357.8	D5	HSS102x102x13	C3	W200x46	B2	W530x66
4th floor	909,357.8	D4	HSS102x102x13			B3	W530x66
3rd floor	909,357.8	D3	HSS127x127x6.4	C2	W200x71	B4	W530x66
2nd floor	909,357.8	D2	HSS127x127x8.0			B5	W530x66
1rst floor	913,761.5	D1	HSS152x152x8.0	C1	W250x101	B6	W530x66

Spring rigidity *k* (kN/m)	
Damper	2,000,000.00
Gap	2,000,000.00

1.12 *6-storey building, exterior bracing, 9m span (9-e-6-mtl)*

Seismic masses (kg)		Steel sections					
		Diagonals		Columns		Beams	
Roof	780,825.7	D6	HSS127x127x6.4			B1	W410x39
5th floor	909,357.8	D5	HSS127x127x6.4	C3	W200x36	B2	W460x52
4th floor	909,357.8	D4	HSS127x127x6.4			B3	W460x52
3rd floor	909,357.8	D3	HSS127x127x8.0	C2	W250x49	B4	W460x52
2nd floor	909,357.8	D2	HSS127x127x9.5			B5	W460x52
1rst floor	913,761.5	D1	HSS152x152x8.0	C1	W310x74	B6	W460x52

Spring rigidity *k* (kN/m)	
Damper	2,000,000.00
Gap	2,000,000.00

1.13 *6-storey building, interior bracing, 9m span (9-int-6-mtl)*

Seismic masses (kg)		Steel sections					
		Diagonals		Columns		Beams	
Roof	780,825.7	D6	HSS127x127x6.4			B1	W530x66
5th floor	909,357.8	D5	HSS127x127x6.4	C3	W250x49	B2	W610x82
4th floor	909,357.8	D4	HSS127x127x6.4			B3	W610x82
3rd floor	909,357.8	D3	HSS127x127x8.0	C2	W250x73	B4	W610x82
2nd floor	909,357.8	D2	HSS127x127x9.5			B5	W610x82
1rst floor	913,761.5	D1	HSS152x152x8.0	C1	W310x97	B6	W610x82

Spring rigidity *k* (kN/m)	
Damper	2,000,000.00
Gap	2,000,000.00

2. Vancouver (BC)

2.1 *2-storey building, exterior bracing, 5.625m span (6-e-2-van)*

Seismic masses (kg)		Steel sections					
		Diagonals		Columns		Beams	
Roof	737,477.1	D2	HSS152x152x9.5			B1	W310x28
1rst floor	913,761.5	D1	HSS178x178x9.5	C1	W200x46	B2	W410x39
Spring rigidity *k* (kN/m)							
Damper	1,500,000.00						
Gap	1,500,000.00						

2.2 *2-storey building, interior bracing, 5.625m span (6-int-2-van)*

Seismic masses (kg)		Steel sections					
		Diagonals		Columns		Beams	
Roof	737,477.1	D2	HSS152x152x9.5			B1	W410x39
1rst floor	913,761.5	D1	HSS178x178x9.5	C1	W200x46	B2	W530x66
Spring rigidity *k* (kN/m)							
Damper	1,500,000.00						
Gap	1,500,000.00						

2.3 *2-storey building, exterior bracing, 9m span (9-e-2-van)*

Seismic masses (kg)		Steel sections					
		Diagonals		Columns		Beams	
Roof	737,477.1	D2	HSS152x152x8.0			B1	W410x39
1rst floor	913,761.5	D1	HSS178x178x9.5	C1	W200x42	B2	W460x52
Spring rigidity *k* (kN/m)							
Damper	1,500,000.00						
Gap	1,500,000.00						

2.4 *2-storey building, interior bracing, 9m span (9-int-2-van)*

Seismic masses (kg)		Steel sections					
		Diagonals		Columns		Beams	
Roof	737,477.1	D2	HSS152x152x8.0			B1	W460x60
1rst floor	913,761.5	D1	HSS178x178x9.5	C1	W200x46	B2	W610x82
Spring rigidity *k* (kN/m)							
Damper	1,500,000.00						
Gap	1,500,000.00						

2.5 *4-storey building, exterior bracing, 5.625m span (6-e-4-van)*

Seismic masses (kg)		Steel sections					
		Diagonals		Columns		Beams	
Roof	737,477.1	D4	HSS152x152x6.4			B1	W310x28
3rd floor	909,357.8	D3	HSS152x152x9.5	C2	W200x46	B2	W410x39
2nd floor	909,357.8	D2	HSS152x152x13			B3	W410x39
1rst floor	913,761.5	D1	HSS178x178x13	C1	W310x97	B4	W410x39

Spring rigidity *k* (kN/m)	
Damper	1,500,000.00
Gap	1,500,000.00

2.6 *4-storey building, interior bracing, 5.625m span (6-int-4-van)*

Seismic masses (kg)		Steel sections					
		Diagonals		Columns		Beams	
Roof	737,477.1	D4	HSS152x152x6.4			B1	W410x39
3rd floor	909,357.8	D3	HSS152x152x9.5	C2	W200x52	B2	W530x66
2nd floor	909,357.8	D2	HSS152x152x13			B3	W530x66
1rst floor	913,761.5	D1	HSS178x178x13	C1	W310x97	B4	W530x66

Spring rigidity *k* (kN/m)	
Damper	1,500,000.00
Gap	1,500,000.00

2.7 *4-storey building, exterior bracing, 9m span (9-e-4-van)*

Seismic masses (kg)		Steel sections					
		Diagonals		Columns		Beams	
Roof	737,477.1	D4	HSS152x152x8.0			B1	W410x39
3rd floor	909,357.8	D3	HSS152x152x13	C2	W200x42	B2	W460x52
2nd floor	909,357.8	D2	HSS178x178x9.5			B3	W460x52
1rst floor	913,761.5	D1	HSS203x203x9.5	C1	W250x73	B4	W460x52

Spring rigidity *k* (kN/m)	
Damper	1,500,000.00
Gap	1,500,000.00

2.8 *4-storey building, interior bracing, 9m span (9-int-4-van)*

Seismic masses (kg)		Steel sections					
		Diagonals		Columns		Beams	
Roof	737,477.1	D4	HSS152x152x8.0			B1	W460x60
3rd floor	909,357.8	D3	HSS152x152x13	C2	W200x46	B2	W610x82
2nd floor	909,357.8	D2	HSS178x178x9.5			B3	W610x82
1rst floor	913,761.5	D1	HSS203x203x9.5	C1	W250x80	B4	W610x82

Spring rigidity *k* (kN/m)	
Damper	1,500,000.00
Gap	1,500,000.00

2.9 *6-storey building, exterior bracing, 5.625m span (6-e-6-van)*

Seismic masses (kg)		Steel sections					
		Diagonals		Columns		Beams	
Roof	737,477.1	D6	HSS127x127x9.5			B1	W310x28
5th floor	909,357.8	D5	HSS152x152x8.0	C3	W250x49	B2	W410x39
4th floor	909,357.8	D4	HSS152x152x9.5			B3	W410x39
3rd floor	909,357.8	D3	HSS152x152x13	C2	W310x86	B4	W410x39
2nd floor	909,357.8	D2	HSS178x178x9.5			B5	W410x39
1rst floor	913,761.5	D1	HSS178x178x13	C1	W310x129	B6	W410x39

Spring rigidity *k* (kN/m)	
Damper	2,000,000.00
Gap	2,000,000.00

2.10 *6-storey building, interior bracing, 5.625m span (6-int-6-van)*

Seismic masses (kg)		Steel sections					
		Diagonals		Columns		Beams	
Roof	737,477.1	D6	HSS127x127x9.5			B1	W410x39
5th floor	909,357.8	D5	HSS152x152x8.0	C3	W250x49	B2	W530x66
4th floor	909,357.8	D4	HSS152x152x9.5			B3	W530x66
3rd floor	909,357.8	D3	HSS152x152x13	C2	W310x97	B4	W530x66
2nd floor	909,357.8	D2	HSS178x178x9.5			B5	W530x66
1rst floor	913,761.5	D1	HSS178x178x13	C1	W310x158	B6	W530x66

Spring rigidity *k* (kN/m)	
Damper	2,000,000.00
Gap	2,000,000.00

2.11 *6-storey building, exterior bracing, 9m span (9-e-6-van)*

Seismic masses (kg)		Steel sections					
		Diagonals		Columns		Beams	
Roof	737,477.1	D6	HSS127x127x9.5			B1	W410x39
5th floor	909,357.8	D5	HSS152x152x9.5	C3	W250x49	B2	W460x52
4th floor	909,357.8	D4	HSS152x152x13			B3	W460x52
3rd floor	909,357.8	D3	HSS178x178x8.0	C2	W310x74	B4	W460x52
2nd floor	909,357.8	D2	HSS178x178x9.5			B5	W460x52
1rst floor	913,761.5	D1	HSS178x178.13	C1	W310x97	B6	W460x52

Spring rigidity *k* (kN/m)	
Damper	2,000,000.00
Gap	2,000,000.00

2.12 *6-storey building, interior bracing, 9m span (9-int-6-van)*

Seismic masses (kg)		Steel sections					
		Diagonals		Columns		Beams	
Roof	737,477.1	D6	HSS127x127x9.5			B1	W460x60
5th floor	909,357.8	D5	HSS152x152x9.5	C3	W250x49	B2	W610x82
4th floor	909,357.8	D4	HSS152x152x13			B3	W610x82
3rd floor	909,357.8	D3	HSS178x178x8.0	C2	W250x73	B4	W610x82
2nd floor	909,357.8	D2	HSS178x178x9.5			B5	W610x82
1rst floor	913,761.5	D1	HSS178x178.13	C1	W310x118	B6	W610x82

Spring rigidity *k* (kN/m)	
Damper	2,000,000.00
Gap	2,000,000.00

3. Los Angeles (CA)

3.1 *2-storey building, exterior bracing, 5.625m span (6-e-2-LA)*

Seismic masses (kg)		Steel sections					
		Diagonals		Columns		Beams	
Roof	661,100.9	D2	HSS178x178x6.4			B1	W310x24
1rst floor	913,761.5	D1	HSS203x203x13	C1	W250x58	B2	W410x39

Spring rigidity *k* (kN/m)	
Damper	1,500,000.00
Gap	1,500,000.00

3.2 *2-storey building, interior bracing, 5.625m span (6-int-2-LA)*

Seismic masses (kg)		Steel sections					
		Diagonals		Columns		Beams	
Roof	661,100.9	D2	HSS178x178x6.4			B1	W410x39
1rst floor	913,761.5	D1	HSS203x203x13	C1	W250x67	B2	W530x66

Spring rigidity *k* (kN/m)	
Damper	1,500,000.00
Gap	1,500,000.00

3.3 *2-storey building, exterior bracing, 9m span (9-e-2-LA)*

Seismic masses (kg)		Steel sections					
		Diagonals		Columns		Beams	
Roof	661,100.9	D2	HSS152x152x13			B1	W360x33
1rst floor	913,761.5	D1	HSS203x203x9.5	C1	W200x46	B2	W460x52

Spring rigidity *k* (kN/m)	
Damper	1,500,000.00
Gap	1,500,000.00

3.4 *2-storey building, interior bracing, 9m span (9-int-2-LA)*

Seismic masses (kg)		Steel sections					
		Diagonals		Columns		Beams	
Roof	661,100.9	D2	HSS152x152x13			B1	W460x52
1rst floor	913,761.5	D1	HSS203x203x9.5	C1	W200x52	B2	W610x82

Spring rigidity *k* (kN/m)	
Damper	1,500,000.00
Gap	1,500,000.00

3.5 *4-storey building, exterior bracing, 5.625m span (6-e-4-LA)*

Seismic masses (kg)		Steel sections					
		Diagonals		Columns		Beams	
Roof	661,100.9	D4	HSS152x152x9.5			B1	W310x24
3rd floor	909,357.8	D3	HSS203x203x8.0	C2	W250x49	B2	W410x39
2nd floor	909,357.8	D2	HSS203x203x13			B3	W410x39
1rst floor	913,761.5	D1	HSS254x254x9.5	C1	W310x129	B4	W410x39

Spring rigidity *k* (kN/m)	
Damper	1,500,000.00
Gap	1,500,000.00

3.6 *4-storey building, interior bracing, 5.625m span (6-int-4-LA)*

Seismic masses (kg)		Steel sections					
		Diagonals		Columns		Beams	
Roof	661,100.9	D4	HSS152x152x9.5			B1	W410x39
3rd floor	909,357.8	D3	HSS203x203x8.0	C2	W250x58	B2	W530x66
2nd floor	909,357.8	D2	HSS203x203x13			B3	W530x66
1rst floor	913,761.5	D1	HSS254x254x9.5	C1	W310x143	B4	W530x66

Spring rigidity *k* (kN/m)	
Damper	1,500,000.00
Gap	1,500,000.00

3.7 *4-storey building, exterior bracing, 9m span (9-e-4-LA)*

Seismic masses (kg)		Steel sections					
		Diagonals		Columns		Beams	
Roof	661,100.9	D4	HSS152x152x13			B1	W360x33
3rd floor	909,357.8	D3	HSS203x203x9.5	C2	W250x49	B2	W460x52
2nd floor	909,357.8	D2	HSS203x203x13			B3	W460x52
1rst floor	913,761.5	D1	HSS254x254x9.5	C1	W310x107	B4	W460x52

Spring rigidity *k* (kN/m)	
Damper	1,500,000.00
Gap	1,500,000.00

3.8 *4-storey building, interior bracing, 9m span (9-int-4-LA)*

Seismic masses (kg)		Steel sections					
		Diagonals		Columns		Beams	
Roof	661,100.9	D4	HSS152x152x13			B1	W460x52
3rd floor	909,357.8	D3	HSS203x203x9.5	C2	W250x49	B2	W610x82
2nd floor	909,357.8	D2	HSS203x203x13			B3	W610x82
1rst floor	913,761.5	D1	HSS254x254x9.5	C1	W310x129	B4	W610x82

Spring rigidity *k* (kN/m)	
Damper	1,500,000.00
Gap	1,500,000.00

3.9 *6-storey building, exterior bracing, 5.625m span (6-e-6-LA)*

Seismic masses (kg)		Steel sections					
		Diagonals		Columns		Beams	
Roof	661,100.9	D6	HSS152x152x9.5			B1	W310x24
5th floor	909,357.8	D5	HSS178x178x9.5	C3	W250x49	B2	W460x60
4th floor	909,357.8	D4	HSS203x203x8.0			B3	W460x60
3rd floor	909,357.8	D3	HSS203x203x9.5	C2	W310x107	B4	W460x60
2nd floor	909,357.8	D2	HSS203x203x13			B5	W460x60
1rst floor	913,761.5	D1	HSS254x254x13	C1	W310x202	B6	W460x60

Spring rigidity *k* (kN/m)	
Damper	2,000,000.00
Gap	2,000,000.00

3.10 *6-storey building, interior bracing, 5.625m span (6-int-6-LA)*

Seismic masses (kg)		Steel sections					
		Diagonals		Columns		Beams	
Roof	661,100.9	D6	HSS152x152x9.5			B1	W410x39
5th floor	909,357.8	D5	HSS178x178x9.5	C3	W250x58	B2	W530x74
4th floor	909,357.8	D4	HSS203x203x8.0			B3	W530x74
3rd floor	909,357.8	D3	HSS203x203x9.5	C2	W310x129	B4	W530x74
2nd floor	909,357.8	D2	HSS203x203x13			B5	W530x74
1rst floor	913,761.5	D1	HSS254x254x13	C1	W310x226	B6	W530x74

Spring rigidity *k* (kN/m)	
Damper	2,000,000.00
Gap	2,000,000.00

3.11 *6-storey building, exterior bracing, 9m span (9-e-6-LA)*

Seismic masses (kg)		Steel sections					
		Diagonals		Columns		Beams	
Roof	661,100.9	D6	HSS152x152x8.0			B1	W360x33
5th floor	909,357.8	D5	HSS178x178x9.5	C3	W200x42	B2	W250x80
4th floor	909,357.8	D4	HSS178x178x13			B3	W250x80
3rd floor	909,357.8	D3	HSS203x203x13	C2	W250x89	B4	W250x80
2nd floor	909,357.8	D2	HSS203x203x13			B5	W250x80
1rst floor	913,761.5	D1	HSS254x254x9.5	C1	W310x158	B6	W250x80

Spring rigidity *k* (kN/m)	
Damper	2,000,000.00
Gap	2,000,000.00

3.12 *6-storey building, interior bracing, 9m span (9-int-6-LA)*

Seismic masses (kg)		Steel sections					
		Diagonals		Columns		Beams	
Roof	661,100.9	D6	HSS152x152x8.0			B1	W460x52
5th floor	909,357.8	D5	HSS178x178x9.5	C3	W250x49	B2	W610x82
4th floor	909,357.8	D4	HSS178x178x13			B3	W610x82
3rd floor	909,357.8	D3	HSS203x203x13	C2	W310x97	B4	W610x82
2nd floor	909,357.8	D2	HSS203x203x13			B5	W610x82
1rst floor	913,761.5	D1	HSS254x254x9.5	C1	W310x202	B6	W610x82

Spring rigidity *k* (kN/m)	
Damper	2,000,000.00
Gap	2,000,000.00

APPENDIX G

CONSTRUCTION BLUEPRINTS OF THE SHAKE TABLE TESTING SETUP

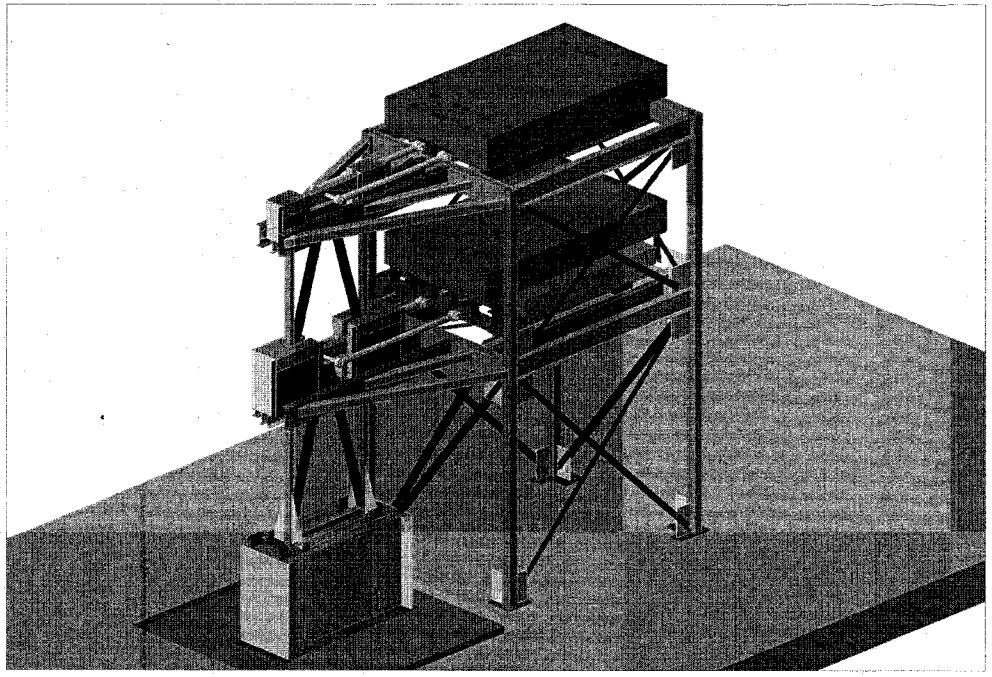

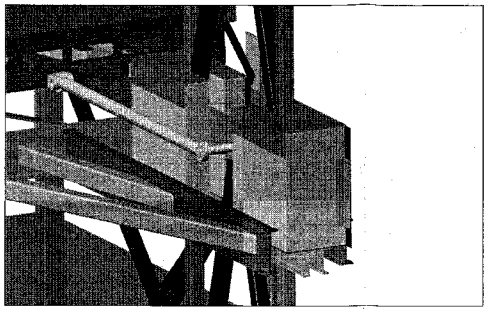

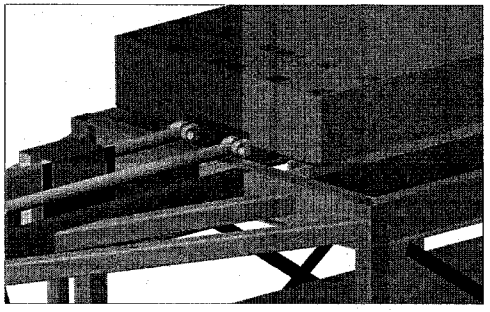

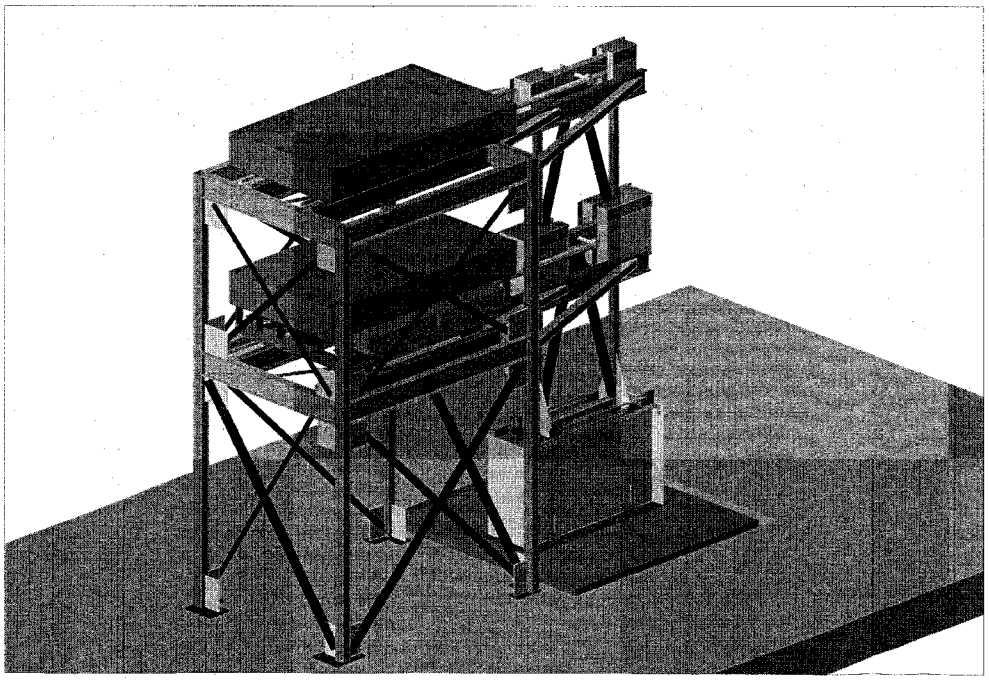

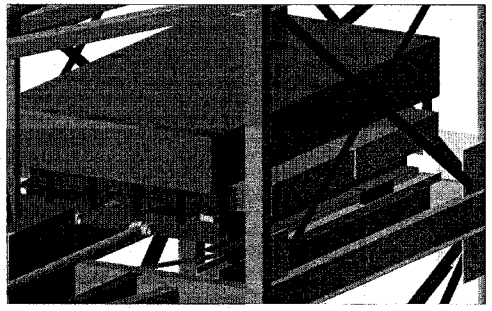

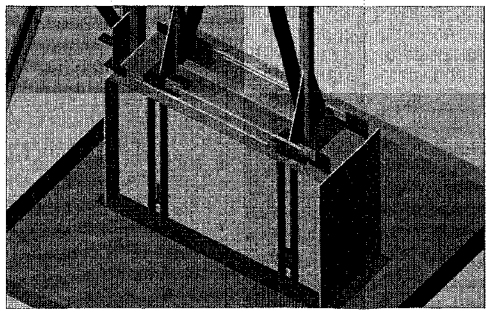

No.	Date	REVISIONS ET OMISSIONS	DO	JPP	SR	RT
1	23 MARS 2007	POUR INFORMATION	DO	JPP	SR	RT

Client:

Projet remplace:

BES inc.
BUREAU D'ETUDES SPECIALISEES Inc.
CONSULTANTS EN STRUCTURE
336 ST-ANTOINE EST
BUREAU 402
MONTREAL, QUEBEC, H2Y 1A3
Tel.: 514-393-1500
Fax.: 514-393-1520

Division:

Projet:

PROJET DE MAÎTRISE
TESTS SUR LA TABLE VIBRANTE

Nom du dessin:

ISOMETRIES
ET
AUTRES VUES

Dessin:	Conception:
D. OUELLET	L.-P. POIRIER
Verification:	Approbation:
S. RIVEST	R. TREMBLAY
Date:	Echelle:
JANVIER 2007	INDIQUEE
Projet no.:	Dessin no.: / Rev.:
05-051-01	S4 / 0

Ref. Cad.:\DESSINS \ 2005 \ 05-051-01 \ PLAN 05510104.dwg

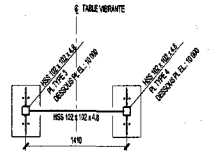

VUE EN PLAN - BASE DU CADRE D'ESSAI
1 : 30

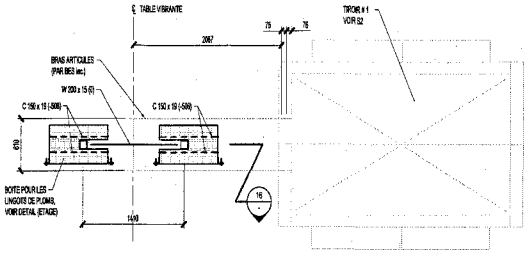

VUE EN PLAN - ETAGE - CADRE D'ESSAI
1 : 30
DESSUS ACIER EL.: 12 259

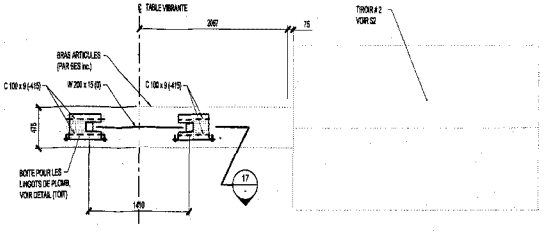

VUE EN PLAN - TOIT - CADRE D'ESSAI
1 : 30
DESSUS ACIER EL.: 14 109

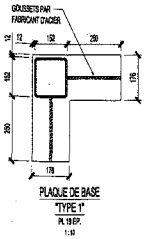

PLAQUE DE BASE
"TYPE 1"
PL 19 EP.
1 : 10

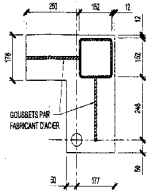

PLAQUE DE BASE
"TYPE 2"
PL 19 EP.
1 - BOULON 36 Ø
(PAR POLYTECHNIQUE)
1 : 10

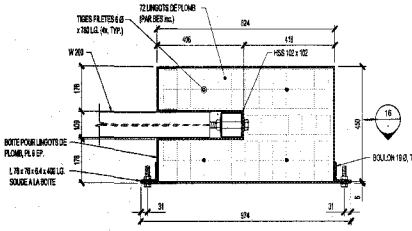

DETAIL - BOITE POUR
LINGOTS DE PLOMB
(ETAGE)
1 : 10

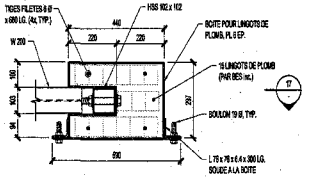

DETAIL - BOITE POUR
LINGOTS DE PLOMB
(TOIT)
1 : 10

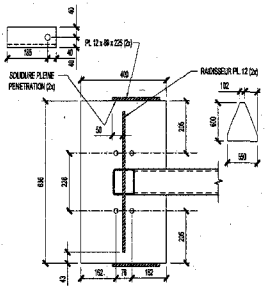

PLAQUE DE BASE
"TYPE 3"
PL 19 EP.
4 - BOULON 19 Ø
1 : 10

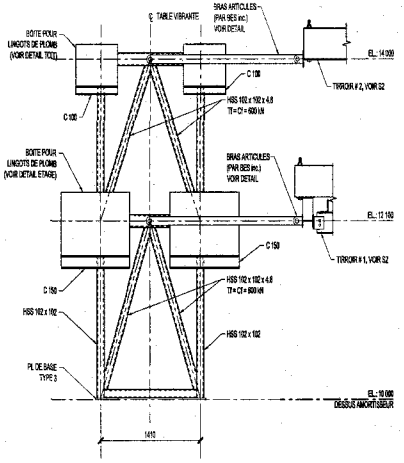

ELEVATION D
1 : 30

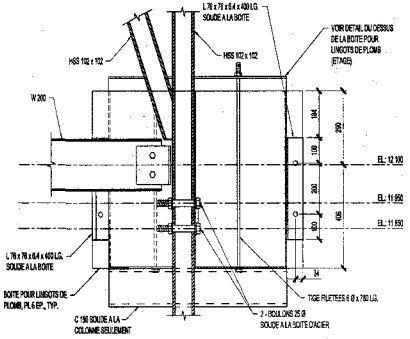

COUPE 16
1 : 10

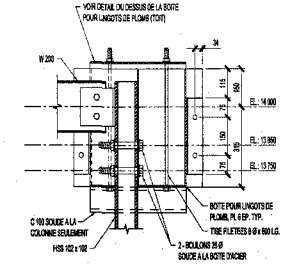

COUPE 17
1 : 10

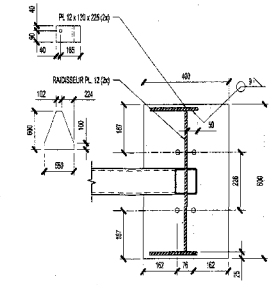

PLAQUE DE BASE
"TYPE 4"
PL 19 EP.
4 - BOULON 19 Ø
1 : 10

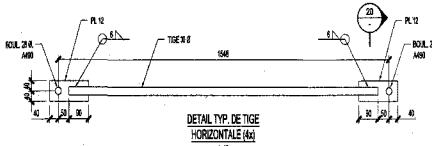

DETAIL TYP. DE TIGE
HORIZONTALE (4x)
1 : 10

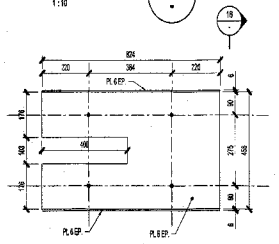

DETAIL - DESSUS BOITE
POUR LINGOTS DE PLOMB
(ETAGE)
1 : 10

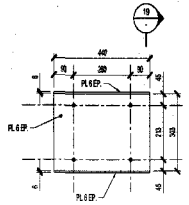

DETAIL - DESSUS BOITE
POUR LINGOTS DE PLOMB
(TOIT)
1 : 10

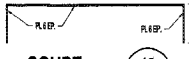

COUPE 18
1 : 10

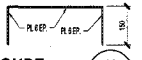

COUPE 19
1 : 10

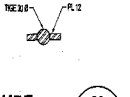

COUPE 20
1 : 5

L'ENTREPRENEUR GÉNÉRAL DOIT VÉRIFIER TOUTES LES DIMENSIONS ET CONDITIONS SUR LE SITE ET AVISER L'INGÉNIEUR DE TOUTE ERREUR OU OMISSION AVANT LE DÉBUT DES TRAVAUX. AUCUNE DIMENSION NE DOIT ÊTRE MESURÉE À L'ÉCHELLE SUR LES PLANS. TOUS LES PLANS DEMEURENT LA PROPRIÉTÉ DE L'INGÉNIEUR.

No.	Date	REVISIONS ET EMISSIONS	PAR	CO	VER.	APP.
3	27 FÉV. 2007	DIRECTIVE No. 2	DO	LPP	SR	RT
2	14 FÉV. 2007	DIRECTIVE No. 1	DO	LPP	SR	RT
1	12 FÉV. 2007	EMIS POUR CONSTRUCTION	DO	LPP	SR	RT
0	01 JUIN 2007	EMIS POUR INFORMATION	DO	LPP	SR	RT

Client:

Experts conseils

BES INC.
BUREAU D'ETUDES SPECIALISEES inc.
CONSULTANTS EN STRUCTURE
330 ST-ANTOINE EST
BUREAU 402
MONTRÉAL, QUÉBEC. H2Y 1A3
Tél.: 514-393-1500
Fax.: 514-393-1500

Entrepreneur:

Projet:

PROJET DE MAÎTRISE
TESTS SUR LA TABLE VIBRANTE

Nom de dessin:

CADRE D'ESSAI

Dessin:	D. OUELLET	Conception:	L.-P. POIRIER
Vérification:	S. RIVEST	Approbation:	R. TREMBLAY
Date:	JANVIER 2007	Échelle:	INDIQUÉE
Projet no.:	05-051-01	Dessin no.:	S3
Rev.:	0		

Ref. Cad.:\DESSINS\ 2005 \ 05-051-01 \ PLAN 50510101.dwg

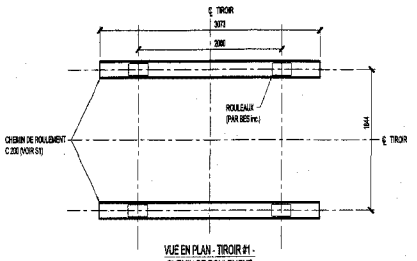

VUE EN PLAN - TIROIR #1 -
CHEMIN DE ROULEMENT

1 : 10

DESSOUS ROULEAUX EL. : 11 818

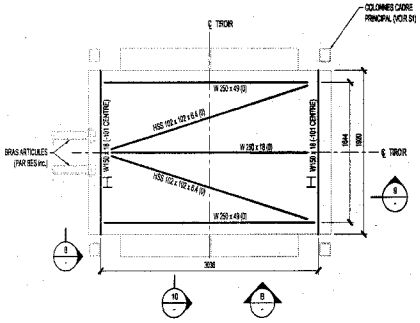

VUE EN PLAN - TIROIR #1

1 : 10

DESSUS ACIER EL. : 12 201

NOTE : ASSEMBLAGES SOUDES

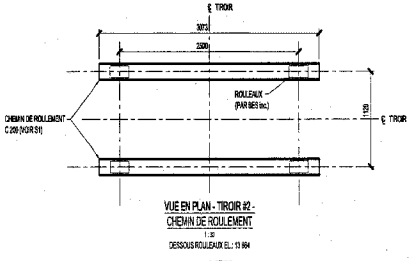

VUE EN PLAN - TIROIR #2 -
CHEMIN DE ROULEMENT

1 : 10

DESSOUS ROULEAUX EL. : 13 884

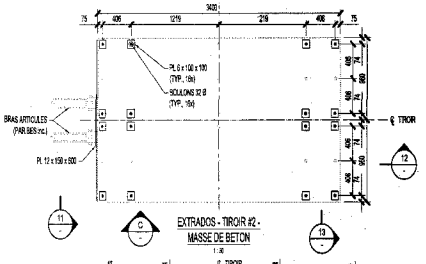

EXTRADOS - TIROIR #2 -
MASSE DE BETON

1 : 10

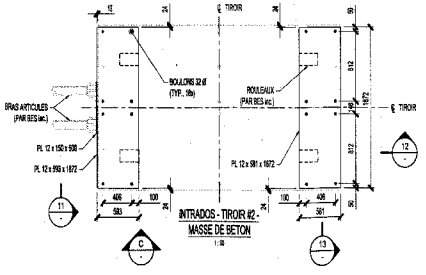

INTRADOS - TIROIR #2 -
MASSE DE BETON

1 : 10

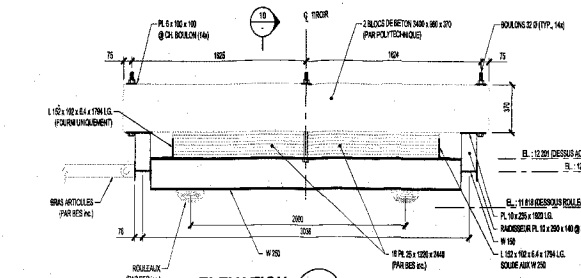

ELEVATION B

1 : 20

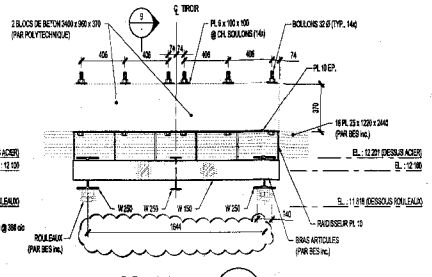

COUPE 8

1 : 20

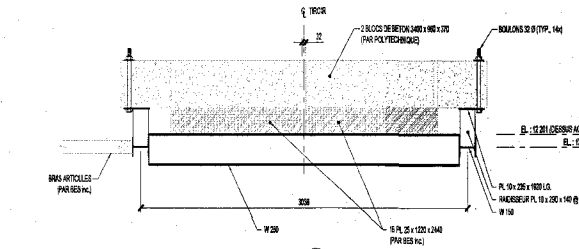

COUPE 9

1 : 20

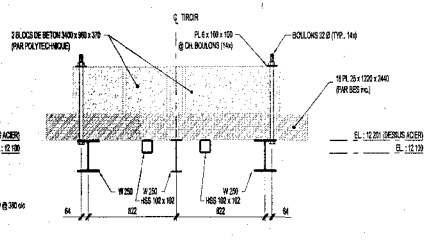

COUPE 10

1 : 20

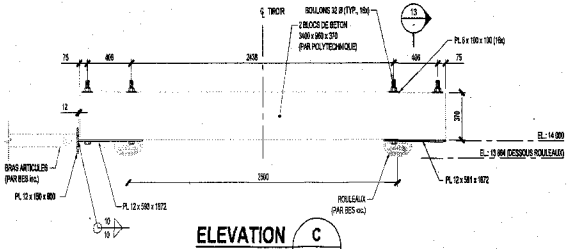

ELEVATION C

1 : 20

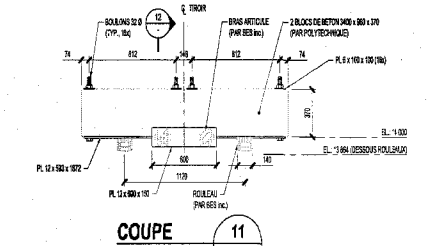

COUPE 11

1 : 20

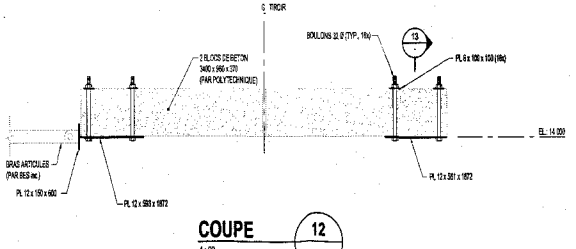

COUPE 12

1 : 20

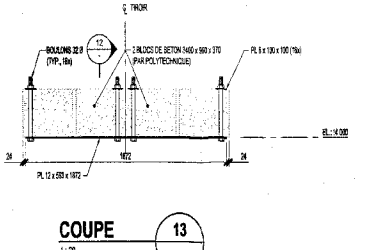

COUPE 13

1 : 20

No.	Date	REVISIONS ET EMISSIONS	PAR	CO	VER.	APP.
3	27 FEV. 2007	DIRECTIVE No. 2	DO	LPP	SR	RT
1	15 FEV. 2007	REVISION No.1	DO	LPP	SR	RT
0	31 JAN. 2007	EMIS POUR CONSTRUCTION	DO	LPP	SR	RT

Client:

Experts-conseils:

BES INC.
BUREAU D'ETUDES SPECIALISEES inc.
CONSULTANTS EN STRUCTURE
338 ST-ANTOINE EST
BUREAU 402
MONTREAL, QUEBEC, H2Y 1A3
Tel.: 514-393-1500
Fax.: 514-393-1550

Sous-sol:

Projet:

PROJET DE MAÎTRISE
TESTS SUR LA TABLE VIBRANTE

Nom du dessin:

TIROIRS POUR LES POIDS

Dessin: D. OUELLET	Conception: L.-P. POIRIER
Vérification: S. RIVEST	Approbation: R. TREMBLAY
Date: JANVIER 2007	Échelle: INDIQUEE

Projet no.:	Dessin no.:	Rév.:
05-051-01	S2	0

Ref. Cad.:\DESSINS \ 2005 \ 05-051-01 \ PLAN 50510101.dwg

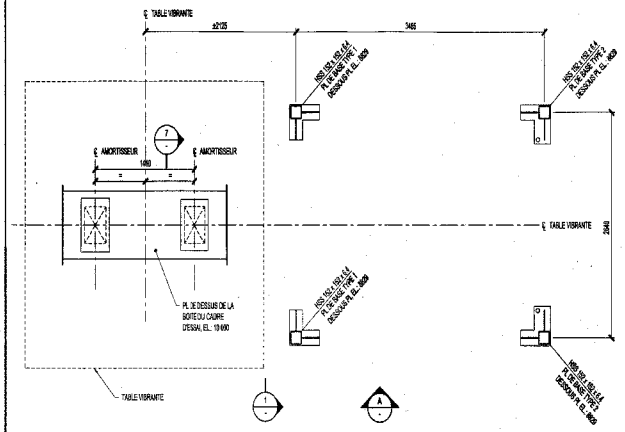

VUE EN PLAN - PLAQUE DE BASE
1 : 30

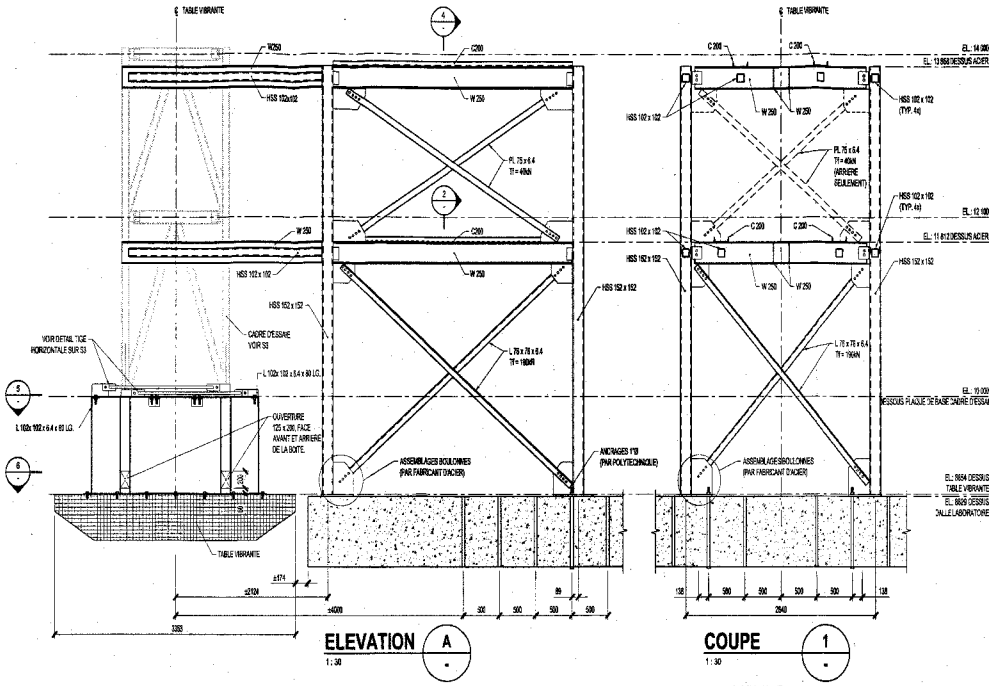

ELEVATION A
1 : 30

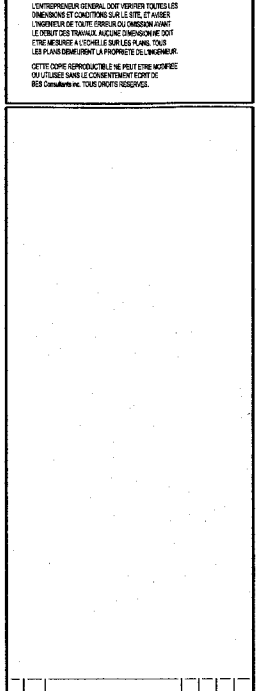

COUPE 1
1 : 30

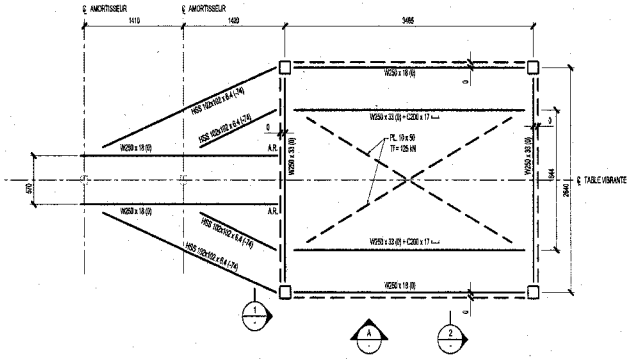

VUE EN PLAN - 1er ETAGE
1 : 30
DESSUS ACIER EL. +11 812

LEGENDE :
— CONTREVENTEMENT VERT. VOIR ELEVATION A ET COUPE 1
A.R. ASSEMBLAGE RIGIDE

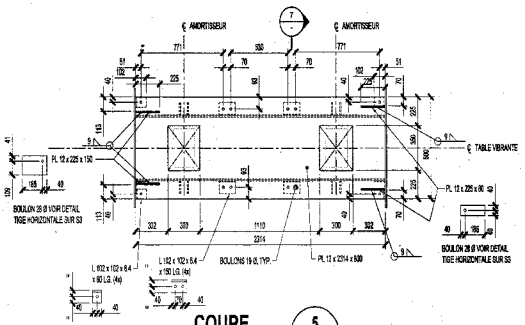

COUPE 5
1 : 20

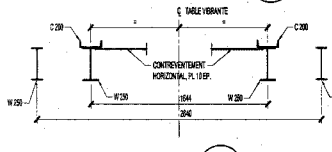

COUPE 2
1 : 20

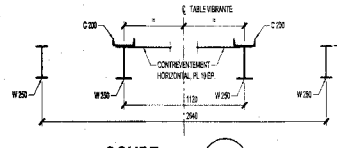

COUPE 4
1 : 20

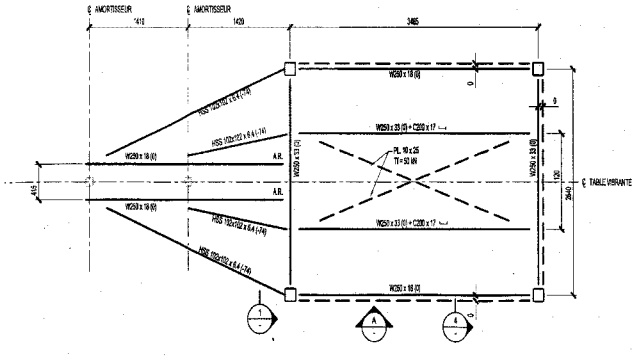

VUE EN PLAN - 2e ETAGE
1 : 30
DESSUS ACIER EL. + 13 838

LEGENDE :
— CONTREVENTEMENT VERT. VOIR ELEVATION A ET COUPE 1
A.R. ASSEMBLAGE RIGIDE

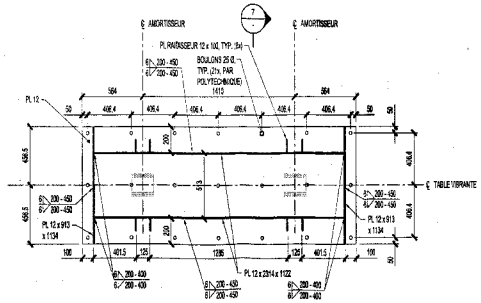

COUPE 6
1 : 20

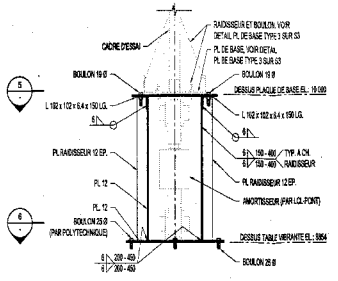

COUPE 7
1 : 20

No.	Date	REVISIONS ET EMISSIONS	PAR	CO	VER.	APP.
3	27 FEV 2007	DIRECTIVE No. 2	DO	LPP	SR	RT
1	12 FEV 2007	EMIS POUR CONSTRUCTION	DO	LPP	SR	RT
0	25 JAN 2007	EMIS POUR INFORMATION	DO	LPP	SR	RT

Client:

Experts conseils:

BES INC.
BUREAU D'ETUDES SPECIALISEES inc.
CONSULTANTS EN STRUCTURE
336 ST-ANTOINE EST
BUREAU 402
MONTREAL, QUEBEC, H2Y 1A3
Tél.: 514-393-1500
Fax.: 514-393-1500

Entrepreneur:

Projet:
PROJET DE MAÎTRISE
TESTS SUR LA TABLE VIBRANTE

Nom du dessin:
CADRE PRINCIPAL

Dessiné: D. OUELLET	Conception: L.-P. POIRIER
Vérifié par: S. RIVEST	Approbation: R. TREMBLAY
Date: JAN 2007	Échelle: INDIQUEE

Projet no.: 05-051-01
Dessin no.: S1
Rev.: 0

Ref. Cad.:\DESSINS\2005\05-051-01\PLAN 5051101.dwg

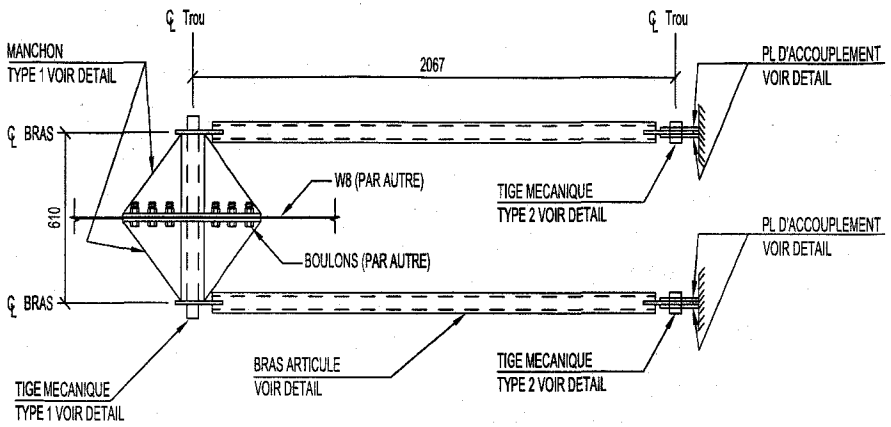

ASSEMBLAGE 1

1:20

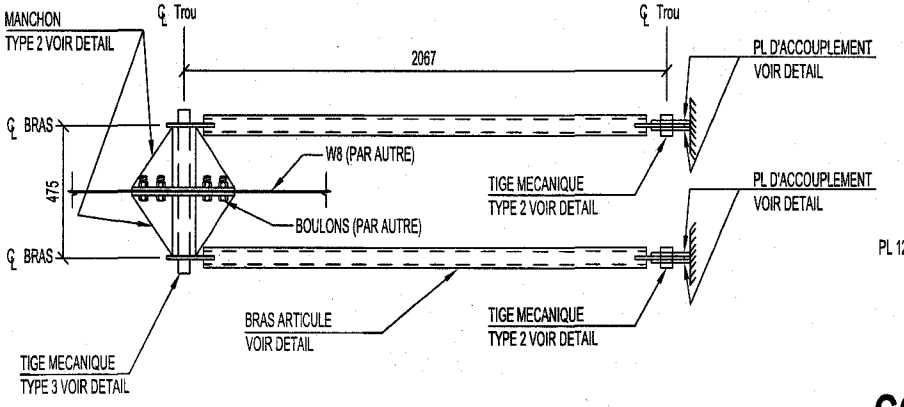

ASSEMBLAGE 2

1:20

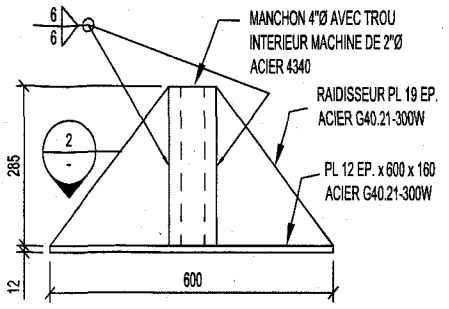

DETAIL MANCHON TYPE 1 (2x)

1:10

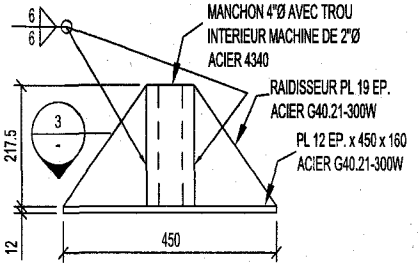

DETAIL MANCHON TYPE 2 (2x)

1:10

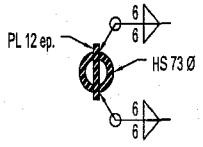

COUPE 1

1 : 10

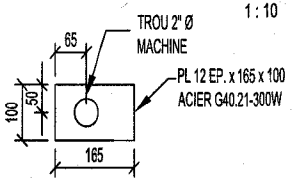

DETAIL PLAQUE D'ACCOUPLEMENT (8x)

1:10

(MATERIEL LIBRE)

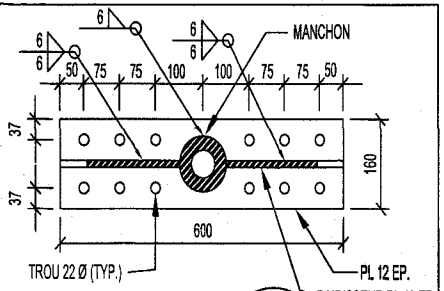

COUPE 2

1 : 10

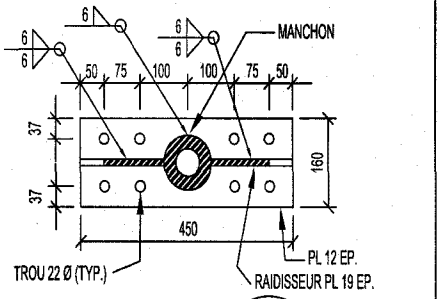

COUPE 3

1 : 10

Experts conseils
BES INC.
BUREAU D'ETUDES SPECIALISEES INC.
CONSULTANTS EN STRUCTURE
338 ST-ANTOINE EST BUREAU 400
MONTREAL, QUEBEC, H2Y 1A3
Tel.: 514-393-1500
Fax.: 514-393-1550

Projet:

PROJET DE MAÎTRISE
TESTS SUR LA TABLE VIBRANTE

Nom du dessin:

ASSEMBLAGE DES BRAS ARTICULES

L.-P. POIRIER, ING.

Projet no.: **05-051-01**

Date: **MARS 2007**

Dessin No: **S1**

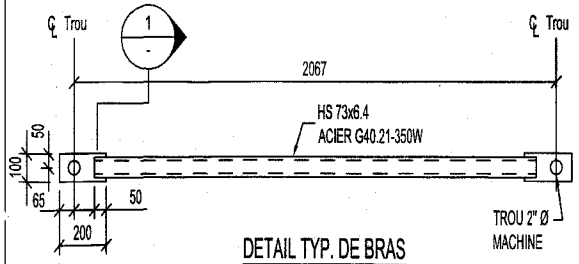

DETAIL TYP. DE BRAS ARTICULE (4x)

1:20

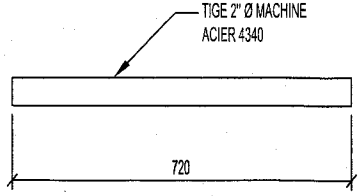

DETAIL TYPE 1 TIGE MECANIQUE (1x)

1:10

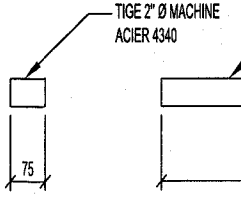

DETAIL TYPE 2 TIGE MECANIQUE (4x)

1:10

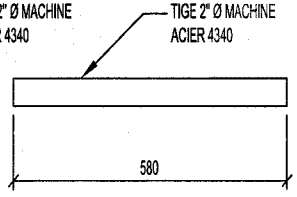

DETAIL TYPE 3 TIGE MECANIQUE (1x)

1:10

APPENDIX H

FRAME MEMBER DEFINITION OF THE LABORATORY FINITE ELEMENT MODEL USED TO EVALUATE THE LAWS OF SIMILITUDE

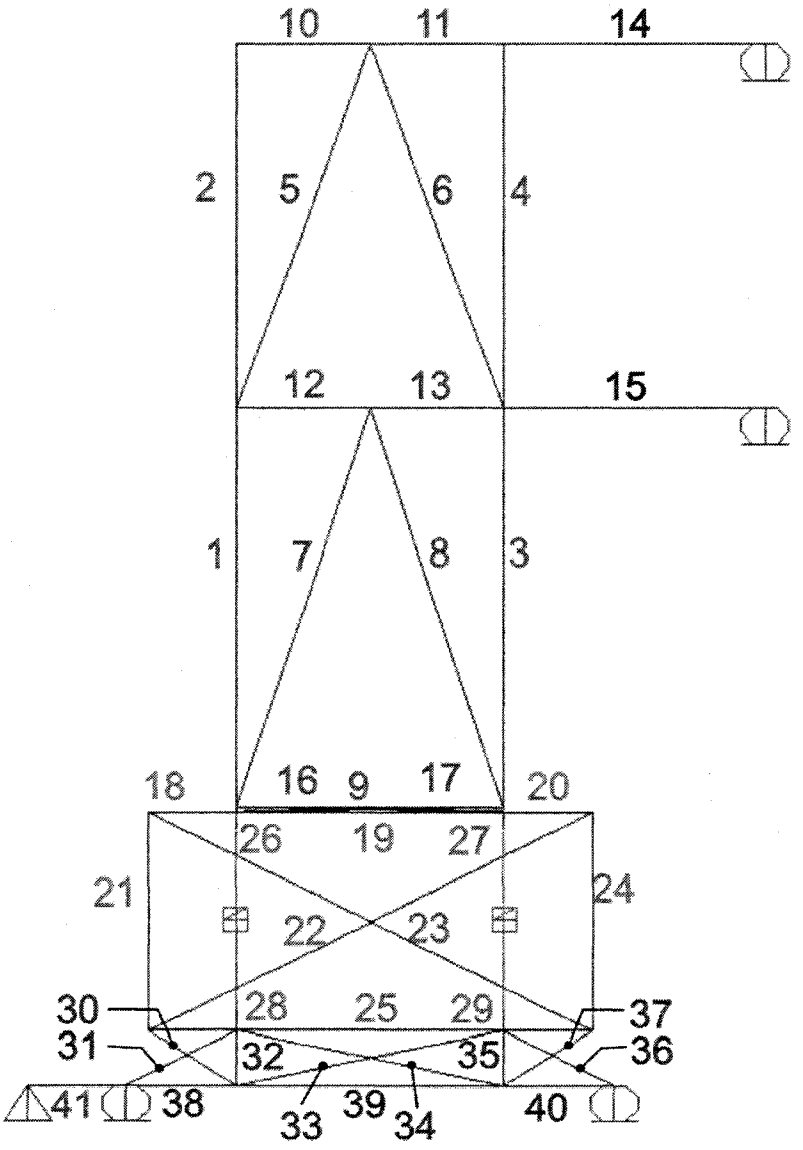

Figure H.1: Laboratory test specimen – Frame labels

Table H.1: Laboratory test specimen – Frame element properties

Frame Label	Section	Material	Length m	Area mm^2	Inertia xx mm^4	Inertia yy mm^4	Modification factor - mass
1	HSS102x102x4.8	Steel	2.100	1787	2.74E+06	2.74E+06	1.0
2	HSS102x102x4.8	Steel	1.900	1787	2.74E+06	2.74E+06	1.0
3	HSS102x102x4.8	Steel	2.100	1787	2.74E+06	2.74E+06	1.0
4	HSS102x102x4.8	Steel	1.900	1787	2.74E+06	2.74E+06	1.0
5	HSS102x102x4.8	Steel	2.027	1787	2.74E+06	2.74E+06	1.0
6	HSS102x102x4.8	Steel	2.027	1787	2.74E+06	2.74E+06	1.0
7	HSS102x102x4.8	Steel	2.215	1787	2.74E+06	2.74E+06	1.0
8	HSS102x102x4.8	Steel	2.215	1787	2.74E+06	2.74E+06	1.0
9	HSS102x102x4.8	Steel	1.410	1787	2.74E+06	2.74E+06	1.0
10	W200x15	Steel	0.705	1910	1.30E+07	8.70E+05	1.0
11	W200x15	Steel	0.705	1910	1.30E+07	8.70E+05	1.0
12	W200x15	Steel	0.705	1910	1.30E+07	8.70E+05	1.0
13	W200x15	Steel	0.705	1910	1.30E+07	8.70E+05	1.0
14	2 x HSS73x6.4	Steel	2.067	2660	1.49E+06	1.49E+06	1.0
15	2 x HSS73x6.4	Steel	2.067	2660	1.49E+06	1.49E+06	1.0
16	30mmØ rods	Steel	1.636	1414	7.95E+04	7.95E+04	1.0
17	30mmØ rods	Steel	1.676	1414	7.95E+04	7.95E+04	1.0
18	Box (rigid)	Steel	0.238	1.00E+08	8.33E+12	8.33E+12	1.0E-08
19	Box (rigid)	Steel	1.902	1.00E+08	8.33E+12	8.33E+12	1.0E-08
20	Box (rigid)	Steel	0.198	1.00E+08	8.33E+12	8.33E+12	1.0E-08
21	Box (rigid)	Steel	1.121	1.00E+08	8.33E+12	8.33E+12	1.0E-08
22	Box (rigid)	Steel	2.121	1.00E+08	8.33E+12	8.33E+12	1.0E-08
23	Box (rigid)	Steel	3.121	1.00E+08	8.33E+12	8.33E+12	1.0E-08
24	Box (rigid)	Steel	1.121	1.00E+08	8.33E+12	8.33E+12	1.0E-08
25	Box (rigid)	Steel	2.338	1.00E+08	8.33E+12	8.33E+12	1.0E-08
26	Box (rigid)	Steel	0.120	1.00E+08	8.33E+12	8.33E+12	1.0E-08
27	Box (rigid)	Steel	0.120	1.00E+08	8.33E+12	8.33E+12	1.0E-08
28	Box (rigid)	Steel	0.120	1.00E+08	8.33E+12	8.33E+12	1.0E-08
29	Box (rigid)	Steel	0.120	1.00E+08	8.33E+12	8.33E+12	1.0E-08
30	Table (rigid)	Steel	0.553	1.00E+08	8.33E+12	8.33E+12	1.0E-08
31	Table (rigid)	Steel	0.652	1.00E+08	8.33E+12	8.33E+12	1.0E-08
32	Table (rigid)	Steel	0.300	1.00E+08	8.33E+12	8.33E+12	1.0E-08
33	Table (rigid)	Steel	1.442	1.00E+08	8.33E+12	8.33E+12	1.0E-08
34	Table (rigid)	Steel	1.442	1.00E+08	8.33E+12	8.33E+12	1.0E-08
35	Table (rigid)	Steel	0.300	1.00E+08	8.33E+12	8.33E+12	1.0E-08
36	Table (rigid)	Steel	0.553	1.00E+08	8.33E+12	8.33E+12	1.0E-08
37	Table (rigid)	Steel	0.652	1.00E+08	8.33E+12	8.33E+12	1.0E-08
38	Table (rigid)	Steel	0.579	1.00E+08	8.33E+12	8.33E+12	1.0E-08
39	Table (rigid)	Steel	1.410	1.00E+08	8.33E+12	8.33E+12	1.0E-08
40	Table (rigid)	Steel	0.579	1.00E+08	8.33E+12	8.33E+12	1.0E-08
41	Hyd. Jack (rigid)	Steel	0.511	1.00E+08	8.33E+12	8.33E+12	1.0E-08